THE HONG KONG POLYTECHNIC UNIVERSITY

DEPARTMENT OF CIVIL AND STRUCTURAL ENGINEERING

EXPERIMENTAL STUDY ON THE INTERFACE BEHAVIOR BETWEEN UNSATURATED COMPLETELY DECOMPOSED GRANITE SOIL AND CEMENT GROUT

By

Md. Akhtar Hossain

A Thesis Submitted in Partial Fulfillment of the Requirements

for the Degree of Doctor of Philosophy

August 2010

CERTIFICATE OF ORIGINALITY

I hereby declare that this thesis entitled "*Experimental Study on the Interface Behavior between Unsaturated Completely Decomposed Granite Soil and Cement Grout*" is my own work and that, to the best of my knowledge and belief, it reproduces no material previously published or written, nor material that has been accepted for the award of any other degree or diploma, except where due acknowledgement has been made in the text.

Signature: _____

Name: Md. Akhtar Hossain

Abstract of the thesis entitled

EXPERIMENTAL STUDY ON THE INTERFACE BEHAVIOR BETWEEN UNSATURATED COMPLETELY DECOMPOSED GRANITE SOIL AND CEMENT GROUT

Soil-structure interaction is an important phenomenon encountered in various geotechnical engineering projects like soil nails, retaining walls, shallow foundations, and pile foundations. One of the most important parameters for the design and safety assessment of these structures is the ultimate interface shear strength at the interface between the structural surface and the surrounding soil surface. The prime focus of this research is to investigate the elementary interface behavior between compacted completely decomposed granite (CDG) soil and cement grout under different matric suctions, net stresses and grouting pressures.

Firstly, a series of single-staged consolidated drained direct shear tests are conducted on compacted CDG soil under different matric suctions and net normal stresses. A soil-water retention curve (SWRC) is obtained from the equilibrium water content corresponding to each applied matric suction at zero net stress. The experimental results show that the influence of suction and net stress on shear behavior of soil is significant. Shear strength of soil increases with matric suction and net stress. The suction envelope is observed as nonlinear. Greater dilation angle is found at higher suction with lower net normal stress, while lower or zero dilation angles are observed under higher net normal stress with lower suction, also at saturated condition. A modified model is proposed for predicting the unsaturated shear strength of soils considering the influence of soil-dilation. The experimental shear strength data are found little bit higher than the

analytical results at higher suction range under higher net stresses.

Secondly, to investigate the elementary behavior of gravity grouted (0 kPa grouting pressure) interface， and compare with the behavior of CDG soil, a number of interface direct shear tests are performed between compacted soil and cement grout under the same matric suctions and net normal stresses. The behavior of stress-displacement curves of soil-cement grout interface tests is similar to those of soil tests. Matric suction and net normal stress have significant influence on the hardening-softening and contractive-dilative behavior of soil-cement interface. The failure envelopes for different matric suctions are observed as linear. The apparent interface friction angle and adhesion intercept increase with matric suction. The apparent interface friction angles for different suctions are equal to the apparent friction angles of soil under the same suctions. However, the apparent adhesion values are higher than the apparent cohesion values of soil in lower suction range, but lower in higher suction range. The suction envelopes for different net normal stresses are nonlinear. The interface shear strength is greater than the strength of soil within the lower suction range for different net stresses. However, the interface shear strength is lower than the strength of soil at higher suction range. A modified model is proposed to consider the influence of dilation on apparent interface friction angle. The experimental shear strength data agrees well with the analytical results for different net normal stresses and matric suctions.

Finally, to examine the influence of grouting pressure on elementary interface behavior, a series of interface direct shear tests are performed under the same net stresses at both saturated and unsaturated conditions. At saturated condition, grouting pressure and net stress have significant influence on the behavior of interface. The behavior of stress-displacement curves for pressure grouted interface is similar to those of soil and

gravity grouted interface. The failure envelopes for different grouting pressures are linear, the apparent effective interface friction angles are constant, and the apparent effective adhesion intercept increases with grouting pressure. The grouting pressure envelope is approximately linear and declivities are constant for different net stresses. A model is proposed for interface shear strength at saturated condition considering grouting pressure as an independent variable. The predicted interface shear strength of the proposed model agrees fairly well with the experimental data. At unsaturated condition, the apparent interface friction angle increases with matric suction for individual grouting pressure, but decreases with grouting pressure for particular matric suction. The apparent adhesion intercept increases with matric suction. and grouting pressure. The interface strength increases with matric suction at lower suction range, but decreases or remains nearly constant at higher suction range. Similar to CDG soil, the suction envelopes for different grouting pressures are nonlinear. The interface shear strength increases with grouting pressure at lower suctions for particular net stress. On the contrary, a downward trend is obvious for the interface strength under higher suctions for different grouting pressures and net stresses. The interface dilatancy (negative) decreases with grouting pressure. The average interface dilation angles for different grouting pressures are lower compared to those of soil under the same suctions and net stresses.

A general model is proposed to predict the shear strength soil-cement interface incorporating the influence of dilation, matric suction, net stress and grouting pressure. The interface shear strength predicted from the proposed model agrees well with the experimental shear strength data. The shear strength of pressure grouted interface is greater than that of soil within the lower suction range for different net stresses. However, the interface strength is lower than the strength of soil at higher suction range.

The strength of higher grouting pressure interface is greater than the strength of CDG soil as well as gravity grouted interface under different net stresses and at saturated condition. This indicates that the stability of slopes can be boosted up at saturated condition by the inclusion of pressure grouted soil nails into the slopes instead of gravity grouted soil nails. At saturated condition and lower suctions, the failure of slope may be happened in the soil as the strength of soil is lower than the strength of interface. On the other hand, at higher suctions, failure of slope may be happened in the interface zone rather than in the soil as the strength of soil is greater than the interface. At saturated condition, the interface behaves as a rough interface for different grouting pressures. However, at unsaturated condition, the behavior of soil-cement interface changes from rough interface towards the smooth interface as the grouting pressure is increased.

ACKNOWLEDGEMENTS

I would like to express my heartiest gratitude to my supervisor, Professor Jian-Hua Yin, for his encouragement and guidance throughout the study. His supports and experienced guidance that made this work possible are highly acknowledged. The privilege of working with Professor Yin has remarkably influenced my professional development and perspectives.

Financial supports from The Hong Kong Polytechnic University and a grant from Research Grants Council (RGC) General Research Fund (GRF) (Grant number: PolyU 5338/08E) of the Hong Kong Special Administrative Region Government of China are gratefully acknowledged.

I would like to express my thanks to Dr. Wan-Huan Zhou, Mr. Eric Ho, the technicians of Concrete Laboratory and Soil Mechanics Laboratory of Department of Civil and Structural Engineering, The Hong Kong Polytechnic University for their co-operation in manufacturing different parts of the testing apparatus, test setup, and installing the computer program.

Finally, I would like to express my sincere thanks to my dear parents, family members, teachers, colleagues, and friends whose encouragement, love and friendship over the last four years have enabled me to reach a new level in my life.

TABLE OF CONTENTS

Chapter 4. TESTING MATERIALS, SPECIMEN PREPARATION AND TEST PROCEDURES

LIST OF TABLES

LIST OF FIGURES

Chapter 1

INTRODUCTION

1.1 BACKGROUND

Every year a large number of structures are constructed all over the world in soils for a variety of civil engineering purposes. One of the most important parameters for the design and safety assessment of these structures in the soil is the ultimate shear strength at the interface between the structural surface and the surrounding soil surface. The interface shear strength is considered in the sliding problem at the base of a retaining structure and a shallow footing or along the surface of a soil nail and a concrete pile.

Researchers have conducted numerous studies on the interface strength between fully saturated or fully dried soil and different construction materials using direct shear apparatus. Beside the direct shear apparatus, some researchers studied interface behavior by using simple shear, torsional shear or annular shear devices. The researchers have found that interface shear strength depends on various aspects such as relative density, surface roughness, normal stress, dilation angle, particle diameter, and moisture content of soil of the interface.

It is recognized that soil suction affects the engineering behavior of unsaturated soils (Burland and Ridley 1996; Fredlund and Rahardjo 1993), and unsaturated soils are common in nature especially in arid and semi-arid regions. Shear strength at the interface between an unsaturated soil and a structural element is one of the most

important parameters in the design of many Civil Engineering projects. The shear resistance of earth structures, pullout resistance of soil nails and shaft resistance of deep foundations depend on the shear strength of the concrete grout against the unsaturated soils.

In Hong Kong, the current practices and GEO-Guide 1 (GEO, 1982) recommend a range of interface friction angle, δ as one half to two-third of the internal friction angle, ϕ' of the surrounding soil in the design of the sliding problem on a shallow footing or a retaining structure. This guidance was originally based on Potyondy (1961), NAVFAC (1982b) and literature on geotextiles. In the case of difficulty to determine the adhesion at the back of the retaining wall, the interface shear strength was simply neglected as a conservative design (Chu 2003).

In 1980s, the soil nailing technique was introduced in Hong Kong to stabilize the unsafe slopes. Soil nailing has been increasingly used and become the most common slope stabilization method in Hong Kong. The pullout capacity of soil nail is a key parameter for the design and safety assessment of soil nailing. This parameter is estimated from an assumed skin friction on the interface between the soil and soil nail cement grout, and this may underestimate or overestimate the pullout capacity (Chu 2003). Moreover, some uncertainties are involved in laboratory or field pullout tests such as stress acting on the surrounding of the nail surface is difficult to measure, less control of saturation (or matric suction), no uniform stress-strain rate, and deformation parameters can not be obtained precisely. Besides, the pullout tests are not elementary tests and the elementary interface behavior can not be obtained. In the current practice of soil nailing, pressure grouted soil nails are being used to stabilize the slopes. Though it is assumed that

pressure grouted soil nail may exhibit more pullout strength (interface strength) compared to normal gravity grouted nails, there is a lack of literatures regarding the influence of grouting pressure on the fundamental interface behavior. To overcome the above mentioned uncertainties and limitations, the present study entitled *'Experimental Study on the Interface Behavior between Unsaturated Completely Decomposed Granite Soil and Cement Grout'* has been conducted to investigate the elementary interface behavior of soil-cement grout under different normal stresses, matric suctions and grouting pressures.

1.2 OBJECTIVES OF THE RESEARCH

Not much literature is available about the interface strength behavior between an unsaturated soil and a construction material. The principal focus of this research is to have a better understanding of the interface strength of unsaturated completely decomposed granite (CDG) soil and cement grout under different normal stresses, matric suctions and grouting pressures. In this project, a large size modified direct shear box (MDSB) is designed, manufactured, and used to measure the shear strength of unsaturated CDG soil from a site in Hong Kong. A special setup is also designed and made for testing the interface between the CDG soil and cement grout under a saturated or unsaturated condition. The main objectives of the current research are as follows:

(i) The shear strength and dilatancy characteristics of the CDG soil will be investigated at both saturated and unsaturated conditions under different net normal stresses. Considering the influence of soil-dilation on shear strength, a modified model for predicting the shear strength of unsaturated soils is to be proposed.

(ii) The shear strength and dilatancy behaviors of the interface between the compacted CDG soil and cement grout will be examined under different net normal stresses and matric suctions. A modified model for predicting the interface shear strength between CDG soil and cement grout is to be proposed considering the influence of interface-dilation.

(iii) The shear strength and deformation characteristics of the interface between compacted CDG soil and cement grout will be investigated under different normal stresses and grouting pressures at saturated condition. A model for predicting the interface strength at saturated condition between CDG soil and cement grout is to be proposed considering the influence of grouting pressure.

(iv) The shear strength and dilatancy characteristics of the interface between compacted CDG soil and cement grout will be examined under different normal stresses and grouting pressures at unsaturated condition. A general model, incorporating the influence of interface-dilatancy, matric suction, net stress and grouting pressure, for predicting the interface strength between CDG soil and cement grout is to be proposed.

(v) The interface shear strength will be compared with the shear strength of CDG soil under different net normal stresses and grouting pressures to provide a general conclusion about the performance of soil-cement interface at different saturated conditions or matric suctions.

1.3 ORGANIZATION OF THE THESIS

This thesis consists of eight chapters as follows:

Chapter 1. Introduction: This chapter presents briefly the background of research, the objectives and specific issues to be investigated, and the organization of the thesis.

Chapter 2. Literature review: The review point out the definition, components and effects of suction on soil characteristics, soil-water retention curve (SWRC) and hysteresis, existing literatures regarding the unsaturated soil shear tests, interface shear tests between soil and different construction materials at both saturated and unsaturated conditions, and pullout interface tests between soil and soil nails. Finally, research gaps in the existing literatures are identified, and the aim of the present study to fill those gaps is proposed.

Chapter 3. Experimental technique and testing apparatus: This chapter illustrates the different techniques to control or measure the matric suction, the technique used for present study, description of different features of the apparatus used in the present testing programs, and calibration of accessories of the apparatus.

Chapter 4. Testing materials, specimen preparation and test procedure: This chapter includes the basic properties of the soil and cement grout, preparatory work for testing apparatus before starting testing program, preparation procedure of soil and interface direct shear specimen, and procedure of conducting suction controlled direct shear tests.

Chapter 5. Unsaturated soil test results and their interpretations: This chapter describes about the SWRC obtained, influence of net stress on SWRC for the soil studied, influence of matric suction and net stress on the behavior of soil and soil dilatancy, and a modified model proposed for predicting the shear strength of unsaturated soils considering soil dilation.

Chapter 6. Unsaturated soil-cement interface test results and their interpretations: This chapter presents the test results and their interpretations of gravity grouted soil-cement

interface under different matric suctions and net stresses, influence of matric suction and net stress on interface stress-strain behavior and dilatancy, influence of interface-dilatancy on interface strength, and a modified model for predicting the interface shear strength taking into account the interface dilatancy.

Chapter 7. Pressure grouted interface test results and their interpretations: This chapter presents the test results and their interpretations of pressure grouted interface under different net stress at both saturated and unsaturated conditions, grouting pressure envelopes at saturated condition, a model for pressure grouted interface strength, influence of matric suction and grouting pressure on pressure grouted interface dilatancy, a general model for predicting interface strength incorporating matric suction, net stress and grouting pressure, comparison between interface shear strength and shear strength of soil at saturated and unsaturated conditions, and general comments on performance of soil-cement interface at different saturated conditions or matric suctions.

Chapter 8. Conclusions and recommendations: In this chapter, the main findings and conclusions obtained form the present study are presented followed by the recommendations for future studies in the topic area.

Chapter 2

LITERATURE REVIEW

2.1 INTRODUCTION

The interface shear strength between compacted soil and structure is an important parameter for various geotechnical engineering projects like soil nails, retaining walls, shallow foundations and pile foundations. Two type of tests such as shear tests (direct shear, simple shear, torsional shear and annular shear) and pullout tests are used to study the behavior of soil-structure interfaces. It is recognized that soil suction affects the engineering behavior of an unsaturated soil and unsaturated soils are common in nature. It is also believed that the interface formed by pressure grouting may exhibit more shearing resistance compared to usual gravity grouted interface. However, there is a lack of sufficient literatures regarding interface behavior of unsaturated soil and different construction materials (especially cement grout) as well as the influence of pressure grouting.

The aim of this chapter is to review the definition of soil suction and its components, mechanical behavior of soil water, effects of suction on soil characteristics, and existing literatures on behavior of unsaturated soils and soil-structures interfaces.

2.2 SOIL SUCTION

The term ‘soil suction’ was firstly used by Schofield (1935) to represent the ‘pressure deficiency’ in the pore water of any soil (saturated and unsaturated) that had the

capacity to absorb water if additional water was supplied at the atmospheric pressure (Sivakumar 1993). It plays an important role in unsaturated soil mechanics. Soil suction is commonly referred to as the free energy state of soil water, which can be measured in terms of its partial vapour pressure. From a thermodynamic standpoint, total suction can be quantitatively described by the Kelvin's equation as follows:

$$\psi = -\frac{RT}{v_{w0}\omega_v}\ln\left(\frac{u_v}{u_{v0}}\right) \qquad 2.1$$

where ψ is total suction (kPa); R is the universal gas constant $[J/(mol \cdot K)]$; T is the absolute temperature (K); v_{w0} is the specific volume of water or the inverse of the density of water (m3/kg); ω_v is the molecular mass of water vapour (g/mol); u_v is the partial pressure of pore-water vapour (kPa); u_{v0} is the saturation pressure of water vapour over a flat surface of pure water at the same temperature (kPa). The term (u_v / u_{v0}) is called relative humidity, RH (%).

2.3 SUCTION COMPONENTS

Total soil suction of soil is composed of two components such as matric component and osmotic component. A change of relative humidity in the soil generally causes a change of total suction. Relative humidity can be reduced due to the presence of a curved water surface produced by capillary phenomenon, that is, contractile skin (Fredlund and Rahardjo 1993). The radius of curvature of the curved water surface is inversely proportional to the difference between air pressure (u_a) and water pressure (u_w) across the surface, that is, $(u_a - u_w)$, which is called matric suction. A reduction in relative humidity due to the presence of dissolved salts in pore water is referred to as osmotic suction. It is a function of the concentration of dissolved salts in the pore fluid, and it is written in terms of a pressure.

Matric suction plays a significant role in the water flow in unsaturated soils as well as the mechanical behaviour of unsaturated soils. However, the influence of osmotic suction on the mechanical behaviour is difficult to identify, and has been controversial (Alonso *et al.* 1987). Since the study in this thesis involves change of only matric suction, the following discussions will concentrate on matric suction.

2.4 MECHANICAL BEHAVIOR OF SOIL WATER

The soil water within an unsaturated soil can be divided into three components such as adsorbed water, bulk water and meniscus water (Wheeler and Karube 1996). Adsorbed soil water is tightly bonded to soil particles and can be considered as a part of the soil skeleton. On the other hand, bulk fluid occupies those void spaces which are completely saturated. Finally, menisci water is surrounding the particle contact points in those void spaces which are not filled by bulk water (see Fig. 2.1). Bulk water, meniscus water and adsorbed water are at the same pressure at a state of hydraulic equilibrium. Those pores which are not filled completely with soil water, present curved menisci at the particle contact points either between individual sand and silt grains or between aggregations of clay particles, as stated by Gens and Alonso (1992). Capillary effects result from the surface tension of the pore fluid in menisci. Based on the Kelvin's model, the value of matric suction is dependent on surface tension (T_s) and the radius of curvature of the menisci characterized by radii R_1 and R_2 (refer to Fig. 2.2):

$$s = u_a - u_w = T_s = \left(\frac{1}{R_1} + \frac{1}{R_2} \right) \qquad 2.2$$

where u_a and u_w are the gas and fluid pressures respectively, acting on both sides of the fluid surface. As degree of saturation decreases, the menisci withdraw into smaller and smaller pore spaces, the radius of curvature of the menisci reduces, and hence matric

suction increases. Because of smaller pore sizes, far higher matric suctions can develop in clayey soils than in granular soils.

Wheeler *et al.* (2003) pointed out that matric suction within bulk water and within meniscus water produces different inter-particle contact forces transmitted through the soil skeleton. To demonstrate the influence of suction on inter-particle forces, an idealized case of two spherical particles having a water meniscus at their contact point is depicted in Fig. 2.3 (Wheeler and Karube 1996). External stresses that applied to the boundary of a soil element produce both normal and tangential forces at particle contacts, even if the external stress state is isotropic. Hence, if the external stress increases sufficiently, the tangential forces at particle contacts can cause interparticle slippage and plastic strains (this is why soils, unlike most metals, undergo plastic volumetric strains if loaded beyond a pre-consolidation pressure). Changes of matric suction within bulk water affect both normal and tangential forces at particle contacts, similar to external stresses. In contrast, the capillary effect arising from suction within the menisci produces only an increase in the normal forces at particle contacts, which in turn increases shear strength and stiffness of unsaturated soils. Therefore, increasing suction (drying) tends to reduce the possibility of slippage at the frictional particle contacts and yielding. In contrast, decreasing suction (wetting) in the initially unsaturated soils causes a decrease in the normal stress at contacts, and may results in inter-particle slippage (collapse) being lack of strength to support the externally applied load. Wheeler and Karube (1996) argued that the difference between suction and external stress was the reason why these two stress state variables could not be combined in a single effective stress parameter. Sharma (1998) carried out an analysis to calculate the contribution of meniscus water to inter-particle contact stress. For the case of the idealized model, the induced inter-particle contact stress by meniscus water

is small for millimeter-sized (or sand-sized) particles, and likely to be insignificant as compared with those caused by external loading. In contrast, much larger values of contact stress can be achieved for micron-sized particles and they may be significant in comparison with those caused by external loading. For the case of micron-sized clay platelets with edge-to-face contact, meniscus water exists only for suctions in excess of about 100 kPa, and its contribution to inter-particle stress is largely dependent on platelet size (i.e. nearly independent of suction value).

2.5 EFFECTS OF SUCTION ON SOIL CHARACTERISTICS

Suction influences soil characteristics significantly in terms of both mechanical and hydraulic properties. The effects of suction on soil characteristics are summarized as follows:

2.5.1 Mechanical characteristics

Numerous researchers have studied suction effects on yielding and compressibility. General conclusions can be reached as follows: an increase of suction stiffens the unsaturated soil against the external loading, resulting in an increase of apparent preconsolidation pressure (yielding stress). The yielding surfaces are enlarged with increased suction, showing a suction-hardening effect. On the contrary, the compressibility of an unsaturated soil increases with decreasing suction in general (Alonso *et al.* 1990). However, the experimental work of Wheeler and Sivakumar (1995) and Chiu and Ng (2003) showed that the compressibility under saturated conditions is smaller than that under unsaturated conditions. The experimental work of Estabragh *et al.* (2004) showed that the compressibility of a compacted silty soil does not change monotonically with suction and there is a maximum value at certain suction. They also found that the compressibility at a given suction is influenced by specimen compaction

effort: a dense specimen has a smaller compressibility. It can be concluded that the compressibility in an unsaturated soil was not only dependent on suction but also affected by compaction conditions and wetting-induced change of fabric. The volumetric response of unsaturated soils is highly stress path dependent due to the irreversibility. Shear strength in an unsaturated soil increases with increased suction, resulting in an increase in apparent cohesion while maintaining constant friction angle ϕ'. However, the increase in shear strength cannot continue indefinitely with the increased suction. Most experimental evidences show a nonlinear increase of shear strength with soil suction (Fredlund *et al.* 1987) and a tendency towards a maximum value at some given (high) suction (Gan and Fredlund 1996). Generally suction has a tendency of increasing elastic shear modulus (Mancuso *et al.* 2002; Ng and Yung 2007). Moreover, suction increases the brittleness and dilatancy of an unsaturated soil (Cui and Delage 1996; Ng and Zhou 2005; Hossain and Yin 2010), opposite to the effect of confining stress.

2.5.2 Hydraulic characteristics

Water permeability of an unsaturated soil depends on degree of saturation. Water flows only through the water-filled pore space, so the percentage of the voids filled with water (degree of saturation) is an important factor. The relationship between degree of saturation and suction can be represented by the soil-water retention curve (SWRC). Therefore the water coefficient of permeability of an unsaturated soil with respect to suction bears a relationship to the SWRC, and it can be estimated from the saturated permeability and the SWRC. Generally the saturated permeability of a sandy soil is larger than that of a clayey soil, but the unsaturated water permeability of the sandy soil decreases more steeply with increased suction and eventually becomes lower than that of the clayey soil. This is caused by the larger desaturation rate (represented by the

slope of the SWRC) of the sandy soil than that of the clayey soil. Saturated and unsaturated permeabilities in a soil are also influenced by void ratio.

2.6 SOIL-WATER RETENTION CURVE (SWRC)

Soil-water retention curve, also known as soil-water characteristic curve, is generally defined as the relationship between matric suction and water content or degree of saturation. This curve depends on the pore-size distribution of a soil, which is co-related with a continuous water phase. This curve is of value for the important role it plays in predicting unsaturated soil property functions (Fredlund 1998). Therefore the curve is believed to play a similar role as the consolidation curve of a saturated soil (Rahadjo and Leong 1997, Barbour 1998). For this reason, the SWRC has been frequently used to investigate different behavior of unsaturated soils like shear strength, permeability, *etc*.

The soil-water retention curve is generally presented in terms of volumetric water content. It is also represented in terns of gravimetric water content or degree of saturation in many cases. An ideal soil-water retention curve with typical features including the hysteresis between the desorption and adsorption curves, air-entry value, residual water content and desorption rate is shown in Fig. 2.4. Typical soil-water retention curves for different types of soils are presented in Fig. 2.5. The plasticity of the soil has significant influence on the SWRC. The saturated volumetric water content and the air entry value generally increase with the plasticity of the soil, whereas the slope of the SWRC in between the air entry value and the residual water content tends to decrease with the plasticity of the soil. Besides plasticity of soil, some other factors such as dry density and stress state also have influence on the shape of SWRC.

A soil-water retention curve starts from saturated condition i.e., at zero suction and ends at completely dry state approximately at 1000000 kPa suction. Vanapalli (1994) divided the entire SWRC into three stages, and they are boundary effect stage, the transition stage and the residual stage. There are several empirical equations proposed in the literature to represent the soil water retention curve (Brooks and Corey 1964; McKee and Bumb 1987; Van Genutchen 1980). These equations have often been restricted to certain types of soils or to soil-water retention curves of a particular shape or to a limited range of suction values. Fredlund and Xing (1994) suggested the following empirical equation of SWRC based on the pore-size distribution curve of the soil matrix:

$$\theta = C(u_a - u_w)\frac{\theta_s}{\left\{\ln\left[e + \left(\frac{(u_a - u_w)}{a}\right)^n\right]\right\}^m} \qquad 2.3$$

where θ is the volumetric water content at unsaturation; θ_s is the volumetric water content at saturation; a, n and m are fitting parameters; $(u_a - u_w)$ is the matric suction; e is the natural number (= 2.71828….); and $C(u_a - u_w)$ is a correction factor function that can be determined by the following equation:

$$C(u_a - u_w) = 1 - \frac{\ln\left[1 + \frac{(u_a - u_w)}{(u_a - u_w)_r}\right]}{\ln\left[1 + \frac{1000000}{(u_a - u_w)_r}\right]} \qquad 0 \le (u_a - u_w) \le 10^6 \text{ kPa} \qquad 2.4$$

where $(u_a - u_w)_r$ is a virtual matric suction corresponding to the residual water content and its magnitude generally varies in the range of 1500 to 3000 kPa (Fredlund and Xing 1994). Equation [2.3] has been frequently used because of its practical applicability (Leong and Rahardjo 1997; Sillers and Fredlund 2001; Lee *et al.* 2005). Equation [2.3] can be rewritten as follows in a normalized form by dividing both sides of the equation by the volumetric water content at saturation, θ_s (Vanapalli *et al.*1996):

$$\Theta = C(u_a - u_w)\left[\frac{1}{\ln\left(e + \left(\frac{(u_a - u_w)}{a}\right)^n\right)}\right]^m \qquad 2.5$$

where Θ is the normalized volumetric water content function and $\Theta = \theta/\theta_s$. Equations [2.3] to [2.5] can be used to best-fit soil-water retention curve data of any soil for the entire suction range of $0 \le (u_a - u_w) \le 10^6$ kPa.

The Fredlund and Xing's equation of SWRC is an empirical equation, but is derived using the assumption that the soil consists of a set of interconnected pores that are randomly distributed. Bao *et al.* (1998) suggested that the portion of SWRC corresponding to the transition stage was most important in the engineering practice associated with unsaturated soils, and the portion of SWRC could be simplified by a linear relationship with suction on the semi-logarithm scale.

The hysteresis is a well-known phenomenon associated with the SWRC. The hysteresis phenomenon of SWRC introduces great difficulties in the application of SWRC in unsaturated soil mechanics. The hysteresis is a complex phenomenon and may be attributed to several causes, like geometric non-uniformity of the individual pores, the contact-angle effect, the encapsulation of air in 'blind' or 'dead-end' pores and swelling, shrinking or aging phenomena (Hillel 1998). Mualem (1973) developed a fairly successful model based on the independent domain theory (Everett and Whitton 1952) to predict the hysteresis within the main wetting and drying curves of SWRC. In that model, only the main drying and wetting curves were required to completely characterize the hysteresis. Mualem (1974) subsequently modified the model and adopted a new physical interpretation of the independent domain theory. A comparison

of predicted and measured hysteresis cycles for a silty loam is shown in Fig. 2.6. It should be noted that the study of hysteresis is not in the scope of the present research.

2.7 STUDIES ON BEHAVIOR OF UNSATURATED SOILS

The shear strength of a soil can be related to the stress state in the soil. The stress state variables generally used for an unsaturated soil are the net normal stress and matric suction. Since 1950s several investigations are carried out to understand the principles of unsaturated soil mechanics. Some studies were performed on unsaturated soils without either controlling or measuring pore-air or pore-water pressure during shear. In some cases, the matric suction of the soil was measured only at the beginning of the test. These results serve as a qualitative indicator of the soil shear strength since the actual stress state variables at failure are unknown. The interpretation of the results from shear strength tests on unsaturated soils become ambiguous when the stress state variables at failure are not known.

Donald (1956) performed a series of direct shear tests on unsaturated fine sand and coarse silt using a modified direct shear box apparatus. The results presented show that as the matric suction is increased, the shear strength increases to a peak value and then decreases to a fairly constant shear strength. Hilf (1956) suggested an indirect measurement of pore-water pressure using axis translation technique when higher matric suction values were involved. An extensive research program on unsaturated soils was performed at Imperial College, London in the early 1960's. At the research conference in Boulder, Colorado, on the Shear Strength of Cohesive Soils, Bishop *et al.* (1960) proposed testing techniques and presented the results of five types of shear strength tests on unsaturated soils. Bishop and Henkel (1962) explained and summarized laboratory testing techniques and details of various types of triaxial tests on

unsaturated soil. Bishop and Blight (1963) examined the use of axis translation technique in the shear strength testing of unsaturated soil and compared between the shear strengths obtained from similar tests with and without axis translation on Talybont clay. The shear stress versus strain curves from the two types of tests agreed closely. Gulhati (1975) performed consolidated drained tests with pore pressure being maintained in a modified triaxial cell of two unsaturated, compacted soils from India. Fredlund and Morgenstern (1977) proposed the use of net normal stress and suction as independent stress state variables.

Fredlund *et al.* (1978) proposed a shear strength equation for unsaturated soils. The shear strength of an unsaturated soil was considered to consist of an effective cohesion and the independent contributions from net normal stress and matric suction. The test data indicated essentially a planar failure surface. The failure envelope was viewed as a three-dimensional plot with net normal stress and matric suction as abscissas can be visualized as an extension of the conventional Mohr-Coulomb failure envelope. Escario (1980) reported a series of consolidated drained direct shear tests and a series of drained triaxial tests on unsaturated Madrid gray clay under controlled matric suction conditions using the axis-translation technique. The results obtained show almost a parallel upward translation indicating an increase in the shear strength as the soil matric suction is increased.

Ho and Fredlund (1982) performed a series of multistage triaxial tests on unsaturated undisturbed specimens of two residual soils from Hong Kong. The soils were a decomposed rhyolite and decomposed granite. The testing program consisted of consolidated drained tests with pore-air and pore-water pressure control during shear. The desired matric suction in the specimen was obtained by controlling the pore-air and

pore-water pressure using axis translation technique. Gan (1986) conducted a program of multistage direct shear tests on an unsaturated glacial till in a modified direct shear box apparatus. The results showed some nonlinearity of the failure envelope. Escario and Saez (1986), Drumright (1989) and Toll (1990) also observed the nonlinearity in the shear strength versus matric suction relationship.

Gan and Fredlund (1992) conducted direct shear testing on fine ash tuff under various applied matric suction. The results indicated that the shear strength increased with matric suction up to a limiting value of about 70 kPa of matric suction. Beyond that matric suction, the applied matric suctions did not appear to contribute further to the shear strength. Campos and Carrillo (1995) performed direct shear testing of unsaturated colluvial and residual soils taken from a large landslide site in Rio de Janeiro, Brazil. The test results obtained suggest that the shear strength of both soils increase with matric suction. Gan and Fredlund (1996) performed direct shear tests and triaxial tests on unsaturated completely decomposed granite (CDG) soil from Hong Kong. The results showed that an increase in matric suction increases the stiffness of the decomposed granite as well as shear strength. Lee *et al.* (2005) studied the effect of stress state on the unsaturated shear strength of a Korean residual soil using modified triaxial tests. Experimental results showed that the soil-water characteristic curve and shear strength of the soil are significantly affected by the change of net normal stresses and this should be taken into consideration in the model to precisely describe the shear strength envelope of unsaturated soils. Feuerharmel *et al.* (2006) conducted suction controlled direct shear tests on two undisturbed colluvium soils taken from Southern Brazil. The shear test results showed that shear strength envelopes were linear for lower matric suction but tended to become bilinear for higher suctions. In addition, the experimental data indicated that for both soils the internal friction angle seems to

increase with matric suction. Ying *et al.* (2006) performed direct shear testing on undisturbed unsaturated loess with suction control. The tests results indicated that net vertical pressure and matric suction have influence on the shear strength. Zhan and Ng (2006) conducted suction controlled direct shear test on an unsaturated expansive clay (both natural and compacted) collected from China. The experimental results showed that the dilatancy and shear strength of the expansive clay increases with an increase in the applied suction. Zhan and Ng (2006) also pointed out that the increase of apparent friction angle with matric suction may be attributed to the increase of dilation angle.

It is generally expected to control total suction or matric suction throughout the testing of an unsaturated soil. The most commonly used technique is axis-translation technique. The focus of the present study is to investigate the effect of matric suction on the shear strength, dilatancy and deformation characteristics of an unsaturated recompacted completely decomposed granite (CDG) soil, collected from Tai Wai, Hong Kong, using a large direct shear box by applying axis-translation technique. The testing of unsaturated CDG soil is to perform to compare the behavior of CDG soil with the behaviour of unsaturated interface between same soil and cement grout. The next section will discuss the study performed on interface between soil and different construction materials.

2.8 SHEAR STRENGTH EQUATIONS OF UNSATURATED SOILS

A number of shear strength equations have been formulated for unsaturated soils in terms of different state variables. Bishop (1959) proposed the following equation for unsaturated soils:

$$\tau_f = c' + [\sigma_n - u_a + \chi(u_a - u_w)]\tan\phi' \qquad 2.6$$

where τ_f = shear strength; c' = effective cohesion; ϕ' = effective friction angle; u_a = pore air pressure; u_w = pore water pressure; σ_n= total stress and χ = coefficient having values ranging from 0 to 1, and is a function of the degree of saturation and soil type. However, Bishop's equation has difficulties in predicting the value of χ, and it can fail to explain phenomena such as the collapse of some soils upon wetting (Alonso *et al.* 1990; Bernier *et al.* 1997; Lee *et al.* 2005). Also, eq. [1] presents a soil parameter χ as in a constitutive equation rather than being a description of the state of stress.

To avoid the limitations of eq. [1], Fredlund and Morgenstern (1977) found that the stress state in an unsaturated soil can be more appropriately described by using two independent variables $(\sigma - u_a)$ and $(u_a - u_w)$. Fredlund *et al.* (1978) formulated the following shear strength equation for an unsaturated soil:

$$\tau_f = c' + (\sigma_{nf} - u_{af})\tan\phi' + (u_a - u_w)_f \tan\phi^b \qquad 2.7$$

where c' = intercept of the extended Mohr-Coulomb failure envelope on the shear stress axis when the net normal stress and the matric suction at failure are equal to zero. It is also referred to as 'effective cohesion'; $(\sigma_{nf} - u_{af})$ = net normal stress variable on the failure plane at failure; u_{af} = pore-air pressure at failure; ϕ' = angle of internal friction associated with the net normal stress state variable $(\sigma_{nf} - u_{af})$; $(u_a - u_w)_f$ = matric suction at failure and ϕ^b = angle indicating the rate of increase in shear strength relative to matric suction $(u_a - u_w)_f$. Though theoretically it is believed that the net normal stress $(\sigma_{nf} - u_{af})$ and matric suction $(u_a - u_w)_f$ are independent of each other, some experimental data show that the net normal stress may affect matric suction and

shear strength (Escario and Saez 1986; Vanapalli *et al.* 1999; Rassam and Williams 1999; Ng and Pang 2000; Lee *et al.* 2005)

Zhan and Ng (2006) proposed a modified form of eq. [2.7] as follows to consider the effect of suction on soil dilatancy, and hence on shear strength:

$$\tau_f = c' + (\sigma_{nf} - u_{af}) \tan(\phi' + \psi) + (u_a - u_w)_f \tan\phi^b \qquad 2.8$$

where ψ is the dilation angle. Equation [3] was simply proposed by Zhan and Ng (2006) without verifying with experimental tests data.

Lamborn (1986) proposed a shear strength equation for unsaturated soils by extending a micromechanics model. The equation is as follows:

$$\tau = c' + (\sigma - u_a) \tan\phi' + (u_a - u_w)\theta_w \tan\phi' \qquad 2.9$$

where θ_w is the volumetric water content, which is defined as the ratio of the volume of water to the total volume of the soil. The volumetric water content decreases as matric suction increases, and it is nonlinear function of matric suction. However, it should be kept in mind that the friction angle associated with matric suction does not become equal to ϕ' at saturation unless the volumetric water content is equal to 1.

Peterson (1988) proposed the following shear strength equation for soils having a degree of saturation less than 85%:

$$\tau = c' + (\sigma - u_a) \tan\phi' + C_\psi \qquad 2.10$$

where C_ψ is the apparent cohesion due to suction. The influence of soil suction on shear strength in eq. [2.10] is considered as an increase in the cohesion of the soil. The apparent cohesion due to suction is dependent on the water content of the soil.

Besides the above mentioned equations, some equations are proposed by Satija (1978), Karube (1988), and Toll (1990). Most of the shear strength equations for unsaturated soils in the literature are either linear or bilinear approximations.

2.9 STUDIES ON SOIL-STRUCTURE INTERFACE BEHAVIOR

Soil-structure interface behavior has been one of the most interesting topics for the geotechnical researchers all over the world as the mechanics of interface are complicated and difficult to model mathematically. For this, experimental observations of interface behavior play a crucial role in advance understanding of this complex behavior. The interface behavior depends on many factors and boundary conditions. Among all the factors water content of the soil (matric suction) is the most important factors which may influence the mechanical behavior of the interface. However, most of the interface studies existing in literatures were conducted either fully saturated or fully dried condition and a less attention was paid on the unsaturated interface behavior. The following sections will describe the existing literatures on interface shear tests at fully saturated (by water or air) and unsaturated conditions.

2.9.1 Interface shear tests at fully saturated or fully dried condition

Researchers conducted extensive study on the interface strength between soil and different construction materials using a variety of equipment including simple shear, direct shear, torsion or annular shear devices. Potyondy (1961) performed several experiments in direct shear apparatus to determine the magnitude of skin friction on various types of soils and construction materials (steel, wood, and concrete) with strictly controlled moisture content. The test results showed that for cohesive soils both cohesion and internal friction should be considered in evaluation of skin friction. Panchanathan and Ramaswamy (1964) studied interface strength tests between soil and

different construction materials in direct shear apparatus. The results indicated that the interface strength depends on the roughness of the construction materials. Kulhawy and Peterson (1979) found that when the concrete is poured directly onto compacted soil, a rougher interface surface is developed and the shear surface is located in the soil away from the interface. Kulhawy and Peterson (1979) also pointed out that the interface friction angle is less than the soil friction angle for smooth interfaces, and equal to or greater than the soil friction angle for rough interfaces. Yoshima and Kishida (1981) used ring torsion apparatus to evaluate friction between dry sand and a steel surface over wide ranges of surface roughness and sand density. The deformation of sand near the steel surface was observed by X-radiography. The test results indicated that frictional resistance is primarily governed by the roughness of the steel surface, irrespective of the density of the sand. Acar *et al.* (1982) studied the interface properties of sand with the finite element method and stated that for all practical purposes, the effect of normal stress and soil density on roughness is negligible. Desai *et al.* (1985) conducted cyclic testing of sand-concrete interface at two densities, loose and dense. The test results indicated that cyclic interface behaviour is influenced by factors such as amplitude of displacement, normal stress, relative density of sand and number of loading cycles. Noorany (1985) investigated the strength behaviour and soil-steel friction of two noncemented calcareous sands, with particular emphasis on the effects of grain crushing on these properties. The tests results indicated that low side friction of steel piles driven in calcareous sands is caused by low effective soil-pile interface stresses. Bosscher and Ortiz (1987) studied the frictional characteristics of various bedrocks and construction materials against sand under cyclic loading. The results indicated that the skin friction is a function of the surface roughness of the solid member against the soil. Jewell and Wroth (1987) gave an interpretation for the plane strain angle of friction and the angle of dilation of sand in a direct shear test. The rate of increase of the reinforcement force

in shearing sand was shown to depend on the angle of dilation. Kishida and Uesugi (1987) performed simple shear tests on the interface between sand and steel. A comparison was made of the test results for sand-steel interfaces with respect to other types of interface testing apparatuses: the direct shear, the annular shear and the ring torsion types. A good correlation was obtained between the coefficient of friction and the normalized roughness over a wide range of sand diameters. O'Rourke *et al.* (1990) performed direct shear tests of sand-polymer interfaces. The interface frictional strength was found to increase with soil density and decrease with hardness of polymer. The shear strength characteristics were found to vary as a function of the type of sand, but were independent of repeated loading. Uesugi *et al.* (1990) reported a series of laboratory tests on dry sand and concrete friction under two-way repeated loading with a simple shear apparatus. The test results indicated that the maximum coefficient of sand-concrete friction depends on the surface roughness of concrete and the mean diameter of sand. Yin *et al.* (1995) performed a large size direct shear test of the interface between soil and concrete. The measured relative slip displacements along the interface showed that the relative displacement distribution is uneven. The traditional method that the shear stiffness or shear modulus is derived from curves of shear stress versus shear relative displacement obtained from direct shear tests is unreasonable. The rigid- plastic model is suggested for interface deformation. And a new kind of interface element with thickness is developed, which can simulate the interface deformation behavior more realistically. Evans and Fennick (1995) used a modified rotation shear device for measuring the interface friction angles between three fine-grained soils and three geosynthetics. Paikowsky *et al.* (1995) developed a dual interface shear apparatus (simple or direct) to evaluate the distribution and magnitude of friction between granular materials and solid inextensible surfaces. The test results indicated that the grain shape and the surface roughness, quantified with respect to the grain size, were the primary

parameters controlling the interfacial shear strength at a given normal stress level. Fakharian and Evgin (1996) developed an automated apparatus to study the behaviour of interfaces between crushed quartz sand and a plate under three-dimensional monotonic and cyclic loading conditions. Rao *et al.* (1996) stated that apart from the roughness of the material surface, the friction angle depends on the manner in which the fill at the interface is prepared. Rao *et al.* (2000) reported that the interface strength is independent of the over consolidation ratio of the soil but increases with roughness of surface by investigating the effective angle of interfacial friction between fine-grained soil and mild steel plate. Zeghal and Edil (2002) modeled the results of sand-structure interface developed under monotonic loading and found that the grain crushing play a major role in the behaviour of the interface. Chu and Yin (2006) performed direct shear tests to investigate the interface shear strength behaviour between completely decomposed granite (CDG) soil and a cement grout plate. The test results indicated that the interface shear strength of the CDG and cement grout material depends on the normal stress level, the soil moisture content and the interface surface waviness.

2.9.2 Interface shear strength equation at saturated condition

Interface shear resistance against displacement relationship can be represented by a linear-elastic-perfectly-plastic formulation. The interface shear strength is governed by the Mohr-Coulomb failure criteria for saturated case. To determine the ratio between interface friction and shearing stress, Potyondy (1961) modified the Mohr-Coulomb's equation as follows with introduction of the coefficient f_a for the reduction of cohesion and a coefficient f_ϕ for the reduction of the internal soil friction angle in the interface model.

$$\tau_f = f_a c' + \sigma'_{nf} \tan(f_\phi \phi') \qquad 2.11$$

where τ_f is the interface shear strength at failure; $f_a = \frac{c'_a}{c'}$; $f_\phi = \frac{\delta'}{\phi'}$; σ'_{nf} is the effective normal stress at failure; c'_a is the effective soil adhesion; δ' is the effective interface friction angle; c' is the effective cohesion of soil; and ϕ' is the effective angle of internal friction of soil. Table 2.1 summarizes the comparison of different modes of shearing on interface friction angle.

2.9.3 Interface shear tests at unsaturated condition

In case of fully saturated or fully dried soil, the soil pores are filled with either water or air. Whereas, soil pores are partially filled with water and air in case of unsaturated soil and the difference of pore-water and pore-air pressure is termed as matric suction or simply suction. Soil suction affects the engineering behavior of unsaturated soils. Thus, the study of unsaturated interface behavior is important to improve the understanding of structures in contact with unsaturated soil to improve the engineering of these systems. However, the role of matric suction in the behavior of interfaces between unsaturated soil and structures has received very little attention.

Miller and Hamid (2007) performed interface tests between unsaturated Minco silt and stainless steel. The test results showed that the interface shear strength increases with the increase of net normal stress and matric suction. The failure envelope and suction envelope were quite linear. However, the shear strength of the soil was greater than the rough interface for similar stress conditions. Sharma *et al.* (2007) carried out soil-geomembrane interface laboratory tests with provision for the measurement of pore pressures close to the soil-geomembrane interface during shearing process. The tests results suggested that soil suction contributes to shearing resistance at low normal stress values. At higher normal stress values, the interface shear behavior appeared to be

governed only by the magnitude of total normal stress. Hamid and Miller (2009) examined the interface behavior between unsaturated Minco silt and steel (smooth and rough surfaces). The test results indicated that matric suction contributes to the peak shear strength of unsaturated interfaces and post-peak shear strength does not vary with changes in matric suction. Net normal stress affects both peak and post-peak shear strength and the suction envelope for interface is nonlinear.

It is very important to understand the mechanical behavior of unsaturated interfaces to design reliable and efficient Civil Engineering projects. However, there is a lack of sufficient literatures regarding interface behavior of unsaturated soil and different construction materials. Unfortunately, no literature is found for interface between unsaturated soil and cement grout though this soil-cement interface is common for different geotechnical structures.

2.9.4 Interface shear strength equation at unsaturated condition

Miller and Hamid (2007) modified the shear strength equation for unsaturated soil proposed by Fredlund *et al.* (1978) to consider for interface between Minco silt and stainless steel. The equation is as follows:

$$\tau_f = c'_a + (\sigma_{nf} - u_{af}) \tan \delta' + (u_a - u_w)_f \tan \delta^b \qquad 2.12$$

where $(\sigma_{nf} - u_{af})$ is the net normal stress variable on the failure plane at failure; u_{af} is the pore-air pressure at failure; $(u_a - u_w)_f$ is the matric suction at failure; and δ^b is the angle indicating the rate of increase in interface shear strength relative to matric suction $(u_a - u_w)_f$.

Sharma *et al.* (2007) used Bishop's (1959) effective stress equation for unsaturated soil to predict the interface strength of silty sand and geomembrane. The equation is given below:

$$\tau = \alpha + [(\sigma - u_a) + \chi(u_a - u_w)]\tan\delta \qquad 2.13$$

where τ is the interface strength; α is the adhesion; σ is the total normal stress; u_a is the pore-air pressure; u_w is the pore-water pressure; δ is the angle of shearing resistance at the soil-geomembrane interface; and χ is a parameter whose value ranges from 0 to 1. Sharma *et al.* (2007) pointed out that eq. [3] does not accurately predict the measured shear strength. At low normal stresses, it overestimates the shear stress relative to the measured values whereas the reverse is true for high normal stresses. Moreover, the resulting χ values ranged from 0.4 to 2.1 for the various series of tests which is not appropriate.

The shear strength equation for unsaturated soils proposed by Vanapalli *et al.* (1996) was modified by Hamid and Miller (2009) as follows to predict the shear strength of unsaturated Minco silt-steel interface:

$$\tau_f = c'_a + (\sigma_{nf} - u_{af})\tan\delta' + (u_{af} - u_{wf})\tan\delta'\left(\frac{\theta - \theta_r}{\theta_s - \theta_r}\right) \qquad 2.14$$

where θ is the current volumetric water content; θ_r is the residual volumetric water content and θ_s is the saturated volumetric water content from a SWRC.

2.10 STUDIES ON PULLOUT INTERFACE BEHAVIOR

Soil nailing is an in-situ ground improvement technique and has become an alternative solution to the conventional slope stabilizing methods such as re-compaction, earth retaining structures, reduce inclination of the slope, etc. Soil nails are divided into

several types, based on the installation methods used, such as driven nails (precast), grouted nails, and jet-grouted nails. An important design parameter of soil nailing is the ultimate shear strength at the interface between the cement grouted nail and surrounding soil. The following sections will discuss the literatures regarding the interface pullout behavior of gravity grouted soil nail and pressure grouted soil nail.

2.10.1 Pullout interface behavior of gravity grouted soil nail

Gravity grouted nails typically consist of a steel bar with a diameter 15 – 46 mm, with 30 – 80 mm thick grout cover. The steel bar is placed in pre-drilled hole (100 – 150 mm in diameter) with a vertical and horizontal spacing, typically varying from 1 to 3 m, depending on the type of in-situ soil. The nails are usually cement-grouted under gravity or low pressure. The safety of the slopes greatly depends on the sliding resistance of soil over the soil nail (cement grout) surface. The pullout shear resistance of gravity grouted nails depends on the interface strength between cement grout and surrounding soil.

An extensive series of investigations have been carried out by researchers to understand the interface shear strength of soil nails. Juran *et al.* (1982) presented the theoretical and experimental studies on the mechanism of interaction between the soil and reinforcing elements during a direct shearing of a nailed soil mass and discussed the influence of different parameters on the efficiency of the reinforcement. Palmeira and Milligan (1989) performed pullout tests of grids buried in sand and found that pullout test results can be influenced by several factors, such as the properties of soil, the roughness and stiffness of the nail, and boundary condition of tests. Heyman *et al*. (1992) established a correlation between pull out resistance of a soil nail and soil parameters that were obtained from routine laboratory and field tests done in a residual soil to demonstrate the importance of soil dilatancy in the prediction of soil nail pullout

resistance. Milligan and Tei (1998) performed a number of pullout tests, direct shear tests of sand and interface tests between three different type sands and nail. The results of the tests indicated that the apparent coefficient of friction (bond) between stiff rough nails and soils is dependent on the friction angle of the soil, the rate of soil dilation during shear, the stiffness of the soil, and the diameter of the nail in relation to the mean particle size of the soil. Lee *et al.* (2001) studied soil nail interaction in loose fill and found that the pullout resistance of nails is a function of vertical pressure, relative compaction, and degree of saturation. Liang and Feng (2002) studied the mechanism and phenomena of the anchor-soil interaction and found that the soil dilatancy due to shearing is the main factor contributing to the increase of the anchor-soil interface friction. Pradhan (2003) performed a series of laboratory soil nail pullout resistance test in a loose completely decomposed granite (CDG) fill. It was noted that the interface strength parameters of the grouted nails at natural moisture contents were very similar to those determined using the direct shear test. The effect of dilatancy was considered for the reasons of high pullout resistance in dense materials. The pullout resistance of the soil nails increases with the increasing of overburden pressure. Chu and Yin (2005) developed a new pullout testing apparatus to investigate the interface shear strength behavior of the soil nail and surrounding soil and a series of laboratory pullout tests were performed with a cement grouted nail in a completely decomposed granite (CDG) soil. The results indicated that the interface strength depends on the normal stress, the soil degree of saturation, and the surface roughness of the nail. Su *et al.* (2007) performed soil nail pullout resistance tests in compacted CDG fill and reported that the degree of saturation influence the soil nail pullout resistance. Su *et al.* (2008) performed soil nail pullout tests on a compacted CDG soil in an unsaturated condition and pointed out that the overburden stress has no influence on the soil nail pullout resistance.

The literatures discussed above are about the interface pullout testing behavior between soil and gravity grouted nail and the following section will discuss the pullout interface behavior of pressure grouted soil nails.

2.10.2 Interface shear resistance equation for soil nail

The average pullout shear stress of a soil nail can be calculated from a measured pullout load by using the following equation:

$$\tau_s = \frac{F}{A} = \frac{F}{(\pi D)L_s} \qquad 2.15$$

where τ_s is the pullout shear stress; F is the pullout load; A is the active nail surface area which can be calculated by multiplying the embedded length L_s (in m) of the nail in contact with the surrounding soil with the perimeter of the pulled-out nail πD (in m).

Wong (1995) proposed the following equation for calculation of a soil nail pullout capacity per lineal meter:

$$T = (\pi D c' + 2D\sigma_v' \tan\phi') \qquad 2.16$$

where T is the pullout capacity per lineal meter, and $T = F/L_s$; D is the diameter of the soil nail; c' is the soil cohesion; and ϕ' is the internal angle of friction of soil.

Schlosser and Guilloux (1981) estimated the pullout force of the soil nail by using the following equation:

$$T_{ult} = \pi D c_a' + 2D\sigma_v'\mu' \qquad 2.17$$

where T_{ult} is the pullout force per lineal meter; c_a' is the effective adhesion of soil-nail interface; D is the nail diameter; σ_v' is the vertical stress at the mid-depth of the soil nail; and μ' is the coefficient of apparent friction of the soil-nail interface. Equation

[2.17] was originally proposed for driven nails and has been adopted by the practicing engineers for grouted nails due to its simplicity. However, the vertical stress acting on the soil nail is not equal to the initial overburden stress after drilling, stress release, and soil nail installation. Based on this understanding, the formula in eq. [2.17] is not suitable to calculate the pullout resistance of grouted nail accurately.

2.10.3 Pullout interface behavior of pressure grouted soil nail

Researchers have great interest on the degree to which the grouting pressure influences the soil nail pullout resistance. However, the literature regarding the effect of grouting pressure on soil nail pullout resistance is limited in references. Yeung *et al.* (2005) conducted field pullout tests on glass fiber reinforced polymer pipe nail in a CDG soil slope in Hong Kong. The test results indicated that pullout resistance increases significantly due to pressure grouting. Au *et al.* (2006a, b) simulated the grout injection in soils and the influence of pressure on the cavity expansion in clay. Yin *et al.* (2008) presented data from a limited number of laboratory pullout tests of pressure grouted soil nail (grouting pressure was 130 kPa or less) at unsaturated condition (S_r = 50%) and pointed out that grouting pressure contributes to the soil nail pullout resistance. A series of laboratory soil nail pullout tests under a combination of different grouting pressures and overburden stresses was carried out by Yin and Zhou (2009) on a CDG soil at nearly saturated condition. The study showed that grouting pressure has influence on soil nail pullout resistance. Yin and Zhou (2009) proposed a equation as follows for soil nail interface shear resistance considering the influence of grouting pressure:

$$\bar{\tau} = c'_G(p_G) + \sigma'_{vi}\mu'_G(p_G) \qquad 2.18$$

where $\bar{\tau}$ is the average soil-nail interface shear resistance; c'_G is the fitting parameter; σ'_{vi} is the initial vertical effective stress; μ'_G is the slope of the fitting line in eq. [2.18];

and p_G is the grouting pressure. The parameter c'_G may be interpreted as the interface shear strength when the initial overburden stress is zero. But c'_G may include the contributions of both bonding and frictional resistance at the interface between soil and cement grout.

It is understandable from the discussion presented in the previous sections that matric suction has significant influence on the engineering behavior of soils, and hence this should be taken into consideration to understand the mechanical behavior of interface between soil and construction materials. However, the existing literatures providing a lack on the unsaturated interface behavior. Moreover, no literature is available till today about the unsaturated interface between soil and cement grout. Though it is believed that pressure grouting may have influence on the interface behavior, there is no such literature in the references regarding the pressure grouted interface shear tests. To fill the above-mentioned gaps in existing literatures, the present study is aimed to perform interface direct shear tests under a combination of different matric suctions, net normal stresses and grouting pressures. Direct shear tests on the interface are more fundamental element tests which measure the shear strength behavior directly. Pullout tests are not elementary tests, the data of which are indirect and need careful interpretation. In the current research, direct shear tests of an unsaturated CDG soil will be performed to compare the behaviors between unsaturated soil and unsaturated interface.

This chapter describes about soil suction, its components, mechanical behavior of soil water, effects of suction on soil behavior, soil-water retention curve, the review of the literatures regarding the unsaturated soil testing as well as interface testing, and existing equations of unsaturated soil and interface. The next chapter will discuss the experimental technique and apparatus used for unsaturated soil tests and interface tests.

Table 2.1 Comparison of different modes of shearing on interface friction angle (after Chu 2003)

Author	**Type of testing apparatus**	**Results of investigation**
Potyondy (1961)	Direct shear test apparatus (Type B model)	(δ/ϕ) values for sand, cohesionless silt, cohesive granular soil and clay with smooth or rough steel, wood and concrete. $\delta = \phi$ in rough materials surfaces
Panchanathan *et al.* (1964)	Direct shear test apparatus (Type B model)	(δ/ϕ) values for sand with smooth or rough steel, cast iron, wood, brick and concrete. The ratio δ/ϕ is obtained between 0.60 to 0.75 for smooth materials and for rough materials 0.90 to 1.00
Kulhawy *et al.* (1979)	Direct shear test apparatus (Type B model)	(δ/ϕ) values for sand with different roughness of concrete surface. δ/ϕ is 0.99 in rough concrete surface and δ/ϕ is 0.89 in smooth concrete surface
Yoshimi and Kishida (1981)	Ring torsion apparatus (Type A model)	δ_{max} depends on surface roughness but does not depend on properties of sand and material type. $\delta_{lim} = \phi_{cv}$ for smooth surface material
Acar *et al.* (1982)	Direct shear test apparatus (Type B model)	δ_{max} increases with density of sand and roughness of steel, wood and concrete materials
Levacher and Sieffert (1984)	Direct shear test apparatus (Type B model)	δ_{max} increases with soil density
Desai *et al.*(1985)	Translational test box (Type B model)	δ_{max} for concrete material depends on density of sand
Noorany (1985)	Direct shear test apparatus (Type A model)	δ_{max} is independent of soil density
Bosscher *et al.* (1987)	Direct shear test apparatus (Type B model)	$\delta = \phi$ in rough concrete and sandstone, δ is lower in granite
Uesugi *et al.* (1990)	Simple shear apparatus (Type A model)	δ_{max} depends on sand density and concrete surface roughness
Subba Rao *et al.* (1998)	Direct shear apparatus (Type A and B models)	δ in Model B depends on sand density while in Model A is independent of density.

*Type A model: Construction materials are placed on the free surface of prepared soil.
*Type B model: Soil is placed against the material surface which functions as a confined boundary.

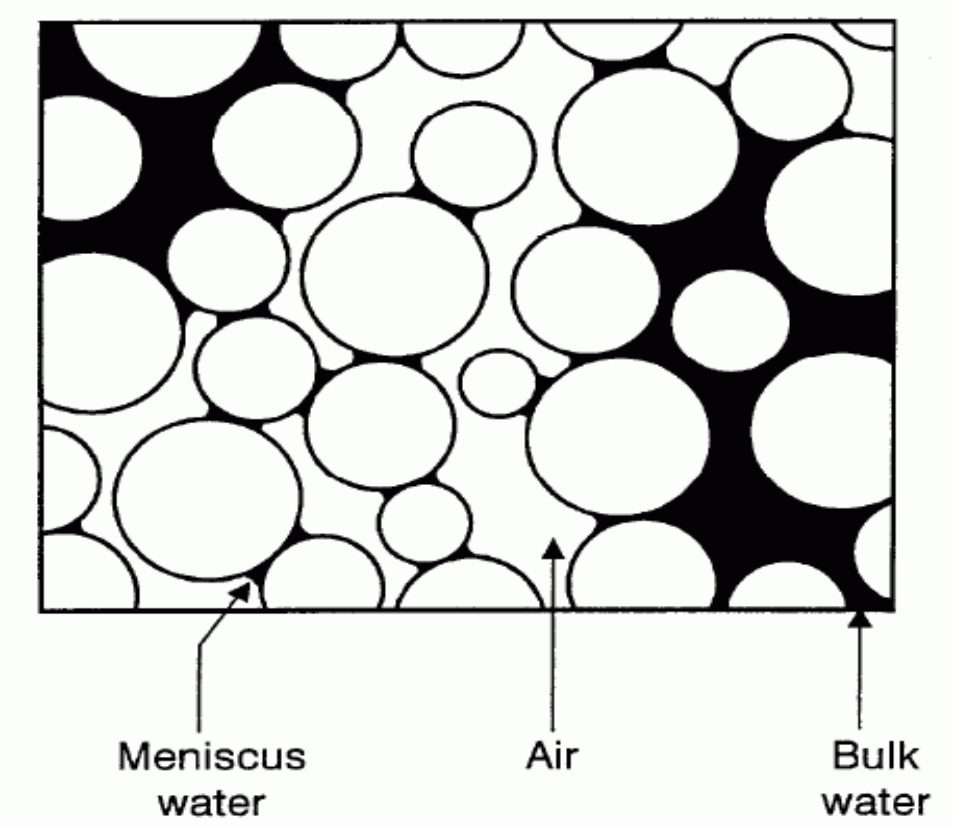

Figure 2.1 Schematic representations of bulk water and meniscus water within an unsaturated soil (after Wheeler and Karube 1996)

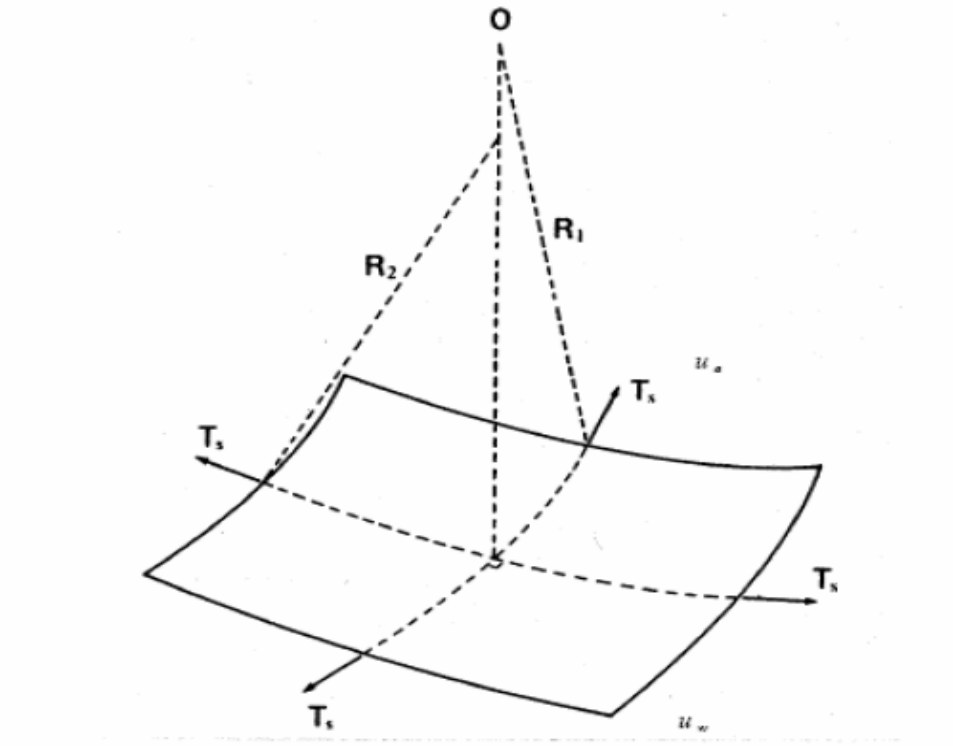

Figure 2.2 Surface tension on a warped membrane (after Fredlund and Rahardjo 1993)

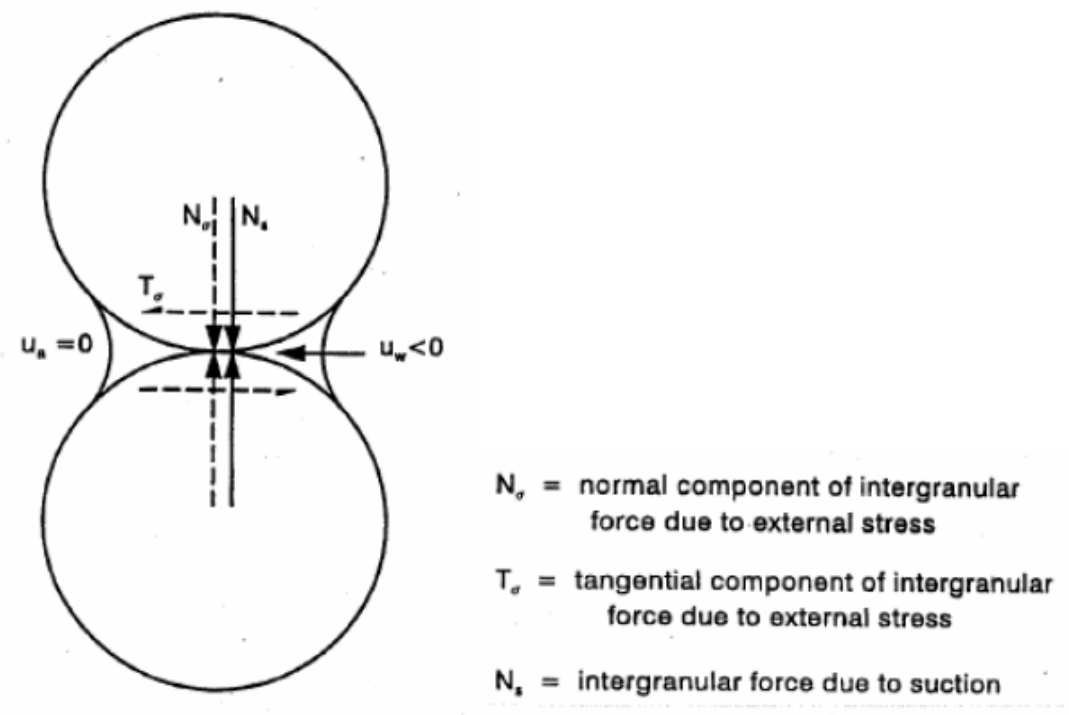

Figure 2.3 Influence of external stress and suction on interparticle forces (after Wheeler and Karube 1996)

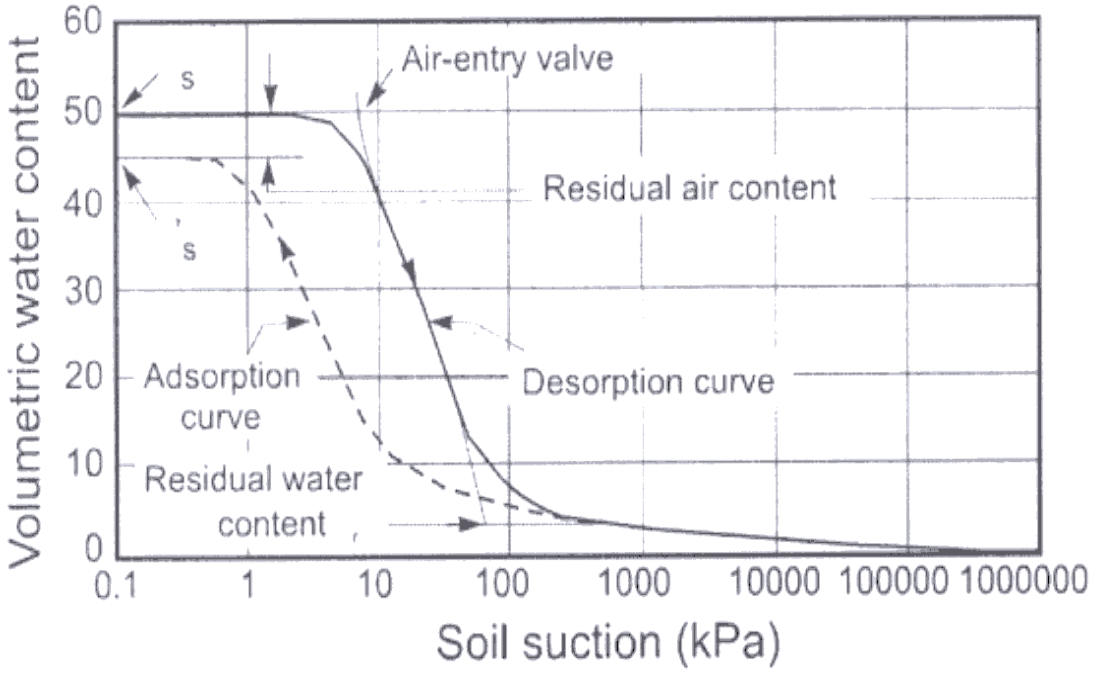

Figure 2.4 Typical soil-water retention curve for a silty soil (after Fredlund and Xing 1994)

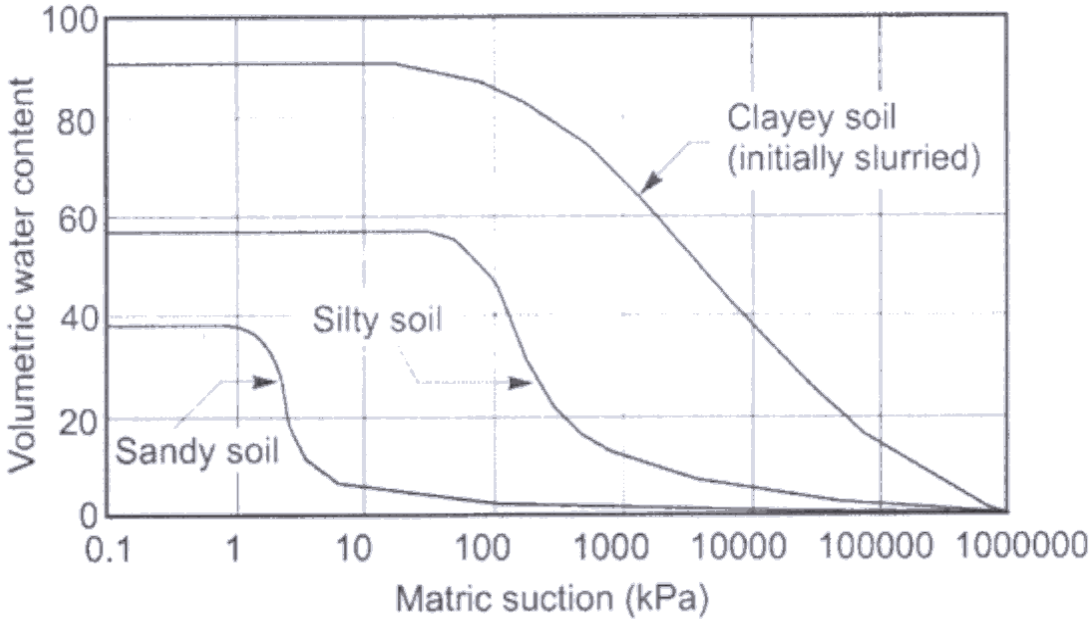

Figure 2.5 Soil-water retention curves for a sandy, silty, and clayey soil (after Fredlund and Xing 1994)

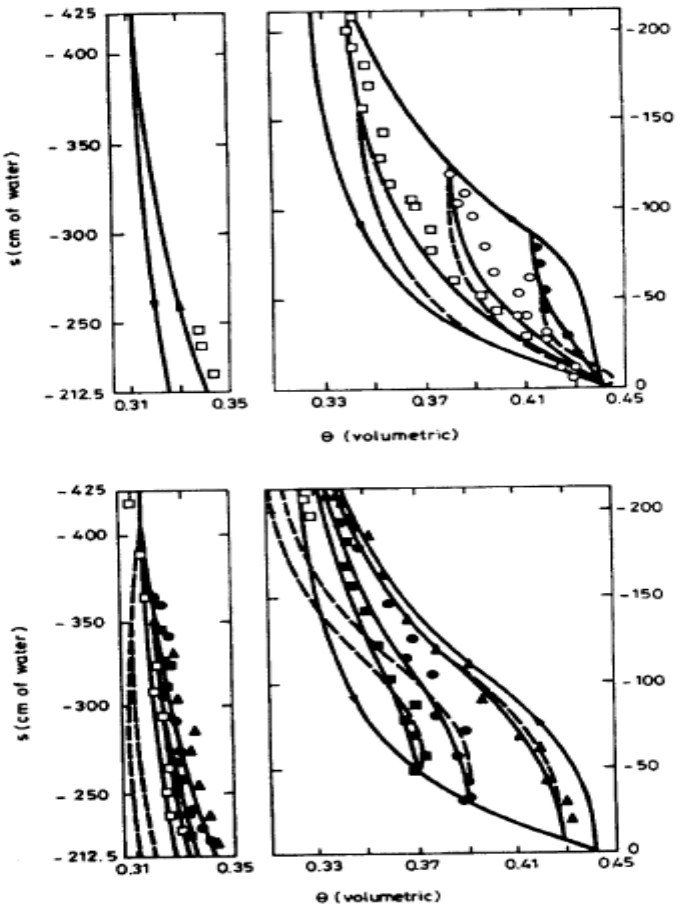

Figure 2.6 Hysteresis predicted by Mualem's model and measured values for Caribou silty loam (after Mualem 1974)

Chapter 3

EXPERIMENTAL TECHNIQUE AND TESTING APPARATUS

3.1 INTRODUCTION

For experimental study on unsaturated soil as well as on unsaturated soil-structure interface, an important issue is the control or measurement of suction in the soil. It is generally expected to control total suction or matric suction. The most commonly used technique is axis-translation technique (Hilf 1956), followed by osmotic technique (Zur 1966) and humidity control technique (Esteban and Saez 1988). These three techniques are briefly introduced and reviewed in the following sections.

3.1.1 Axis-translation technique

This technique was developed by Hilf (1956), and since then become the most common method used in unsaturated soil mechanics. The basic principle of axis-translation technique is to elevate pore air pressure u_a to increase pore water pressure u_w to be positive, preventing cavitations in water drainage system. Total stress σ is increased with air pressure u_a at the same amount to remain net stress $(\sigma - u_a)$ unchanged. This process is termed as 'axis-translation'. Axis-translation is accomplished by separating air and water phases in a soil through porous material with high air-entry value. Lloret *et al.* (2003) stated that when saturated, these materials allow water passage, but prevent flow of free air when the applied matric suction does not exceed air-entry-value of the porous material, which can be as high as 1500 kPa for sintered ceramic or 15 MPa for

special cellulose membrane.

In axis-translation technique, both pore-water pressure and pore-air pressure are controlled and measured independently, which enables controlled variation of suction. Suction can be controlled automatically if a feedback system is used. The axis-translation technique is frequently used for majority of experimental results about unsaturated soils in the literature due to its easy measurement and control of suction. One limitation of the axis-translation technique pertains to the maximum value of suction that can be applied. It is limited by the maximum value of cell pressure and the air entry value of porous material. For this reason, this technique is generally used for controlling suction in the order of several hundred kPa.

The validity of axis-translation technique has been investigated by relatively limited experimental evidences. Bishop and Blight (1963) examined the effect of the axis-translation technique on measured shear strength by conducting unconfined triaxial compression tests on compacted Selset clay and compacted Talybont clay. It was found that the measured shear strength was not affected by the application of the axis-translation technique. However, Bishop and Blight (1963) did not provide complete information about the specimen characteristics, especially degree of saturation, which is regarded as an indicator of continuity of air phase in unsaturated soil. Therefore, consideration should be given to the state of air phase in unsaturated soil when using these experiments to verify the axis-translation technique. Null tests by Fredlund and Morgenstern (1977) confirmed the validity of the axis-translation technique at a high degree of saturation (ranging from 0.833 to 0.95 with one exception of 0.759), when air phase is believed to be occluded (Juca and Frydman 1996). Null tests by Tarantino *et al.* (2000) verified the axis-translation technique for the case when the air phase is

continuous. In contrast, analysis presented by Bocking and Fredlund (1980), suggested that the axis-translation technique is no longer valid when the air phase in an unsaturated soil is occluded. Hence, the validity of the axis-translation technique is controversial for the case when the air phase is occluded. Moreover, since cavitations of pore water are hindered in the axis-translation technique, elevation of pore air pressure may alter desaturation mechanism of soil (Dineen and Burland, 1995). Thus, it is essential to understand whether experimental results obtained from the axis-translation technique can be extrapolated to interpret behavior of unsaturated soil under atmospheric conditions in the field.

3.1.2 Osmotic technique

An alternative method of controlling the matric suction in testing unsaturated soil is osmotic technique. Delage *et al.* (1998) reported that this technique was initially developed by biologist (Lagerwerff *et al.* 1961), and then adopted by soil scientist (Zur 1966) and geotechnical researcher (Kassif and Ben Shalom 1971; Komornik *et al.* 1980; Cui and Delage 1996).

The osmosis phenomenon is observed whenever a solvent and a solution are separated by a semi-permeable membrane, which only allows diffusion of solvent molecules (i.e. water molecules in this case). In the osmotic technique, suction control in a soil specimen is based on the principle of osmosis. A semi-permeable membrane is used to separate a soil specimen from an osmotic solution. The membrane is permeable to water and ions in the soil but impermeable to large solute molecules and soil particles (Zur 1966). Therefore, at equilibrium, the component of osmotic suction related soil salts is the same on both sides of the membrane, and the component of osmotic suction related

to the solute is zero in the soil. Then the difference of osmotic suction on both sides of the membrane is equal to the component of osmotic suction related to the solute in the solution. Similar to natural condition in the field, the pore air pressure in the soil is generally kept at the atmospheric pressure. Zur (1966) discussed the principle of osmotic technique in a view of energy analysis on soil water. At the state of equilibrium water exchange through the membrane, the energy potential in soil water is equal to that in solution water, that is, total suction in the soil is equal to that in the solution. Therefore, the difference of osmotic suction is equal to the difference of matric suction on both sides of membrane. Since the matric suction in the solution is zero, the matric suction in the soil in equilibrium is equal to the difference of osmotic suction on both sides of the membrane, that is, equal to the component of osmotic suction related to the solute. If the osmotic pressure of the solution is greater than initial suction in the specimen, water will be drawn from the soil into the solution, increasing the suction in the specimen to achieve equilibrium.

Polyethylene glycol (PEG) is the most commonly used solute to produce a solution for soil testing, because of its safety and simplicity. The value of osmotic pressure depends on the concentration of the solution: the higher the concentration, the higher the osmotic pressure. Delage *et al.* (1998) reported that the maximum value of osmotic pressure for a PEG solution was above 10 MPa.

Since the air pressure around a soil specimen remains atmospheric in osmotic technique, field stress path is better simulated by using the osmotic technique. Moreover, high value of suction can be applied without a use of very high cell pressure. However, an evaluation on the performance of three different semi-permeable membranes by Tarantino and Mongiovi (2000) showed that these membranes experienced a chemical

breakdown as the osmotic pressure of PEG solution exceeded a threshold value (in the order of several hundred kPa), which was found to depend on the type of membrane. Beyond this value, solute molecules were no longer retained by the semi-permeable membrane and passed into soil specimen, resulting in a reduction of concentration gradient and a decay of soil suction. This means that the maximum applied suction in the osmotic technique is also limited by the performance of semi-permeable membranes. One of the limitations of osmotic technique is that it can not be used in its current form to control suction in a continuous manner, because in existing technology, suction changes are applied in steps by exchanging PEG solution with different concentrations manually.

In addition, calibration of osmotic pressure against concentration of PEG solution is essential in the osmotic technique. Calibration for PEG solution can be carried out with a use of psychrometer (Williams and Shaykewich 1969), osmotic tensiometer (Peck and Rabbidge 1969), high suction probe (Dineen and Burland 1995) and osmotic pressure cell (Slatter *et al.* 2000). All these methods involve a semi-permeable membrane except the method using the psychrometer, which requires strict temperature control. Researchers have found that the relationship between osmotic pressure and concentration of PEG solution is affected significantly by calibration method (Dineen and Burland 1995; Slatter *et al.* 2000). That is why, Dineen and Burland (1995) suggested a need for direct measuring negative pore water pressure in soil specimen when using the osmotic technique. Hence, an important issue in the osmotic technique is the calibration of osmotic pressure against PEG concentration or direct measurement of applied suction in the soil.

3.1.3 Humidity control technique

According to thermodynamic definition of total suction, it can be imposed on an unsaturated soil specimen by controlling relative humidity of the atmosphere surrounding the soil. Humidity can be controlled by using aqueous solutions (Esteban and Saez 1988) or by mixing vapour-saturated gas with dry gas via a feedback system (Likos and Lu 2003). Delage *et al.* (1998) reported that humidity control with solutions was initially developed by soil scientist and the first application to geotechnical testing was by Esteban and Saez (1988). To apply this technique, a soil specimen is placed in a closed thermodynamic environment containing an aqueous solution of a given chemical compound. According to physico-chemical properties of the compound, a given relative humidity is imposed within the sealed environment. Water exchanges occur by vapour transfer between the solution and the specimen, and the given suction is applied to the specimen when vapour equilibrium is achieved. The solution can be the same product at various concentrations or various saturated saline solutions.

A feedback system for controlling humidity in a soil specimen was reported by Likos and Lu (2003). Humidity is controlled by proportioned mixing of vapour-saturated nitrogen gas and desiccated nitrogen gas in a closed environmental chamber. The vapour-saturated and desiccated gas streams are reintroduced in a three-neck flask where the resulting gas stream has a relative humidity that is a direct function of the wet to dry gas flow ratio (w/d). The humid gas stream is routed into an acrylic environmental chamber containing a soil sample. An effluent gas vent on the top cap of the chamber allows the influent humid gas to escape after flowing around the soil. Relative humidity and temperature in the chamber are continuously monitored with a polymer capacitance probe. Signals from the probe form a feedback loop with a control computer for automated regulation of the wet to dry gas flow ratio, enabling to control

relative humidity. Humidity variation is controlled to approximately 0.6% RH in this system. Similar to the osmotic technique, humidity control techniques can maintain the pore water pressure within a soil specimen at its negative value and high values of suction can be applied without a use of very high cell pressure. Very high values of suction (up to 1000 MPa) can be applied if solutions are used to control humidity. However, Delage *et al.* (1998) pointed out those uncertainties in this technique, limit applications under 10 MPa suction. When using a feedback system to control humidity, suction control range is determined by the measuring range and accuracy of the used humidity probe. Likos and Lu (2003) reported that in their system suction control range was from 7 MPa to 700 MPa.

Only fixed values of suction can be applied and cannot be used for varying suction in a continuous manner if solutions are used to control humidity. If the humidity is controlled by proportioning vapour-saturated gas with dry gas via a feedback system, suction can be controlled automatically as the axis-translation technique. Accuracy of this method depends on the accuracy of humidity probe and the resolution of feedback loop for automated regulation of relative humidity. When humidity is controlled by using solutions, temperature must be strictly controlled during testing as activity of the solutions is very sensitive to thermal fluctuation. The control of suction by this technique is much slower than the techniques involving liquid transfer (axis-translation and osmotic techniques) due to the very low kinetics of vapour transfer. When humidity is controlled by proportioning vapour-saturated gas with dry gas, test durations can be reduced due to active gas circulation. Likos and Lu (2003) reported that equilibrium water contents in several clays were reached within 12 hours. The short suction equalization duration (within 12 hours) is rather surprising, since it has been reported by Mazo *et al.* (1995) that months testing durations were required when humidity was

controlled by using solutions. Characteristics of the three suction control techniques (i.e. axis-translation, osmotic and humidity control) are summarized in Table 3.1.

3.1.4 Suction control technique used in present study

In present study, axis-translation technique was used to control matric suction for unsaturated soil tests and unsaturated soil-cement grout interface tests. To control the matric suction, water pressure (200 kPa) was applied in the water chamber below (top for interface tests) the high air entry ceramic disk, and required air pressure was applied in the air pressure chamber. The difference between the air pressure and water pressure applied is the desired matric suction. A higher water pressure was applied in the water chamber for two reasons- (a) to prevent the desaturation of the bottom (top for interface tests) of ceramic disk due to accumulation of diffused air during tests, and (b) to facilitate the control of matric suction to be constant during shearing.

3.2 TESTING APPARATUS

The shear behavior of unsaturated soils can be observed by performing either triaxial tests or direct shear tests. Most of the past studies are mainly based on triaxial tests. However, triaxial tests for unsaturated soils require a relatively long time for conducting one experiment, and may become an obstacle in solving the in-situ problem which should be treated within a short period of time. Additionally, the dilation tendency of soils may not be observed clearly in case of triaxial tests as the net mean stress increases with deviator stress during shearing. The increase of net mean stress tends to cause the contraction of the specimen, and consequently, the effect of suction on the dilation may be masked by the contraction (Zhan and Ng 2006). For these reasons, several studies have been conducted with direct shear tests. The results obtained from direct shear tests are compared with the theory on the basis of triaxial test results and found that some

theories proposed on the basis of the triaxial tests can be applied (Donald 1956; Escario 1980; Escario and Saez 1986; Gan *et al.* 1988).

Numerous studies have been performed to describe the behavior of soil-structures interface using different types of apparatus. However, each apparatus has some merits and limitations. The stress-strain relationships, mode of deformation, and dilatancy have to be studied critically to understand the interface behavior. The elementary interface behavior can be obtained by performing the direct shear testing. To overcome the limitations presented above, a direct shear apparatus was selected to conduct soil-soil direct shear tests and soil-cement grout interface tests program. The following section will discuss about the different features of the testing apparatus used for present study.

3.3 MODIFIED DIRECT SHEAR APPARATUS (MDSA)

Conventional direct shear apparatus requires modifications prior to their use for testing unsaturated soils and interface. Several factors related to the nature of an unsaturated soil must be considered in modifying the equipment. The modifications must accommodate the independent measurement or control of the pore-air and pore-water pressures. Gan and Fredlund (1988) developed a modified shear box by using the basic ideas presented by Escario (1980). The main difference between these two direct shear boxes is that in the design by Escario (1980), the lower portion of the shear box was immovable and the shear force was applied through the upper portion of the box. This resulted in problems related to eccentric normal loading of the specimen. The shear load in Escario's design was measured on the loading ram, thereby including the friction of the roller bearings. The main modification to the conventional direct shear apparatus was the design of an air pressure chamber. The air chamber completely enclosed the direct shear box.

A modified direct shear apparatus (MDSA), as shown in Fig. 3.1, slightly different from Gan and Fredlund (1988), is manufactured and set in the Soil Mechanics Laboratory, Department of Civil and Structural Engineering, The Hong Kong Polytechnic University. Schematic diagrams of MDSA used for soil-soil direct shear tests and soil-cement interface tests are shown in Fig. 3.2 and Fig. 3.3 respectively. The difference of present MDSA with the conventional one, used for unsaturated soil testing, is that different air entry value ceramic disks can be attached in present MDSA with steel plates. These disk plates can be placed tightly over the water chamber by screws and rubber O-ring, and can be replaced according to the desired suction values. One end of the water chamber is connected with auto volume change (AVC) device (after Wykeham Farrance Engineering Ltd.), as shown in Fig. 3.4(a), to monitor the movement of water from or into the specimen. The other end of water chamber is connected with a diffused air flushing (DAF 200M) device (after Geotechnical Consulting & Testing System), as shown in Fig. 3.4(b) to measure the volume of diffused air. A GDS pressure/volume controller (after Geotechnical Digital System), as shown in Fig. 3.5(a) is used to drain out all the air bubbles from the connecting tubes and water chamber. The air pressure inside the pressure chamber and water pressure in water chamber are applied and controlled by using a pressure regulators panel (after Wykeham Farrance Engineering Ltd.) (see Fig. 3.5(b)). The MDSA is equipped with five measuring or monitoring devices. These are two LVDTs (Linear Variable Differential Transformer) for monitoring horizontal and vertical displacements, a pressure transducer for monitoring pore-water pressure, a load cell (capacity 20 kN), as shown in Fig. 3.6(a), for measuring the horizontal shear load, and a electric volumemeter, AVC.

For interface direct shear testing, some modifications were made in the MDSA used for unsaturated soil. The water chamber was constructed inside the top steel platen, (see Fig. 3.6(b)), instead of shear box base since the bottom part of specimen was cement grout material. High air entry ceramic disk was set below the water chamber at same level of the bottom of top steel platen. The main features of the MDSA are discussed briefly in the following sections.

3.3.1 Shear box base and shear box

A photographic view of the shear box base used for unsaturated soil testing and interface testing is shown in Fig. 3.7. The shear box base is made of stainless steel. Water is allowed to circulate from entry port to the exit port below (top for interface tests) the high air entry disk. This ensures a thorough flushing of the channels and compartment of water chamber. The base of the shear box is seated on rollers which are set on the chamber base.

The shear box is consisted of two parts- top part and bottom part (see Fig. 3.8(a)), which are made of stainless steel. The top and bottom part of the shear box has an internal dimension of 100.05 mm square for soil testing and 100.07 mm square for interface testing, and a thickness of 15 mm. A steel mould, as shown in Fig. 3.8(b), having a dimension of 100 mm square and 50 mm high, was used for compaction of soil in case of unsaturated soil tests specimen preparation. Shearing is induced by applying the shear load on the base of the shear box using a digital motor having a displacing capacity of 0.001 mm/min to 2 mm/min. Horizontal resisting shear load is measured on top part of the shear box. Since the shear resistance is measured on the top part of shear box, the resistance to movement of the lower part with the base resulting from the

frictional resistance with the rollers may not introduce errors or inaccuracies to the resisting shear load measured.

3.3.2 Air pressure chamber

The entire shear box is enclosed in a pressure chamber, as shown in Fig. 3.9(a), to maintain the desired air pressure inside and around the specimen. The cylindrical chamber is built of stainless steel which can withstand a pressure up to 1000 kPa. The chamber body has an internal diameter of 300 mm, and a thickness of 8 mm. The chamber is comprised with three components such as (i) the chamber cap, (ii) the chamber body, and (iii) the chamber base which are made of stainless steel. Two rubber O-rings seal, one on the chamber cap and the other on the chamber base, are used to ensure air tightness of the entire chamber. The chamber cap, as shown in Fig 3.9(b), is held to the body through the use of six cap screws. The chamber cap has an air inlet valve, an air outlet valve, and an axial loading ram. A Teflon ring seal is used in the circular hole for the axial loading ram to ensure air tightness when the loading ram is in-place. Two holes, diametrically opposite each other, provide the necessary housing for the pistons that apply the shear force acting on the shear box assembly, and measure the resisting shear load. These holes are lined on the inside with an airtight Teflon seal. Two holes are provided on the chamber base to connect the two tubes with water chamber. The chamber base is attached with the frame by screws.

3.3.3 High air entry ceramic disk and disk plate

The key element for both controlling and measuring the pore-water pressure is the high air entry ceramic disk. The thickness of the disk is 7.14 mm, and the diameter is 79.38 mm. The disk acts as a semi-permeable membrane that separates the air and water phases. The ceramic disk is used not to allow the passage of free air, however, dissolved

air can diffuse through the water. The separation of the air and water phases can be properly achieved only when the air entry value of the disk is greater than the matric suction of the soil. The air entry value of the disk depends on the maximum pore size in the disc. The air entry value refers to the maximum matric suction to which the high air entry disk can be subjected before free air passes through the disk. The selection of a high air entry disk for testing an unsaturated soil should be primarily based upon the maximum possible matric suction that can occur during the test. The water coefficient of permeability and the thickness of a high air entry disk affect the time required for the pore-water pressure to equalize across high air entry disk.

In the present study, for unsaturated soil testing, the ceramic disk was attached with stainless steel plate, as shown in Fig. 3.10(a), having a dimension of 100 mm square and a thickness similar to the disk. The steel plate has a circular cut in the middle having a diameter of 85 mm. The disk is placed in the middle of steel plate, and properly attached with the plate by using Araldite (A & B) glue in such a manner that no air or water can pass through the interface between steel and disk. To ensure that, a groove of 2 mm wide and 3 mm deep was made inside the steel to be filled with glue when attaching the disk with steel plate. In case of interface testing, the ceramic disk is attached with the top platen (shear box cap) (see Fig. 3.10(b)) below the water chamber. Water pressure was applied to the water chamber below/top of the ceramic disk via the air-water interface Perspex cell (see Fig. 3.11(a), and controlled by a pressure control panel.

3.4 CALIBRATION OF MDSA ACCESSORIES

Two miniscanners (VJ Technology), as shown in Fig. 3.11(b), were used for logging the shear test data, and LabVIEW program was used to transfer the collected data from miniscanners to a computer.

The pore-water pressure transducers were used to measure the applied air and water pressure, and were calibrated by using the GDS pressure/volume controller. The pore-water pressure transducers were calibrated within the range of 0 to 600 kPa. The auto volume change (AVC) device used to measure the total volume change of water from or into the specimen had a capacity of 110 ml, and was calibrated within the range of 0 to 100 ml with the help of GDS pressure/volume controller. The DAF 200M used to flush and measure the volume of diffused air was calibrated within the range of 0 to 10 ml. Figures 3.12, 3.13 and 3.14 present the calibration curves for pressure transducers, AVC device and DAF 200M respectively. The load cell used for measuring the horizontal resisting shear load was calibrated with the help of a universal testing machine by applying compressive load within the range of 0 to 15 kN. The calibration curve for the load cell is shown in Fig. 3.15. The displacement capacity of horizontal LVDT was 50 mm and vertical LVDT was 25 mm. The displacement capacity was checked and calibrated with the help of a slidecaliperse. Figures 3.16 and 3.17 show the calibration curve for LVDTs. Necessary corrections were made for calculation or control of the net normal stress and shear load for different air pressures in the chamber. Figure 3.18 presents the correction on load cell reading corresponding to different air pressure inside the pressure chamber, and the load cell correction was considered and applied during calculation of resisting shear load. The frictional resistance between top and bottom parts of shear box was determined negligible as the contact area was reduced by providing a groove of 2 mm wide and 3 mm deep at the bottom of top part of shear box, and grease was also used between the two parts of shear box. Table 3.2 summarizes the additional load applied in the hanger for the correction of net normal stress due to different air pressure applied in the chamber. It should be noted that the ratio of hanger load to actual applied load on the specimen was 1: 20. The frictional resistance of

moving loading rams (vertical and horizontal) were determined very negligible, and was neglected during calculation.

3.5 SUMMARY

This chapter states the different techniques in existing literatures used to control or measure the matric suction with their advantages and limitations. The axis translation technique is used in the present study to control pore-air and pore-water pressure by applying a high water pressure at the bottom of ceramic disk and required air pressure inside the pressure chamber for particular suction. The descriptions of the modified direct shear apparatus used in the present testing programs are discussed with the calibration of different accessories. The next chapter will present the elaborate description of testing materials properties, preparation of specimens for direct shear tests, and the test procedure adopted for the present study.

Table 3.1 Summary of characteristics of three suction control techniques (after Rui 2007)

	Axis-translation	Osmotic	Humidity control	
			using solutions	using feedback system
Controlled suction	matric	matric	total	total
Automatization	automatic	manual	manual	automatic
Suction range	zero to hundreds of kPa	zero to 10 MPa (maximum is limited by performance of semi-permeable membrane)	10 MPa to 1000 MPa	determined by measuring range and accuracy of humidity probe
Similarity with field condition	positive pore-water pressure	negative pore-water pressure (similar to field condition)	negative pore-water pressure (similar to field condition)	negative pore-water pressure (similar to field condition)
Verification	valid (continuous air phase); controversial (occluded air phase)	Nil	Nil	Nil
Requirement	continuous air and water phases	calibration of PEG solution or direct measurement of negative pore-water pressure	strict temperature control; time-consuming	accurate humidity probe and feedback loop

Table 3.2 Additional hanger load applied for the correction of net normal stress due to different air pressure applied inside the chamber

Air pressure inside the pressure chamber (kPa)	Additional hanger load (N)
200	3.08
250	3.85
300	4.62
400	6.16
500	7.7

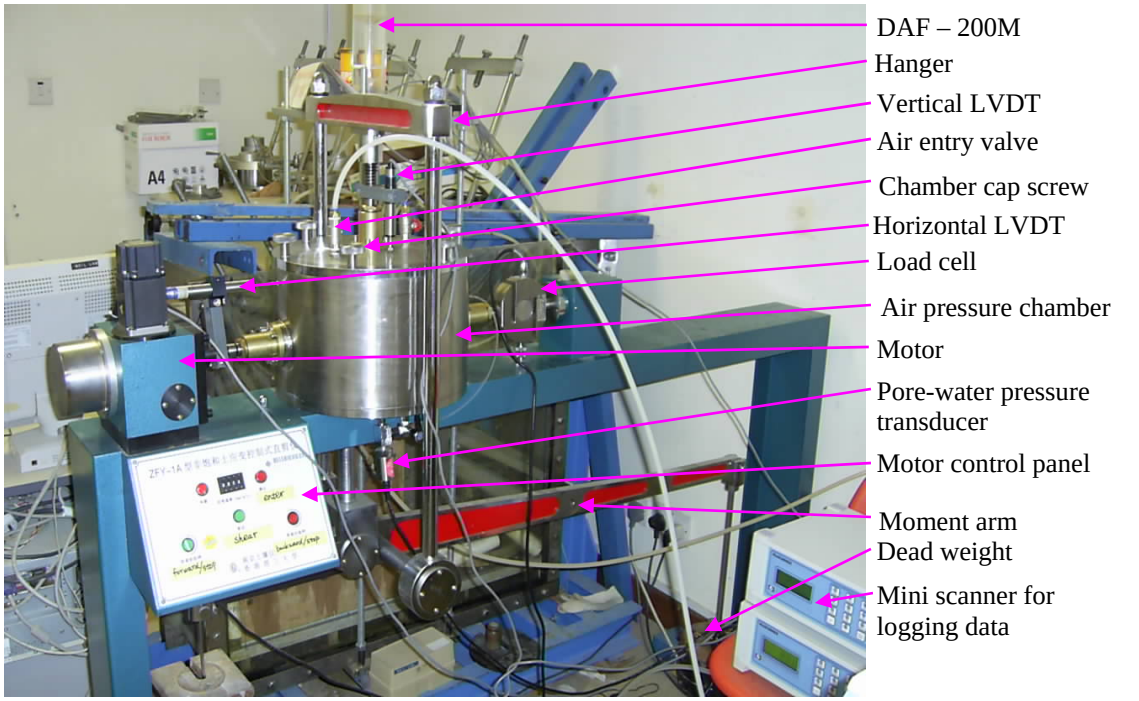

Figure 3.1 A photograph of the modified direct shear apparatus used in the present study

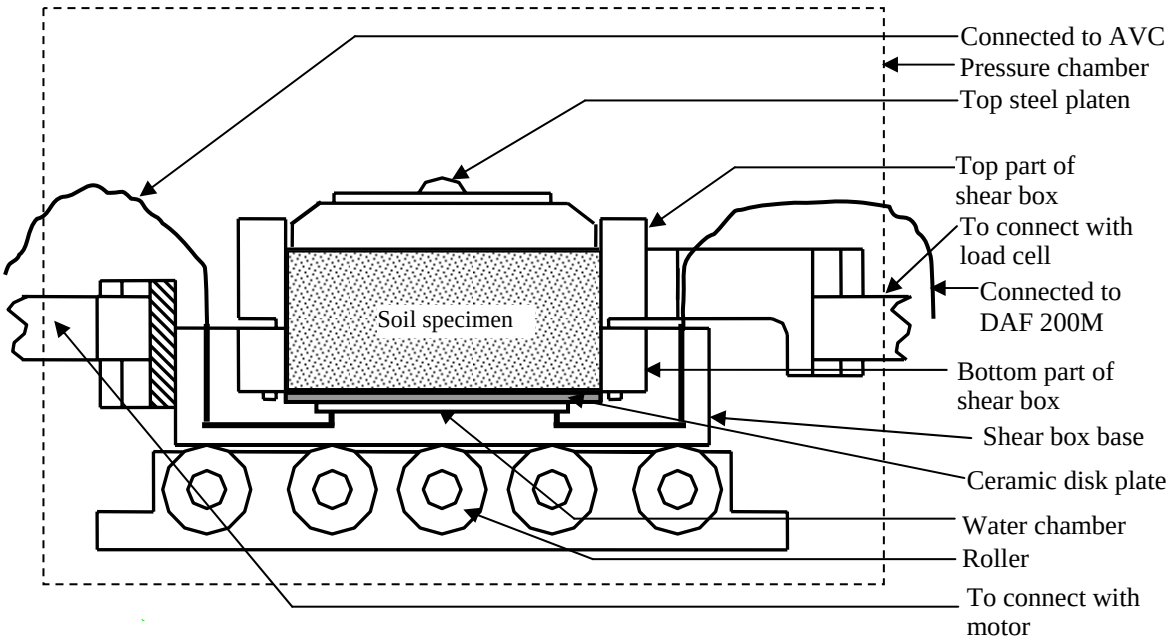

Figure 3.2 Schematic diagram of modified direct shear apparatus used for soil-soil direct shear test

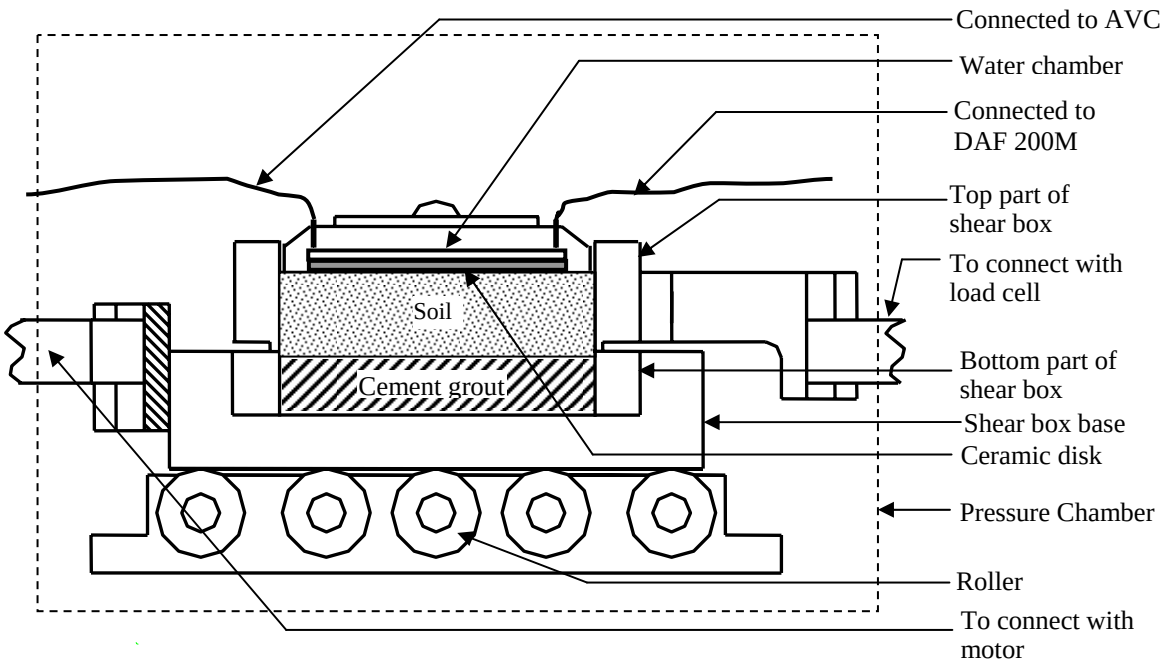

Figure 3.3 Schematic diagram of modified direct shear apparatus used for soil-cement grout interface test

(a) Auto volume change device (b) diffused air flushing device

Figure 3.4 Devices used for measuring the volume change of water and diffused air

(a) GDS pressure/volume controller (b) air and water pressure regulator panel

Figure 3.5 Air and water pressure applying and controlling devices

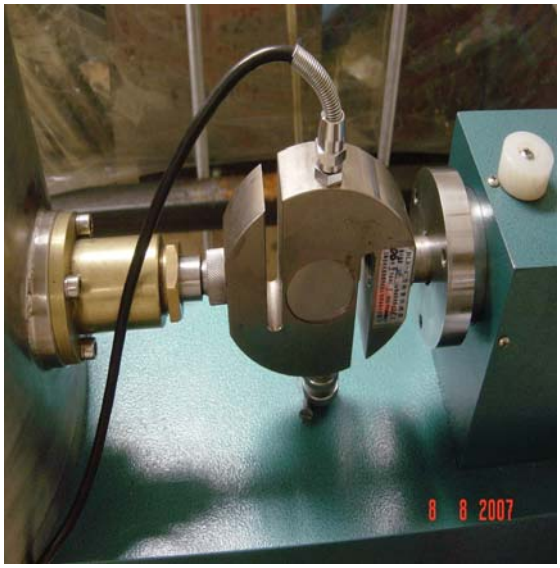

(a) load cell (b) top platen

Figure 3.6 Load cell, and top platen for interface tests

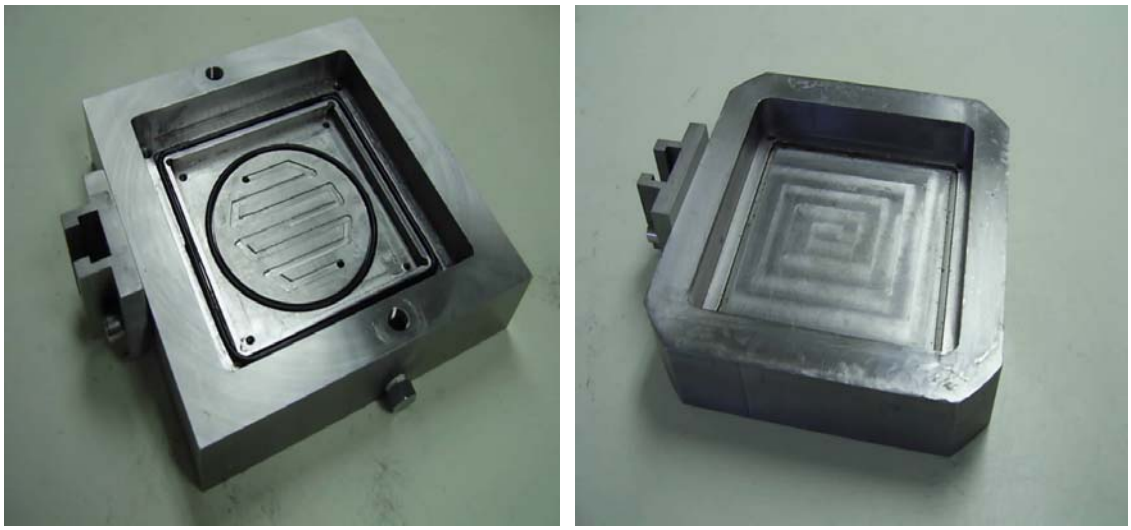

(a) for unsaturated soil tests (b) for unsaturated interface tests

Figure 3.7 Shear box bases used for unsaturated soil and interface tests

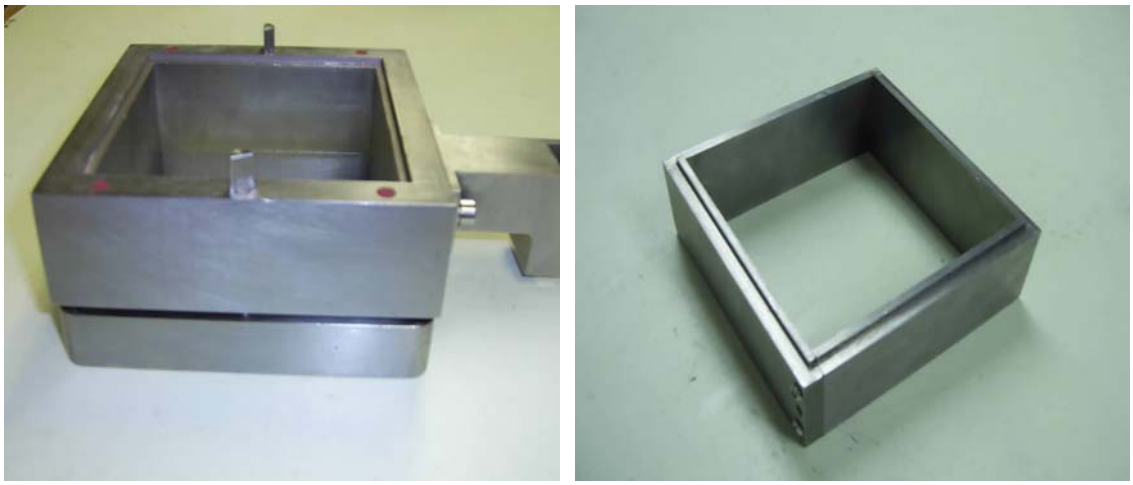

(a) shear box (a) steel mould

Figure 3.8 Shear box, and steel mould used for compaction of soil

(a) pressure chamber (b) chamber cap

Figure 3.9 Air pressure chamber and chamber cap of MDSA

(a) steel plate with ceramic disk (b) top platen with ceramic disk

Figure 3.10 High air entry ceramic disk attached with steel plate and top platen

(a) Perspex cell (b) miniscanners

Figure 3.11 Air-water interface Perspex cell, and shear test data logging device

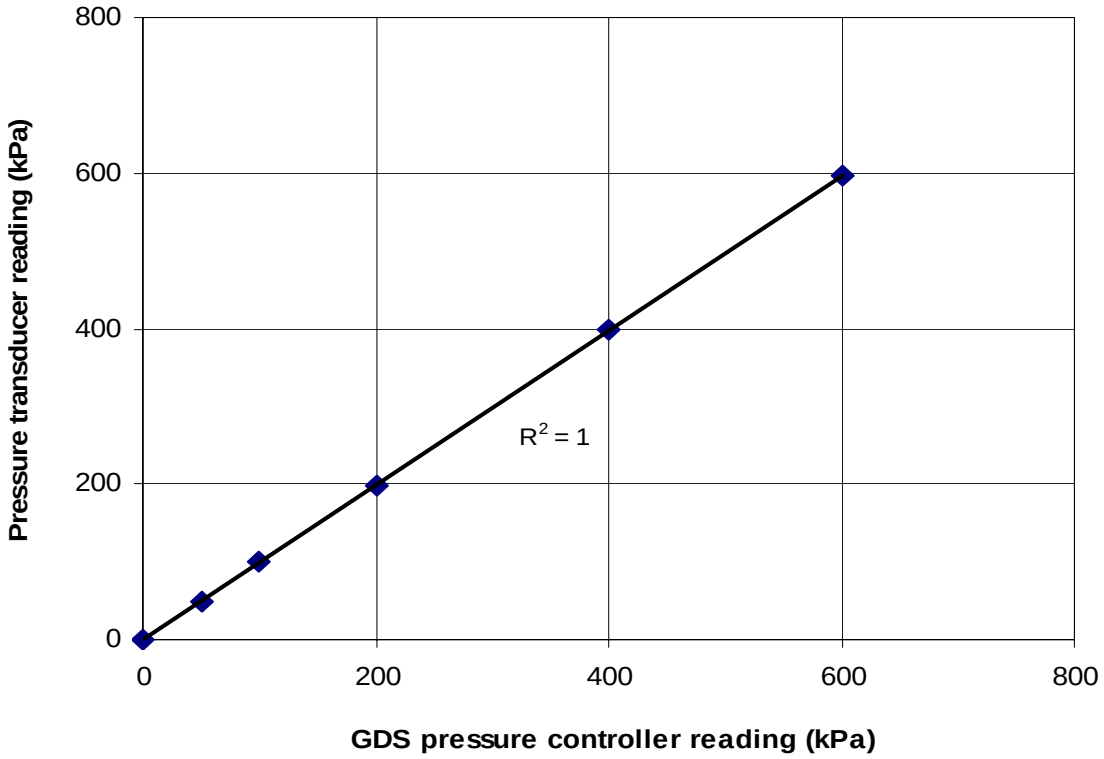

Figure 3.12 Calibration curve for pore-water pressure transducer

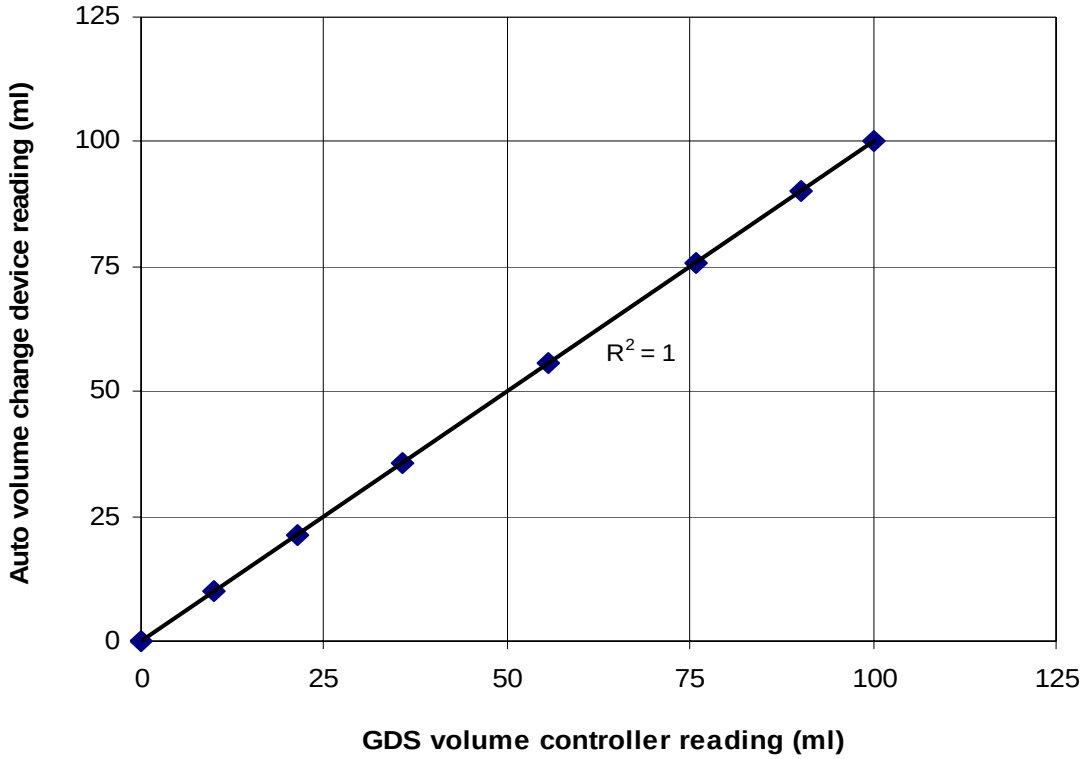

Figure 3.13 Calibration curve for auto volume change (AVC) device

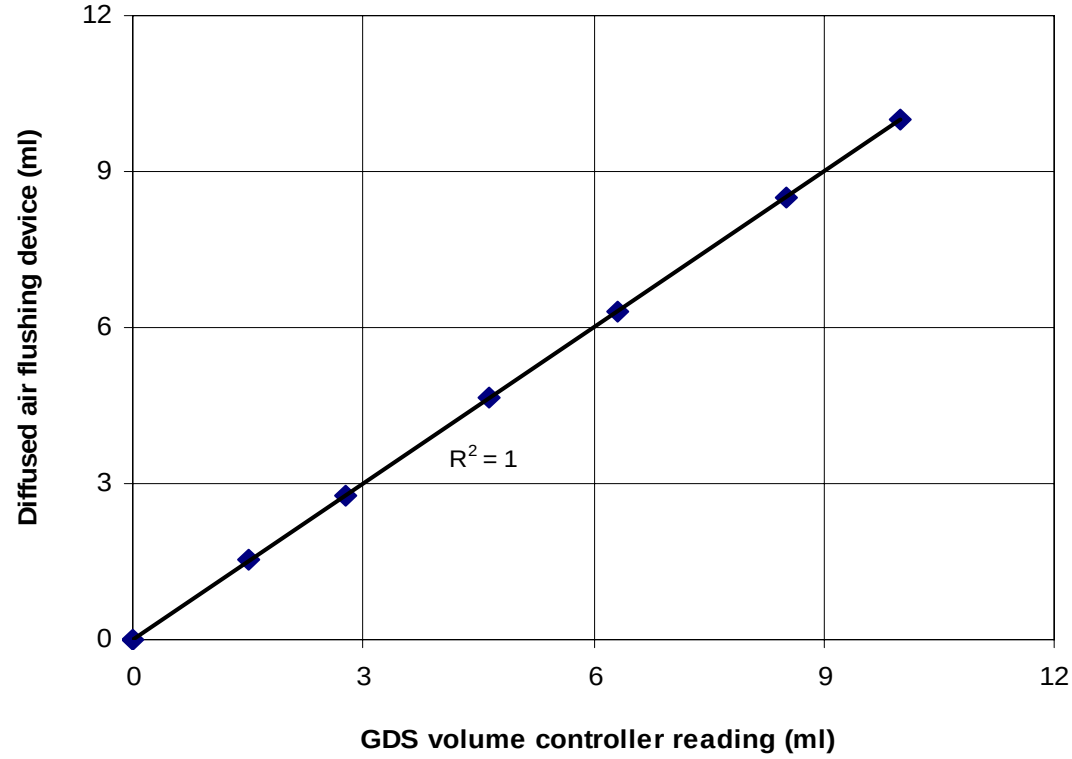

Figure 3.14 Calibration curve for diffused air flushing (DAF 200M) device

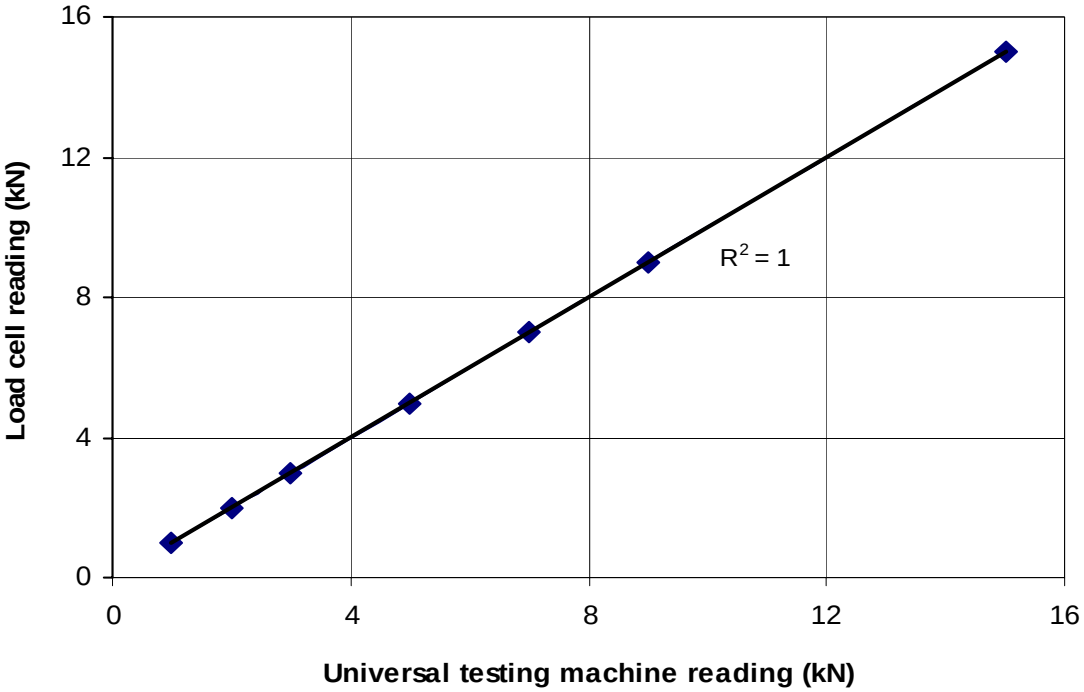

Figure 3.15 Calibration curve for load cell

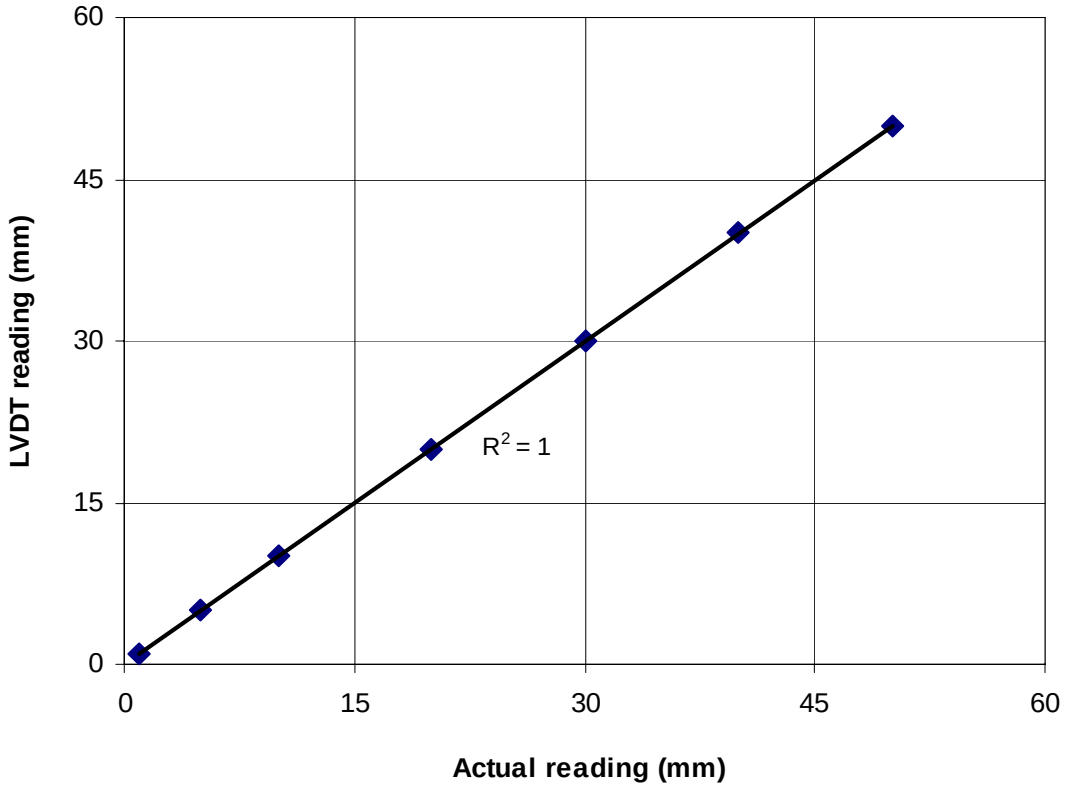

Figure 3.16 Calibration curve for horizontal LVDT

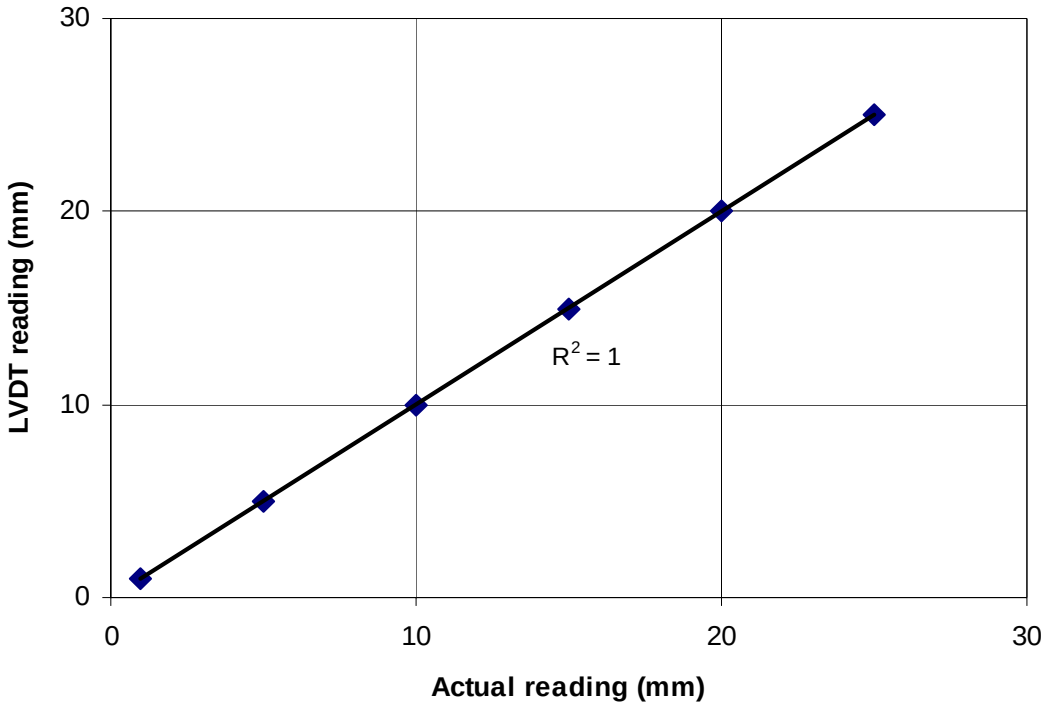

Figure 3.17 Calibration curve for vertical LVDT

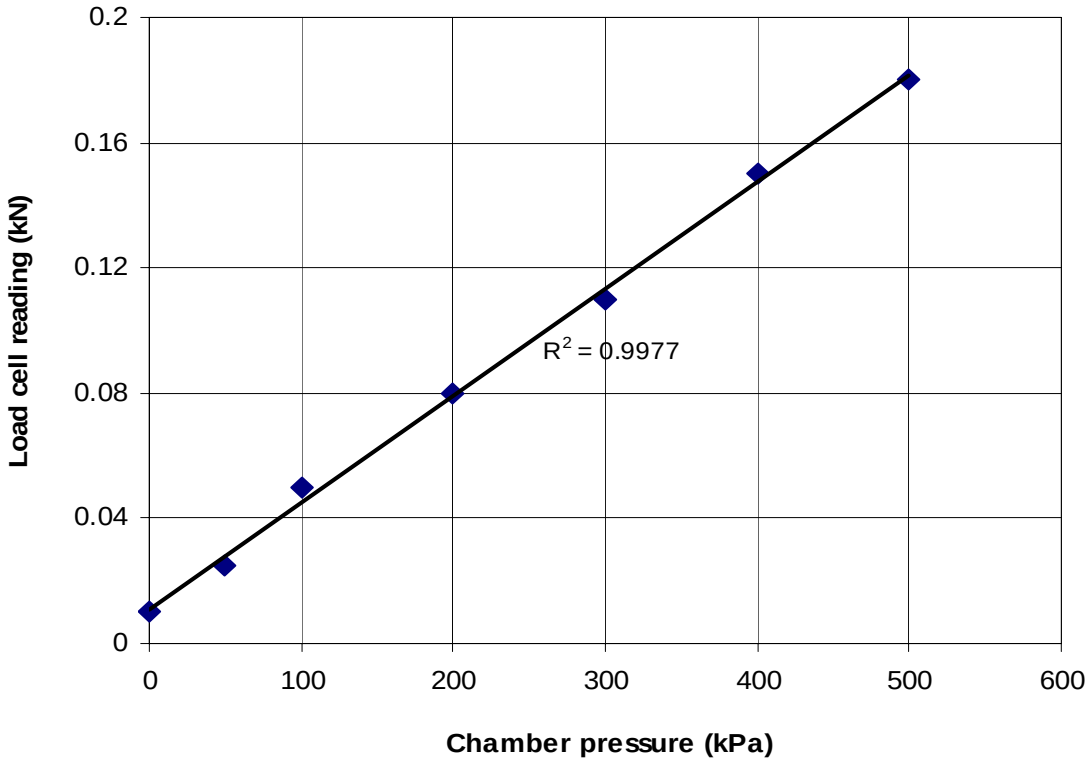

Figure 3.18 Correction on load cell reading for chamber pressure

Chapter 4

TESTING MATERIALS, SPECIMEN PREPARATION AND TEST PROCEDURE

4.1 INTRODUCTION

The main focus of the present study was to investigate the interface direct shear behavior between compacted soil and cement grout under different suctions, net normal stresses and grouting pressures. To compare the interface behavior with the behavior of soil, soil-soil direct shear tests were performed under the same suctions and net normal stresses. The following sections will discuss the properties of materials, preparation of specimen and tests procedure adopted to attain the objectives of the research.

4.2 MATERIAL PROPERTIES

4.2.1 Basic properties of the soil studied

The soil used in this study was a Completely Decomposed Granite (CDG) soil which is a typical in-situ soil in Hong Kong. Many geotechnical projects are related to this type of soils. Therefore the study of this soil has significant applications in Hong Kong, and is of great interests to local engineers and scholars.

The CDG tested in this study was taken from a highway construction site at Tai Wai, Hong Kong. All the tests on this soil followed the procedures as described in BS 1377:

1990 to determine the basic properties. The tests included particle size distribution, compaction, specific gravity, liquid and plastic limit, and permeability tests.

The particle size distribution of the soil was determined by wet sieving and hydrometer tests following the procedures in BS 1377-2 (1990) and GEO REPORT No. 36 (Chen 1992). The results of the particle size distribution are shown in Fig. 4.1. According to British Standards (BS 5930:1999), the sample soil is composed of 5.8% gravel, 44.1% sand, 36.8% silt and 13.3% clay. The soil can be classified as silty sand or SM according to the Unified Soil Classification System (ASTM D2487-90 1992). The average diameter of the soil (D_{50}) is 0.063 mm. The plastic limit and liquid limit of the soil are 22.7% and 32.8% respectively. The soil plasticity index I_p is 10.1%.

A standard compaction test was conducted by using a 2.5 kg rammer and a container of 1000 cm^3. The relationship between the dry density and moisture content of the soil is shown in Fig. 4.2. The obtained maximum dry density $(\rho_{d\max})$ of the soil is 1.75 Mg/m^3 with an optimum moisture content of 14.3%. The specific gravity G_s of the soil is 2.599. The falling-head permeability test was performed to determine the hydraulic conductivity of the soil, and the obtained water permeability (k_{20}) of the soil is 2.36×10^{-8} m/s. All the basic properties of CDG soil has been summarized in Table 4.1.

4.2.2 Properties of cement grout material

The cement grout was prepared in the way same as for the previous study (Su 2006; Zhou 2008). Therefore, there was no need to do duplicate tests on the cement grout properties. Uniaxial Compressive Strength (UCS) tests were carried out on both cylindrical and cubic specimens. The average uniaxial compressive strength σ_c of the

cement grout on the cylindrical specimens was 32.1 MPa. The average compressive strength from four cubic specimens was 32.2 MPa. The density of the cement grout was 1.89 Mg/m^3. The properties of the cement grout from Su (2006) are shown in Table 4.2.

4.3 PREPARING MDSA BEFORE STARTING TEST PROGRAM

Before starting the direct shear testing program, the modified direct shear apparatus (MDSA) was made prepared by saturating the high air entry ceramic disk and inspecting the leakage. The procedure of saturating the disk and inspecting the leakage are discussed in the following sections.

4.3.1 Saturation of high air entry disk

It is necessary to saturate the high air entry disk first with deaired water before starting the testing program. The saturation of ceramic disk was done according to Fredlund and Rahardjo (1993) by flooding the base of the shear box with deaired water and subsequently pressurizing the pressure chamber by air pressure of 500 kPa to force the water through the ceramic disk. The valves connecting the water chamber and measuring device are closed, and water was allowed to flow through the porous disk for about 1 hr. After that, the water chamber was flushed to remove diffused air from below the high air entry disk. The shear box base was then again flooded and air pressure is applied inside the pressure chamber. The water above, inside, and below the porous disk took on a pressure equal to the applied pressure. The pressure was applied for about 1 hr, and the air bubbles were then flushed from below the ceramic disk. The procedure was repeated for several times. When the process was completed, the air pressure chamber was opened, and the shear box base was again flooded with deaired water. This time the air pressure chamber was covered with a plastic sheet to reduce evaporation and drying

out of the high air entry disk until such time that the testing was to commence. The same procedure is applied to saturate the ceramic disk embedded inside the top platen for interface testing. After completing the saturation of the disk, the top platen was kept submerged under deaired distilled water until the test was commenced.

4.3.2 Inspection of leakage

4.3.2.1 Leakage of high air entry disk

After saturation of high air entry disk, it is very essential to check that there are no detectable leaks in the disk. Leakage through the high air entry disk was checked by applying air pressure inside the chamber stepwise upto the air entry value of the disk and flushing the water chamber. At first, 100 kPa air pressure was applied inside the chamber and retained for 1 hr. After that, the water chamber was flushed to observe air bubble, if any. The air pressure was then increased to 200 kPa, kept for another 1 hr, and the water chamber was flushed again. The same procedure of increasing the sir pressure was repeated upto the air entry value of the high air entry disk, and finally the water chamber was flushed. No significant amount of air bubble appear means no leakage of the disks. After completing the checking of leakage, the disk was again saturated following the procedure mentioned in the previous section.

4.3.2.2 Leakage of pressure chamber

Air-tightness of pressure chamber is important as leakage of air can render the equilibration of the applied suction difficult due to the loss of continuous loss of moisture from the system. Leakage from the chamber was checked by means of applying soap solution to all sealed areas around the moving parts. After applying the soap solution to all sealed areas, chamber cap was closed, and air pressure was applied inside the chamber stepwise upto the maximum possible pressure to be applied for

testing program. If no soap foam comes out from the sealed areas, the chamber is free of leakage.

4.4 PREPARATION OF DIRECT SHEAR TEST SPECIMEN

Three types of specimens were prepared for the testing program. They were soil-soil direct shear specimens, soil-cement grout interface specimens under gravity grouting, and soil-cement grout interface specimens under pressure grouting. The following sections will describe the preparation of different specimens for direct shear tests.

4.4.1 Preparation of soil-soil direct shear test specimen

The preparation of compacted soil-soil direct shear specimens generally includes: pretreatment of disturbed soil which includes drying of soil, breaking down of aggregation, sieving by 2 mm BS sieve, drying of the portion passing through 2 mm BS sieve, mixing with water, and compaction of soil.

4.4.1.1 Pretreatment of disturbed soil

The collected disturbed wet soil was kept in the oven for seven days where the temperature was maintained at 105 °C to dry completely. After drying, the aggregations of large particles were broken down into small particles by a hammer. The small particles were then broken down to sizes smaller than 2 mm by a rubber pestle so that the gravel particles did not get broken. Then, the broken particles were sieved by 2 mm BS sieve for 15 minutes. The portion remained on the 2 mm sieve was gravel and was discarded for the preparation of specimen to ensure the uniformity of the soil specimens. The portion passing through the 2 mm sieve was collected, mixed thoroughly and kept in the oven for two days. After that the required amount of prepared dried soil was taken

in a mixing bowl and sufficient amount of distilled water was added to flood the soil. The mixing bowl with wet soil was placed on a balance and kept in a room where the temperature was kept constant (17 °C) for three days. Continuous monitoring of the water content of the soil was made during this period and more water was added if the water content reached below the optimum moisture content which was 14.3%. After two days, the soil was mixed thoroughly so that no coagulation of soil particles took place and uniform water content could be assured.

4.4.1.2 Compaction of soil

A special square mould was produced having an inner cross-section of 100.05 mm by 100.05 mm and a height of 50 mm. The treated soil was compacted in four layers of 10 mm thickness each inside the mould to produce a specimen having a cross-section area of 100.05 mm x 100.05 mm, and a thickness of 40 mm. Each layer was compacted at the optimum moisture content (14.3%) to achieve a controlled dry density of 1.663 Mg /m^3, which was 95% of the maximum dry density of 1.75 Mg /m^3, obtained using a standard compaction test. The required mass of wet soil for a particular layer was calculated, then placed and compacted. After completing the compaction, the weight of specimen was recorded. After that, the mould with the specimen was turned over (upside down) and placed over the shear box which was made ready to place the sample prior to compaction of the soil. The specimen was pushed slowly inside the shear box and stopped pushing when the specimen set properly over the high air-entry ceramic disk. As the dimensions of the sample and the dimension of the shear box are exactly the same, the disturbance of the specimen is negligible. The as-compacted soil specimens had a void ratio of 0.563 and bulk density of 1.895 Mg/m^3. Figure 4.3 shows a compacted CDG soil specimen for direct shear test after compaction.

4.4.2 Preparation of soil-cement grout specimen

4.4.2.1 Gravity grouted soil-cement specimen

Treatments of disturbed CDG soil and preparation procedures of soil-soil direct shear specimen are elaborately discussed in the previous sections. The procedure for preparing soil-cement grout specimen is described in the followings. To simulate the cast in-situ installation, cement grout was poured on the compacted surface of CDG soil.

Before starting the compaction of treated soil in the shear box, the two parts of shear box are tightened together by using screws. The gap between the two part of shear box was filled with grease. The side walls of the shear box were polished with lubricating oil to reduce the friction between soil and side walls. A wooden block (wrapped with scotch tape) having a section of 100 mm by 100 mm and a height of 18 mm was placed at the bottom of the shear box. It should be noted that the height of bottom part of shear box is 20 mm.

The treated soil was compacted over the wooden block in two layers having a thickness of 10 mm each. Similar to soil-soil direct shear specimen, each layer was compacted at optimum moisture content of 14.3% to achieve a controlled dry density of 1.663 Mg/m^3, which was 95% of the maximum dry density of 1.75 Mg/m^3. The required mass of wet soil for a particular layer was calculated, then placed inside the shear box and compacted. After completing the compaction, the weight of compacted soil was recorded and the top part of the shear box was covered by another wooden block (wrapped with scotch tape) to prevent movement of moisture from or into the soil.

The amount of cement and water needed to fill a section of 100.07 mm by 100.07 mm and a height of 18 mm with cement grout was calculated before mixing. The cement and water was mixed (water/cement ratio 0.42) in such a way that no cement particle could coagulate and no lumps could present in the grout. After the preparation of cement grout, the shear box with the soil was turned over (top part down and bottom part up) and the first wooden block was removed to pour cement grout on the prepared surface of soil. The cement grout was poured smoothly over the prepared surface so that the bottom part of shear box could be filled fully with no air voids.

The cement grout was kept open in atmosphere for about 12 hours to facilitate the setting. After setting, the surface of the cement grout was leveled carefully by using a spatula. The cement grout surface and shear box was wrapped with scotch tape (see Fig. 4.4) to ensure self-curing of cement grout (to simulate the field condition) for a period of 5 days. After completing the curing period, the wrapping scotch tape was removed and the shear box was turned over again (soil at top and cement grout at bottom) and set on the shear box base kept inside the pressure chamber. It should be noted that soil-cement grout specimen was prepared inside the shear box instead of using any mould, and shear box was placed directly over the shear box base to conduct the direct shear test. This would cause no disturbance of soil-cement interface before testing.

4.4.2.2 Pressure grouted soil-cement specimen

The CDG soil was compacted over the wooden block in two layers having a thickness of 10 mm each following the same procedure mentioned in previous section. After completing the compaction, the weight of compacted soil was recorded and the top part of the shear box was covered by a steel plate and a wooden block. The gaps between

wooden block and side walls of shear box were filled properly with a sealer so that no air can flow through the gaps during pressure grouting. After that the shear box with the compacted soil was turned over (top part down and bottom part up) and placed inside the pressure chamber.

The cement grout was prepared in the same way as for gravity grouted soil-cement specimen. After the preparation of cement grout, the first wooden block was removed to pour cement grout on the prepared surface of soil. The cement grout was poured smoothly over the prepared surface so that the bottom part of shear box could be filled fully with no air voids. Immediately after filling the bottom part of shear box with cement grout, the pressure chamber was closed with the chamber cap and the preset air pressure (grouting pressure) was applied inside the chamber. The air pressure inside the chamber was contained for about half an hour (similar to Yin and Zhou 2009) until the initial setting of the cement grout had almost finished. After that the air pressure valve was closed and pressure was released from the chamber at a very slow rate (approximately 3 kPa per minute) so that no back pressure could be developed which might affect the interface surface.

After completing the release of air pressure, the shear box was moved out from the chamber and kept open in atmosphere for about 12 hours to facilitate the setting of cement grout. After that the same procedure was followed as that of gravity grouted specimen.

4.5 TEST PROCEDURE

4.5.1 Determination of soil-water retention curve for CDG soil

It should be noted that the same procedure of preparing the soil-soil direct shear specimen mentioned in previous section was applied to prepare the specimen for determining the water retention curve (SWRC) under zero net normal stress. After compaction of the soil, the specimen was set on the ceramic disk, a porous disk was placed over the specimen and ample amount of water was poured on the disk to submerge. The specimen was kept for overnight saturation. After saturation, the excess water from the porous disk was removed, chamber cap was closed, and then the experiment was started. It should be noted that no swelling was detected for the soil after saturation. In the present study, only drying SWRC was measured as hysteresis is not in the scope of the study.

During drying SWRC measurement, the soil suction was decreased in steps by increasing the air pressure inside the chamber. In each step, the suction was maintained until the drainage of water was essentially ceased or less than 1% of degree of saturation per day. Then the drained water volume from the soil specimen was recorded, and air pressure was increased to the next step. At the end of the last step, the valve of air pressure and volume change device were closed, and the specimen was dismantled quickly from the MDSA to take the wet weight of the specimen. After that the specimen was kept in an oven for 24 hrs. to determine the water content of the specimen after the last step. By performing back calculations, the water content after each step was obtained. Finally, the equilibrium suctions and water contents at different steps were plotted in a semi-logarithm graph to determine the drying SWRC for the studied soil.

4.5.2 Direct shear testing program

4.5.2.1 Stress path of direct shear test

Single-staged consolidated drained direct shear tests were performed to investigate the behavior of compacted CDG soil as well as soil-cement grout interface under different matric suctions, net normal stresses and grouting pressures. The test procedure of conducting direct shear test consisted of three steps: saturation, equilibration of matric suction and drained shearing at constant net normal stress and suction. Figure 4.5 shows the stress paths of direct shear testing program. The direct shear specimen was brought to a saturated condition without applying any net normal stress following path *IO*. After saturation, the desired matric suction (equilibration) was attained by simultaneously applying specified net normal stress following path *OA* and matric suction following path *AB*. When the equilibration of suction attained, the specimen was sheared at constant matric suction following path *BC*.

4.5.2.2 Selection of interface zone thickness for direct shear test

No definite criterion has been found in the existing literatures for the selection of interface layer thickness for different soil-structures interface. The interface layer thickness may depend on many factors such as way of forming the interface, water-cement ratio of grout, void ratio (porosity) and water content of soil. Kulhawy and Peterson (1979) pointed out that when the concrete (mortar with aggregate) is poured directly onto compacted soil, a rough interface surface is developed and the shear surface is located in the soil away from the interface. Desai *et al.* (1985) considered that the interface action for many soil-structure interfaces occurs in a thin zone near the interface. In the present study, the interface of cement grout (water-cement ratio 0.42) is formed with a compacted CDG soil which is a granular soil (maximum particle size 2 mm) having a porosity of 36%, water content 14.3% and

degree of saturation 65%. The properties of the as-compacted CDG soil indicate that cement grout may penetrate a significant distance into the soil when poured over the compacted soil surface. Chu (2003) and Zhou (2008) studied interface direct shear tests and soil nail laboratory pullout tests using the same CDG soil and cement grout (water-cement ratio 0.42) and found that failure surface was likely to happen in the surrounding soil but not at the interface. Chu and Yin (2006) performed interface direct shear tests at saturated and submerged conditions with different waviness surfaces of cement grout considering an interface layer thickness of about 2.78 mm from the teeth of the waviness surfaces. Zhou (2008) conducted the pullout laboratory tests of pressure grouted soil nails at saturated condition and pointed out that the thickness of adhered soil on the grout column ranges from 1.9 mm to 7.8 mm for different grouting conditions. Considering all the facts mentioned above, an interface zone thickness of 2 mm was selected for the present interface direct shear testing program. This means that the soil thickness inside the bottom part of shear box is 2 mm as no gap is provided between the top part and bottom part of shear box (see Fig. 4.6). However, due to limitation of required time, further study was not possible to investigate the soil-cement grout interface behaviors by varying the interface layer thickness in order to determine the exact extent of cement penetration into the soil.

4.5.2.3 Saturation of direct shear specimen

After placing the soil-soil direct shear specimen inside the shear box, a porous disk plate was placed over the specimen and ample amount of water was poured on the disk plate. The specimen was allowed to soak for 18 to 24 hr. It should be noted that, the degree of saturation of the compacted CDG soil specimen was examined after soaking, and found that more than 98% saturation was attained by soaking. The height of the specimen before and after soaking was monitored to detect change in the specimen height at the

end of soaking and no detectable change was found. After soaking, the excess water above the disk was removed and the loading cap was mounted.

For soil-cement interface tests, the specimen (soil part at top and cement part at bottom) with the shear box was placed on the shear box base inside the air pressure chamber, a porous disk plate was placed over the soil, ample amount of water was poured on the disk plate, and the chamber cap was closed. The specimen was allowed to saturate by applying 200 kPa air pressure inside the chamber for about 10 to 12 hours. It should be noted that the saturation of soil-cement specimen was accomplished by applying water pressure to ensure the complete saturation of interface zone which might not possible by simply soaking. After saturation, the excess water and the disk were removed, the top steel platen fitted with ceramic disk was mounted and the water chamber was connected with AVC device. The height of the specimen was checked before and after saturation to measure the swelling/contraction. A swelling value of about 1.5 mm was found for different soil-cement specimens after saturation.

4.5.2.4 Equilibration of matric suction

To attain the equilibration of desired matric suction, the pre-calculated axial load, air pressure and water pressure were applied (by opening the valve of AVC) sequentially. The connecting valves of DAF-200M and pressure controller devices were remaining closed during the equilibration process. It was already mentioned that axis-translation technique was used to attain the desired matric suction by applying 200 kPa water pressure in the water chamber and the required air pressure in the pressure chamber. Matric suction value is zero for saturated case and the magnitudes of air pressure and water pressure were equal to 200 kPa. During the equilibration process, vertical deformation and water movement were recorded. Equilibration was assured when the

vertical deformation was constant and flow of water essentially ceased (≤ 1% of degree of saturation per day). Equilibration was assured when the flow of water essentially ceased. The duration of the equilibration stage depended on the target suction and net normal stress applied. It should be noted that the effect of volume change, due to equilibration of matric suction, on shear strength was not considered separately as all the specimens were firstly saturated, and the volume change due to equilibration was approximately equal for different suctions under particular net stresses.

4.5.2.5 Shearing at constant suction and net stress

After suction equilibration attained, single-staged shearing was carried out under a drained condition. Shearing rate is an important factor for testing of unsaturated soils for both triaxial and direct shear tests to equalize the excess pore-water pressure during drained shearing. Gan (1986) conducted direct shear tests on statically and dynamically compacted specimens of clay to sand using displacement rates in the range of 0.1-0.6 mm/h and pointed out that the shearing rate should be selected in such way that the shear strength should remain constant when sheared at rates below the selected displacement rate. Gan and Fredlund (1994) performed modified direct shear tests on a completely decomposed granite (CDG) soil of Hong Kong with a shearing rate of 0.005 mm/min. Han (1997) investigated the shearing rate for the compacted residual soil and found that the shearing rate of 0.004 mm/min satisfied the criterion addressed by Gan (1986). Melinda *et al.* (2004) followed the same shearing criterion for a residual soil in their study. Considering the above mentioned discussion, in the present study the specimen was sheared with a constant shearing rate of 0.004 mm/min for both soil-soil direct shear tests and soil-cement interface tests until the horizontal displacement reached to 15 mm. The suction in the specimen was maintained constant throughout the shearing. During shearing, the horizontal shear load, horizontal displacement and

vertical displacement were measured and recorded automatically in a computer at an interval of two minutes. Shearing was accomplished during a period of approximately 2.5 days. After the completion of shearing, all the valves were closed, the air pressure was released and the specimen was quickly dismantled from the shear box for the determination of wet weight of soil.

4.6 SUMMARY

The properties of CDG soil and cement grout are presented in this chapter. The testing apparatus was made ready before starting the test program by saturating the ceramic disk and inspecting the leakage through the ceramic disk and pressure chamber. The procedure of specimen preparation for soil-soil direct shear test and soil-cement interface test and interface direct shear tests are elaborately discussed in this chapter. Finally, the adopted stress path for direct shear testing program, and the steps of test procedure for the present study are illustrated. The next chapter will present the direct shear test results of unsaturated soil and their interpretations.

Table 4.1 Basic properties of completely decomposed granite (CDG) soil

Soil Property	Unit	Value
Specific gravity (G_s)	-	2.60
Maximum dry density ($\rho_{d(\max)}$)	Mg/m^3	1.75
Optimum moisture content (w_{opt})	%	14.3
Gravel	%	5.8
Sand	%	44.1
Silt	%	36.8
Clay	%	13.3
Plastic limit (w_p)	%	22.7
Liquid limit (w_L)	%	32.8
Plasticity index (I_P)	%	10.1
Permeability (k_{20})	m/s	2.36×10^{-8}

Table 4.2 Properties of the cement grout (after Su 2006)

Property	Unit	Value
Density (ρ_d)	Mg/m^3	1.89
Uniaxial compressive strength (σ_c)	MPa	32.1
Secant Young's modulus (E_{50})	GPa	12.6
Poisson's ratio (υ)	-	0.21

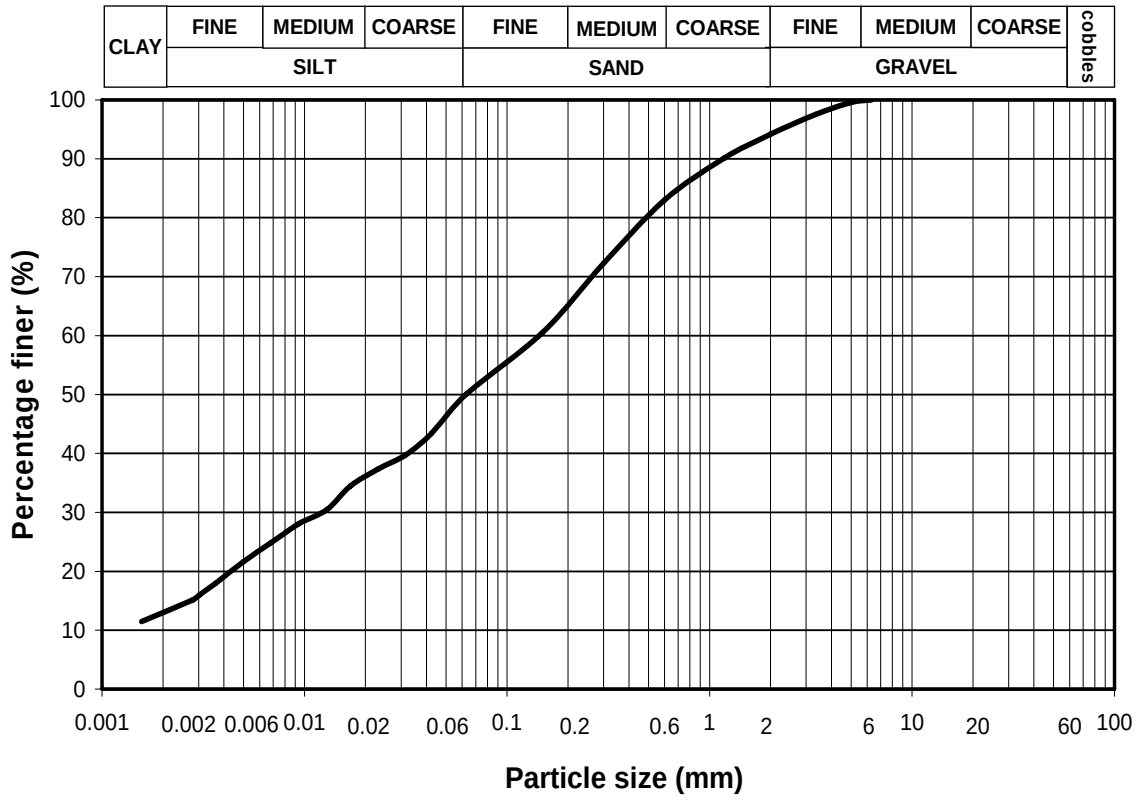

Figure 4.1 Particle size distribution of completely decomposed granite

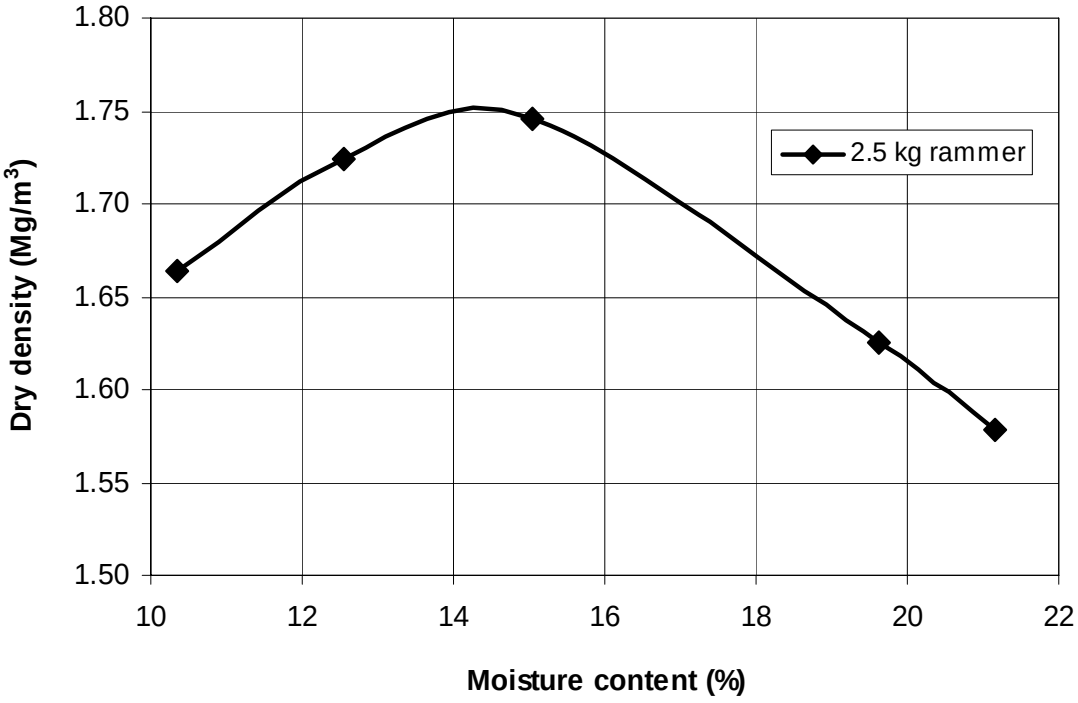

Figure 4.2 Variation of dry density with moisture content for CDG soil

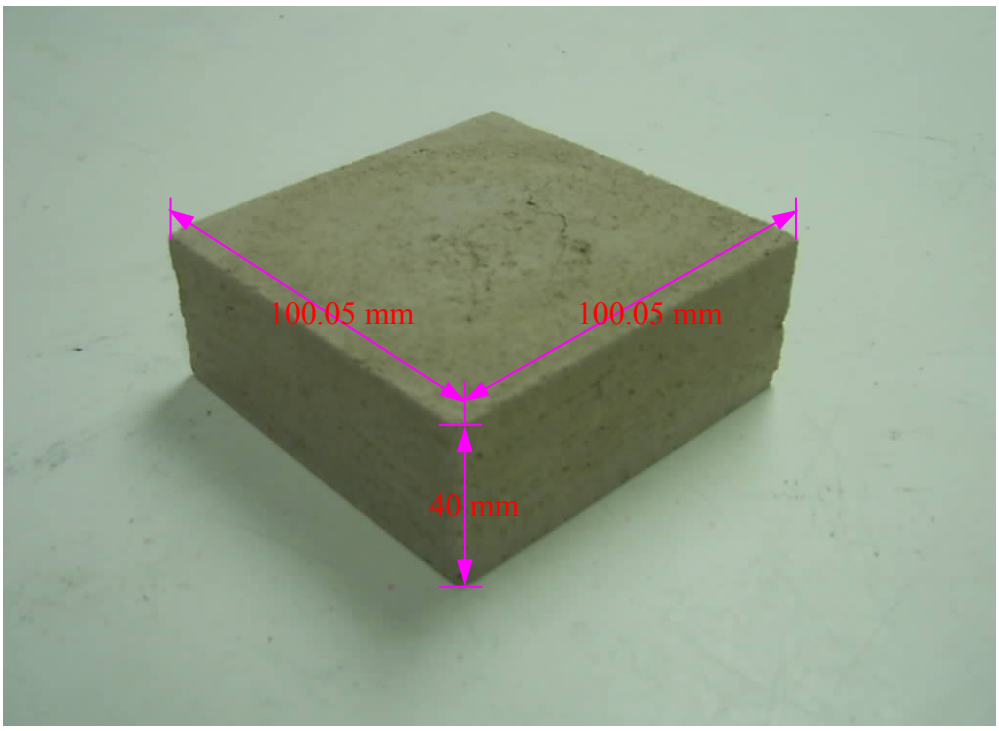

Figure 4.3 Photograph of a CDG soil specimen for direct shear test

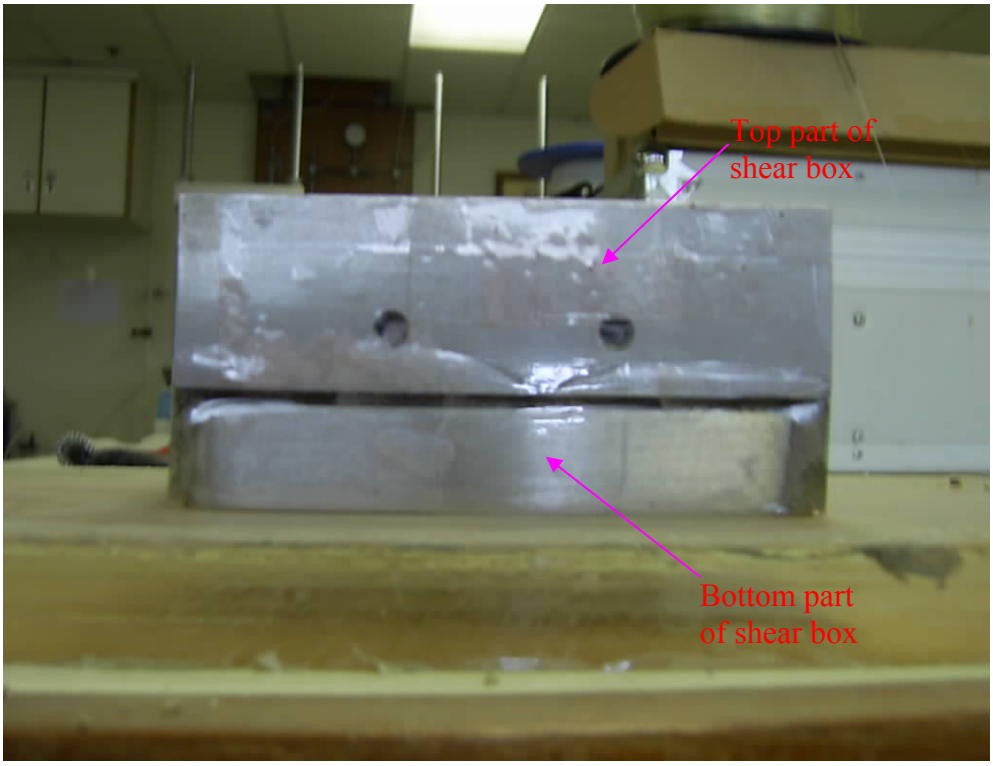

Figure 4.4 Direct shear box wrapped with scotch tape for interface specimen

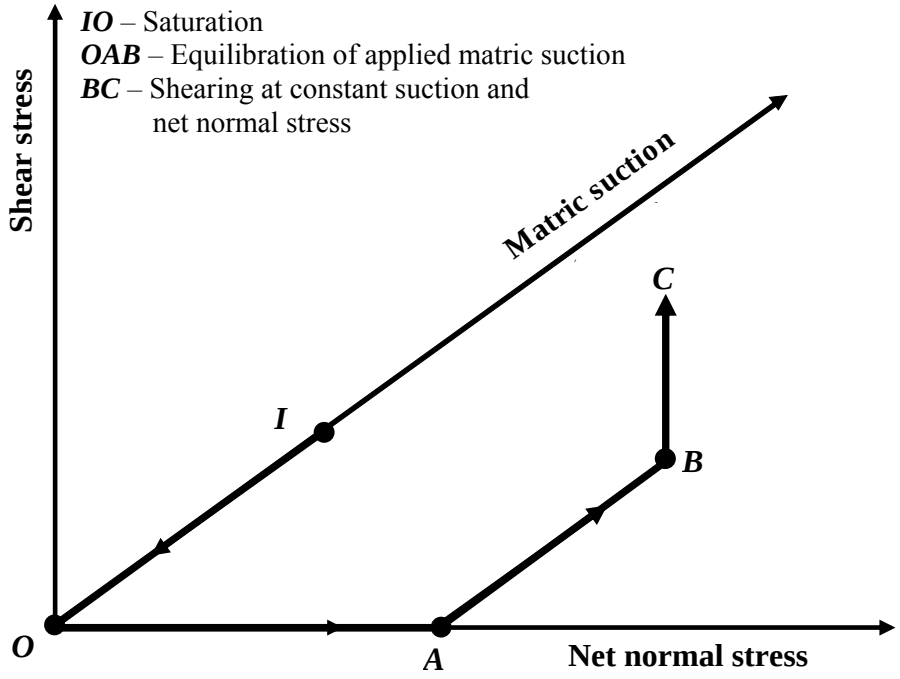

Figure 4.5 Stress paths of direct shear testing program

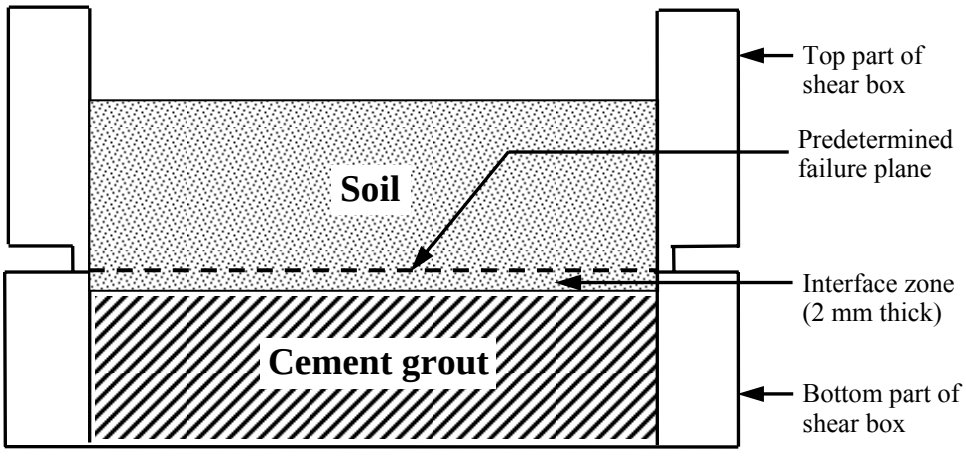

Figure 4.6 Selected interface layer thickness for direct shear tests

Chapter 5

UNSATURATED SOIL TEST

RESULTS AND INTERPRETATIONS

5.1 INTRODUCTION

A series of single-staged consolidated drained direct shear tests were conducted on compacted completely decomposed granite (CDG) soil under different matric suctions and net normal stresses. Matric suction was controlled by applying air pressure in the pressure chamber and water pressure at the bottom of the high air-entry ceramic disk. A soil-water retention curve (SWRC) was obtained for the CDG soil from the equilibrium water content corresponding to each applied matric suction value for zero net normal stress by using the modified direct shear apparatus. The experimental study concentrates on estimating the shear strength of unsaturated compacted CDG soil. The effect of dilation angle on apparent internal friction angle and consequently on shear strength are investigated and considered to estimate the shear strength of unsaturated compacted CDG soil. A modified shear strength model for unsaturated soil is proposed and considered to establish the effect of dilation angle on apparent internal friction angle as well as shear strength by using analytical values of dilation angles obtained from dilatancy curves. The experimental shear strength data are also compared with the analytical results obtained from the proposed modified model.

A total of 20 direct shear tests are performed under different suction values of 0, 50, 100, 200, and 300 kPa with net normal stresses of 50, 100, 200, and 300 kPa. The effect of suction and net normal stress on the behavior of compacted CDG soil are observed and presented in the following sections.

5.2 SOIL-WATER RETENTION CURVE FOR CDG SOIL

The data points of the soil-water retention curve (SWRC) for the compacted specimen obtained from the equilibrium water content corresponding to each applied matric suction value for zero net normal stress by using the modified direct shear apparatus are presented in Fig. 5.1. The water content decreases as the suction value increases and the rate of decrement is higher in the suction range of 0 to 100 kPa than the remaining suction range. Figure 5.2 shows the best-fit to experimental data by using eq. [2.5], described in chapter 2, for zero net normal stress. The values of three fitting parameters a, n and m in eq. [2.5] of soil-water retention curve are determined by using nonlinear regression and summarized in Table 5.1. It is found from SWRC that the air entry value of the re-compacted CDG soil is about 11 kPa.

5.3 INFLUENCE OF NET NORMAL STRESS ON SWRC

There are two approaches used for determining shear strengths using SWRC. One approach uses one SWRC obtained at zero net normal stress to predict shear strengths at different net normal stresses. This approach is commonly used because of its simplicity. The other approach uses all SWRCs performed at different net normal stresses so that the effect of net normal stress on matric suction can be considered in predicting shear strengths. Vanapalli *et al.* (1996) pointed out that in low plasticity soils, net normal stress has limited influence on suction pressure if ϕ' is not influenced significantly.

However, Lee et al. (2005) studied the effect of stress state on the SWRC of weathered granite, and found that net normal stress has significant influence on SWRC. In present study, the equilibrium water content (total water content including diffused air) of specimen under different net normal stresses are obtained for different matric suctions before starting shearing, and plotted together with the SWRC obtained under zero net normal stress in Fig. 5.3. It is obvious from Fig. 5.3 that all the data points under different net normal stresses are nearly same as that of SWRC obtained under zero net normal stress. This indicates that for this particular CDG soil net normal stress has limited influence on SWRC, and SWRC obtained for zero net normal stress can be used for predicting unsaturated shear strengths of the studied CDG soil.

5.4 DIRECT SHEAR TEST RESULTS AND INTERPRETATIONS

5.4.1 Influence of net normal stress on stress-strain-strength behavior

Figures 5.4, 5.5, 5.6, 5.7 and 5.8 show the relationships between (a) shear stress and horizontal displacement, and (b) vertical displacement and horizontal displacement under different net normal stresses of 50, 100, 200 and 300 kPa for the same matric suction of 0, 50, 100, 200 and 300 kPa respectively. The behavior of the CDG soil from these figures is discussed in the followings with attention on the influences of net normal stress:

(a) For zero suction, all curves of the shear stress and horizontal displacement show gradually hardening behavior and all vertical displacements increase with horizontal displacement indicating shear-compression. The higher the net stress, the more the shear compression.

(b) For suction 50 kPa, all curves of the shear stress and horizontal displacement still show gradually hardening behavior. But the two curves of vertical displacement and horizontal displacement for net stresses 50 and 100 kPa show shear-dilation (vertical displacement negative), the two curves for net stresses 200 and 300 kPa show shear-compression. The higher the net stress, the more the shear compression.

(c) For suction 100 kPa, all curves of the shear stress and horizontal displacement still show gradually hardening behavior. The two curves of vertical displacement and horizontal displacement for net stresses 50 and 100 kPa show shear-dilation (vertical displacement negative) from the start to the end; while the two curves for net stresses 200 and 300 kPa show shear-compression in the initial period and a little shear dilation in the ending period.

(d) For suctions 200 and 300 kPa, the two curves of the shear stress and horizontal displacement for net stresses 50 and 100 kPa show clear peak shear stresses, indicating a strain (or displacement) softening behavior. The corresponding two curves of vertical displacement and horizontal displacement show strong shear-dilation (vertical displacement negative). The two curves of the shear stress and horizontal displacement for net stresses 200 and 300 kPa show no peak (or no clear peak) shear stresses, indicating mostly a strain hardening behavior. The corresponding two curves of vertical displacement and horizontal displacement show a little shear-compression at beginning, followed by large shear-dilation.

5.4.2 Influence of suction on stress-strain-strength behavior

The same data presented in Figs. 5.4, 5.5, 5.6, 5.7 and 5.8 are plotted in Figs. 5.9, 5.10, 5.11 and 5.12 in order to study the influences of the suction on the shear and volumetric behavior of the same soil. Figures 5.9, 5.10, 5.11 and 5.12 show the relationships between (a) shear stress and horizontal displacement, and (b) vertical displacement

and horizontal displacement under different suction of 0, 50, 100, 200 and 300 kPa for the same net normal stress of 50, 100, 200 and 300 kPa respectively. The behavior of the CDG soil from these figures is discussed in the followings with attention on the influences of suction:

(a) For the net stresses of 50 and 100 kPa as shown in Figs. 5.9 and 5.10, with the increase of suction, curves of the shear stress and horizontal displacement change from gradually hardening behavior (showing no peak shear stress) to hardening-softening (showing a peak shear stress) behavior. The corresponding curves of vertical displacement and horizontal displacement show shear-compression for zero suction and shear-dilation for higher suction. The higher the suction, the more significant strain-softening, the more shear dilation.

(b) For the net stresses of 200 kPa and 300 kPa as shown in Figs. 5.11 and 5.12, with the increase of suction, curves of the shear stress and horizontal displacement change from gradually hardening behavior (showing no peak shear stress) to a little hardening-softening (showing a small peak shear stress) behavior. The corresponding curves of vertical displacement and horizontal displacement show shear-compression for suction of zero and 50 kPa, and then shear-dilation for higher suction (100, 200 and 300 kPa). The higher the suction, the more the shear dilation.

5.4.3 Influence of suction on friction angle and cohesion

Using the experimental test data, the failure envelopes of the shear stress τ_f at failure versus the net normal stress $(\sigma_{nf} - u_{af})$ are shown in Fig. 5.13 for different matric suctions $(u_a - u_w)_f$. It should be noted that area correction for direct shear tests is applied to calculate the shear stress. For this reason, the stress-displacement curves

seem to increase even after failure. The failure criterion is considered as the point at which the shear load starts decreasing (peak shear load) or starts to remain fairly constant observed from the raw test data. Figure 5.13 indicates that the shear strength increases with the net normal stress and matric suction. The shear strength envelopes of the shear stress τ_f versus the net normal stress $(\sigma_{nf} - u_{af})$ for a given suction are approximately linear. The declivity of those envelopes is represented by $\phi_{\max}$ which is the combination of ϕ' at saturated condition and dilation angle ψ at different suction i.e., $\phi_{\max} = (\phi' + \psi)$. $\phi_{\max}$ increases with matric suction under different net normal stresses. At saturated condition, $\phi_{\max} = \phi'$ and $\psi = 0$ as no dilation is observed for different net normal stresses. Table 5.2 presents the values of apparent friction angle $\phi_{\max}$ and cohesion intercept c for different suction values. The cohesion intercept can be defined by the following equation:

$$c = c' + (u_a - u_w)_f \tan \phi^b \qquad 5.1$$

where c' is the cohesion at saturated condition; $(u_a - u_w)_f$ is the matric suction at failure; and ϕ^b is the angle indicating the rate of increase in shear strength relative to matric suction $(u_a - u_w)_f$. The cohesion intercept indicates an increase in strength as matric suction increases. The effective angle of internal friction, ϕ' = 29.9° and effective cohesion, c' = 0 kPa are obtained for the compacted CDG soil from Fig. 5.13 at suction 0 kPa (saturated condition). It should be noted that the effect of suction induced volume change on shear strength was not considered separately as all the specimens were firstly saturated, and the volume change due to equilibration was approximately equal for different suctions under particular net stresses. Table 5.3 presents the values of suction induced volume change (contraction) during equilibration of suction under different net stresses.

5.4.4 Suction envelope for CDG soil

The variation of shear strength τ_f with different matric suction $(u_a - u_w)_f$ (suction envelope) for different net stresses $(\sigma_{nf} - u_{af})$ is shown in Fig. 5.14. The shear strength increases with matric suction and net normal stress. However, the relationships between shear stress τ_f at failure and matric suction $(u_a - u_w)_f$ are obviously nonlinear, indicating that the ϕ^b parameter in eq. [2.7] defined by Fredlund *et al*. (1978), is not constant. This agrees with the observation made by other researchers who studied the behavior of different types of unsaturated soils (Escario and Saez 1986; Gan 1986; Fredlund *et al*. 1987; Gan and Fredlund 1992; Campos and Carrillo 1995; Melinda *et al*. 2004; Lee *et al*. 2005; Ying *et al*. 2006; Zhan and Ng 2006). Table 5.4 summarized the values of ϕ^b angle for different matric suctions. Figure 5.15 indicates that the ϕ^b angle varies nonlinearly, and decreases with matric suction.

5.4.5 Influence of suction and net stress on soil dilatancy

Figures 5.16, 5.17, 5.18 and 5.19 describe the effect of suction on soil dilatancy $(\delta y / \delta h)$ under different net normal stresses. The dilatancy essentially increases with an increase of suction. Figure 5.20 shows the variation of the maximum dilatancy with matric suction under different net normal stresses. The peak dilatancy is observed at lower net normal stress (50 kPa) under higher suctions. The soil dilation under different net normal stresses is found to have significant influences on the shear strength of unsaturated CDG soils. The dilation angle increases with matric suction and peak dilation angle is observed under lower net normal stress (50 kPa) with higher suction (100 to 300 kPa). This can be explained by the fact that when the soil starts to desaturate from saturated condition, the effective contact area between the soil and water starts decreasing as the water content decreases. When the water content continues decreasing

due to increase in suction and the soil is sheared under lower net normal stress, the soil particles can not move around each other but move up or over each other which cause dilation of the soil and this dilation rate depends on the rate of decreasing water content. From Fig. 5.1, it is obvious that the rate of decreasing the degree of saturation is greater in the suction range of 0 to 100 kPa than the remaining suction range. Thus the rate of decreasing the effective contact area between soil particles and water is greater in lower suction range than higher suction range which causes higher dilation in lower suction values. This means that matric suction has significant influence on dilation of the unsaturated compacted CDG soil.

The dilation angle ψ under different net normal stresses and suctions are calculated from dilatancy curves shown in Figs. 5.16, 5.17, 5.18 and 5.19 by using the following equation:

$$\tan\psi = -\frac{\delta y}{\delta h} \qquad 5.2$$

where δy is the increment in vertical displacement (expansion '-' and contraction '+'); and δh is the increment in horizontal displacement. The average dilation angle is obtained by taking the algebraic mean of all dilation angles under different net normal stresses for particular matric suction. Table 5.5 summarizes the analytical values of dilation angles and apparent friction angles for different suctions.

5.5 PROPOSED MODIFIED MODEL FOR UNSATURATED SOILS

Vanapalli *et al.* (1996) proposed a practical model for predicting the shear strength of unsaturated soils using the SWRC and the saturated shear strength parameters without

obtaining ϕ^b values from laboratory tests. It is understandable from the discussion presented in previous section that soil dilation has significant influence on the apparent friction angle and hence, on the shear strength. That is why, it is essential to incorporate soil dilation in the model predicting shear strength of unsaturated soils. A modified version of Vanapalli's model is proposed to consider the effect of suction on soil dilatancy and hence on the shear strength of unsaturated soil. The proposed model is as follows:

$$\tau = c' + (\sigma_n - u_a)\tan(\phi' + \psi) + (u_a - u_w)(\Theta^{\kappa})\tan(\phi' + \psi) \qquad 5.3$$

where ψ is the dilation angle; and $(\phi' + \psi)$ is the apparent friction angle $(= \phi_{\max})$. To obtain the value of fitting parameter κ for the studied CDG soil, a better correlation between predictions and experimental shear strength data is essential. Figure 5.21 shows the correlation between experimental shear strength data and the shear strength value from the model proposed by Vanapalli *et al.* (1996) by using the SWRC for zero net normal stress, apparent friction angles $\phi_{\max}$ obtained from failure envelopes for different suctions, and effective cohesion at saturated condition. After correlating the prediction of Vanapalli's model with the experimental data, the value of parameter κ for the studied compacted CDG soil is determined as 2.2.

5.6 VERIFICATION OF PROPOSED MODIFIED MODEL

Figure 5.22 shows the comparison between experimental shear strength data and the analytical shear strength results obtained from the modified model (eq. [5.3]) using SWRC, effective shear strength parameters (c' and ϕ') of compacted CDG soil and analytical values of soil dilation angle (refer to Table 5.4) . Figure 5.22 indicates that the experimental shear strength data are little bit higher than the analytical shear strength

results under higher net normal stresses (200 and 300 kPa) at higher suction range (100 to 300 kPa). This may be due to:

(i) increase of soil skeleton stiffness under higher matric suction. When the suction value is increased from saturated state, the proportion of bulk water starts to decrease and the proportion of meniscus water starts to increase which causes the increase of soil skeleton stiffness resulting in greater resistance during shearing, and consequently the shear strength is increased.

(ii) existence of some frictional resistance between soil and sidewalls of large shear box which may retard the actual dilation of soil resulting in lower dilation angles, and consequently lower analytical shear strength results.

5.7 SUMMARY

To study the influence of both matric suction and net normal stress on the behavior of compacted CDG soil, a series of direct shear tests have been conducted under consolidated drained condition. A total of 20 tests were performed under different suctions and net normal stresses. In this chapter, typical test results and their interpretations have been presented and discussed. A soil-water retention curve (SWRC) has been obtained from the equilibrium water content corresponding to different suctions for zero net normal stress. The influence of net normal stress on the SWRC is examined, and found that for this particular CDG soil, net normal stress has limited influence on SWRC. The initial presentation of the results in this chapter illustrates the variations of hardening-softening and contractive-dilative behavior under different suction and net normal stresses. The failure envelopes under different suctions are found to be linear. However, a nonlinearity is obvious for suction envelopes under different net normal stresses. An especial attention has been paid on the influence of suction on soil dilatancy. The soil dilation increases with matric suction. A modified model has

been proposed to consider the influence of soil dilation on apparent friction angle and hence, on the shear strength of unsaturated soils. The prediction of the proposed model is compared with the experimental results. It is found that soil stiffness increases with matric suction and consequently offers greater resistance during shearing.

This chapter presents the direct shear test results of compacted CDG soil under different matric suctions and net stresses, their interpretations and discussions with an especial attention on soil-dilatancy, and a modified model for shear strength of unsaturated soil. The next chapter will state the direct shear test results of unsaturated soil-cement interface for zero grouting pressure, and their interpretations with discussions.

Table 5.1 Input parameters of SWRC to predict the shear strength of compacted CDG soil

Preload stress (kPa)	a	n	m	κ	$(u_a - u_w)_r$ (kPa)
0	15.63	1.71	0.29	2.2	3000

Table 5.2 Variation of apparent friction angle $\phi_{\max}$ and cohesion intercept c with matric suction for compacted CDG soil

Matric suction (kPa)	0	50	100	200	300
$\phi_{\max} = (\phi' + \psi)$ (deg)	29.9	33.1	37.1	37.6	38.7
c (kPa)	0.0	20.6	36.2	68.2	93.5

Table 5.3 Values of suction induced volume change (in mm) during equilibration of suction under different net normal stresses for compacted CDG soil

Matric suction (kPa)	0	50	100	200	300
Net normal stress (kPa)					
50	1.10	1.05	0.97	1.08	1.12
100	1.52	1.52	1.51	1.54	1.52
200	1.97	1.91	1.97	2.11	2.12
300	2.30	2.27	2.29	2.45	2.33

Table 5.4 Variation of ϕ^b angle with matric suction for compacted CDG soil

Matric suction (kPa)	0	50	100	200	300
ϕ^b (deg)	29.9	22.4	19.9	18.8	17.3

Table 5.5 Analytical values of dilation angle and apparent friction angle for different matric suctions obtained from dilatancy curves

Matric suction (kPa)	Net normal stress (kPa)	Dilation angle (^{0})	Average dilation angle ψ (^{0})	Effective cohesion c' (kPa)	Effective internal friction angle ϕ' (^{0})	Apparent friction angle $\phi_{max} = (\phi' + \psi)$ (^{0})
0	50	0.0	0.0	0.0	29.9	29.9
	100	0.0				
	200	0.0				
	300	0.0				
50	50	7.5	2.4	0.0	29.9	32.3
	100	1.9				
	200	0.0				
	300	0.0				
100	50	9.5	3.5	0.0	29.9	33.4
	100	4.4				
	200	0.2				
	300	0.0				
200	50	9.2	5.3	0.0	29.9	35.2
	100	7.7				
	200	3.6				
	300	0.8				
300	50	8.6	6.3	0.0	29.9	36.2
	100	8.9				
	200	5.4				
	300	2.4				

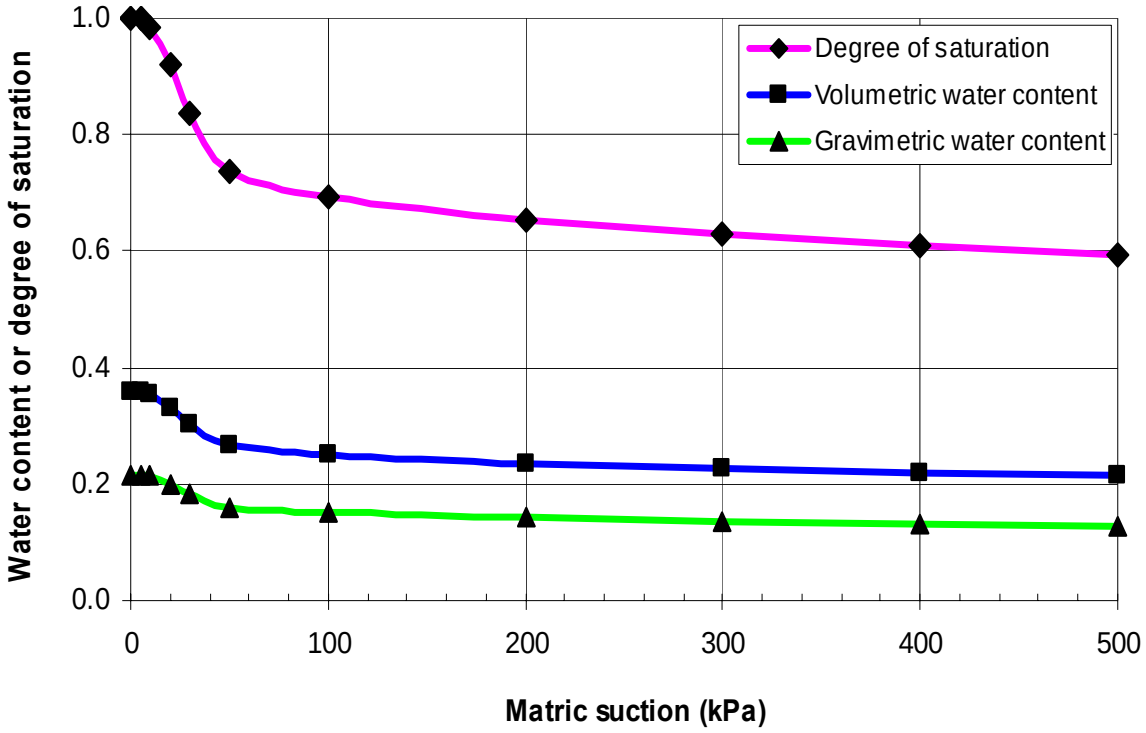

Figure 5.1 Variation of water content with matric suction (SWRC)

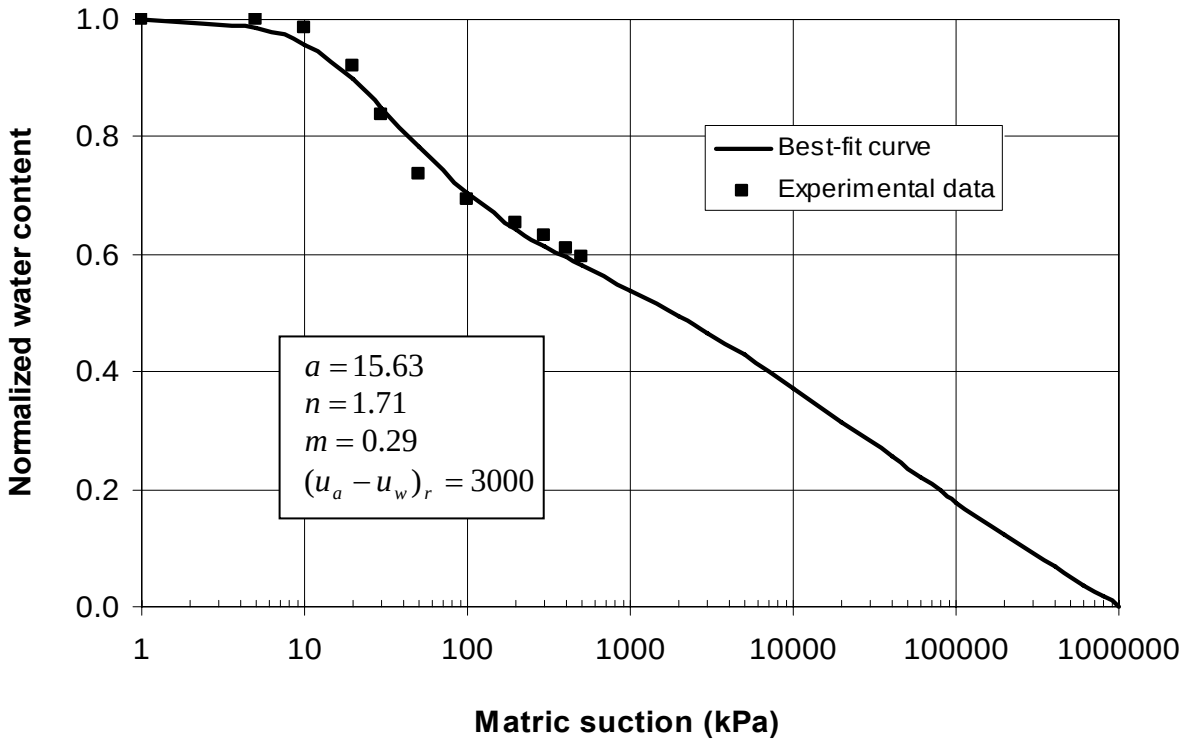

Figure 5.2 Soil-water retention curve for 0 kPa net normal stress

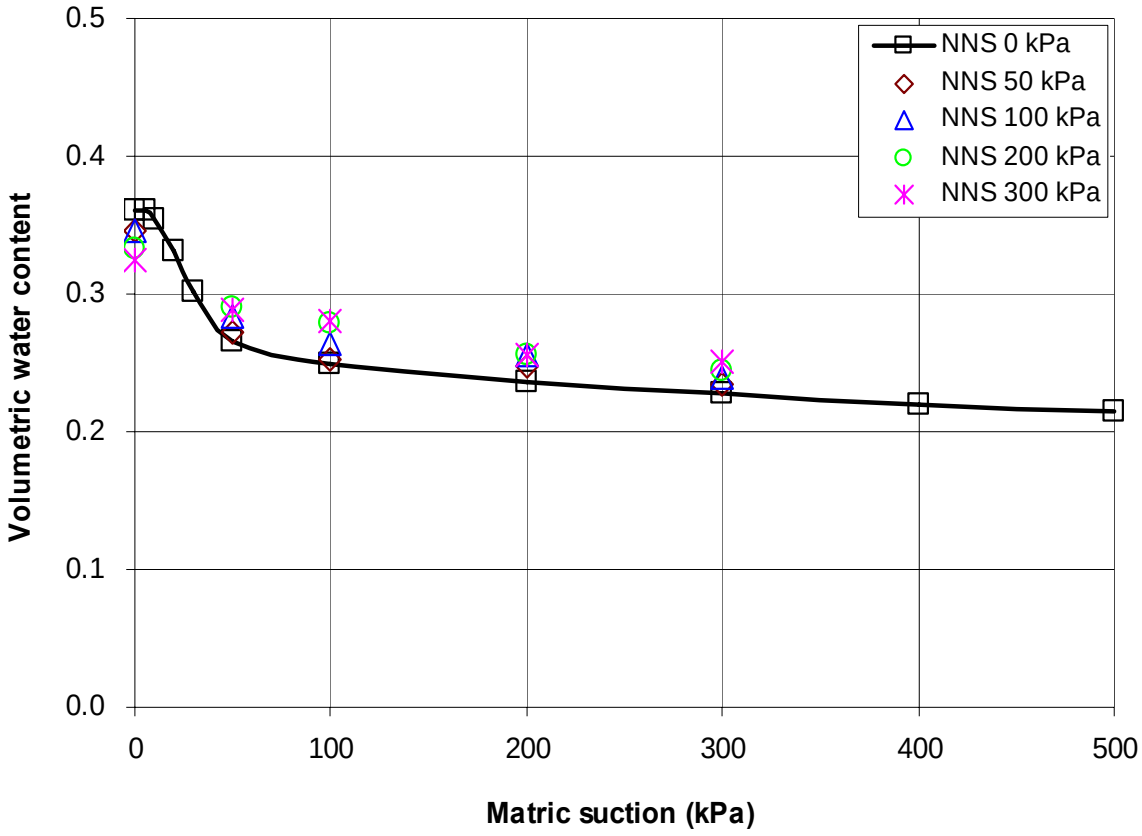

Figure 5.3 Variation of volumetric water content with matric suction for different net normal stresses

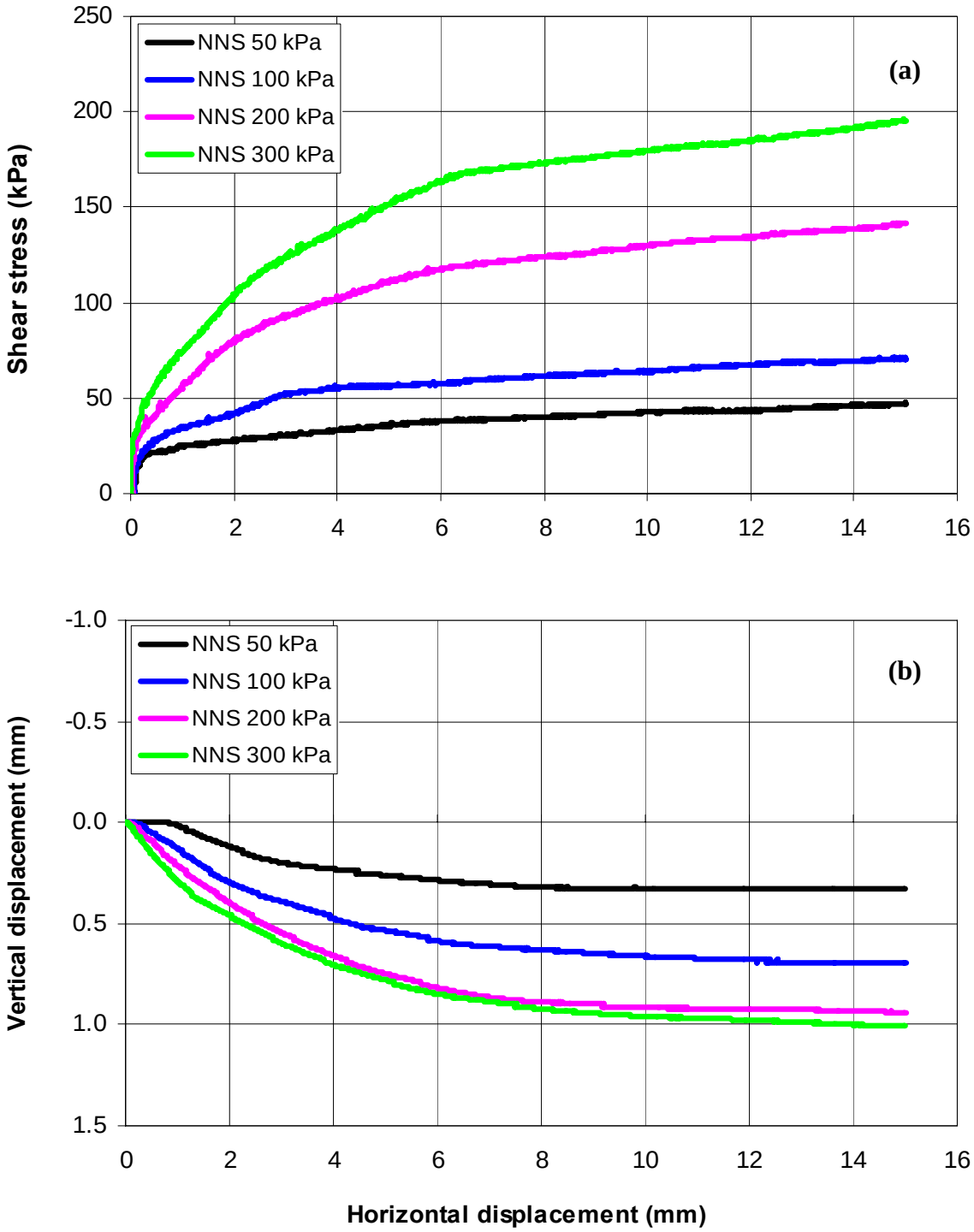

Figure 5.4 Curves of (a) shear stress versus horizontal displacement; and (b) vertical displacement versus horizontal displacement for different net normal stresses under 0 kPa matric suction (saturated condition)

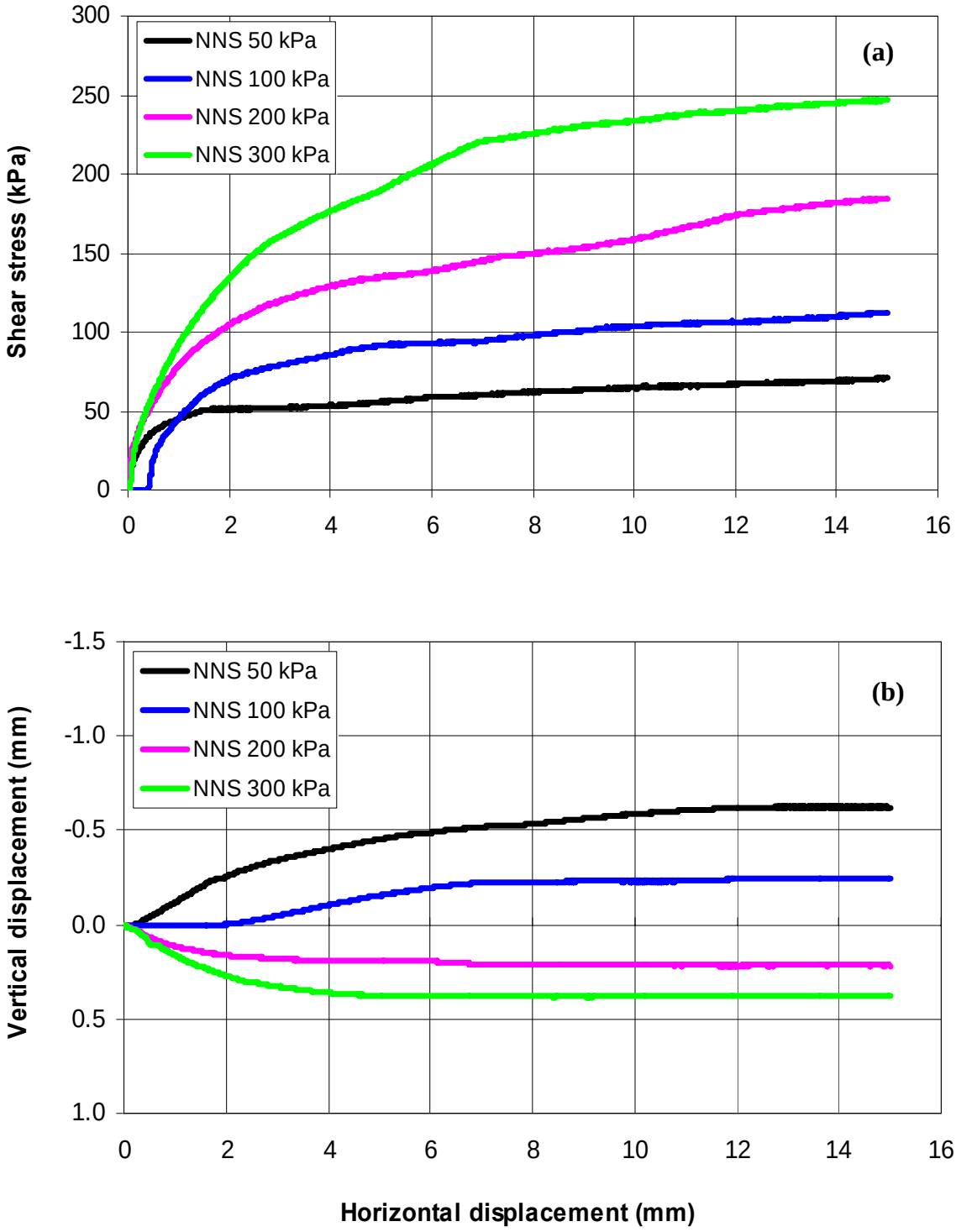

Figure 5.5 Curves of (a) shear stress versus horizontal displacement; and (b) vertical displacement versus horizontal displacement for different net normal stresses under 50 kPa matric suction

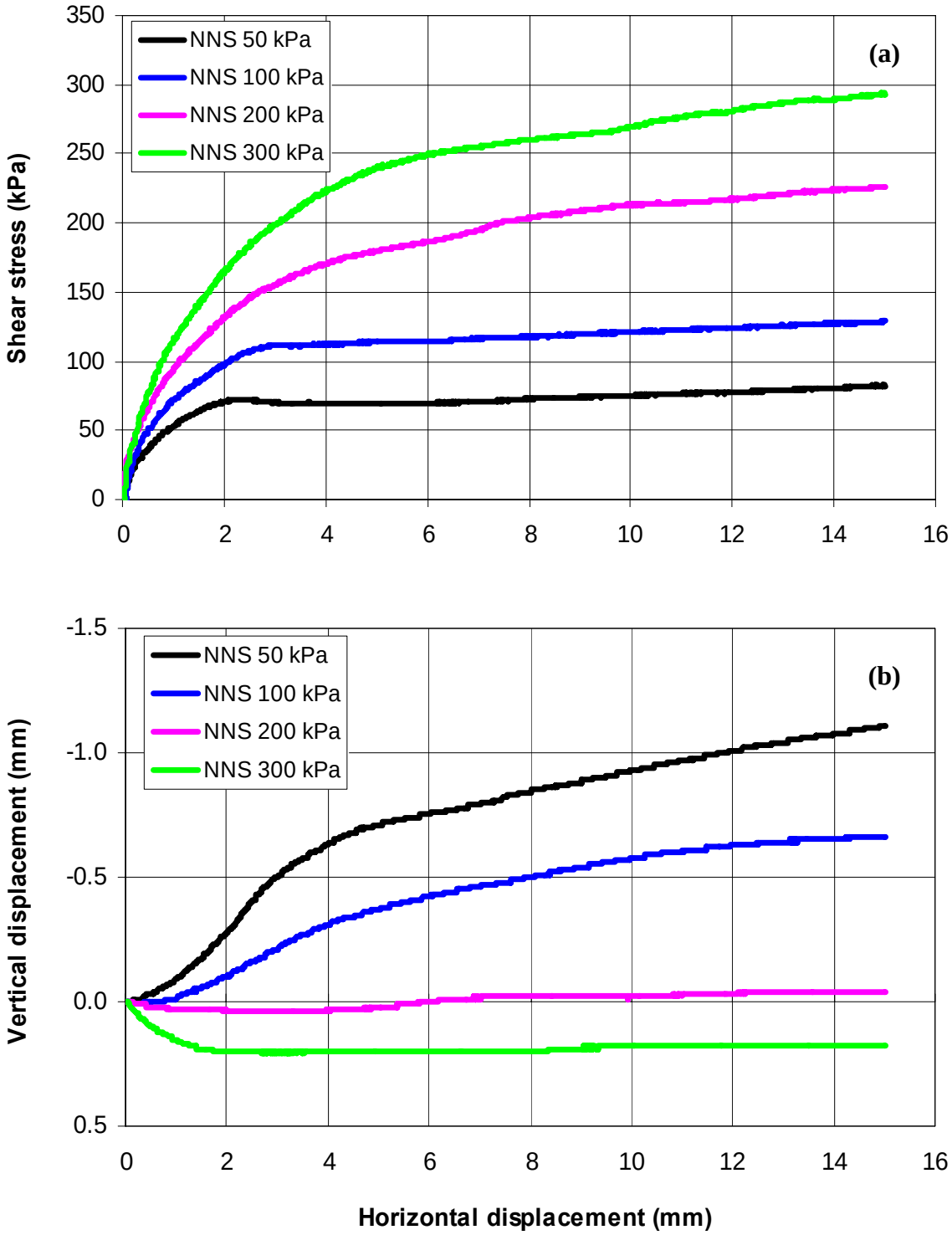

Figure 5.6 Curves of (a) shear stress versus horizontal displacement; and (b) vertical displacement versus horizontal displacement for different net normal stresses under 100 kPa matric suction

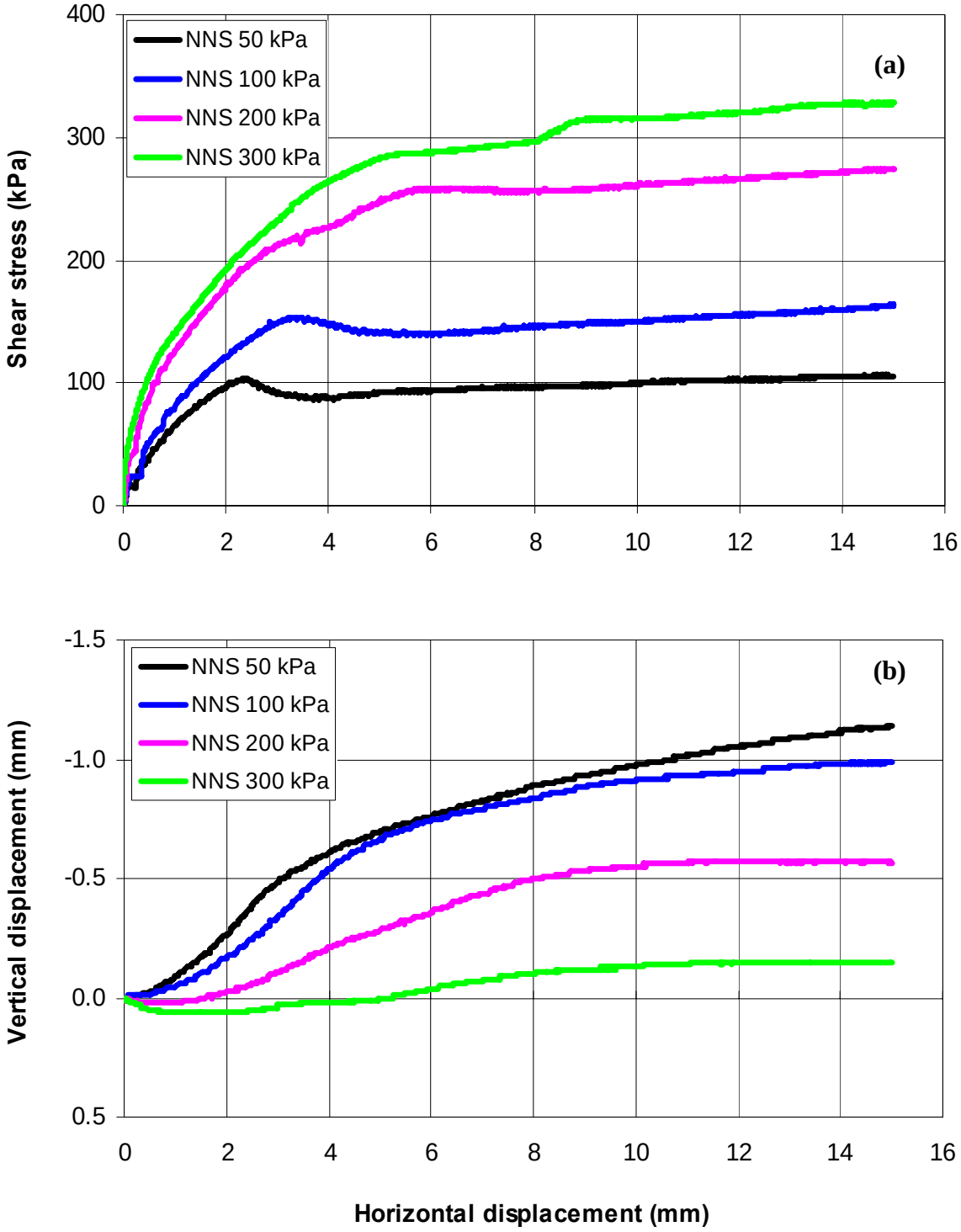

Figure 5.7 Curves of (a) shear stress versus horizontal displacement; and (b) vertical displacement versus horizontal displacement for different net normal stresses under 200 kPa matric suction

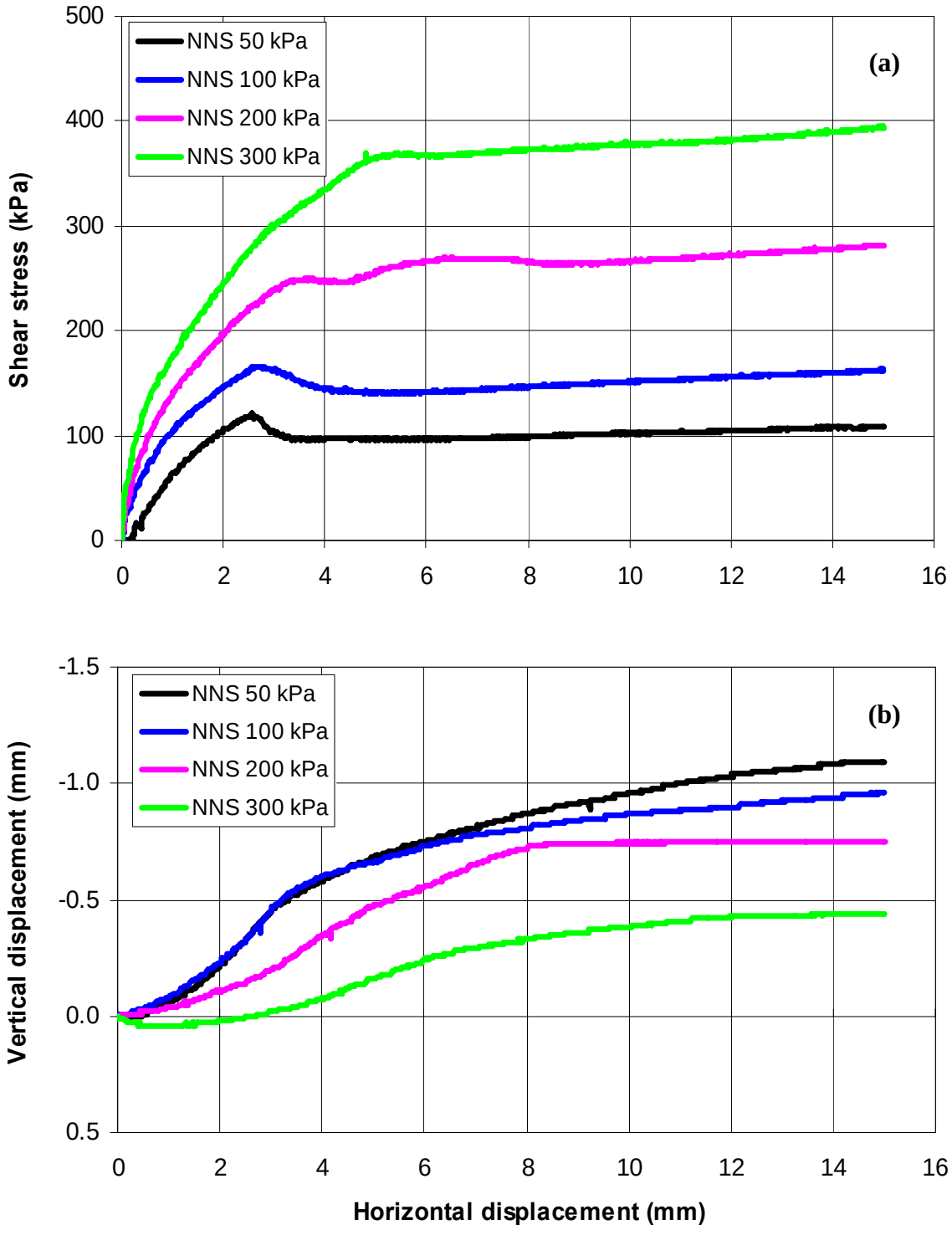

Figure 5.8 Curves of (a) shear stress versus horizontal displacement; and (b) vertical displacement versus horizontal displacement for different net normal stresses under 300 kPa matric suction

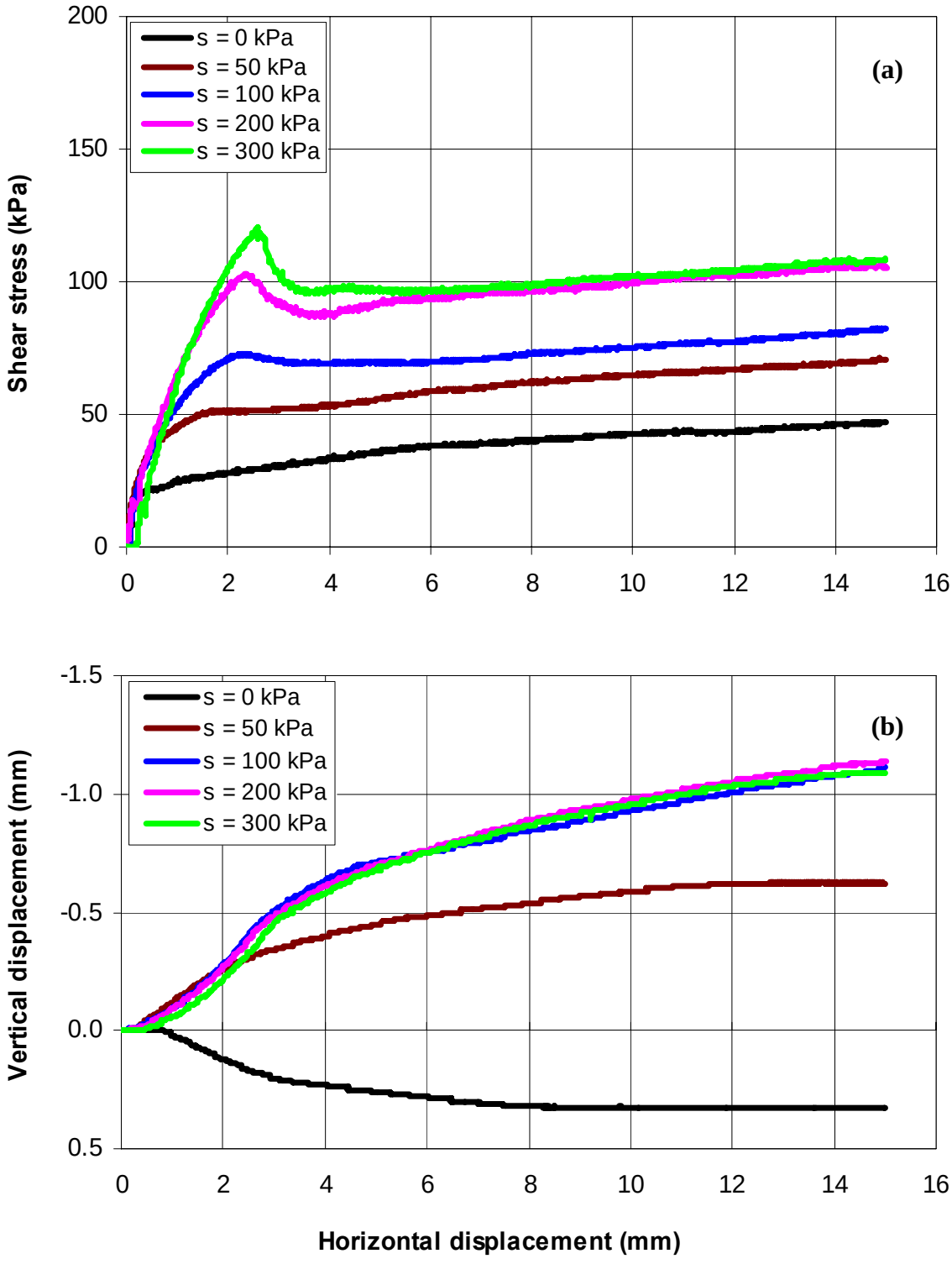

Figure 5.9 Curves of (a) shear stress versus horizontal displacement; and (b) vertical displacement versus horizontal displacement for different suctions under 50 kPa net normal stress

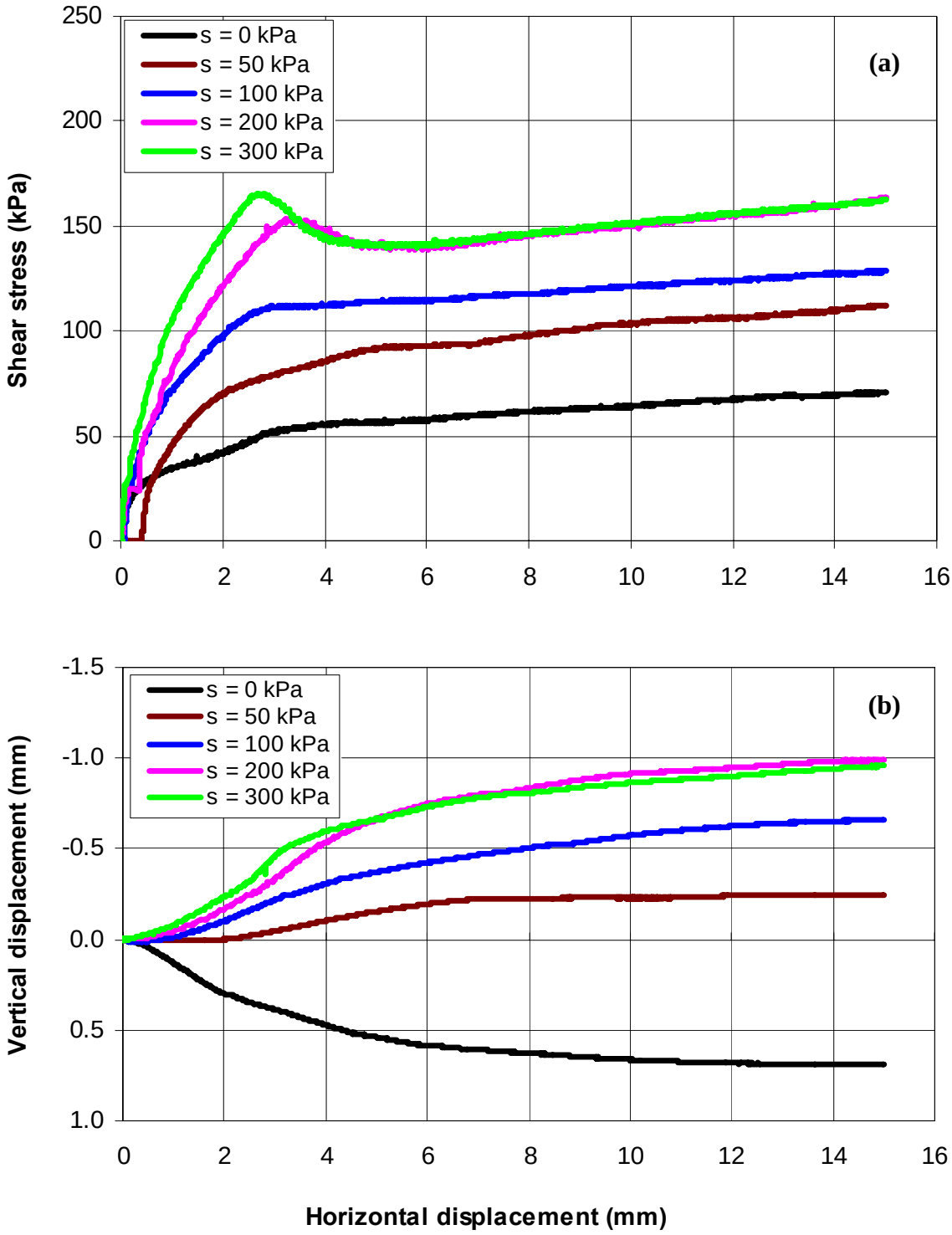

Figure 5.10 Curves of (a) shear stress versus horizontal displacement; and (b) vertical displacement versus horizontal displacement for different suctions under 100 kPa net normal stress

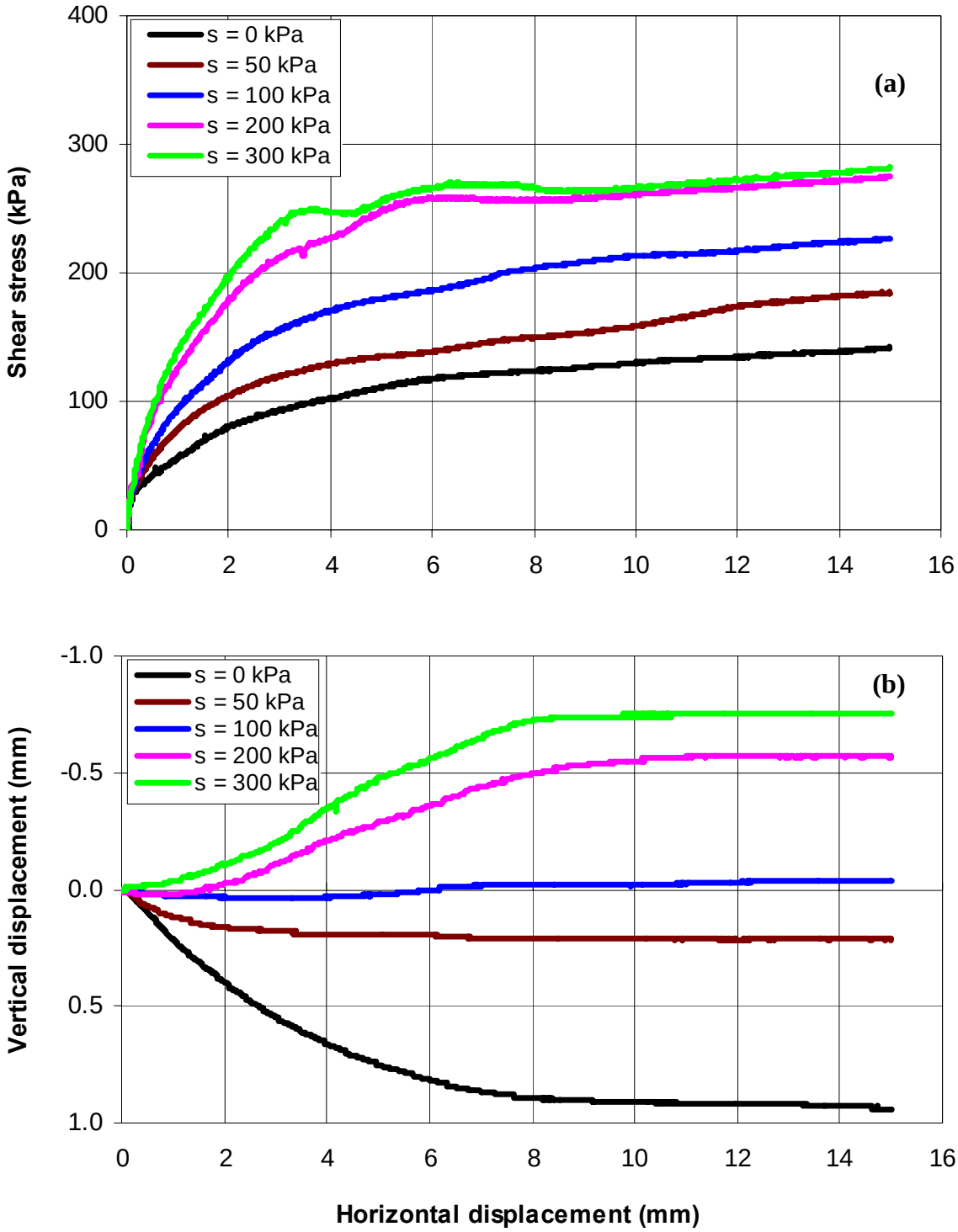

Figure 5.11 Curves of (a) shear stress versus horizontal displacement; and (b) vertical displacement versus horizontal displacement for different suctions under 200 kPa net normal stress

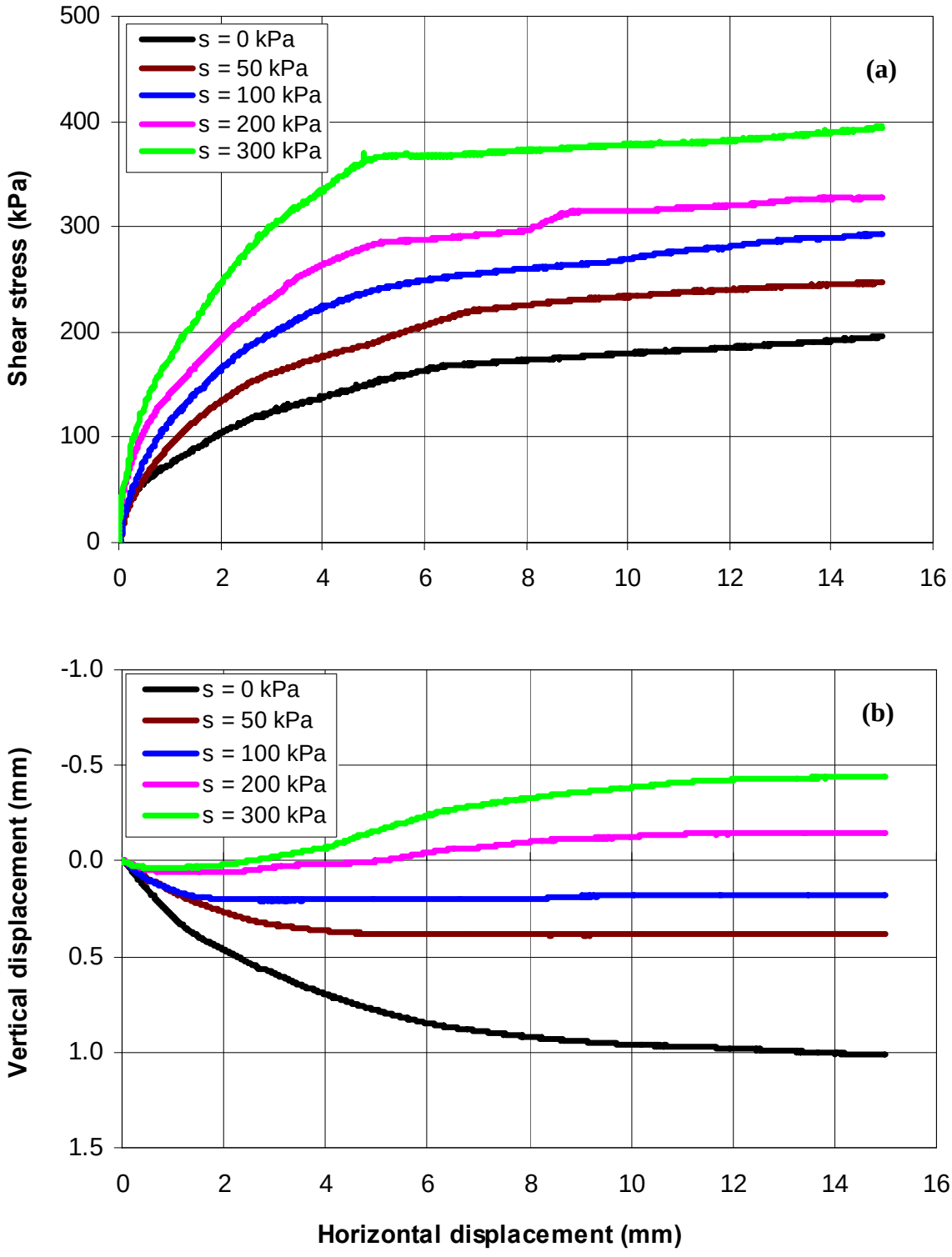

Figure 5.12 Curves of (a) shear stress versus horizontal displacement; and (b) vertical displacement versus horizontal displacement for different suctions under 300 kPa net normal stress

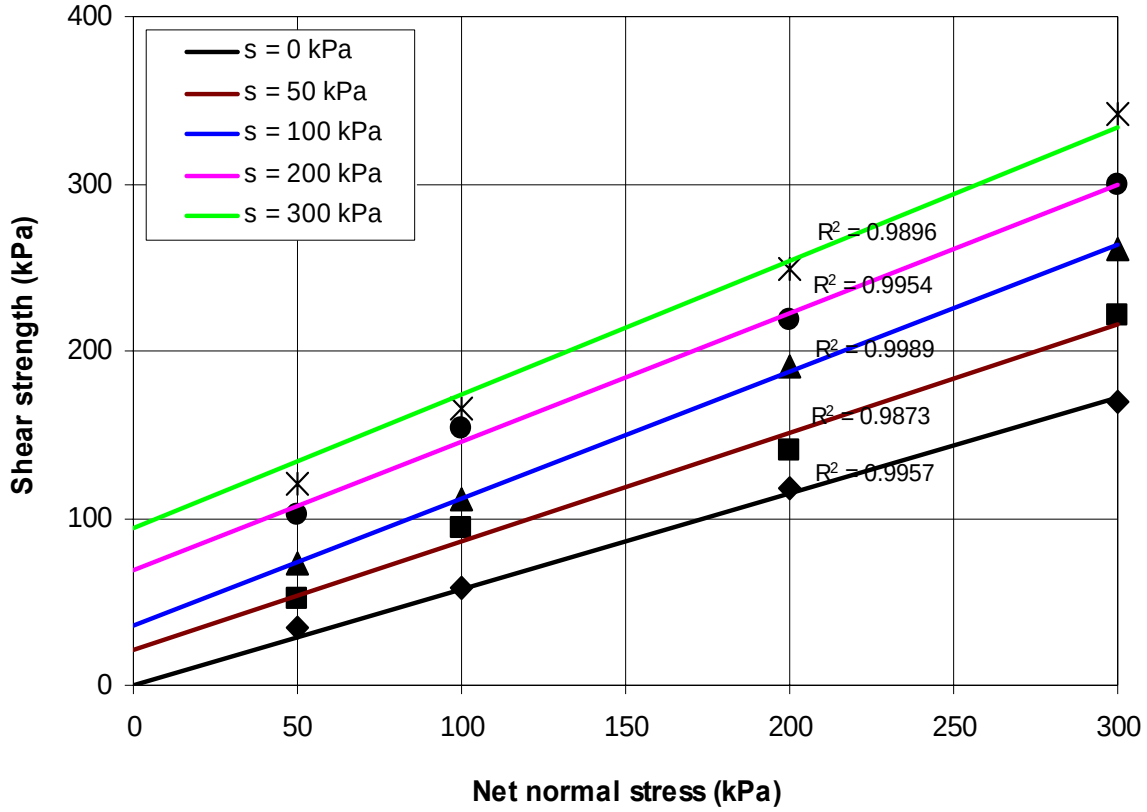

Figure 5.13 Failure envelopes corresponding to different suctions

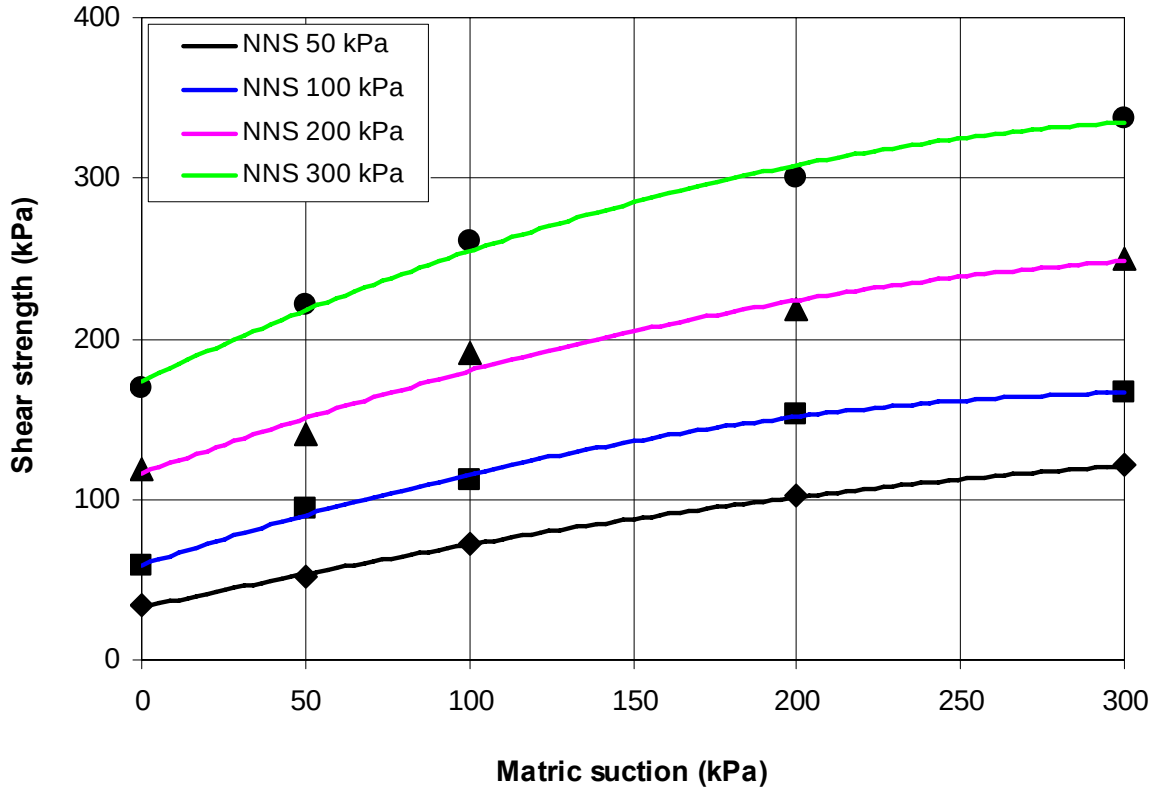

Figure 5.14 Suction envelopes corresponding to different net normal stresses

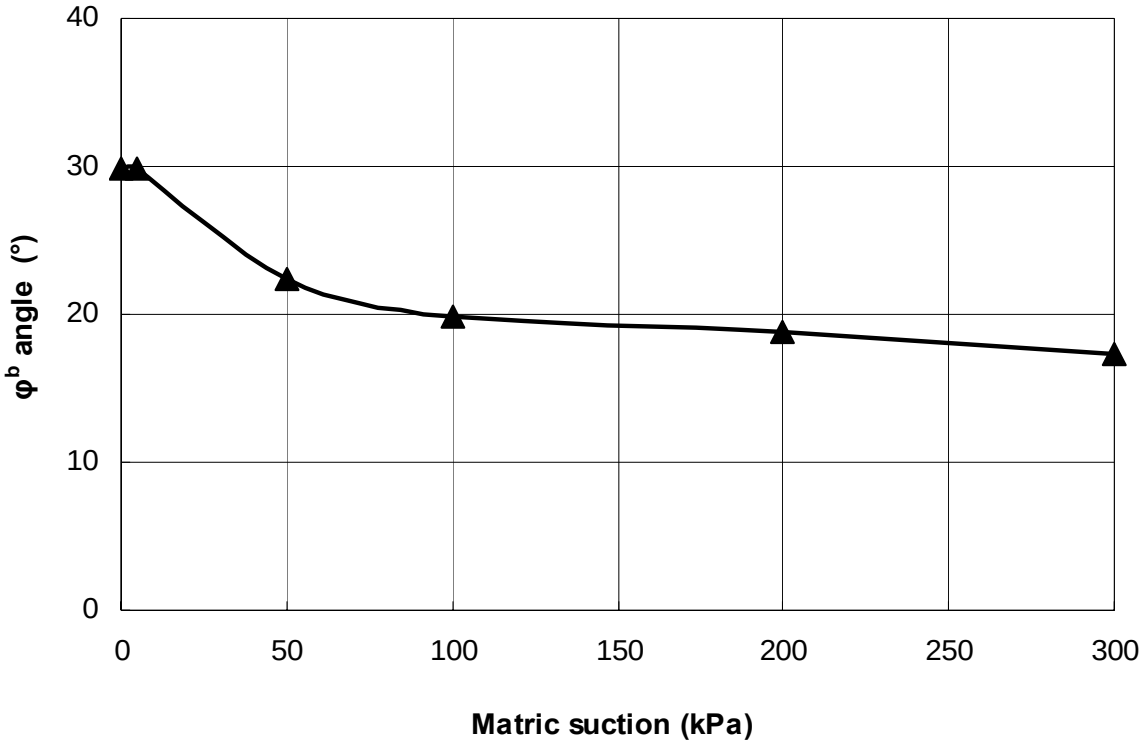

Figure 5.15 Variation of ϕ^b angle with matric suction

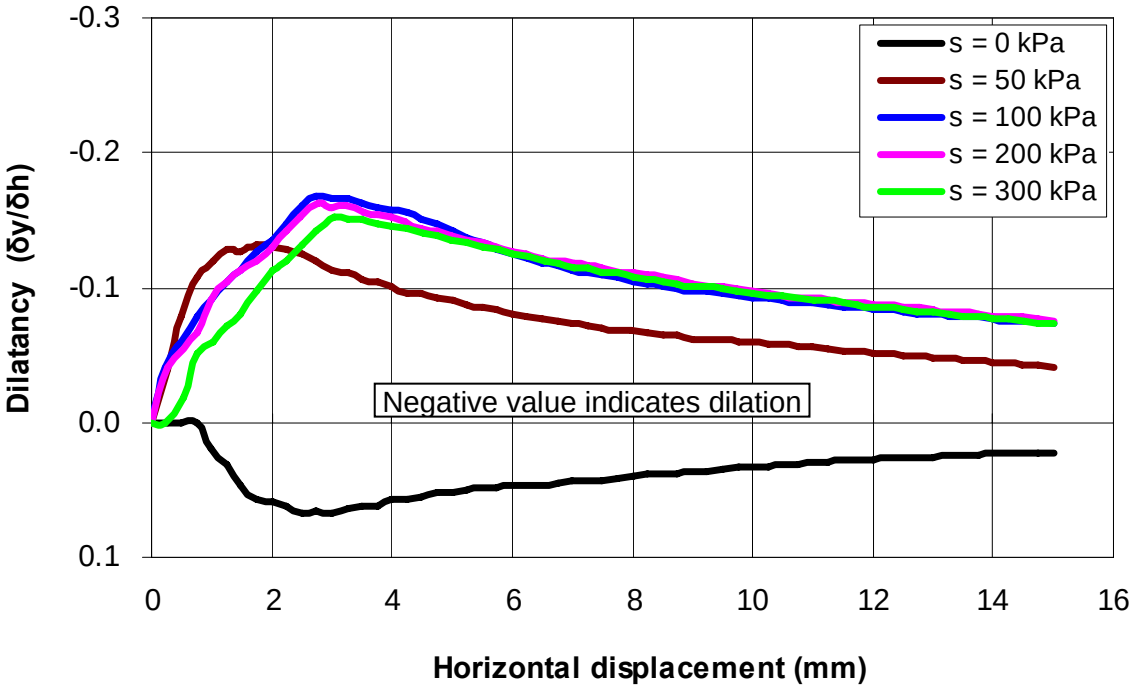

Figure 5.16 Curves of soil dilatancy versus horizontal displacement for different suctions under 50 kPa net normal stress

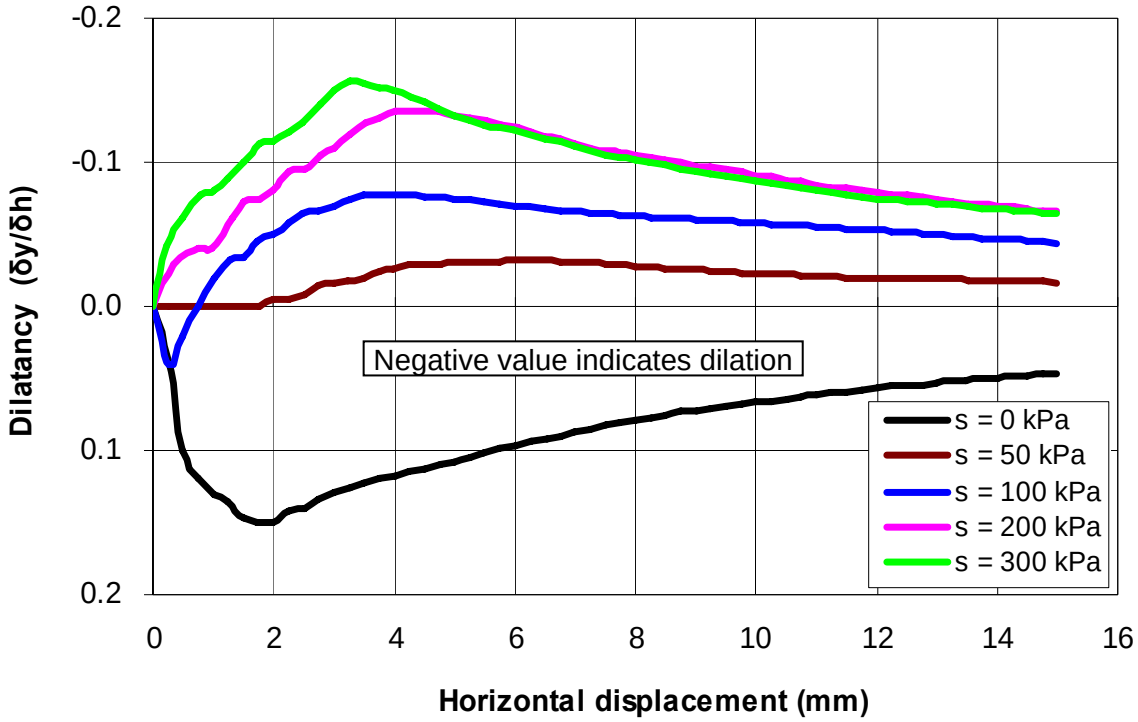

Figure 5.17 Curves of soil dilatancy versus horizontal displacement for different suctions under 100 kPa net normal stress

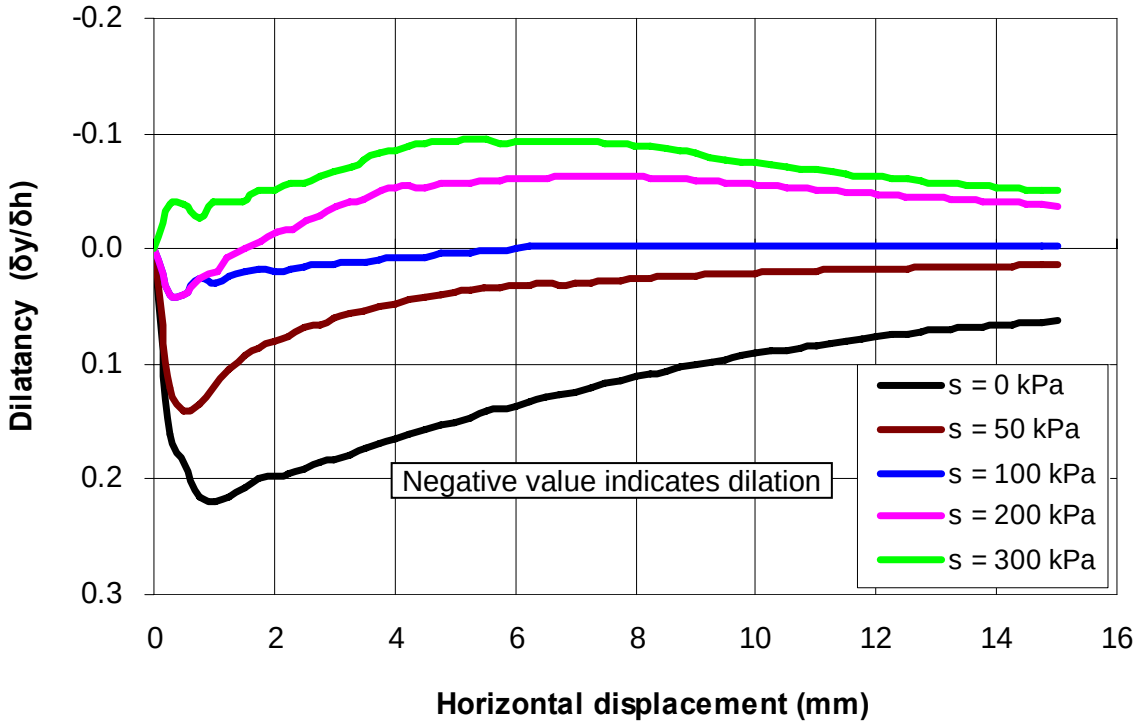

Figure 5.18 Curves of soil dilatancy versus horizontal displacement for different suctions under 200 kPa net normal stress

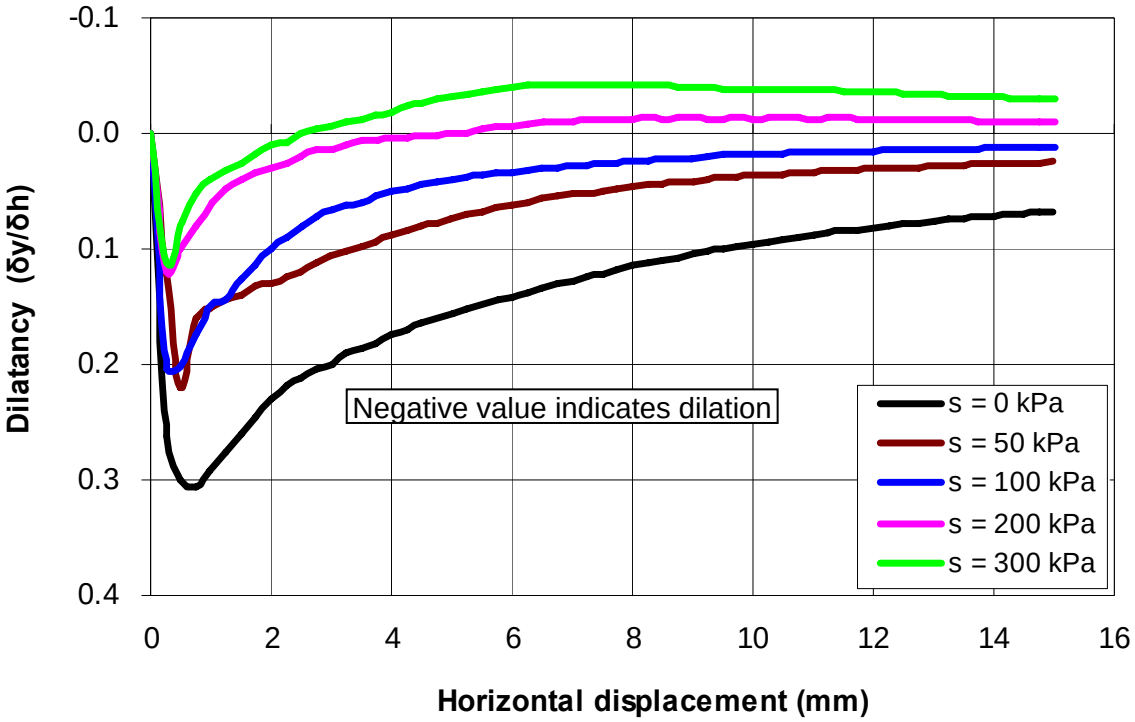

Figure 5.19 Curves of soil dilatancy versus horizontal displacement for different suctions under 300 kPa net normal stress

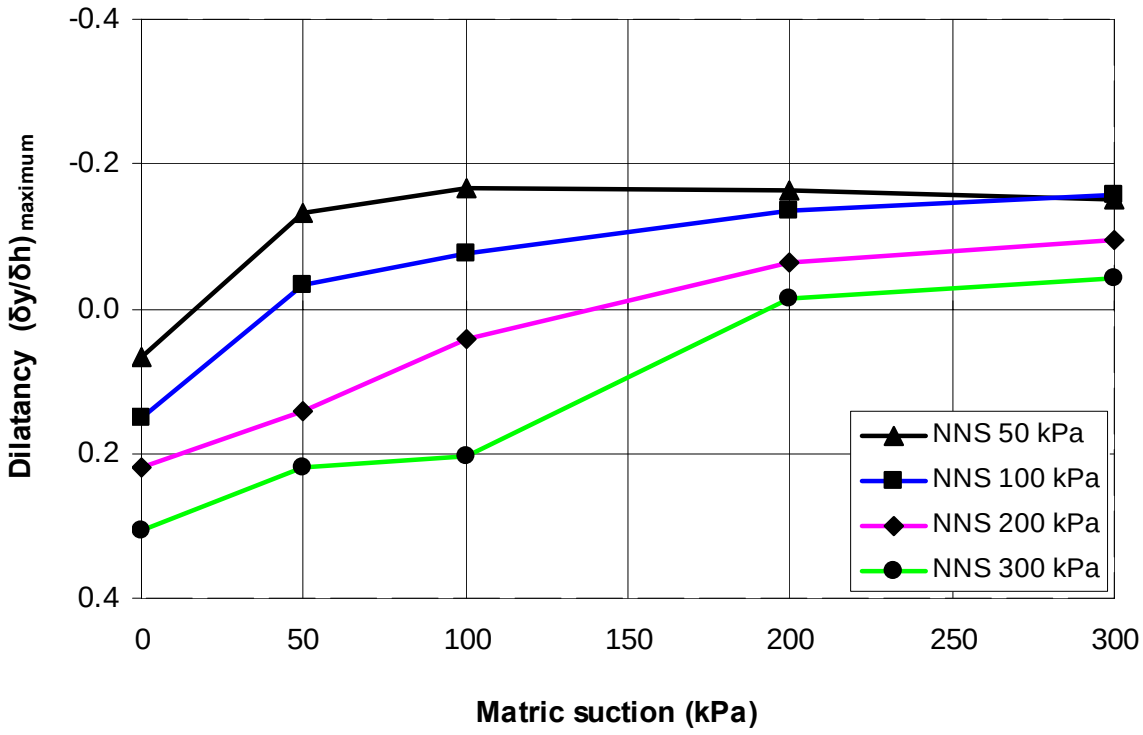

Figure 5.20 Variation of maximum dilatancy with suction under different net normal stresses

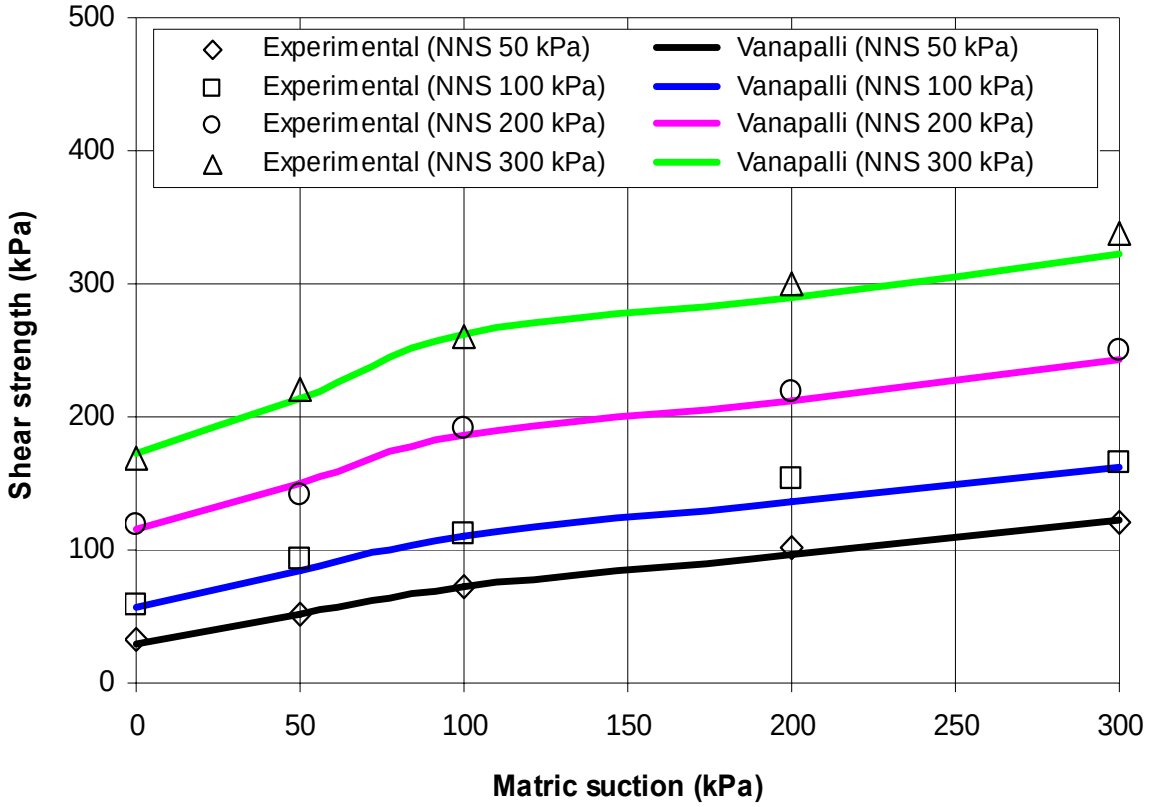

Figure 5.21 Correlation between experimental data and Vanapalli's model to determine the value of fitting parameter κ

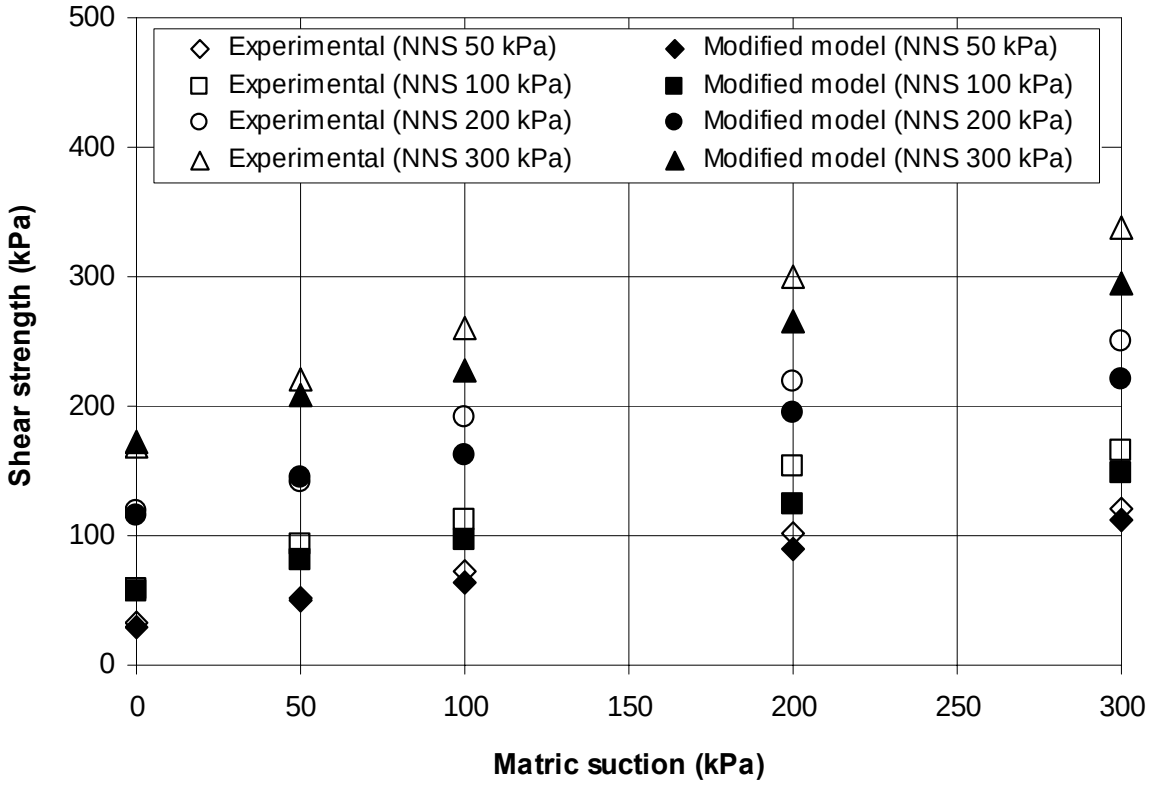

Figure 5.22 Comparison between experimental shear strength data and analytical results obtained from the modified model

Chapter 6

UNSATURATED INTERFACE TEST RESULTS AND INTERPRETATIONS

6.1 INTRODUCTION

To some extend, the interface behavior depends on the way by which it is formed. There are two ways of forming the interface: (i) Cast in-situ interface - construction materials is applied over a prepared soil surface, and (ii) Pre-cast interface - soil is compacted over a construction material. The cast in-situ interface is very common in geotechnical projects and can be formed by (i) normal gravity grouting, and (ii) pressure grouting. To investigate the influence of matric suction and net normal stress on the behavior of a cast in-situ interface formed between a compacted completely decomposed granite (CDG) soil and cement grout (grouting pressure 0 kPa), a series of direct shear box tests were performed under consolidated drained condition. Axis-translation technique was applied to control the matric suction, that is, to control pore-water and pore-air pressure. This chapter focuses on the interface direct shear tests results, their interpretations, and discussion. The effect of interface dilation angle on apparent interface friction angle, and consequently on shear strength are investigated, and considered to estimate the shear strength of unsaturated CDG soil-cement grout interface. A modified interface shear strength model is proposed to establish the effect of dilation angle on apparent interface friction angle and shear strength, by using analytical values of interface dilation angles obtained from dilatancy curves. The experimental shear strength data are also compared with the analytical results obtained from the model.

A total of 15 interface direct shear tests are performed under different suction values of 0, 50, 100, 200, and 300 kPa with net normal stresses of 50, 100, and 300 kPa. The influence of suction and net normal stress on the behavior of compacted CDG soil-cement grout interface are observed and presented in the following sections.

6.2 INTERFACE TEST REULTS AND INTERPRETATIONS

6.2.1 Influence of net normal stress on stress-strain-strength behavior

The relationships between (a) shear stress and horizontal displacement, and (b) vertical displacement and horizontal displacement under different net normal stresses (50, 100, and 300 kPa) for the same matric suction (0, 50, 100, 200 and 300 kPa) are shown in Figs. 6.1, 6.2, 6.3, 6.4 and 6.5 The behavior of the soil-cement interface from these figures is discussed in the followings with attention on the influences of net normal stress:

(a) For zero suction, all curves of the interface shear stress and horizontal displacement show gradually hardening behavior and all vertical displacements increase with horizontal displacement indicating shear-compression. The higher the net stress, the more the shear compression.

(b) For suction 50 kPa, curves of the interface shear stress and horizontal displacement for 50 and 100 kPa net normal stress show hardening-softening behavior. Whereas, the curve for 300 kPa net normal stress shows still hardening behavior. The two curves of vertical displacement and horizontal displacement for net stresses 50 and 100 kPa show shear-dilation (vertical displacement negative). On the other hand, the curve for net stress 300 kPa shows shear-compression.

(c) For suction 100 kPa, the curves of the interface shear stress and horizontal displacement show softening behavior with clear peak stress. But, the curve for 300 kPa still shows hardening behavior. The two curves of vertical displacement and horizontal displacement for net stresses 50 kPa and 100 kPa show shear-dilation (vertical displacement negative) from the start to the end; while the curve for net stress 300 kPa show shear-compression in the initial period and a little shear dilation at the ending period.

(d) For suctions 200 and 300 kPa, all the curves of interface shear stress and horizontal displacement show clear peak shear stresses, indicating a strain (or displacement) softening behavior. The two curves of vertical displacement and horizontal displacement for 50 and 100 kPa net normal stresses show strong shear-dilation (vertical displacement negative). The curve of vertical displacement and horizontal displacement for 300 kPa show a little shear-compression at beginning, followed by large shear-dilation.

6.2.2 Influence of suction on stress-strain-strength behavior

The experimental interface tests data presented in Figs. 6.1, 6.2, 6.3, 6.4 and 6.5 are plotted in Figs. 6.6, 6.7 and 6.8 in order to study the influences of the suction on the shear and deformation behavior of the soil-cement interface. The relationships between (a) interface shear stress and horizontal displacement, and (b) vertical displacement and horizontal displacement under different suction of 0, 50, 100, 200 and 300 kPa for the same net normal stress of 50, 100 and 300 kPa are shown in Figs. 6.6, 6.7 and 6.8. The behavior of the CDG soil-cement grout interface from these figures is discussed in the followings with attention on the influences of suction:

(a) For both the net stresses of 50 and 100 kPa as shown in Figs. 6.6 and 6.7, the curves of interface shear stress and horizontal displacement change from gradually hardening behavior (showing no peak shear stress) to hardening-softening behavior (showing a clear peak shear stress) with the increase of suction. The corresponding curves of vertical displacement and horizontal displacement show shear-compression for zero suction and shear-dilation for higher suction. The higher the suction, the more significant strain-softening, the more shear-dilation.

(b) For the net stress 300 kPa, with the increase of suction, the curves of interface shear stress and horizontal displacement change from gradually hardening behavior (showing no peak shear stress) to a little hardening-softening behavior (showing a small peak shear stress), as shown in Fig. 6.8. The corresponding curves of vertical displacement and horizontal displacement show shear-compression for suction of zero and 50 kPa, a little shear-dilation for 100 kPa suction, and then more shear-dilation for higher suction of 200 and 300 kPa.

6.2.3 Influence of suction on interface friction angle and adhesion

The relationships between the interface shear strength and the net normal stress (failure envelopes) corresponding to different suctions is shown in Fig. 6.9. The failure strength is obtained from the raw test data as that point where the shear load starts decreasing (peak shear load) or where the shear load starts to remain nearly constant. The shear strength envelopes of the shear stress τ_f *versus* the net normal stress $(\sigma_{nf} - u_{af})$ for a given suction are approximately linear. The declivity of those envelopes is represented by apparent interface friction angle $\delta_{\max}$. At saturated condition, $\delta_{\max} = \delta'$. The effective angle of interface friction, $\delta' = 31.5°$ and effective adhesion, $c'_a = 16.4$ kPa are found for the soil-cement grout interface from Fig. 6.9 for 0 kPa suction (at

saturated condition). The apparent interface friction angle $\delta_{\max}$ and adhesion intercept c_a increase with matric suction. The change of the apparent friction angle is likely attributed to the change of dilation angle with matric suction (Zhan and Ng 2006; Hossain and Yin 2010). The change of adhesion intercept is due to change of suction and δ^b angle. The values of $\delta_{\max}$ and c_a for different suctions are summarized in Table 6.1. The adhesion intercept, c_a can be defined by the following equation:

$$c_a = c'_a + (u_a - u_w)_f \tan \delta^b \qquad 6.1$$

where c'_a is the adhesion at saturated condition; $(u_a - u_w)_f$ is the matric suction at failure; and δ^b is the angle indicating the rate of increase in interface shear strength relative to matric suction $(u_a - u_w)_f$.

6.2.4 Suction envelope for soil-cement interface

The variation of interface shear strength τ_f with different matric suction $(u_a - u_w)_f$ (suction envelope) for different net stresses $(\sigma_{nf} - u_{af})$ is shown in Fig. 6.10. The interface shear strength increases with matric suction and net normal stress. However, the relationships between interface shear stress τ_f at failure and matric suction $(u_a - u_w)_f$ are obviously nonlinear, indicating that the δ^b parameter in eq. [6.1] is not constant. The values of δ^b angles obtained from eq. [6.1] for different matric suctions are tabulated in Table 6.2. Figure 6.11 shows that the variation of δ^b angle with matric suction is nonlinear, and decreases with matric suction.

6.2.5 Influence of suction and net stress on interface dilatancy

The interface dilation under different net normal stresses may have significant influences on the unsaturated interface shear strength. The effect of suction on interface dilatancy $(\delta y / \delta h)$ under different net normal stresses is presented in Figs. 6.12, 6.13 and 6.14. The dilatancy essentially increases with an increase of matric suction. The peak dilatancy (negative) is observed at lower net normal stress (50 kPa) under higher suctions. The dilatancy decreases as the net stress is increased. The explanation of increase of dilation angle at higher suctions and lower net stresses is already mentioned in the previous chapter (Chapter 5) of this thesis.

The interface dilation angle ψ_i under different net normal stresses and suctions can be calculated from dilatancy curves shown in Figs. 6.12, 6.13 and 6.14 by using the following equation:

$$\tan \psi_i = -\frac{\delta y}{\delta h} \qquad 6.2$$

where δy is the increment in vertical displacement (expansion '-' and contraction '+'); and δh is the increment in horizontal displacement. The average interface dilation angle is obtained by taking the algebraic mean of all interface dilation angles under different net normal stresses for particular matric suction. Table 6.3 summarizes the analytical values of interface dilation angles and apparent interface friction angles for different suctions. It is obvious from Table 6.3 that the average dilation angle increases with matric suction.

6.3 PROPOSED MODIFIED MODEL FOR UNSATURATED INTERFACE

Miller and Hamid (2007) modified the shear strength equation for unsaturated soil proposed by Fredlund *et al.* (1978) to consider for interface between Minco silt and stainless steel. The modified model of Miller and Hamid (2007) is proposed to further modify as follows following the same theory behind for predicting the interface shear strength between unsaturated compacted CDG soil and cement grout considering the influence of interface dilation angle on apparent interface friction angle:

$$\tau_f = c_a + (\sigma_n - u_a)_f \tan(\delta' + \psi_i) \qquad 6.3$$

where c_a is the adhesion intercept, and can be defined by eq. [6.1]; δ' is the effective interface friction angle at saturated condition; ψ_i is the interface dilation angle; and $(\delta' + \psi_i) = \delta_{\max}$ is the apparent interface friction angle. In saturated case, $\delta_{\max} = \delta'$ as $\psi_i = 0$, since no dilation is observed.

6.4 VERIFICATION OF PROPOSED MODIFIED MODEL

The modified model (eq. [6.3]) proposed in the previous section is used to obtain a better correlation between experimental interface shear strength data and analytical results. Figure 6.15 shows the comparison between experimental data and the analytical shear strength results obtained from the proposed modified model (eq. [6.3]), using effective interface shear strength parameters (c'_a and δ') of compacted CDG soil-cement grout interface at saturated condition, and analytical values of interface dilation angle, ψ_i and δ^b angles under different suctions (refer to Table 6.3). It is obvious from Fig. 6.15 that the interface shear strength predicted from the proposed modified model agrees well with the experimental shear strength data for different net

normal stresses and matric suctions. This indicates that interface dilation has significant influence on apparent friction angle, and consequently on interface shear strength, and should be considered during design and safety assessment of different CDG soil-structure interactions.

6.5 SOIL SHEAR STRENGTH AND INTERFACE STRENGTH

Figure 6.16 presents the comparison of experimental shear strengths of soil and soil-cement grout interface under different suctions and net normal stresses. Similar to soil-soil direct shear tests, the interface shear strength increases with net normal stress and matric suction. It is obvious from Fig. 6.16 that interface shear strength is greater than the shear strength of soil within the suction range of 0 to 100 kPa for different net normal stresses. However, the interface shear strength is slightly lower than the shear strength of soil for the higher suction range of 200 to 300 kPa. The decrease of interface shear strength may be due to lower apparent adhesion intercept values and lower δ^b angle compared to apparent cohesion, and ϕ^b angle of soil, as the apparent interface friction angle remain equal to the apparent friction angle for the entire suction range (refer to Table 6.4).

Kulhawy and Peterson (1979) pointed out that the interface friction angle is less than the soil friction angle for smooth interfaces, and equal to or greater than the soil friction angle for rough interfaces. It is obvious from Table 6.4 that the apparent interface friction angles $\delta_{\max}$ under different suctions are greater than or equal to the apparent friction angle for soil $\phi_{\max}$ under the same suctions (ratio of $\delta_{\max}/\phi_{\max}$ varies from 1.00 to 1.05). This implies that CDG soil-cement grout interface behaves like a rough interface according to the finding of Kulhawy and Peterson (1979). The rough interface

is likely formed due to infiltration of cement particles into the failure plane. From Table 6.4, it is obvious that the apparent adhesion c_a is greater than the apparent cohesion c of CDG soil within the suction range of 0 to 100 kPa. But, in higher suction range of 200 to 300 kPa, the apparent adhesion values are lower than the apparent cohesion values of soil. This decrease of apparent adhesion may be due to (i) weakening of bonding between soil and cement particles along the shear plane under higher suctions as bulk water content of the soil pore is decreased, and (ii) weakening of air-water menisci (contractile skin) at higher suctions along the failure plane when sheared due to presence of cement particles.

6.6 SUMMARY

The influences of both matric suction and net normal stress on the behavior of compacted CDG soil-cement grout interface are investigated by conducting a series of direct shear tests at consolidated drained condition. The counterface of CDG soil was formed by cement grout with gravity grouting (grouting pressure 0 kPa). A total of 15 interface direct shear tests are performed under different suctions and net normal stresses. In this chapter, typical test results and their interpretations have been presented and discussed. The initial presentation of the test results in this chapter illustrates the variations of hardening-softening and contractive-dilative behaviors under different suction and net normal stresses. The interface failure envelopes under different suctions are found to be linear. Whereas, nonlinearity is obvious for interface suction envelopes under different net normal stresses. The main focus has been paid on the influence of suction on interface dilatancy. The interface dilation angle increases with matric suction. A modified model has been proposed to consider the influence of interface dilation angle on apparent interface friction angle and hence, on the shear strength of unsaturated soil-cement interface. The prediction of the proposed model is found to

match well with the experimental results. The interface shear strength data is compared with the shear strength of CDG soil under the same suctions and net normal stresses. It is obvious from the experimental interface shear strength data that interface stiffness decreases with matric suction, and consequently offers some lower resistance during shearing at higher suctions compared to CDG soil. It was observed after shearing that the true failure plane did not form exactly at 2 mm from the counterface but propagated along the weakest zone (little bit lower than 2 mm form the cement surface in the middle). This may be due to the facts that the shear box size is large (100.07 mm square), shearing rate is very slow (0.004 mm/min), and shearing is accomplished upto 15 mm horizontal displacement.

This chapter illustrates the interpretations and discussions on direct shear test results of unsaturated soil-cement grout interface for zero grouting pressure with an especial attention on interface dilatancy under different suctions and net stresses, and a proposed model for interface strength for unsaturated soil-cement interface. The next chapter will discuss about the direct shear test results and their interpretations of pressure grouted soil-cement interface under different matric suctions and net normal stresses.

Table 6.1 Variation of apparent interface friction angle $\delta_{\max}$ and adhesion intercept c_a with matric suction for soil-cement interface

Matric suction (kPa)	0	50	100	200	300
$\delta_{\max}$ (deg)	31.5	33.2	37.0	37.5	38.1
c_a (kPa)	16.4	37.5	41.6	54.0	58.5

Table 6.2 Variation of δ^b angle with matric suction for gravity grouted soil-cement interface

Matric suction (kPa)	0	50	100	200	300
δ^b (deg)	31.5	22.9	14.2	10.7	8.0

Table 6.3 Analytical values of interface dilation angle and apparent interface friction angle for different matric suctions obtained from interface dilatancy curves

Matric suction (kPa)	Net normal stress (kPa)	Interface dilation angle (°)	Average dilation angle ψ_i (°)	Effective adhesion c'_a (kPa)	Effective interface friction angle δ' (°)	Apparent interface friction angle $\delta_{max} = (\delta' + \psi_i)$ (°)
0	50	0.0	0.0	16.4	31.5	31.5
	100	0.0				
	300	0.0				
50	50	4.6	2.0	16.4	31.5	33.5
	100	1.4				
	300	0.0				
100	50	5.2	3.6	16.4	31.5	35.1
	100	5.6				
	300	0.1				
200	50	8.5	5.7	16.4	31.5	37.2
	100	7.3				
	300	1.2				
300	50	9.1	6.4	16.4	31.5	37.9
	100	7.8				
	300	2.3				

Table 6.4 Different parameters of CDG soil and gravity grouted soil-cement interface for different matric suctions

Matric suction (kPa)	0	50	100	200	300
ϕ_{max} (deg)	29.9	33.1	37.1	37.6	38.7
δ_{max} (deg)	31.5	33.2	37.0	37.5	38.1
δ_{max}/ϕ_{max}	1.05	1.00	1.00	1.00	1.00
c (kPa)	0.0	20.6	36.2	68.2	93.5
c_a (kPa)	16.4	37.5	41.6	54.0	58.5
c_a/c	-	1.82	1.15	0.79	0.63
ϕ^b (deg)	29.9	22.4	19.9	18.8	17.3
δ^b (deg)	31.5	22.9	14.2	10.7	8.0
δ^b/ϕ^b	1.05	1.02	0.71	0.57	0.46
ψ (deg)	0	3.1	4.6	5.9	6.6
ψ_i (deg)	0	2.0	3.6	5.7	6.4
ψ_i/ψ	-	0.65	0.78	0.97	0.97

*ψ is the average of dilation angles under 50, 100 and 300 kPa net stresses for CDG soil

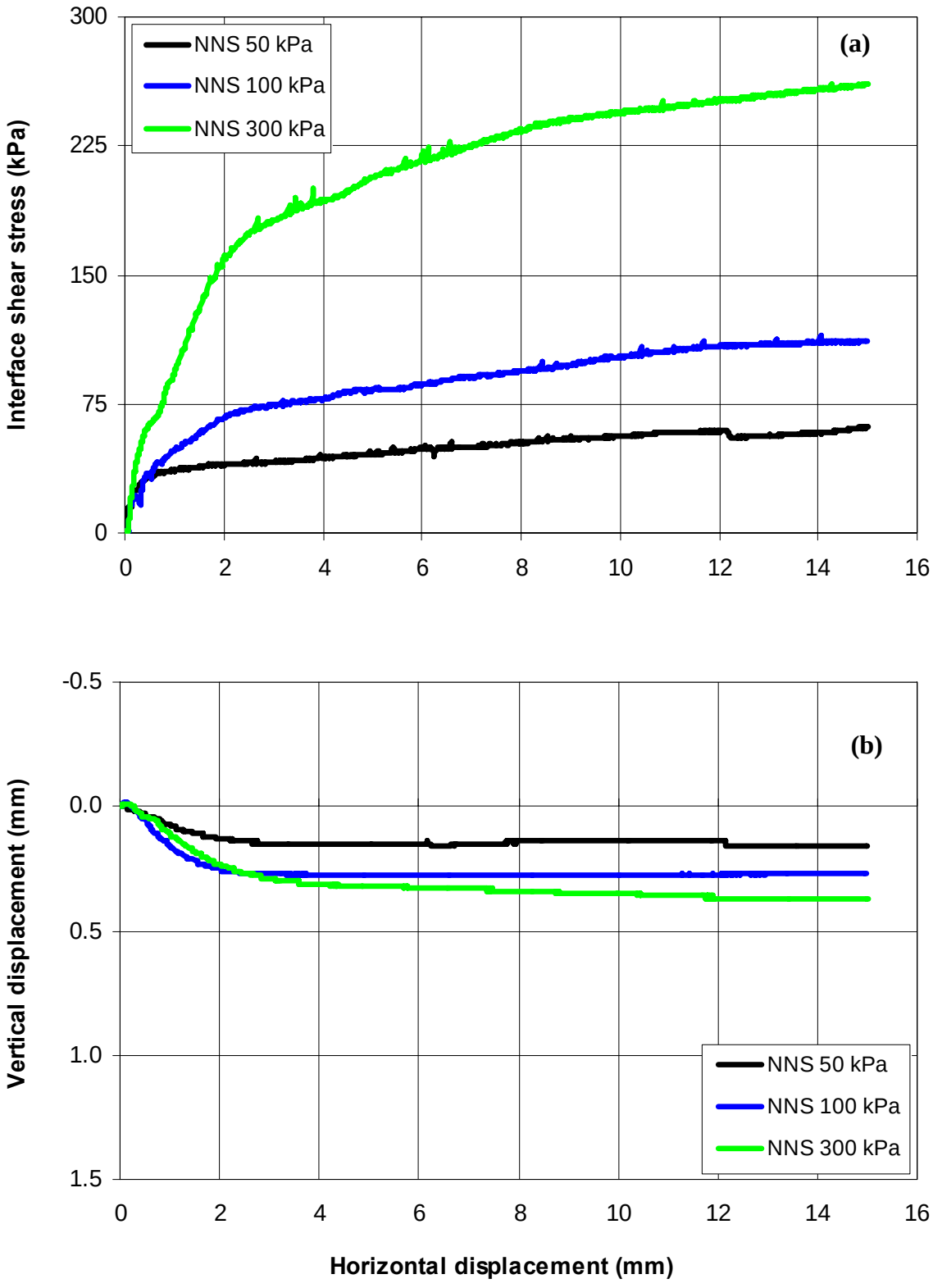

Figure 6.1 Curves of (a) interface shear stress versus horizontal displacement; and (b) vertical displacement versus horizontal displacement for different net normal stresses under 0 kPa matric suction (saturated condition)

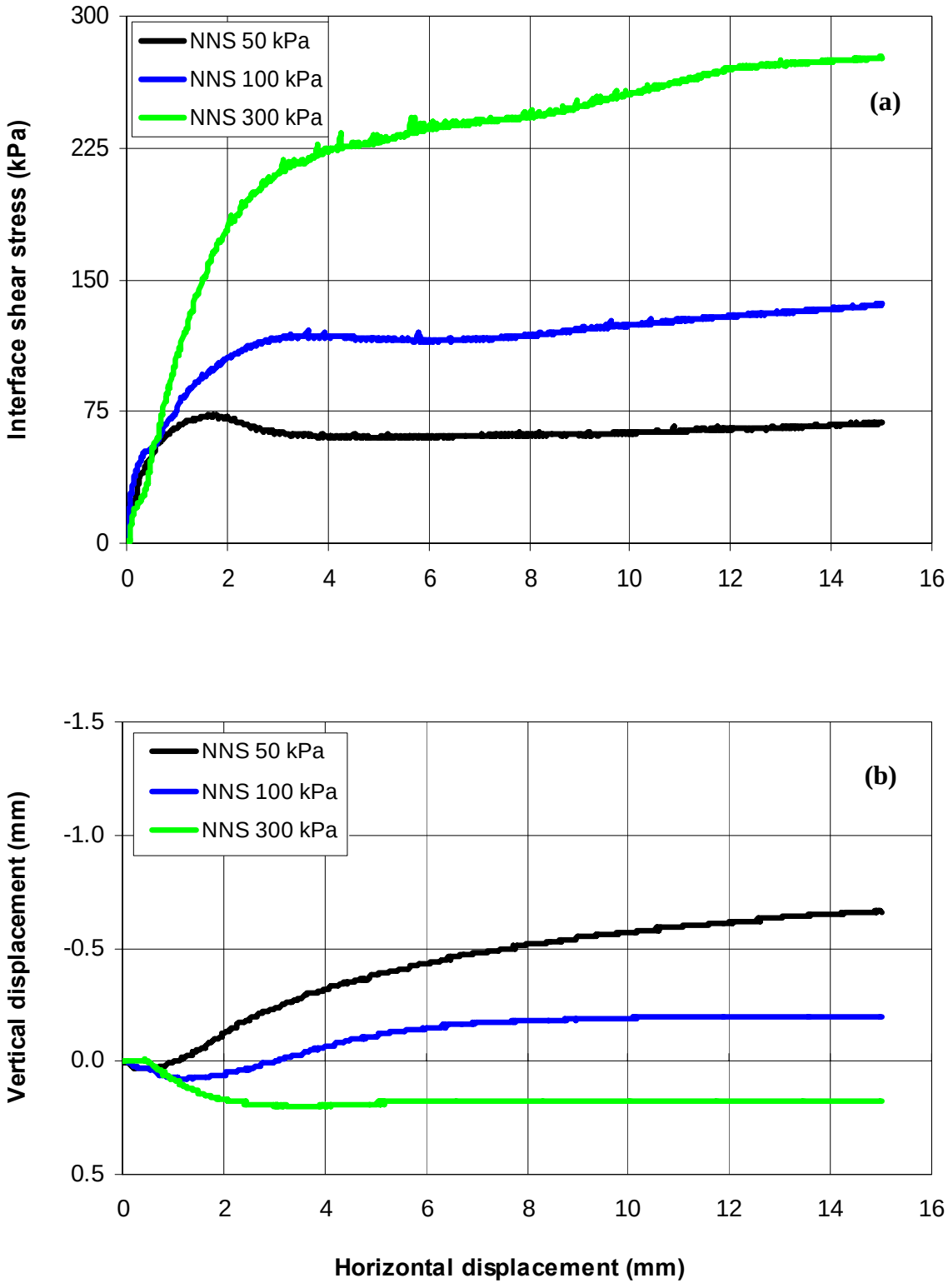

Figure 6.2 Curves of (a) interface shear stress versus horizontal displacement; and (b) vertical displacement versus horizontal displacement for different net normal stresses under 50 kPa matric suction

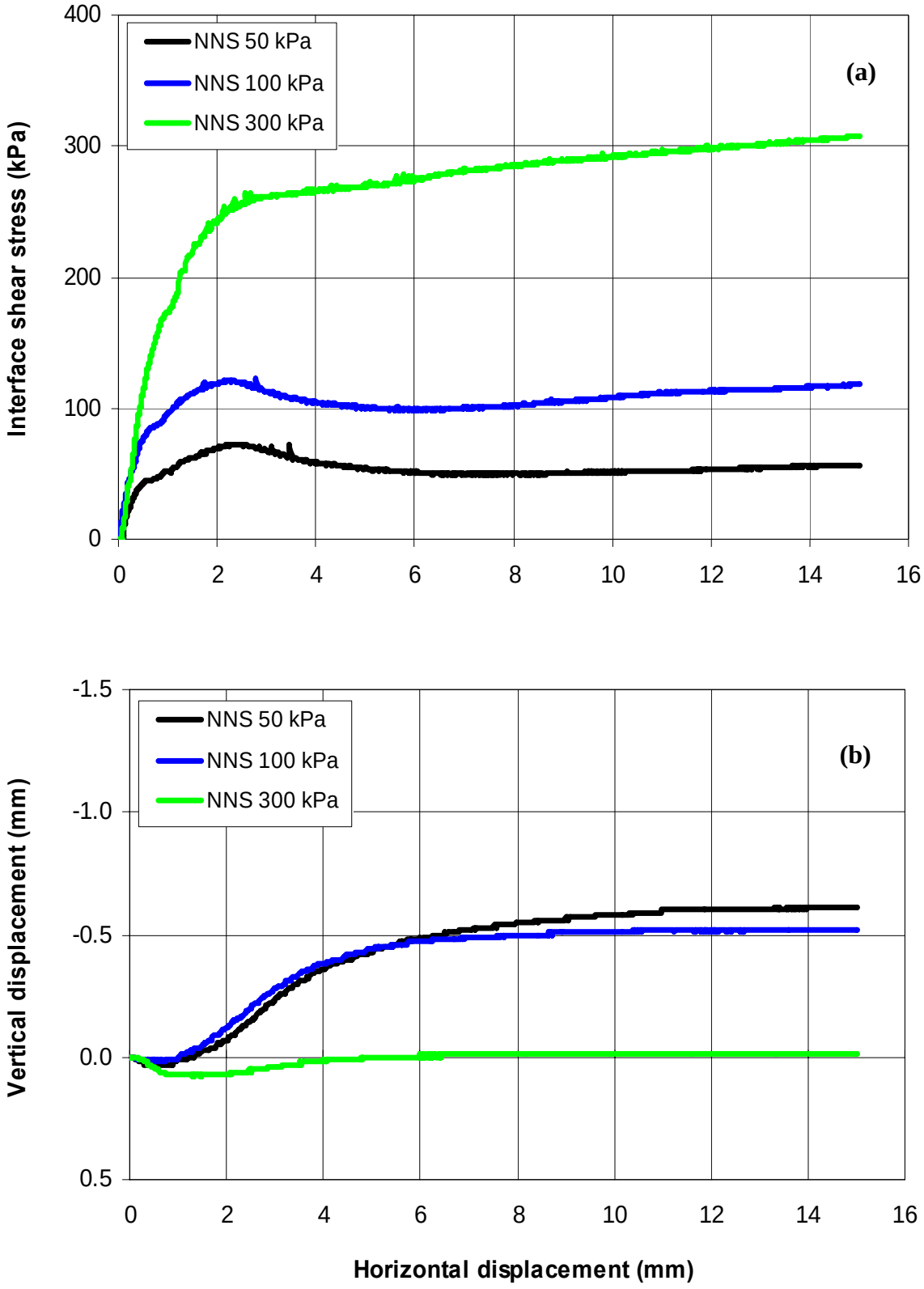

Figure 6.3 Curves of (a) interface shear stress versus horizontal displacement; and (b) vertical displacement versus horizontal displacement for different net normal stresses under 100 kPa matric suction

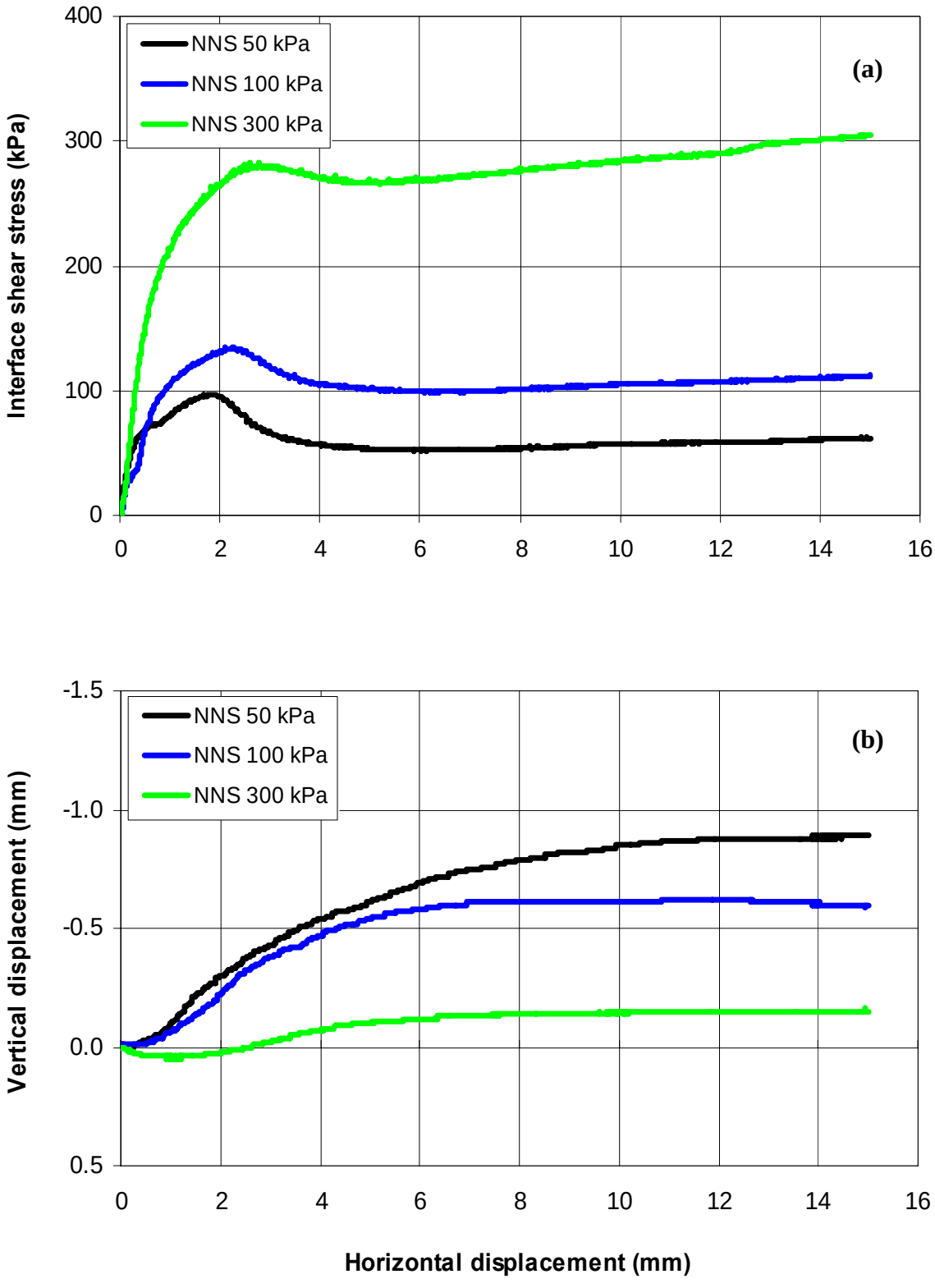

Figure 6.4 Curves of (a) interface shear stress versus horizontal displacement; and (b) vertical displacement versus horizontal displacement for different net normal stresses under 200 kPa matric suction

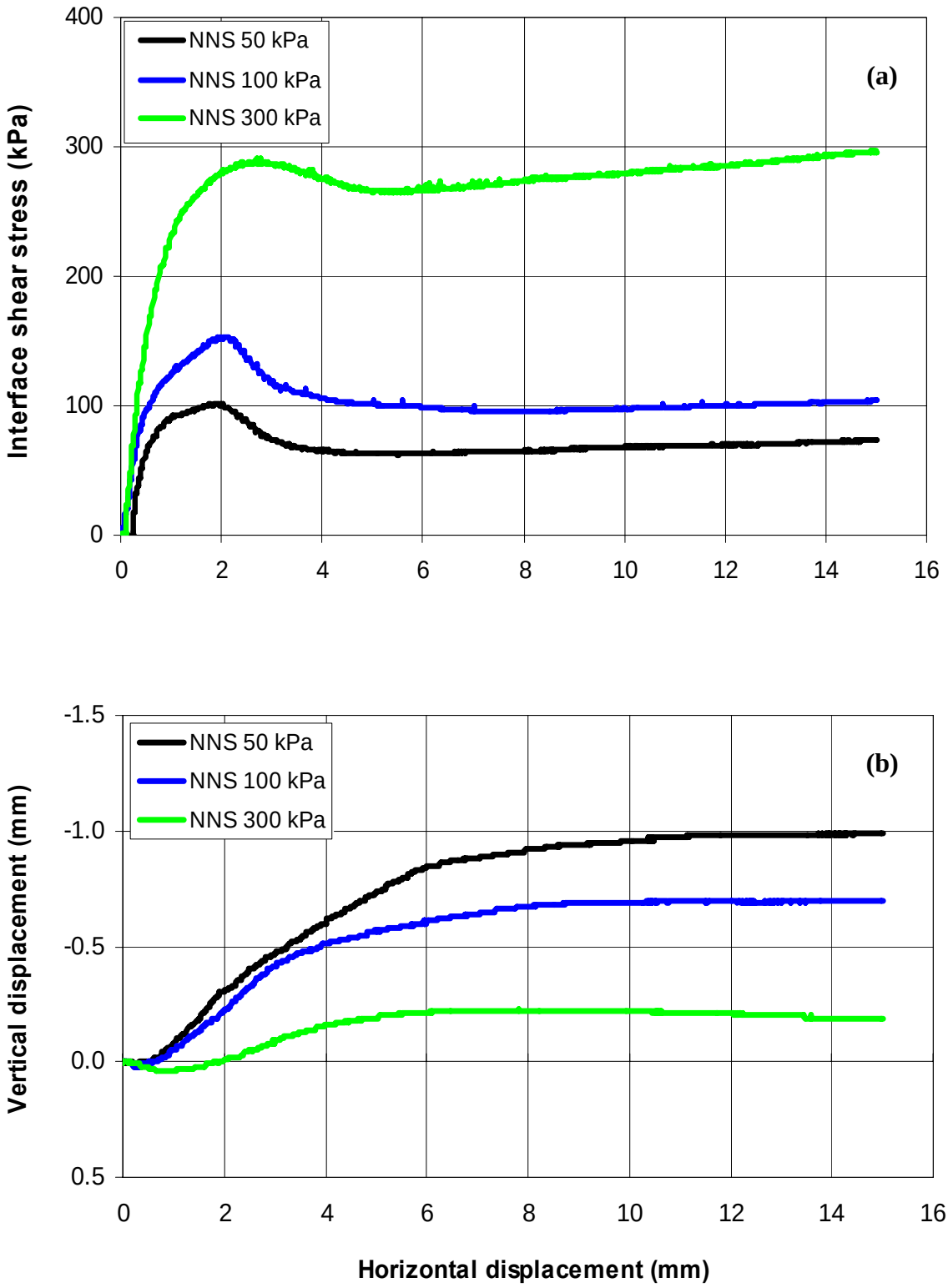

Figure 6.5 Curves of (a) interface shear stress versus horizontal displacement; and (b) vertical displacement versus horizontal displacement for different net normal stresses under 300 kPa matric suction

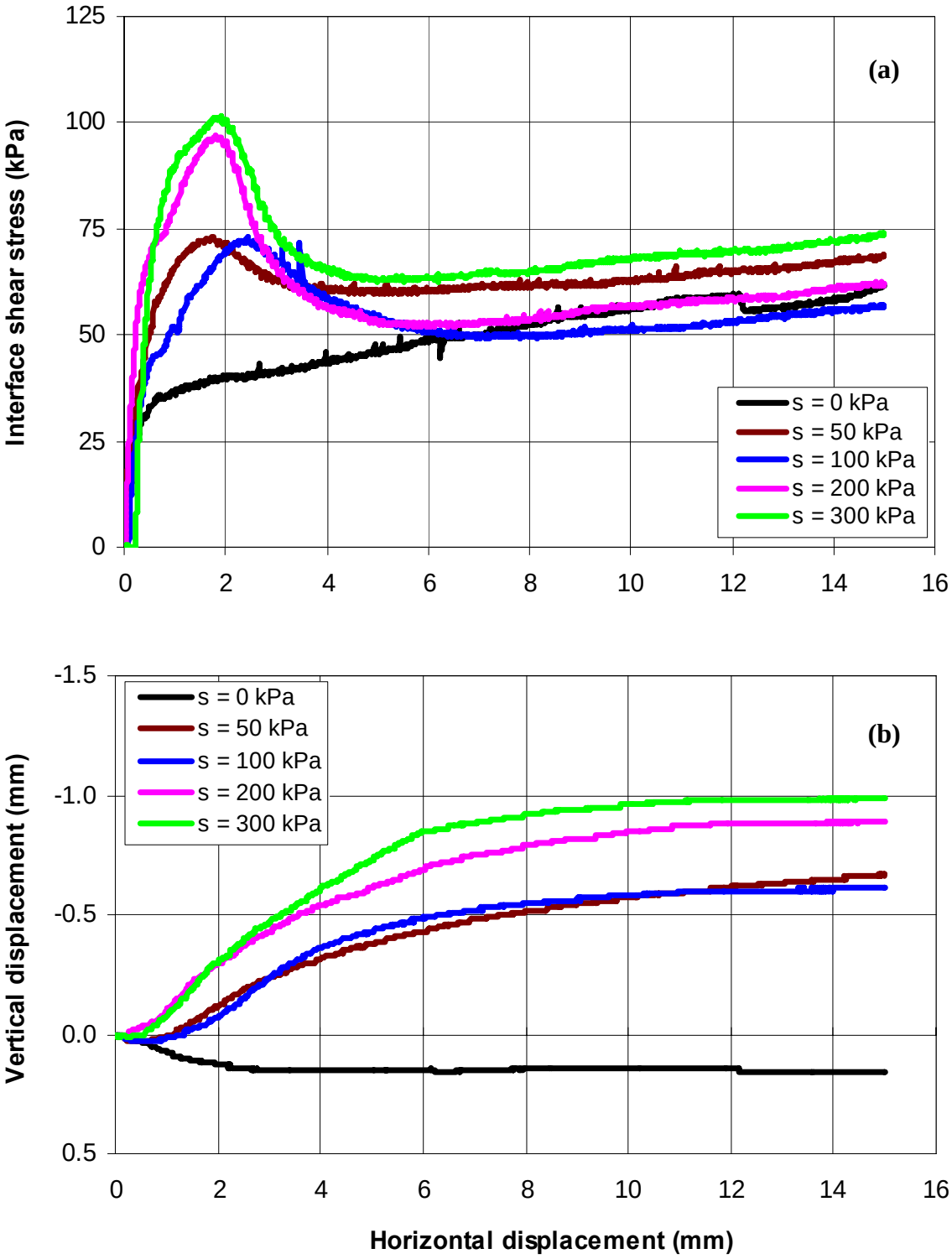

Figure 6.6 Curves of (a) interface shear stress versus horizontal displacement; and (b) vertical displacement versus horizontal displacement for different matric suctions under 50 kPa net normal stress

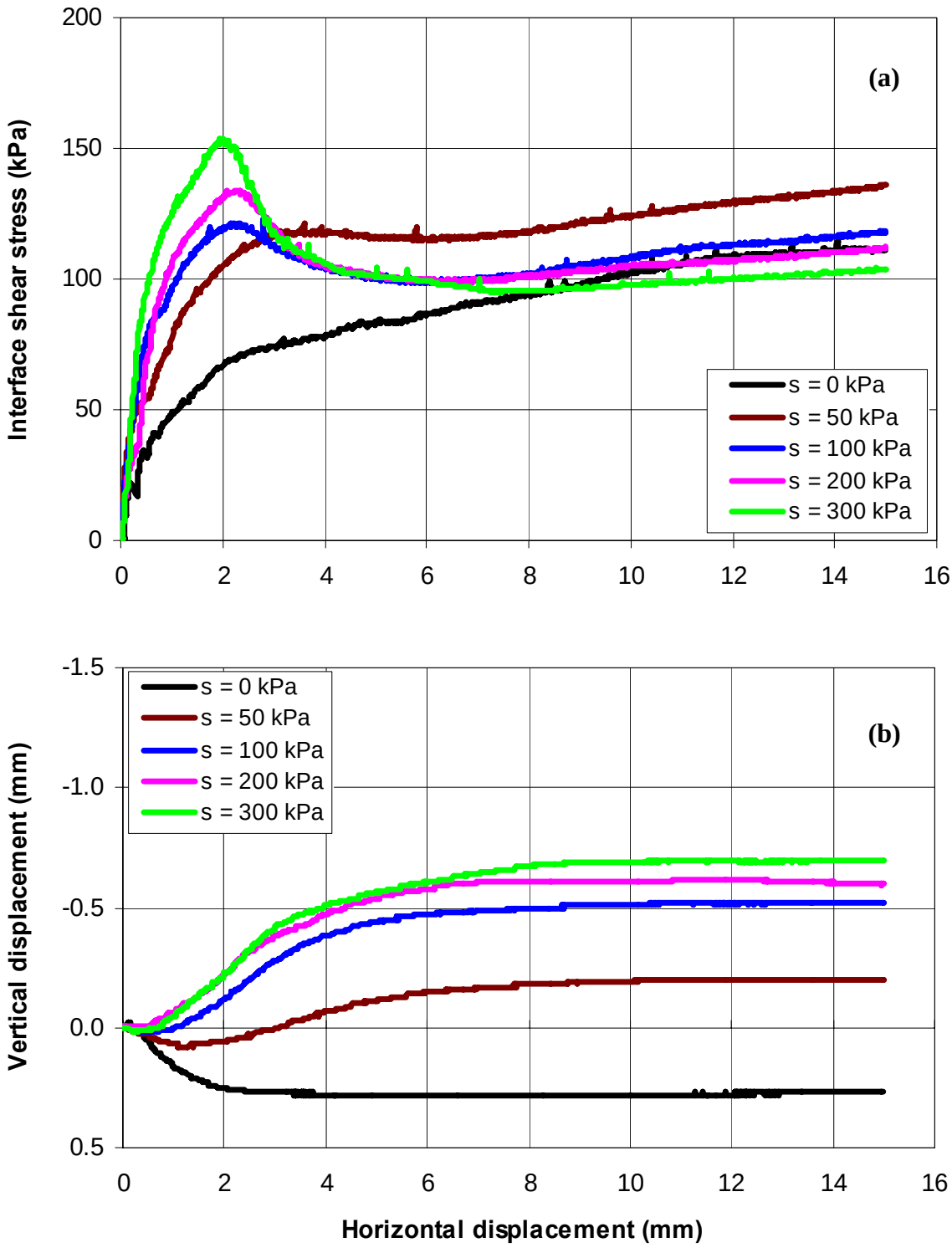

Figure 6.7 Curves of (a) interface shear stress versus horizontal displacement; and (b) vertical displacement versus horizontal displacement for different matric suctions under 100 kPa net normal stress

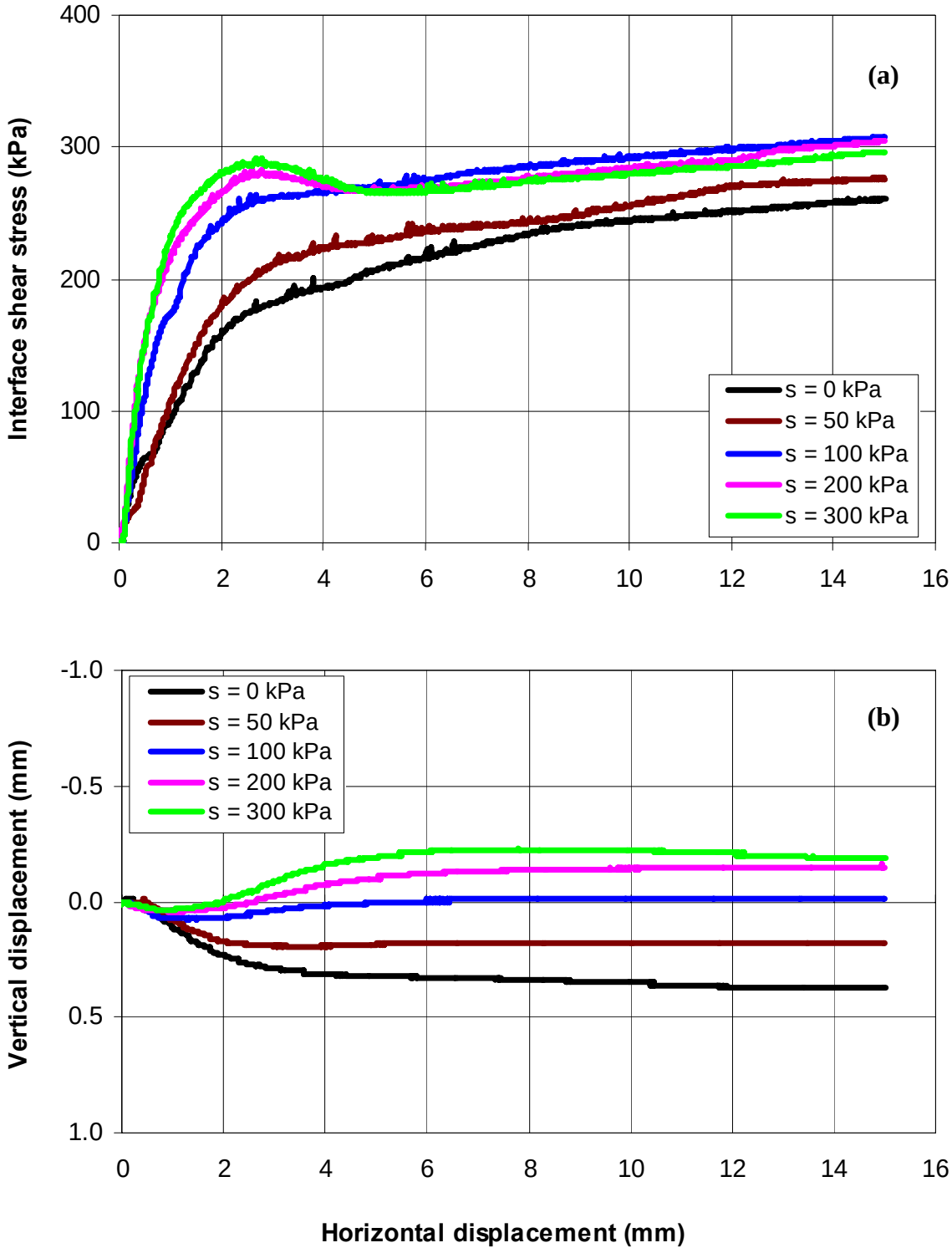

Figure 6.8 Curves of (a) interface shear stress versus horizontal displacement; and (b) vertical displacement versus horizontal displacement for different matric suctions under 300 kPa net normal stress

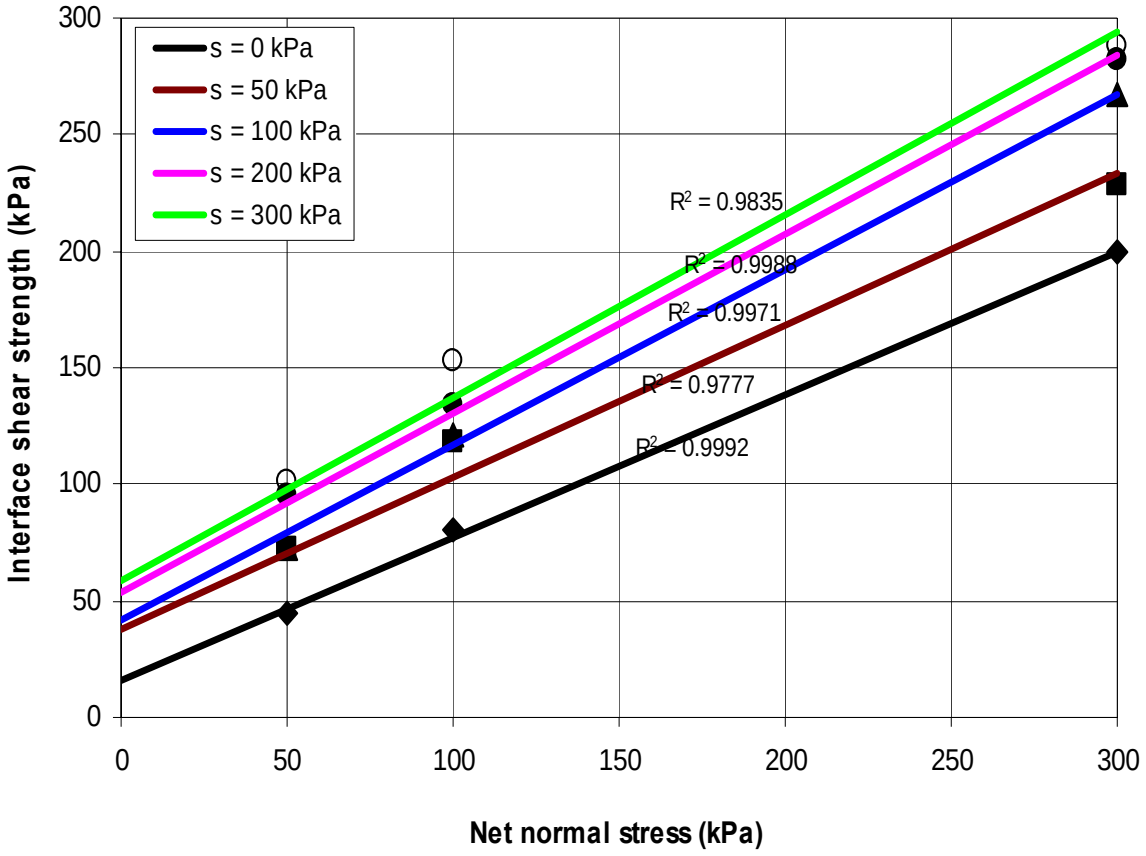

Figure 6.9 Interface failure envelopes corresponding to different suctions

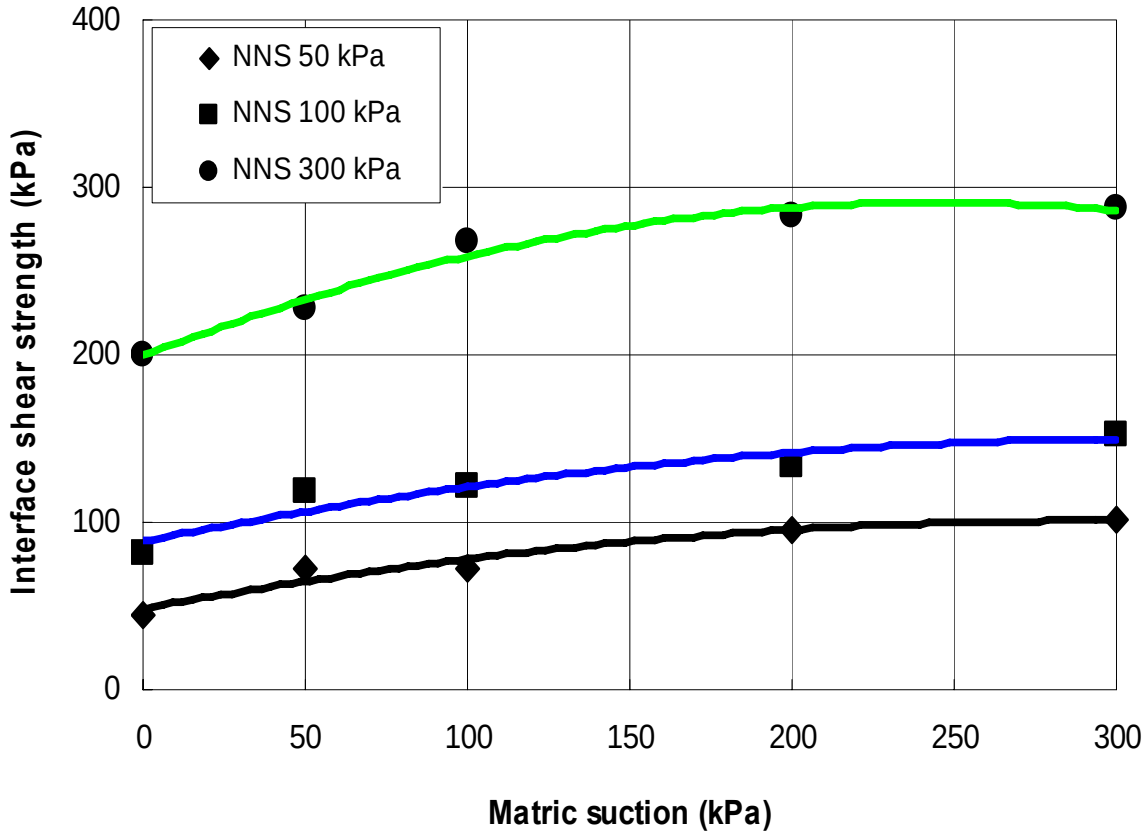

Figure 6.10 Interface suction envelopes corresponding to different net normal stress

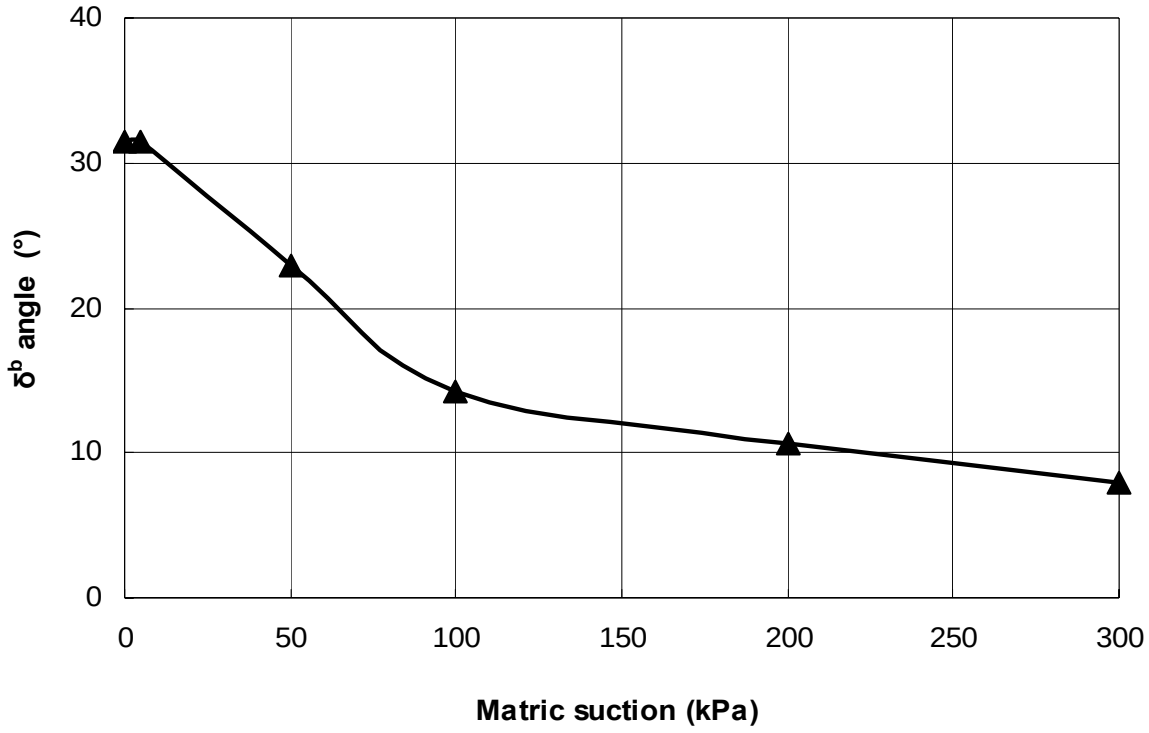

Figure 6.11 Variation of δ^b angle with matric suction for gravity grouted (grouting pressure 0 kPa) soil-cement interface

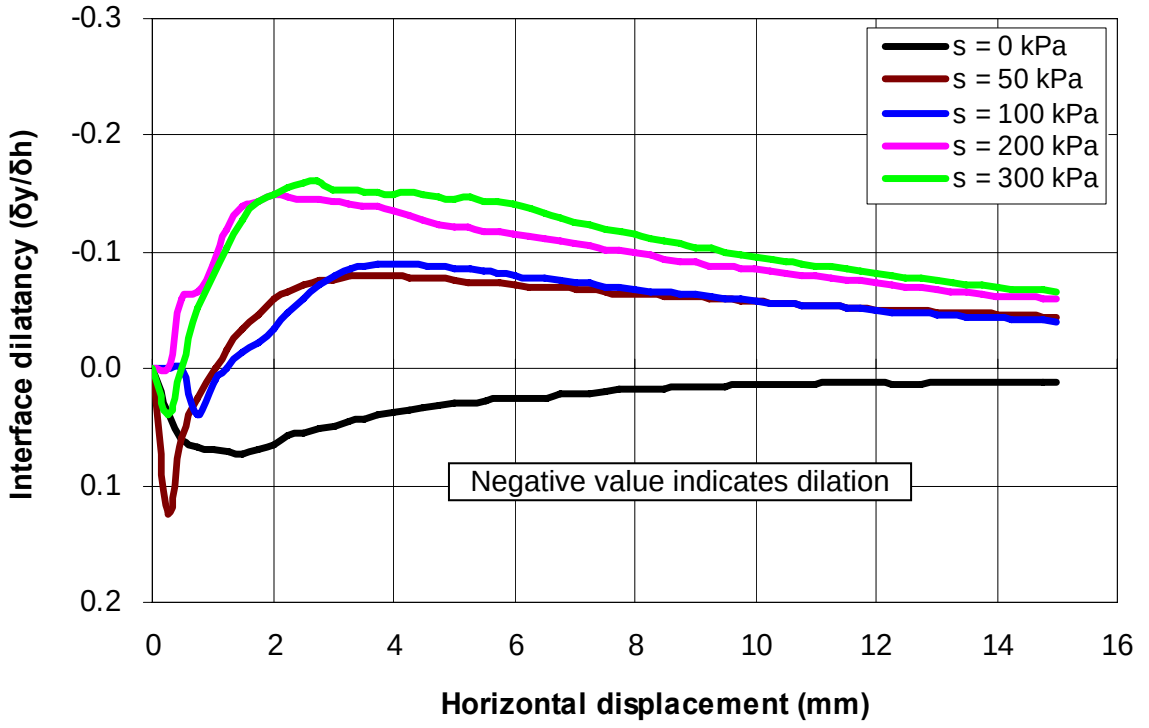

Figure 6.12 Curves of interface dilatancy versus horizontal displacement for different suctions under 50 kPa net normal stress

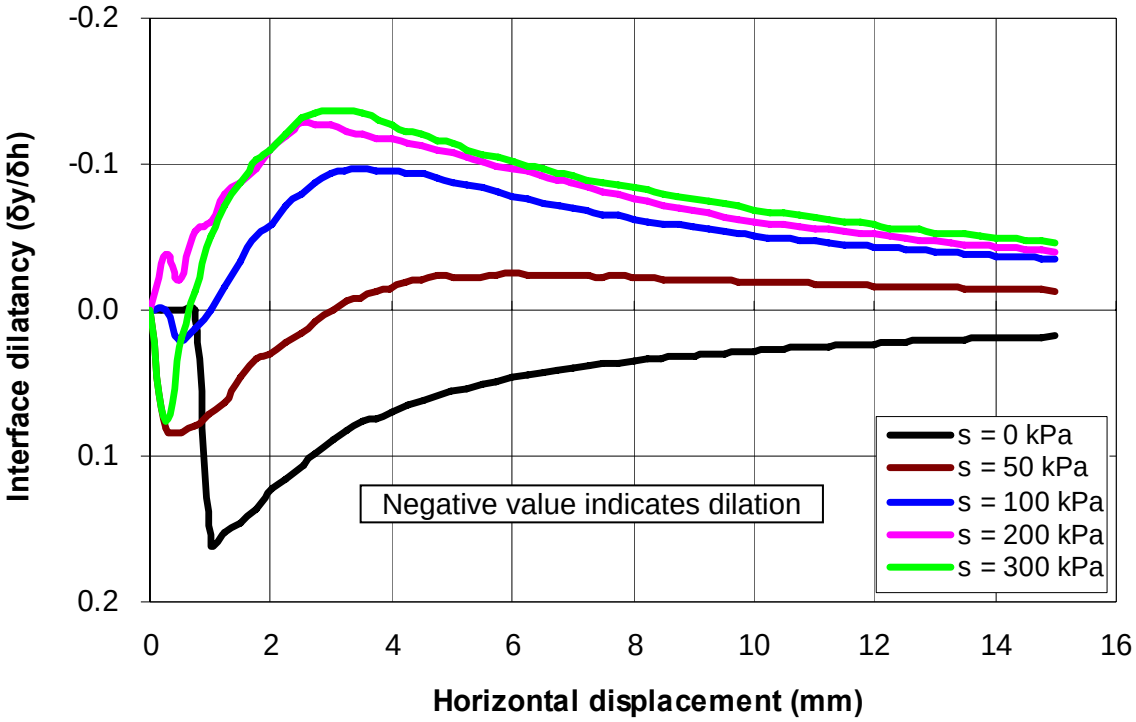

Figure 6.13 Curves of interface dilatancy versus horizontal displacement for different suctions under 100 kPa net normal stress

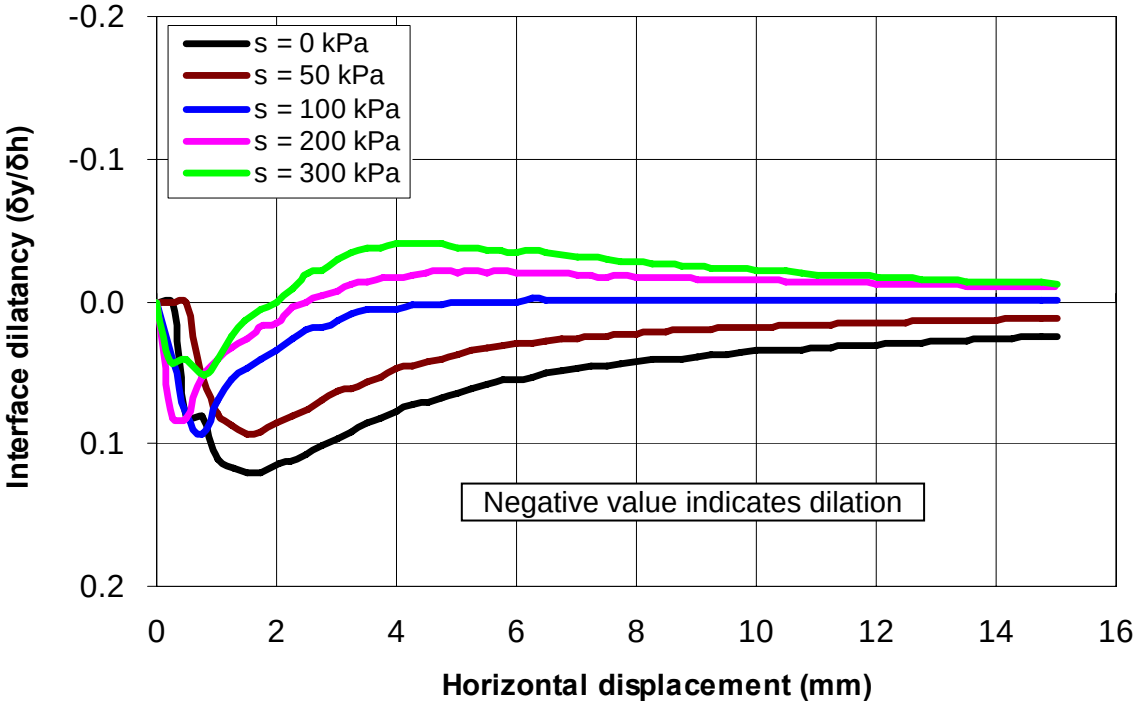

Figure 6.14 Curves of interface dilatancy versus horizontal displacement for different suctions under 300 kPa net normal stress

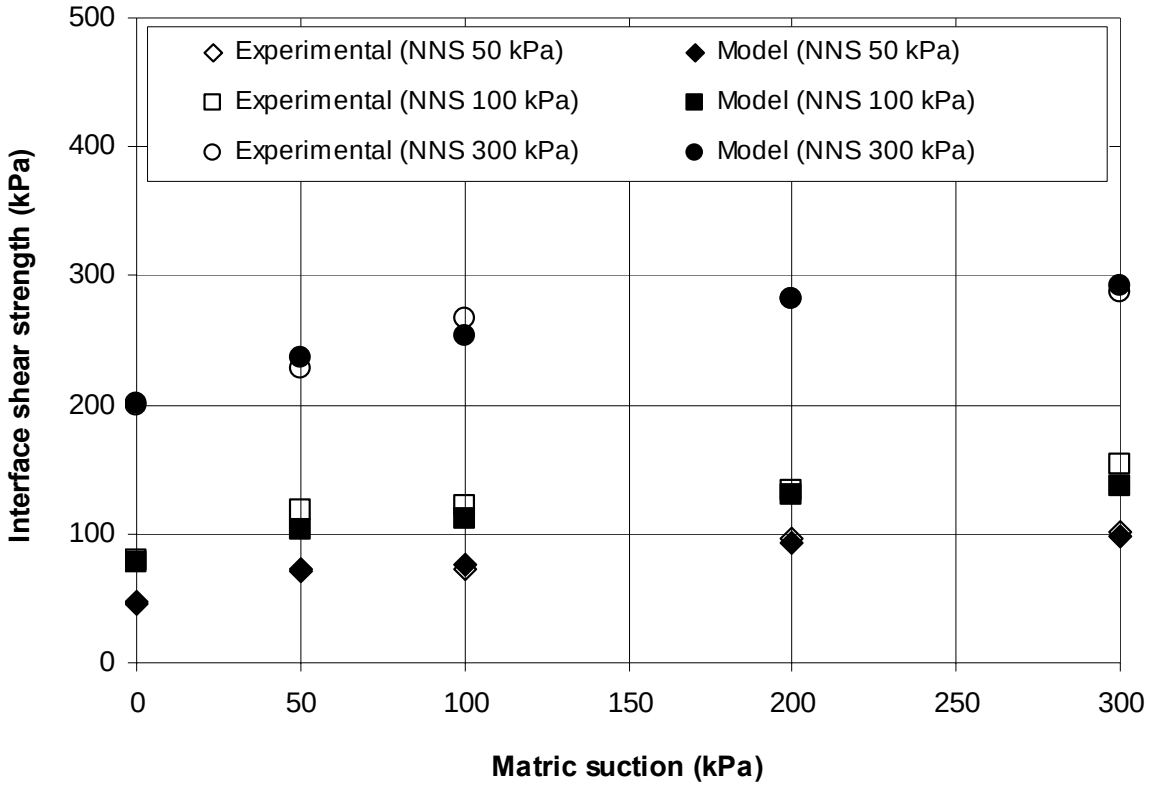

Figure 6.15 Comparison between experimental interface shear strength data and analytical results obtained from the modified model

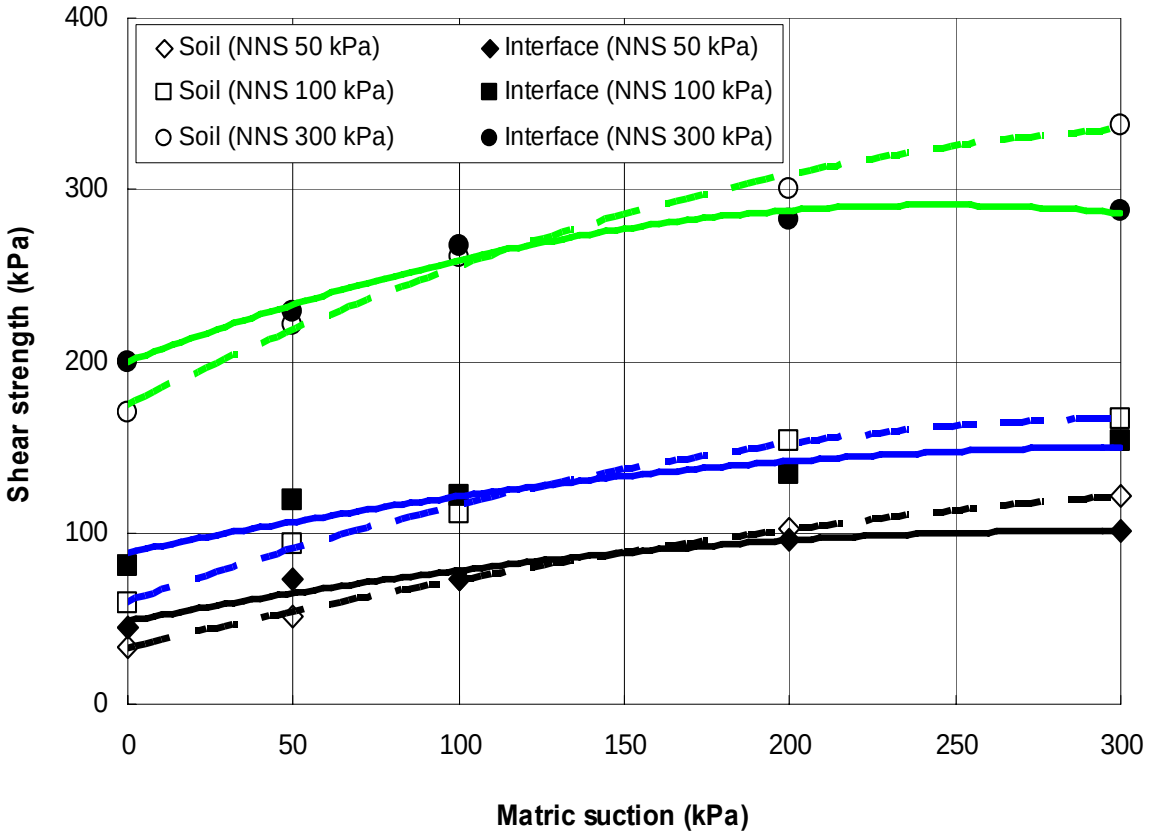

Figure 6.16 Comparison of shear strengths of CDG soil and gravity grouted soil-cement interface under different matric suctions

Chapter 7

PRESSURE GROUTED INTERFACE TEST RESULTS AND INTERPRETATIONS

7.1 INTRODUCTION

It is believed that grouting pressure may have an influence on the interface behavior. Unfortunately, there is a lack of literature regarding the influence of grouting pressure on the fundamental interface behavior especially on direct shear interface behavior. To investigate the influence of grouting pressure on the interface behavior of compacted CDG soil and cement grout at both saturated and unsaturated conditions, a series of consolidated drained direct shear tests were performed under the same net normal stresses and grouting pressures as that of gravity grouted interface tests. Similar to soil-soil direct shear tests, axis-translation technique was applied to control the matric suction. This chapter concentrates on the interface direct shear tests results, their interpretations, and discussions. The influence of grouting pressure on the interface behavior at both saturated and unsaturated conditions are investigated. An especial attention has been paid on variation of interface dilation angle due to grouting pressures. The different parameters obtained from interface tests are compared with those of soil-soil direct shear tests. A general interface shear strength model is proposed incorporating matric suction, net normal stress and grouting pressure to establish the effect of dilation angle on apparent interface friction angle and shear strength by using analytical values of interface dilation angles obtained from dilatancy curves. The experimental shear strength data are compared with the analytical results obtained from

the proposed model. At last, the interface shear strengths for different grouting pressures are compared with the shear strength of compacted CDG soil under same matric suctions and net stresses.

7.2 INTERFACE TESTS AT SATURATED CONDITION

A series of interface direct shear tests were performed at saturated condition (0 kPa matric suction) under different net stresses of 50, 100 and 300 kPa and grouting pressures of 0, 80, 130 and 250. It should be noted that, at saturated condition, the both applied pore-air pressure and pore-water pressure were 200 kPa. The influence of grouting pressure and net normal stress on the behavior of compacted CDG soil-cement grout interface are observed and presented in the following sections.

7.2.1 Influence of net stress and grouting pressure on stress-strain-strength behavior

Figures 7.1, 7.2, 7.3 and 7.4 show the relationships of (a) interface shear stress versus horizontal displacement and (b) vertical displacement versus horizontal displacement from saturated soil-cement grout interface tests under different net normal stresses and grouting pressures. The variation of interface shear stress with horizontal displacement for different grouting pressures (0, 80, 130 and 250 kPa) under the normal stresses of 50, 100 and 300 kPa are presented in Figs. 7.1(a), 7.2(a), 7.3(a) and 7.4(a). The behavior of shear stress-displacement curves of soil-cement grout interface tests is similar to that of soil-soil direct shear tests. The interface shear stress increases with increase of grouting pressure and net normal stress. Under different net normal stresses the stress-displacement curves show strain-hardening behavior for different grouting pressures. It is obvious that the interface shear stress under different grouting pressure is

greater than the shear stress of CDG soil under the same net normal stresses. Hence, it can be concluded that grouting pressure and normal stress have significant influence on the interface behavior of soil-cement grout interface.

Figures 7.1(b), 7.2(b), 7.3(b) and 7.4(b) describe the variation of vertical displacement with horizontal displacement for net normal stress of 50, 100, and 300 kPa under different grouting pressures of 0, 80, 130 and 250 kPa respectively. A contractive behavior is observed for the curves under different net normal stresses and the deformation (contraction) value increases with net stress. The vertical displacement (downward) values of interface tests are lower for different grouting pressures compared to that of CDG soil under the same net stresses. This reflects that soil particles along the failure surface may be locked in place by cement bonds which resist the vertical deformation during shearing.

7.2.2 Influence of net stress and grouting pressure on interface friction angle and adhesion

The relationship between the interface shear strength and net normal stress (failure envelopes) corresponding to different grouting pressures is shown in Fig. 7.5. Similar to soil-soil direct shear tests, the failure point is obtained from the raw test data as that point where the shear load starts decreasing (peak shear load) or where the shear load starts to remain nearly constant. Also, area correction for direct shear test is applied to calculate the interface shear stress.

It is observed that the failure points under different net normal stresses shift towards a larger horizontal displacement as the grouting pressure is increased. This indicates that more cement particles infiltrate into the failure surface as the grouting pressure is

increased, and a strong bonding is formed with the soil particles along the failure plane. The interface shear strength envelopes of the shear stress τ_f *versus* the net normal stress σ'_{nf} for different grouting pressures are approximately linear. The declivity of those envelopes is defined by the effective interface friction angle δ''. The effective interface friction angle δ'' and effective adhesion c''_a for different grouting pressures are obtained from the failure envelopes, and tabulated in Table 7.1. The effective interface friction angle δ'' for different grouting pressures is constant, and can be represented by δ', that is, effective interface friction angle for 0 kPa grouting pressure. However, the effective adhesion intercept c''_a increases with grouting pressure. The increase of adhesion intercept with grouting pressure is attributed to the bonding of soil particles with hydrated cement particles. More the grouting pressure, more the infiltration of cement particles into the soil, resulting stronger bonding, and consequently higher adhesion intercept at higher grouting pressure. The effective adhesion intercept c''_a can be defined by the following equation:

$$c''_a = c'_a + p_g \tan \delta^g \qquad 7.1$$

where c'_a is the effective adhesion for gravity grouted interface (grouting pressure 0 kPa); p_g is the grouting pressure; and δ^g is the angle indicating the rate of increase of interface shear strength with grouting pressure. For gravity grouted interface, $c''_a = c'_a$.

Table 7.1 illustrates that the effective interface friction angles δ'' under different grouting pressures are greater than the effective friction angle of soil ϕ' under the same net normal stress (δ''/ϕ' = 1.05). This implies that CDG soil-cement grout

interface behaves like a rough interface for different grouting pressures at saturated condition, and consistent with the finding of previous chapter (Chapter 6). The rough interface is likely formed due to infiltration of cement particles in the failure plane. However, the infiltration of cement particles may not only depend on grouting pressure but also on void ratio and compaction water content of soil.

7.2.3 Grouting pressure envelope for interface

The variation of interface shear strength with grouting pressure (grouting pressure envelope) for different normal stresses is presented in Fig. 7.6. The interface shear strength increases with grouting pressure and net normal stress. The increase of interface shear strength is approximately linear and the declivity of those envelopes can be represented by δ^g. δ^g is defined as the angle indicating the rate of increase of interface shear strength with grouting pressure under different net normal stresses. The increase of interface shear strength is attributed to the increase of effective adhesion intercept under different grouting pressures as the effective interface frictional angles remain constant.

7.2.4 Proposed model for pressure grouted interface

Though it is considered that grouting pressure may have influence on the interface strength, no interface shear strength equation with due consideration of grouting pressure can be found in existing literatures. To observe the influence of grouting pressure on the interface strength at saturated condition, the following interface shear strength equation is proposed considering grouting pressure as an independent parameter:

$$\tau_f = c_a'' + \sigma_{nf}' \tan\delta'' \qquad 7.2$$

where τ_f is the interface shear strength at failure; c_a'' is the effective adhesion intercept for different grouting pressures; σ_{nf}' is the effective net normal stress variable on the failure plane at failure; δ'' is the effective interface friction angle for different grouting pressures. Combining the eqs. [7.1] and [7.2], the general interface shear strength equation for different grouting pressures at saturated condition can be obtained as follows:

$$\tau_f = c_a' + \sigma_{nf}' \tan\delta' + p_g \tan\delta^g \qquad 7.3$$

where c_a' is the effective adhesion for gravity grouted interface (grouting pressure 0 kPa); σ_{nf}' is the effective net normal stress variable on the failure plane at failure; δ' is the effective interface friction angle for gravity grouted interface; p_g is the grouting pressure; and δ^g is the angle indicating the rate of increase of interface shear strength relative to grouting pressure p_g. The value of δ^g angle under different normal stress is found as 6.6° obtained from grouting pressure envelopes shown in Fig. 7.6.

For the present study, a general form of interface shear strength equation at saturated condition can be obtained as follows by substituting the values of c_a', δ' and δ^g from Table 7.1 and Fig. 7.6 in eq. [7.1]:

$$\tau_f = 16.4 + \sigma_{nf}' \tan 31.5° + p_g \tan 6.6° \qquad 7.4$$

7.2.5 Verification of proposed model for pressure grouted interface

The experimental interface shear strength results and predicted data obtained from proposed model (eq. [7.3]), using effective interface shear strength parameters (c_a' and δ') of compacted CDG soil-cement grout interface at saturated condition, and grouting pressure, are compared and presented in Fig. 7.7. It is obvious from Fig. 7.7 that the

experimental data agrees well with the predictions of proposed model. This indicates that grouting pressure has influence on interface shear strength, and should be considered during design and safety assessment of different CDG soil-cement grout interfaces.

In the present study, the range of grouting pressure applied was 0 - 250 kPa. However, after a certain higher grouting pressure, the interface strength may be constant as the failure surface will be saturated by cement particles, and no change of cement particles quantity is possible along the failure plane after that higher grouting pressure. Hence, further study may be conducted to establish the range of grouting pressure within which eq. [7.3] will be effective.

7.3 INTERFACE TESTS AT UNSATURATED CONDITION

To investigate the behavior of pressure grouted interface at unsaturated condition, a number of direct shear tests are performed under different grouting pressures of 80, 130 and 250 kPa, with the same matric suctions and net stresses of gravity grouted interface tests. All the tests are single-staged consolidated drained direct shear tests. The effect of grouting pressure, matric suction and net normal stress on the behavior of soil-cement grout interface are examined and presented in the following sections.

7.3.1 Influence of suction and net stress on stress-strain-strength behavior

Figures 6.6, 6.7 and 6.8 presented in previous chapter (Chapter 6) show the stress-strain-deformation relationships of gravity grouted (grouting pressure 0 kPa) soil-cement interface for different matric suctions of 0, 50, 100, 200 and 300 kPa and

net stresses of 50, 100 and 300 kPa respectively. The behavior of soil-cement interface for different grouting pressures of 80, 130 and 250 kPa under the same matric suctions and net stresses are shown in Figs. 7.8, 7.9, 7.10, 7.11, 7.12, 7.13, 7.14, 7.15 and 7.16. The variation of interface shear stress with horizontal displacement for different grouting pressures (80, 130 and 250 kPa) under the normal stresses of 50, 100 and 300 kPa are presented in Figs. 7.8(a), 7.9(a), 7.10(a), 7.11(a), 7.12(a), 7.13(a), 7.14(a), 7.15(a) and 7.16(a). The behavior of shear stress-displacement curves of pressure grouted soil-cement interface tests is similar to that of soil-soil direct shear tests and gravity grouted soil-cement interface tests. The interface shear stress increases with increase of grouting pressure and net normal stress. The stress-displacement curves show strain-softening behavior with clear peak shear stress for different grouting pressures under lower net stresses (50 and 100 kPa) as the suction value is increased from saturated condition. On the other hand, a strain-hardening behavior (with no peak or no clear peak shear stress) is observed for different grouting pressures and suctions under higher net stress of 300 kPa. Hence, it can be concluded that similar to gravity grouted soil-cement interface, matric suction and net normal stress have significant influence on the interface behavior of pressure grouted soil-cement interface.

The variation of vertical displacement with horizontal displacement for net normal stress of 50, 100, and 300 kPa under different grouting pressures of 80, 130 and 250 are presented in Figures 7.8(b), 7.9(b), 7.10(b), 7.11(b), 7.12(b), 7.13(b), 7.14(b), 7.15(b) and 7.16(b). A dilative behavior is observed for different grouting pressures at suction range of 50 to 300 kPa under lower net stresses of 50 and 100 kPa, and at suction range of 200 to 300 kPa under higher net stress of 300 kPa. In contrast, a contractive behavior is observed for different grouting pressures and net stresses at saturated condition, also at lower suction range (0 to 100 kPa) under higher net stress of 300 kPa. Hence, it can

be concluded that matric suction and net stress influence significantly the contractive-dilative behavior of pressure grouted interface, which is similar to CDG soil and gravity grouted interface.

7.3.2 Influence of net stress and grouting pressure on interface friction angle and adhesion

The failure envelopes for different matric suctions corresponding to different grouting pressures (80, 130 and 250 kPa) are shown in Fig. 7.17, 7.18 and 7.19. Similar to soil-soil direct shear tests and gravity grouted interface tests, the failure point is obtained from the raw test data as that point where the shear load starts decreasing (peak shear load) or where the shear load starts to remain nearly constant. Also, area correction for direct shear test is applied to calculate the interface shear stress.

The interface shear strength envelopes for different matric suctions corresponding to different grouting pressures are approximately linear. The declivity of those envelopes is represented by apparent interface friction angle $\delta_{\max}$. At saturated condition, $\delta_{\max} = \delta'$. The values of effective angle of interface friction δ' and effective adhesion c'_a obtained from failure envelopes are tabulated in Table 7.2. Similar to CDG soil, the apparent interface friction angle $\delta_{\max}$ increases with matric suction for particular grouting pressure. On the contrary, it decreases with pressure grouting for different matric suctions except saturated condition. The decrease of apparent interface friction angle with pressure grouting may be attributed to the decrease of interface dilation angle. The interface dilation angle may be decreased due to slippage of the interface soil particles as the cement particles infiltrates into the failure plane. The more the grouting pressure, the more the infiltration of cement particles. The apparent adhesion intercept

for different grouting pressures $c_{a(g)}$ increases with matric suction and grouting pressure. The increase of adhesion intercept at saturated condition (0 kPa suction) is attributed to the bonding of soil particles with hydrated cement particles. The change of adhesion intercept at unsaturated condition is due to change of suction and δ^b angle. The adhesion intercept $c_{a(g)}$ can be defined by the following equation:

$$c_{a(g)} = c_a'' + (u_a - u_w)_f \tan\delta^b \qquad 7.5$$

where c_a'' is the effective adhesion for different grouting pressures at saturated condition; $(u_a - u_w)_f$ is the matric suction at failure; and δ^b is the angle indicating the rate of increase in interface shear strength relative to matric suction $(u_a - u_w)_f$. By substituting the value of c_a'' from eq. [7.1] into eq. [7.5], the general equation of adhesion intercept $c_{a(g)}$ can be rewritten as follows considering the influence of matric suction and grouting pressure:

$$c_{a(g)} = c_a' + p_g \tan\delta^g + (u_a - u_w)_f \tan\delta^b \qquad 7.6$$

where p_g is the grouting pressure; and δ^g is the angle indicating the rate of increase of interface shear strength relative to grouting pressure p_g.

7.3.3 Suction envelope for pressure grouted interface

The variation of interface shear strength τ_f with different matric suction $(u_a - u_w)_f$ (suction envelope) for different net stresses and grouting pressures are shown in Fig. 7.20, 7.21 and 7.22. For gravity grouted interface, the interface shear strength increases with matric suction under different net normal stresses. On the other hand, for pressure grouted interface, the interface strength increases with matric suction at lower suction range (upto 150 to 200 kPa) and after that the strength decreases or remain nearly

constant at higher suction range (200 to 300 kPa). However, the relationships between interface shear stress τ_f at failure and matric suction, $(u_a - u_w)_f$ for different grouting pressures are obviously nonlinear, indicating that the δ^b parameter in eq. [7.5] is not constant. The value of δ^b angle obtained from eq. [7.5] for different matric suctions and grouting pressures are tabulated in Table 7.3. Figure 7.23 shows that the variation of δ^b angle with matric suction for different grouting pressures is nonlinear, and decreases with matric suction as well as grouting pressure.

7.3.4 Influence of grouting pressure and suction on interface strength

The relationship between grouting pressure and interface shear strength under different suctions are presented in Figs. 7.24, 7.25 and 7.26 for net stresses of 50, 100 and 300 kPa respectively. Figures 7.24, 7.25 and 7.26 indicate that the interface shear strength increases with grouting pressure under lower suctions of 0 to 50 kPa for particular net stresses. This may be due to the fact that more infiltration of cement particles into the soil as grouting pressure is increased, and existence of strong bonding between soil and cement particles in presence of water. In contrasts, a downward trend is obvious for the interface strength under higher suctions of 200 to 300 kPa for different grouting pressures and net stresses. This may be attributed to the breaking of bonding between cement particles and soil, and slippage provided by the cement particles during shearing at higher suctions due to shortage of water content. The SWRC presented in Fig. 5.1 (chapter 5) shows that the water content starts to decrease as the suction value is increased from air entry value of CDG soil, and reaches to the residual water content about suction of 200 kPa. Figure 5.1 also indicates that the rate of decrement of water content is higher within the suction range of 0 to 100 kPa than the higher suction range of 100 to 300 kPa. Figures 7.24, 7.25 and 7.26 present that the interface shear strength

remains nearly constant with grouting pressure under suction of 100 kPa for different net stresses.

7.3.5 Influence of suction, net stress and grouting pressure on interface dilatancy

Figures 7.27, 7.28 and 7.29 describe the effect of suction on interface dilatancy ($\delta y / \delta h$) under different net normal stresses of 50, 100 and 300 kPa and grouting pressures of 80, 130 and 250 kPa. The peak dilatancy (negative) is observed at higher matric suction under lower net normal stress for particular grouting pressures. The interface dilatancy decreases with net stress. The interface dilatancy essentially increases with an increase of matric suction for particular net stress (similar to CDG soil and gravity grouted interface), but decreases with grouting pressure. The rate of decrement of dilatancy with grouting pressure is higher at higher suction range of 200 to 300 kPa than the lower suction range of 50 to 100 kPa. This may be due to the fact that under higher grouting pressure more cement particles infiltrate into the soil, and at higher suctions the bonding between soil and cement particles completely breaks down due to shortage of water and cement particles existing at surrounding the soil particles facilitate the slippage of soil particles during shearing. The interface dilation angle ψ_i under different net normal stresses, grouting pressures and suctions are calculated from dilatancy curves shown in Figs. 7.27, 7.28 and 7.29 by using the eq. [6.3] mentioned in chapter 6. Similar to CDG soil and gravity grouted interface, the average interface dilation angle is obtained by taking the algebraic mean of all interface dilation angles under different net normal stresses for particular matric suction and grouting pressure. Tables 7.4, 7.5 and 7.6 summarize the analytical values of interface dilation angles and apparent interface friction angles under different suctions for 80, 130 and 250 kPa grouting pressures

respectively. Comparing the average interface dilation angle values for different grouting pressures presented in Tables 6.3 (chapter 6), 7.4, 7.5, and 7.6, it is obvious that the average dilation angle increases with matric suction for particular grouting pressure, but decreases with grouting pressure.

7.3.6 Proposed model for unsaturated pressure grouted interface

It is understandable from the interpretations and discussions presented in previous sections that grouting pressure has significant influence on the behavior of soil-cement grout interface. The interface dilation and adhesion intercept are remarkably influenced by grouting pressure. That is why, it is necessary to consider the influence of grouting pressure while estimating the interface strength. The model (eq. [6.3]) proposed for predicting the unsaturated shear strength of gravity grouted interface can be rewritten as follows for determining the shear strength of soil-cement interface considering the influence of matric suction and grouting pressure on interface dilation angle as well as on adhesion intercept:

$$\tau_f = c_{a(g)} + (\sigma_n - u_a)_f \tan(\delta' + \psi_i) \qquad 7.7$$

where $c_{a(g)}$ is the adhesion intercept for different grouting pressure, and can be defined by eq. [7.6]; $(\sigma_n - u_a)_f$ is the net normal stress at failure; δ' is the effective interface friction angle of gravity grouted interface at saturated condition; ψ_i is the interface dilation angle; and $(\delta' + \psi_i) = \delta_{\max}$ is the apparent interface friction angle. By substituting the value of $c_{a(g)}$ from eq. [7.6] into eq. [7.7], the general equation for interface shear strength of soil-cement grout interface under different matric suctions, net stresses and grouting pressures can be obtained as follows:

$$\tau_f = c'_a + (\sigma_n - u_a)_f \tan(\delta' + \psi_i) + (u_a - u_w)_f \tan\delta^b + p_g \tan\delta^g \qquad 7.8$$

where c'_a is the effective adhesion of gravity grouted interface (0 kPa grouting pressure) at saturated condition; $(\sigma_n - u_a)_f$ is the net normal stress at failure; δ' is the effective interface friction angle of gravity grouted interface at saturated condition; ψ_i is the interface dilation angle; $(u_a - u_w)_f$ is the matric suction at failure; δ^b is the angle indicating the rate of increase in interface shear strength relative to matric suction $(u_a - u_w)_f$; p_g is the grouting pressure; and δ^g is the angle indicating the rate of increase of interface shear strength relative to grouting pressure p_g.

7.3.7 Verification of proposed pressure grouted interface model

The model (eq. [7.8]) proposed for predicting shear strength of pressure grouted soil-cement interface needs to be verified. That is why, a better correlation between experimental interface shear strength data and prediction of proposed model is essential. The comparison between experimental data and the analytical shear strength results obtained from the proposed model (eq. [7.8]) is shown in Figs. 7.30, 7.31, 7.32 and 7.33 for 0, 80, 130 and 250 kPa grouting pressures respectively. The analytical shear strength results is obtained using effective interface shear strength parameters at saturated condition (c'_a and δ') of gravity grouted interface between compacted CDG soil and cement grout, analytical values of interface dilation angle ψ_i, δ^b angles under different suctions (refer to Table 7.3), grouting pressure, and δ^g angle under different grouting pressures (refer to Fig. 7.6). It is obvious from Figs. 7.30, 7.31, 7.32 and 7.33 that the interface shear strength predicted from the proposed model agrees well with the experimental shear strength data for different net normal stresses, matric suctions and grouting pressures. This indicates that matric suction, normal stress and grouting pressure have significant influence on shear behavior of compacted CDG soil and

cement grout interface. However, the proposed model should be verified for different types of soil, suction, net stress and grouting pressure range before apply for cast in-situ soil-cement grout interface.

7.3.8 Soil shear strength and pressure grouted interface strength

The comparison between experimental shear strength of compacted CDG soil and pressure grouted soil-cement interface shear strength for different suctions and grouting pressures are presented in Figs. 7.34, 7.35 and 7.36 under net normal stresses of 50, 100 and 300 kPa respectively. Figures 7.34, 7.35 and 7.36 indicate that the shear strength of pressure grouted interface is greater than the shear strength of CDG soil within the suction range of 0 to 100 kPa for different net normal stresses. The increase of interface shear strength at lower suction is due to strong bonding between soil and cement particles in presence of bulk water. However, the interface shear strength is lower than the shear strength of CDG soil at higher suction range of 200 to 300 kPa. The decrease of interface shear strength at higher suction range may be attributed to breaking of bonding due to shortage of bulk water, slippage provided by the cement particles present around the soil particles during shearing. For the above mentioned reasons, lower values of interface friction angle, δ^b angle and interface dilation angle ψ_i are found for different grouting pressures at higher matric suctions compared to CDG soil (refer to Table 7.7). It is obvious from Figs. 7.34, 7.35 and 7.36 that the strength of higher grouting pressure (250 kPa) interface is greater than the strength of CDG soil as well as gravity grouted interface under different net stresses at saturated condition. This indicates that the stability of slopes can be boosted up at saturated condition by the inclusion of pressure grouted soil nails into the slopes instead of gravity grouted soil nails. At saturated condition and lower suctions, the failure of slope may be happened in

the soil as the strength of soil is lower than the strength of interface. On the other hand, at higher suctions, failure of slope may be happened in the interface zone rather than in the soil as the strength of soil is greater than the interface.

From Table 7.7, it is obvious that the ratio of δ_{max}/ϕ_{max} is greater than or equal to 1 under different matric suctions for gravity grouted interface, which indicates a rough interface (Kulhawy and Peterson 1979). However, δ_{max}/ϕ_{max} becomes lower than 1 as the grouting pressure is increased, which indicates a smooth interface (Kulhawy and Peterson 1979). Thus, it can be concluded that the behavior of compacted CDG soil-cement grout interface changes from rough interface towards the smooth interface due to influence of grouting pressure.

7.4 SUMMARY

A series of consolidated drained direct shear tests are conducted on compacted CDG soil-cement grout interface to investigate the influence of grouting pressure on the behavior of interface. The direct shear tests are performed under the same net stresses and matric suction as that of gravity grouted interface tests. A total of 45 interface tests are performed for grouting pressures of 80, 130 and 250 kPa. Typical tests results and their interpretations have been presented and discussed. The initial presentation of the test results in this chapter illustrates the influence of grouting pressure on interface behavior at saturated condition. A model has been proposed to take into account the influence of grouting pressure on interface strength at saturated condition. Finally, the influence of grouting pressure on interface behavior at unsaturated condition is presented and discussed. Variations of hardening-softening and contractive-dilative behaviors of soil-cement interface under different grouting pressures, suctions and net

normal stresses are illustrated. Similar to CDG soil and gravity grouted interface, the interface failure envelopes for different grouting pressures under different suctions are found to be linear. Whereas, nonlinearity is obvious for interface suction envelopes for different grouting pressures under different net normal stresses. An especial attention has been paid on the influence of grouting pressure and suction on interface dilatancy. The interface dilation angle increases with matric suction, but decrease with grouting pressure. The different parameters obtained from interface tests are compared with those of CDG soil tests. A general model has been proposed to consider the influence of grouting pressure, matric suction and net stress on the cast in-situ soil-cement interface strength. The prediction of the proposed model is found to agree well with the experimental results for different grouting pressure, matric suction and net normal stress. The interface shear strength data for different grouting pressures is compared with the shear strength of CDG soil under the same suctions and net normal stresses. The overall interface strength for different grouting pressures and matric suctions under particular net stress is greater than the strength of CDG soil at saturated condition. It is obvious from the analysis that the soil-cement grout interface behavior changes from rough interface towards the smooth interface at unsaturated condition due to influence of pressure grouting.

This chapter illustrates the direct shear test results of pressure grouted soil-cement interface under different suctions and net stresses, their interpretations and discussions concentrating on the influence of grouting pressure on interface dilatancy and shear strength, a general model for soil-cement grout interface incorporating the influence of matric suction, net stress and grouting pressure, and comparison between shear strength of CDG soil and soil-cement interface strength for different grouting pressure. The next chapter will present the important findings and conclusions of soil-soil direct shear test

results and soil-cement interface test results, and recommendations for future study in the topic area.

Table 7.1 Variation of effective interface friction angle δ'', effective adhesion c_a'' and δ''/ϕ' ratio with grouting pressure obtained from failure envelopes at saturated condition

Grouting pressure (kPa)	0	80	130	250
δ'' (deg)	31.5	31.5	31.5	31.5
c_a'' (kPa)	16.4	22.5	30.5	41.8
δ''/ϕ'	1.05	1.05	1.05	1.05

Table 7.2 Variation of apparent interface friction angle $\delta_{\max}$ and adhesion intercept c_a with matric suction and grouting pressure obtained from failure envelopes

Matric suction (kPa) / Grouting pressure (kPa)		0	50	100	200	300
0	$\delta_{\max}$ (deg)	31.5	33.2	37.0	37.5	38.1
	c_a (kPa)	16.4	37.5	41.6	54.0	58.5
80	$\delta_{\max}$ (deg)	31.5	32.4	37.0	37.3	38.0
	c_a (kPa)	22.5	36.2	47.7	56.4	64.5
130	$\delta_{\max}$ (deg)	31.5	33.2	35.5	35.6	37.5
	c_a (kPa)	30.5	51.3	55.5	57.4	65.8
250	$\delta_{\max}$ (deg)	31.5	32.5	35.0	35.6	36.2
	c_a (kPa)	41.8	54.7	64.7	70.9	73.9

Table 7.3 Variation of δ^b angle with matric suction for different grouting pressures

	δ^b (deg)				
Matric suction (kPa) / Grouting pressure (kPa)	0	50	100	200	300
0	31.5	22.9	14.2	10.7	8.0
80	31.5	15.3	14.1	9.6	8.0
130	31.5	22.5	14.0	7.7	6.7
250	31.5	14.5	12.9	8.3	6.1

Table 7.4 Analytical values of interface dilation angle and apparent interface friction angle for different matric suctions obtained from dilatancy curves (GP 80 kPa)

Matric suction (kPa)	Net normal stress (kPa)	Interface dilation angle (°)	Average dilation angle ψ_i (°)	Effective adhesion c'_a (kPa)	Effective interface friction angle δ' (°)	Apparent interface friction angle $\delta_{\max} = (\delta' + \psi_i)$ (°)
0	50	0.0	0.0	22.5	31.5	31.5
	100	0.0				
	300	0.0				
50	50	3.4	2.0	22.5	31.5	33.5
	100	2.6				
	300	0.0				
100	50	7.4	3.9	22.5	31.5	35.4
	100	4.4				
	300	0.0				
200	50	8.2	5.2	22.5	31.5	36.7
	100	6.5				
	300	1.0				
300	50	8.7	6.3	22.5	31.5	37.8
	100	8.0				
	300	2.1				

Table 7.5 Analytical values of interface dilation angle and apparent interface friction angle for different matric suctions obtained from dilatancy curves (GP 130 kPa)

Matric suction (kPa)	Net normal stress (kPa)	Interface dilation angle (°)	Average dilation angle ψ_i (°)	Effective adhesion c'_a (kPa)	Effective interface friction angle δ' (°)	Apparent interface friction angle $\delta_{max} = (\delta' + \psi_i)$ (°)
0	50	0.0	0.0	30.5	31.5	31.5
	100	0.0				
	300	0.0				
50	50	3.2	1.5	30.5	31.5	33.0
	100	1.3				
	300	0.0				
100	50	6.5	3.0	30.5	31.5	34.5
	100	2.5				
	300	0.0				
200	50	7.6	4.1	30.5	31.5	35.6
	100	4.2				
	300	0.6				
300	50	8.8	5.9	30.5	31.5	37.4
	100	6.4				
	300	2.4				

Table 7.6 Analytical values of interface dilation angle and apparent interface friction angle for different matric suctions obtained from dilatancy curves (GP 250 kPa)

Matric suction (kPa)	Net normal stress (kPa)	Interface dilation angle (°)	Average dilation angle ψ_i (°)	Effective adhesion c'_a (kPa)	Effective interface friction angle δ' (°)	Apparent interface friction angle $\delta_{max} = (\delta' + \psi_i)$ (°)
0	50	0.0	0.0	41.8	31.5	31.5
	100	0.0				
	300	0.0				
50	50	3.4	1.7	41.8	31.5	33.2
	100	1.7				
	300	0.0				
100	50	5.2	2.4	41.8	31.5	33.9
	100	2.0				
	300	0.0				
200	50	7.9	4.0	41.8	31.5	35.5
	100	3.8				
	300	0.4				
300	50	8.7	5.3	41.8	31.5	36.8
	100	5.9				
	300	1.4				

Table 7.7 Variation of δ_{max}/ϕ_{max}, c_a/c and δ^b/ϕ^b ratio with matric suction and grouting pressure

Grouting pressure (kPa)	Matric suction (kPa)	0	50	100	200	300
0	δ_{max}/ϕ_{max}	1.05	1.00	1.00	1.00	1.00
	c_a/c	-	1.82	1.15	0.79	0.63
	δ^b/ϕ^b	1.05	1.02	0.71	0.57	0.46
	ψ_i/ψ	-	0.65	0.78	0.97	0.97
80	δ_{max}/ϕ_{max}	1.05	0.98	1.00	0.99	0.98
	c_a/c	-	1.58	1.33	0.82	0.69
	δ^b/ϕ^b	1.05	0.68	0.71	0.51	0.46
	ψ_i/ψ	-	0.65	0.85	0.88	0.96
130	δ_{max}/ϕ_{max}	1.05	0.98	0.96	0.95	0.97
	c_a/c	-	2.49	1.53	0.83	0.70
	δ^b/ϕ^b	1.05	1.00	0.70	0.41	0.39
	ψ_i/ψ	-	0.48	0.65	0.69	0.89
250	δ_{max}/ϕ_{max}	1.05	0.98	0.94	0.95	0.94
	c_a/c	-	2.65	1.79	1.04	0.79
	δ^b/ϕ^b	1.05	0.64	0.65	0.42	0.35
	ψ_i/ψ	-	0.55	0.52	0.68	0.80

*ψ is the average of dilation angles under 50, 100 and 300 kPa net normal stresses for CDG soil

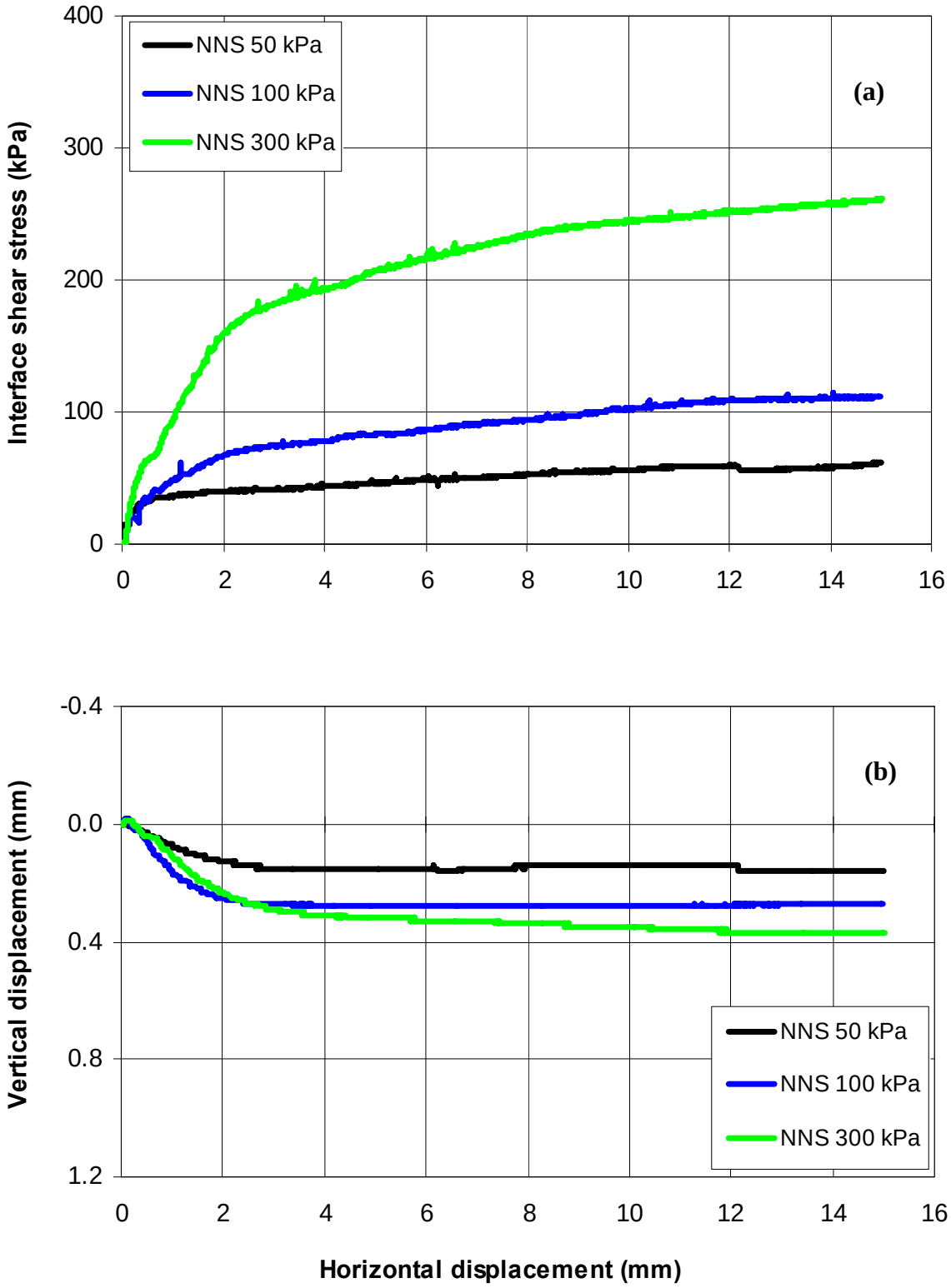

Figure 7.1 Curves of (a) interface shear stress versus horizontal displacement; and (b) vertical displacement versus horizontal displacement for different net normal stresses under 0 kPa suction and 0 kPa grouting pressure

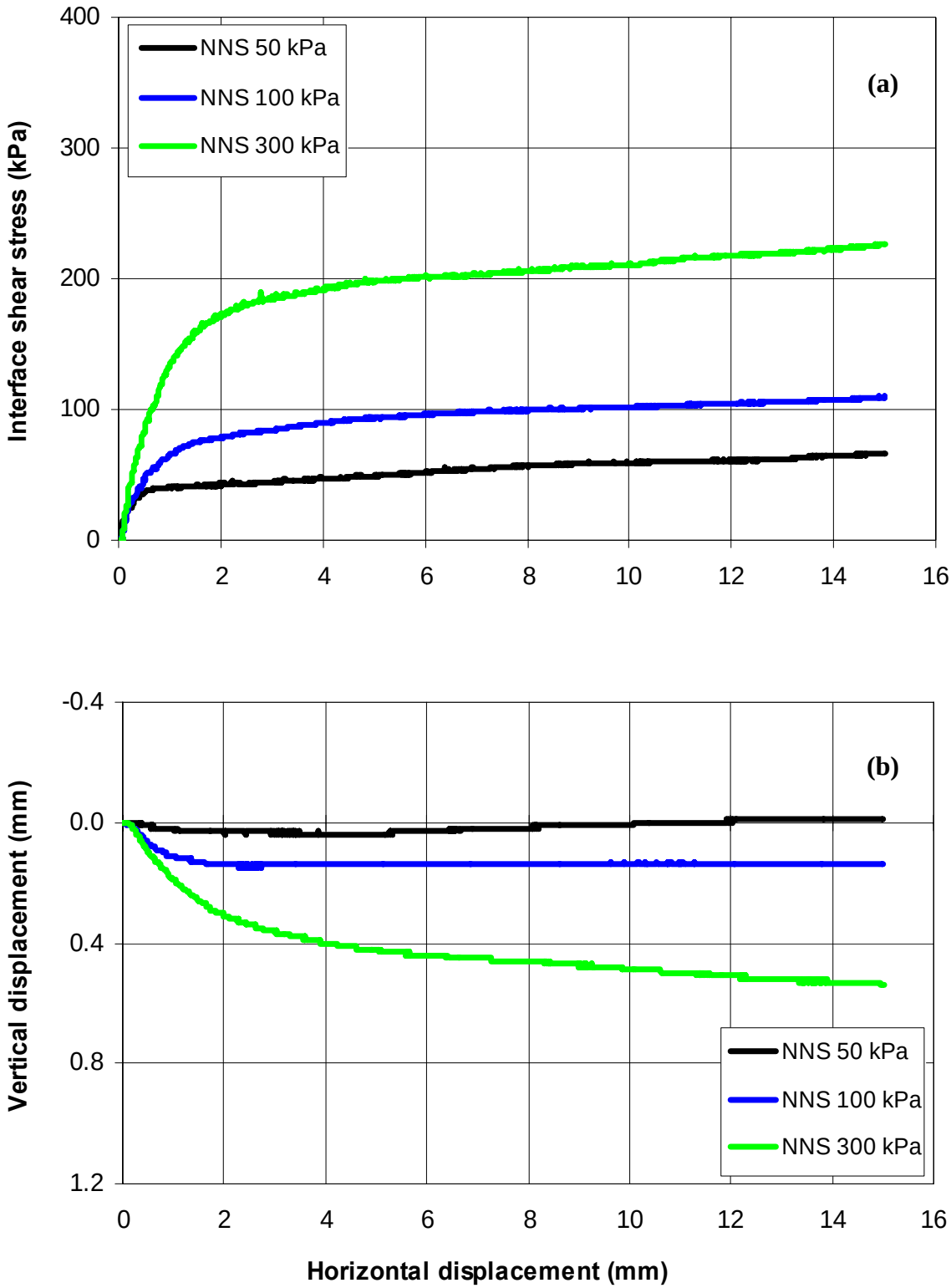

Figure 7.2 Curves of (a) interface shear stress versus horizontal displacement; and (b) vertical displacement versus horizontal displacement for different net normal stresses under 0 kPa suction and 80 kPa grouting pressure

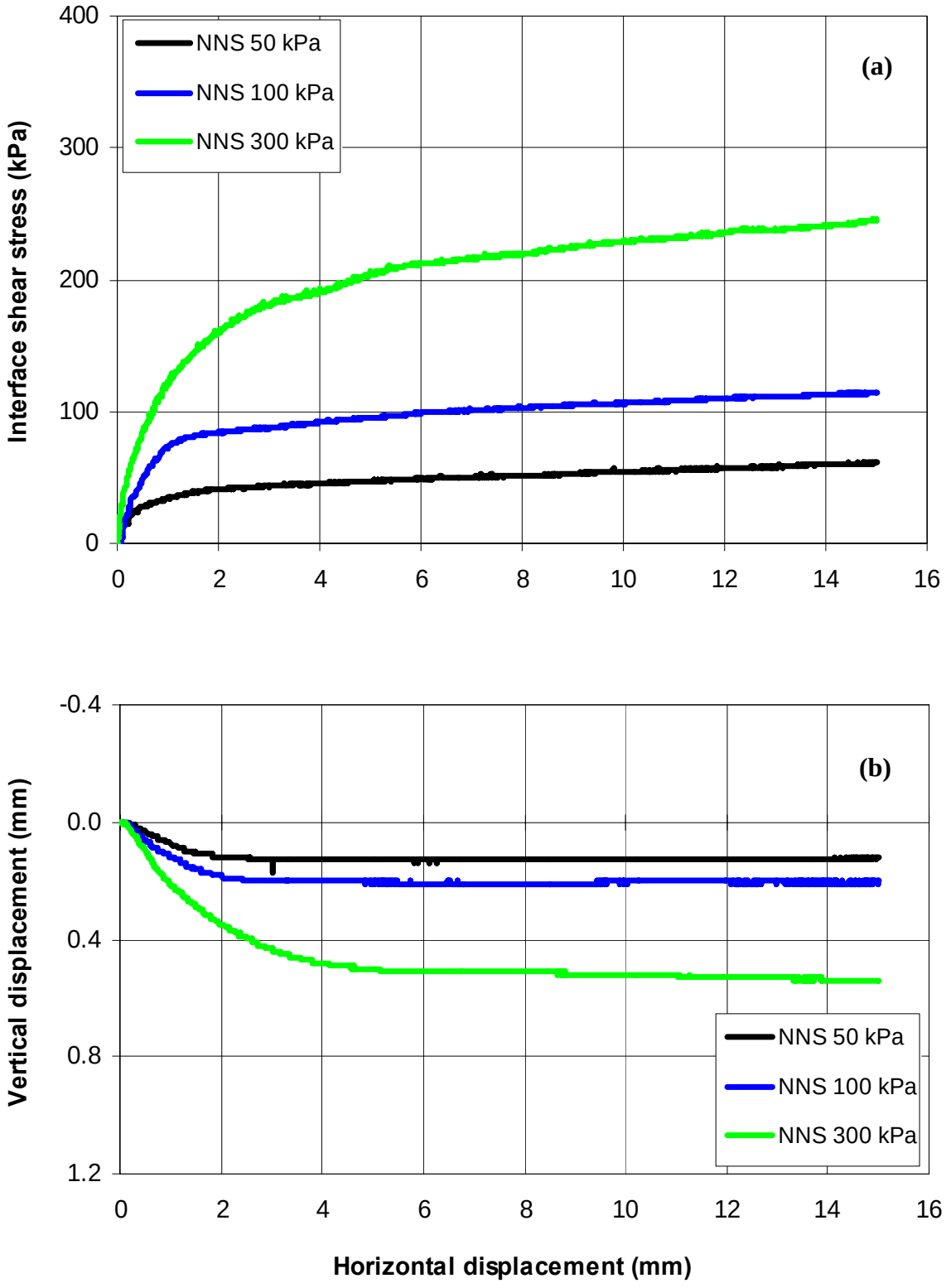

Figure 7.3 Curves of (a) interface shear stress versus horizontal displacement; and (b) vertical displacement versus horizontal displacement for different net normal stresses under 0 kPa suction and 130 kPa grouting pressure

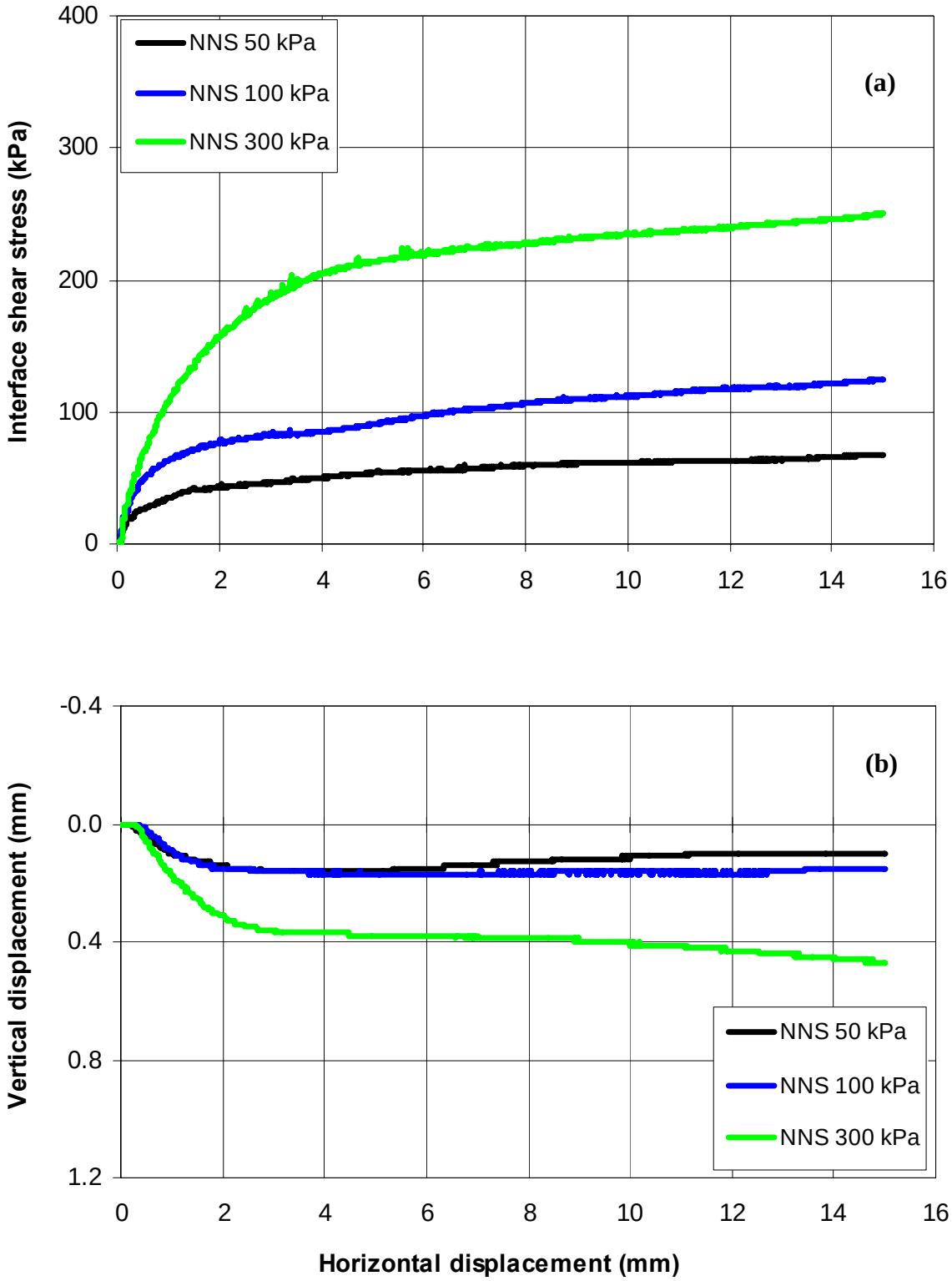

Figure 7.4 Curves of (a) interface shear stress versus horizontal displacement; and (b) vertical displacement versus horizontal displacement for different net normal stresses under 0 kPa suction and 250 kPa grouting pressure

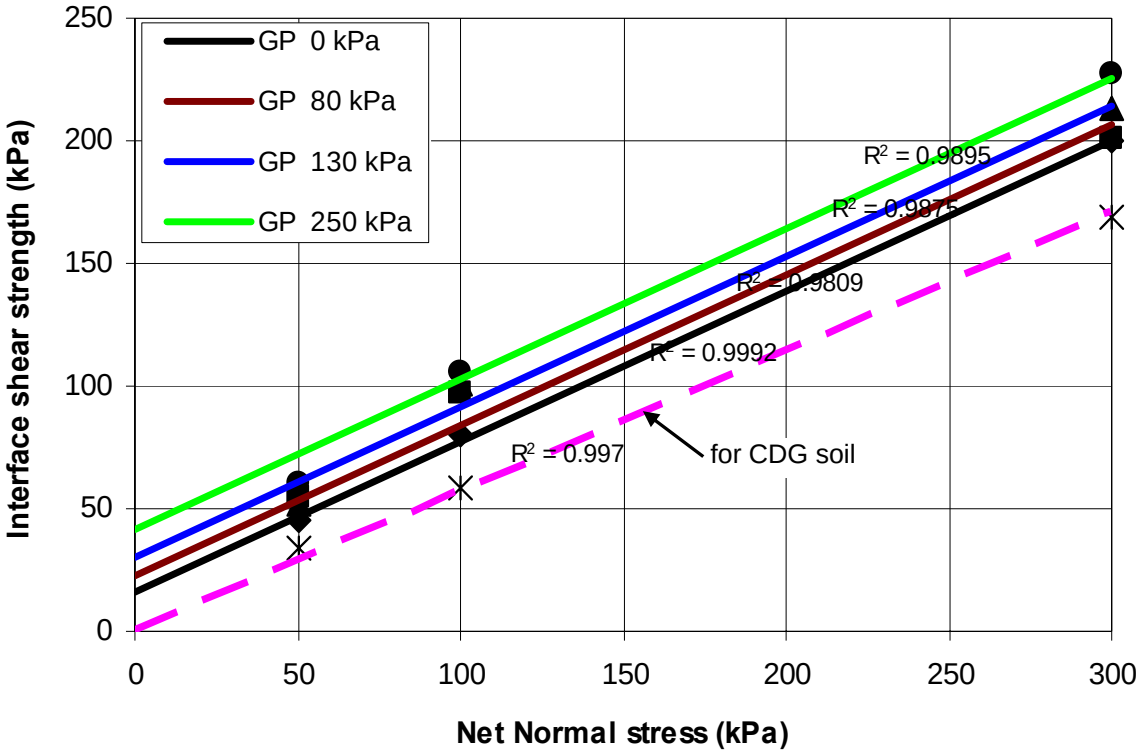

Figure 7.5 Interface failure envelopes corresponding to different grouting pressures at saturated condition (0 kPa matric suction)

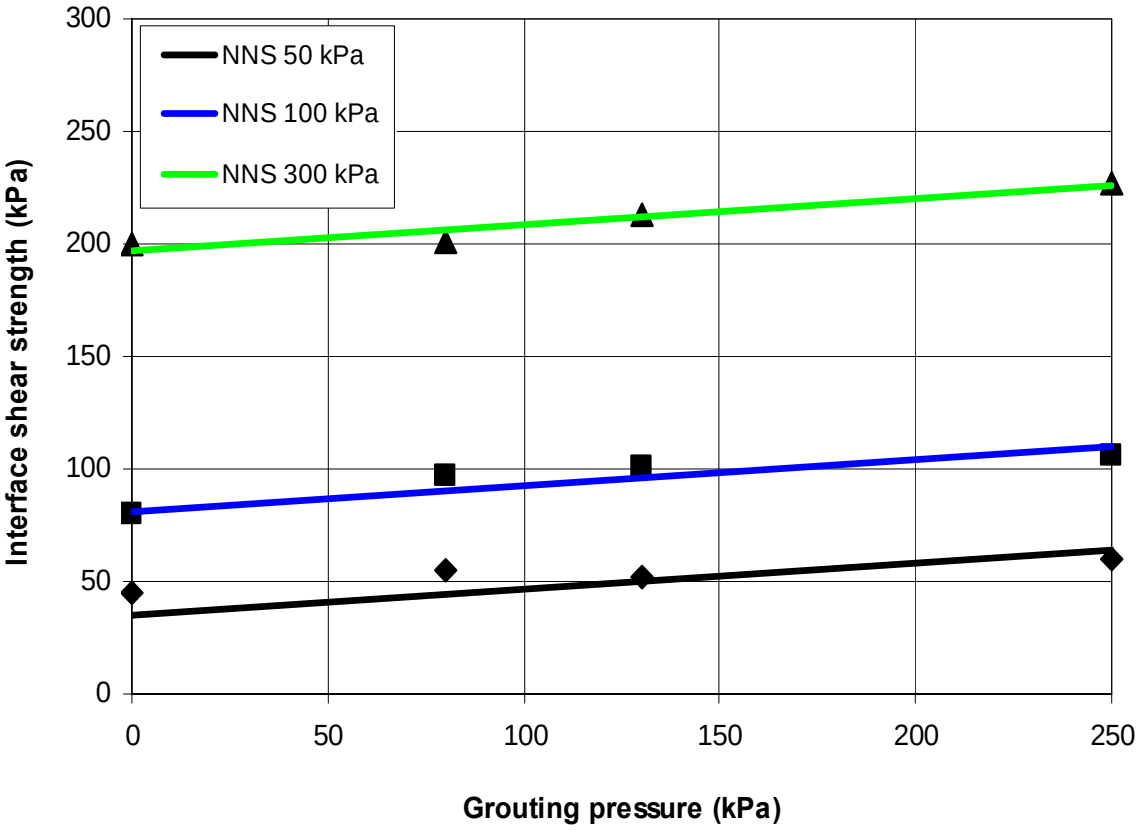

Figure 7.6 Grouting pressure envelopes corresponding to different net normal stresses at saturated condition (0 kPa matric suction)

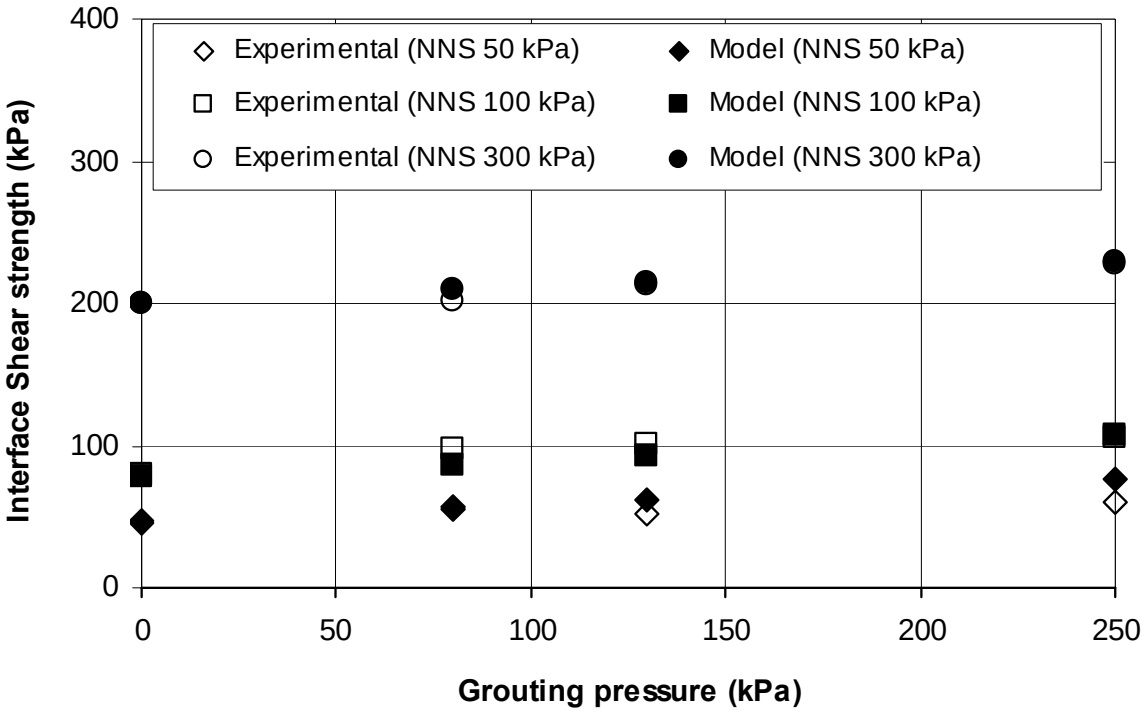

Figure 7.7 Comparison between experimental interface shear strength data and predictions of the modified model at saturated condition

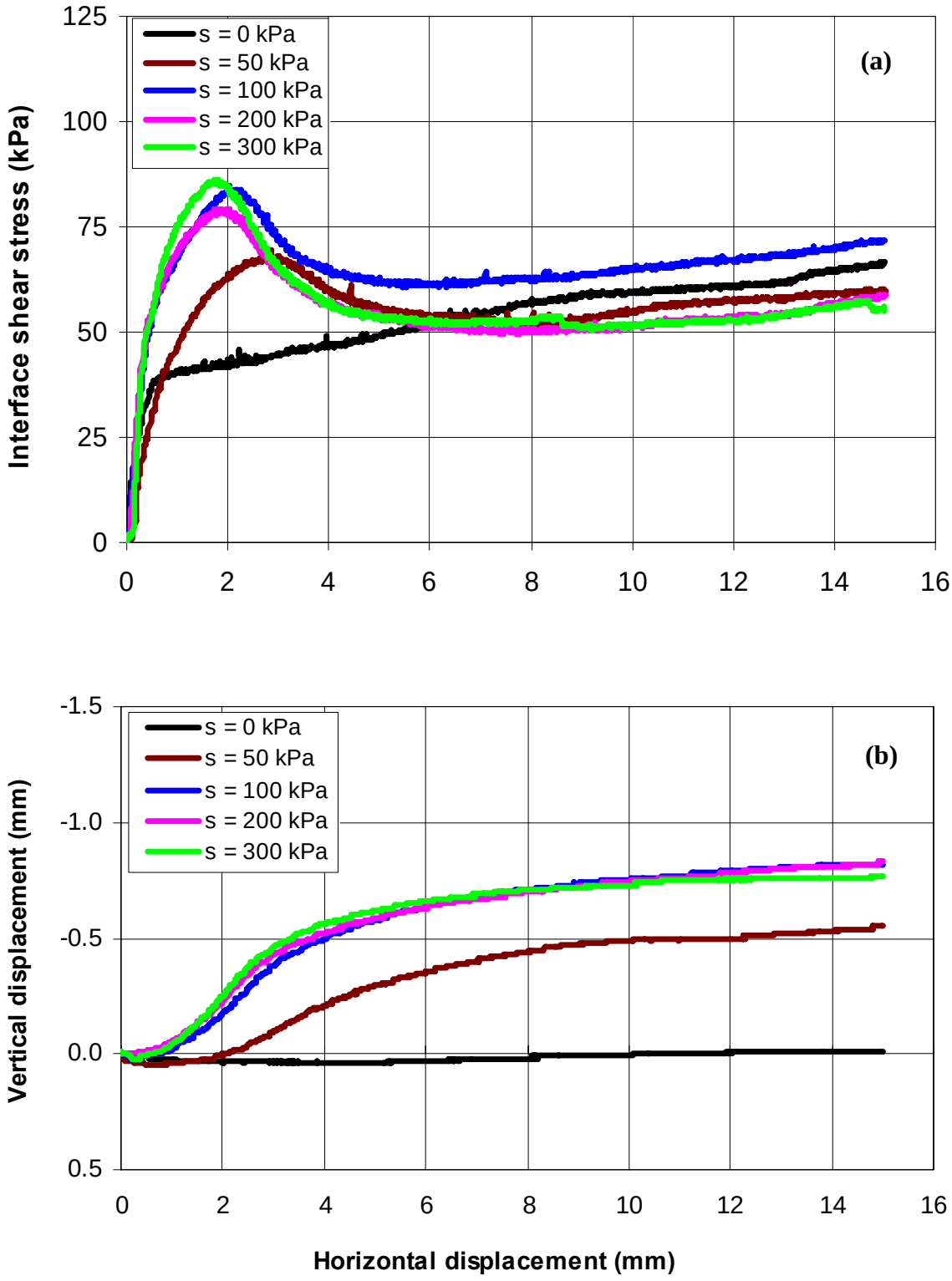

Figure 7.8 Curves of (a) interface shear stress versus horizontal displacement; and (b) vertical displacement versus horizontal displacement for different suctions under 50 kPa net normal stress and 80 kPa grouting pressure

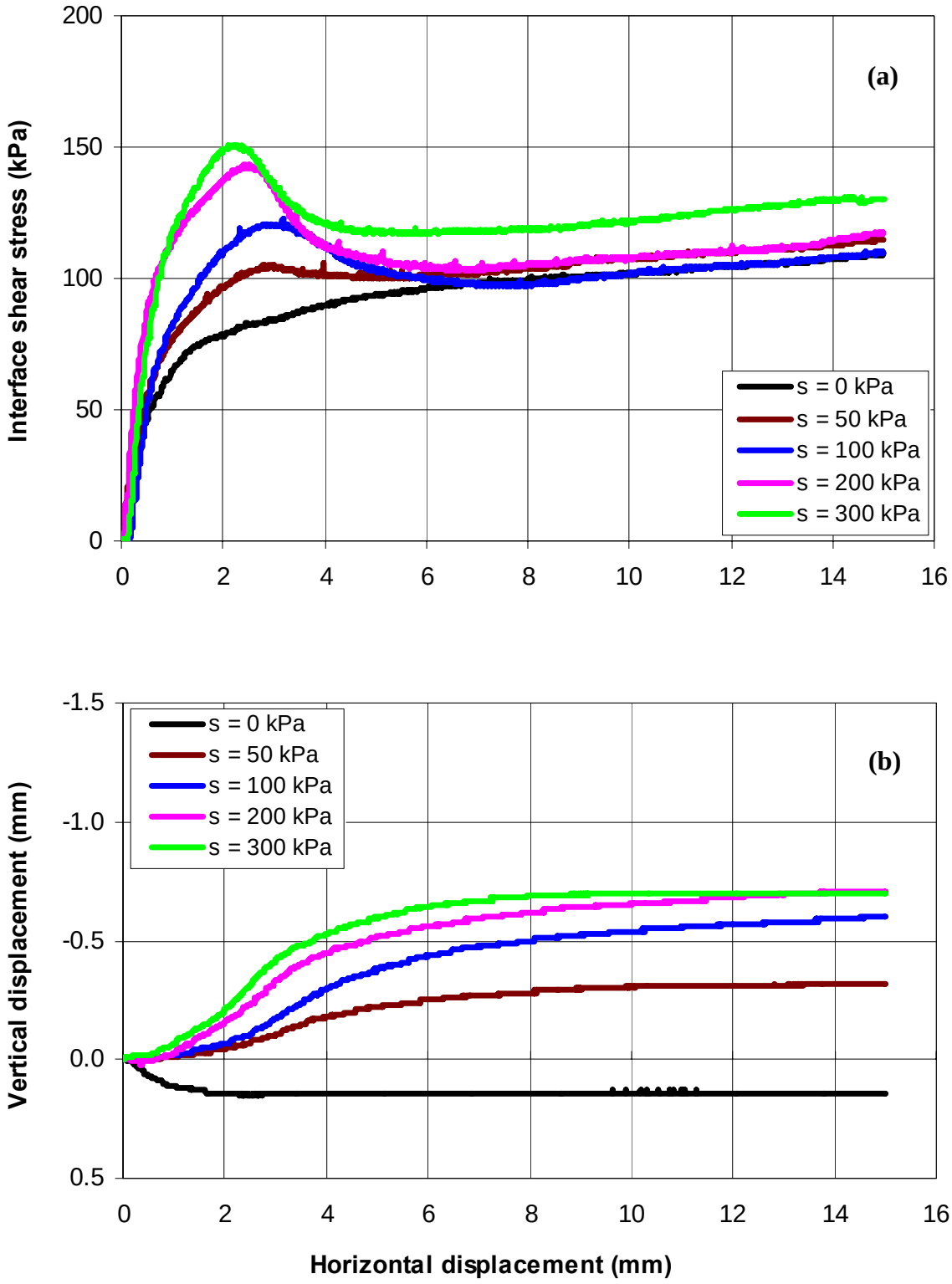

Figure 7.9 Curves of (a) interface shear stress versus horizontal displacement; and (b) vertical displacement versus horizontal displacement for different suctions under 100 kPa net normal stress and 80 kPa grouting pressure

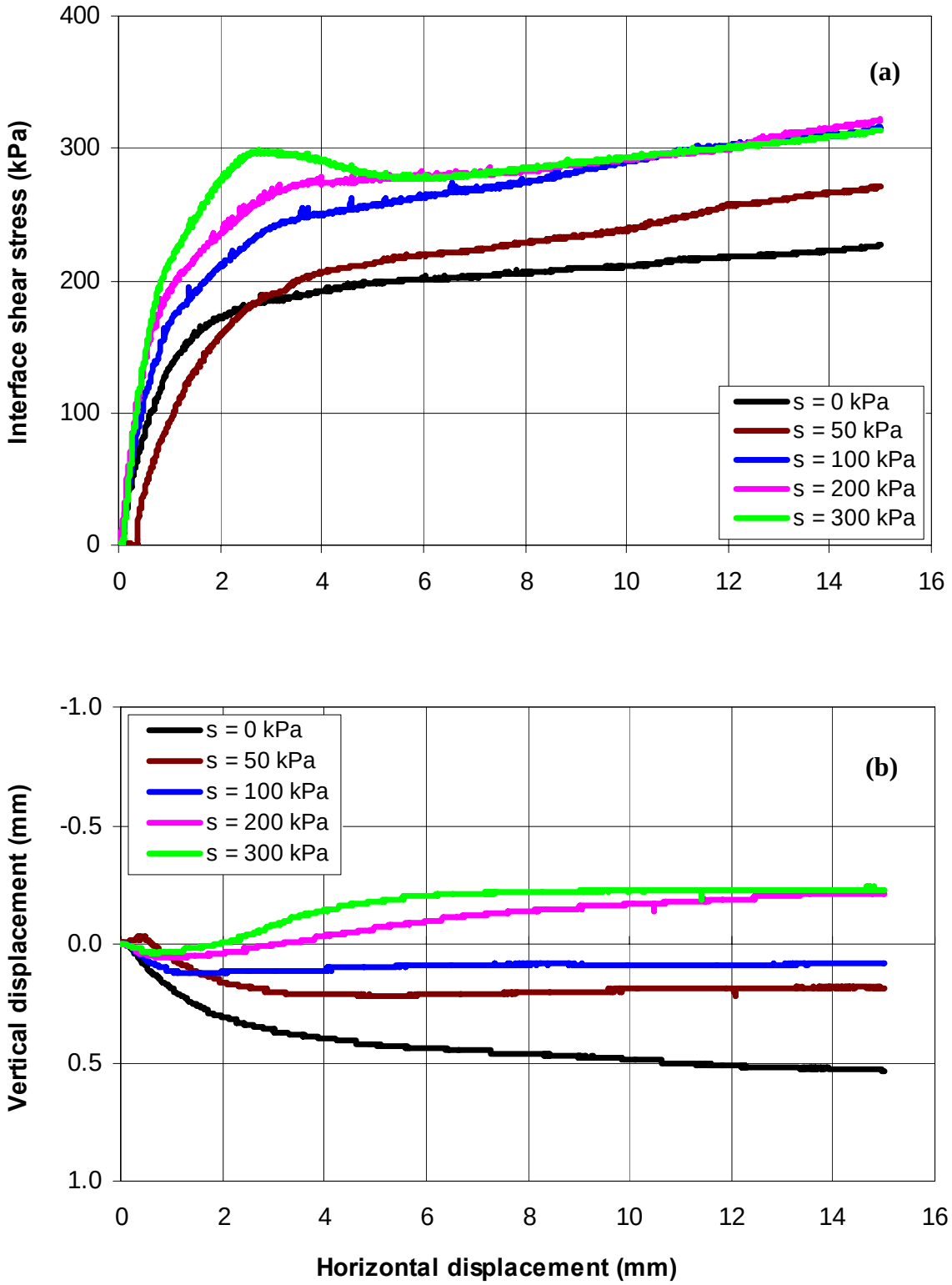

Figure 7.10 Curves of (a) interface shear stress versus horizontal displacement; and (b) vertical displacement versus horizontal displacement for different suctions under 300 kPa net normal stress and 80 kPa grouting pressure

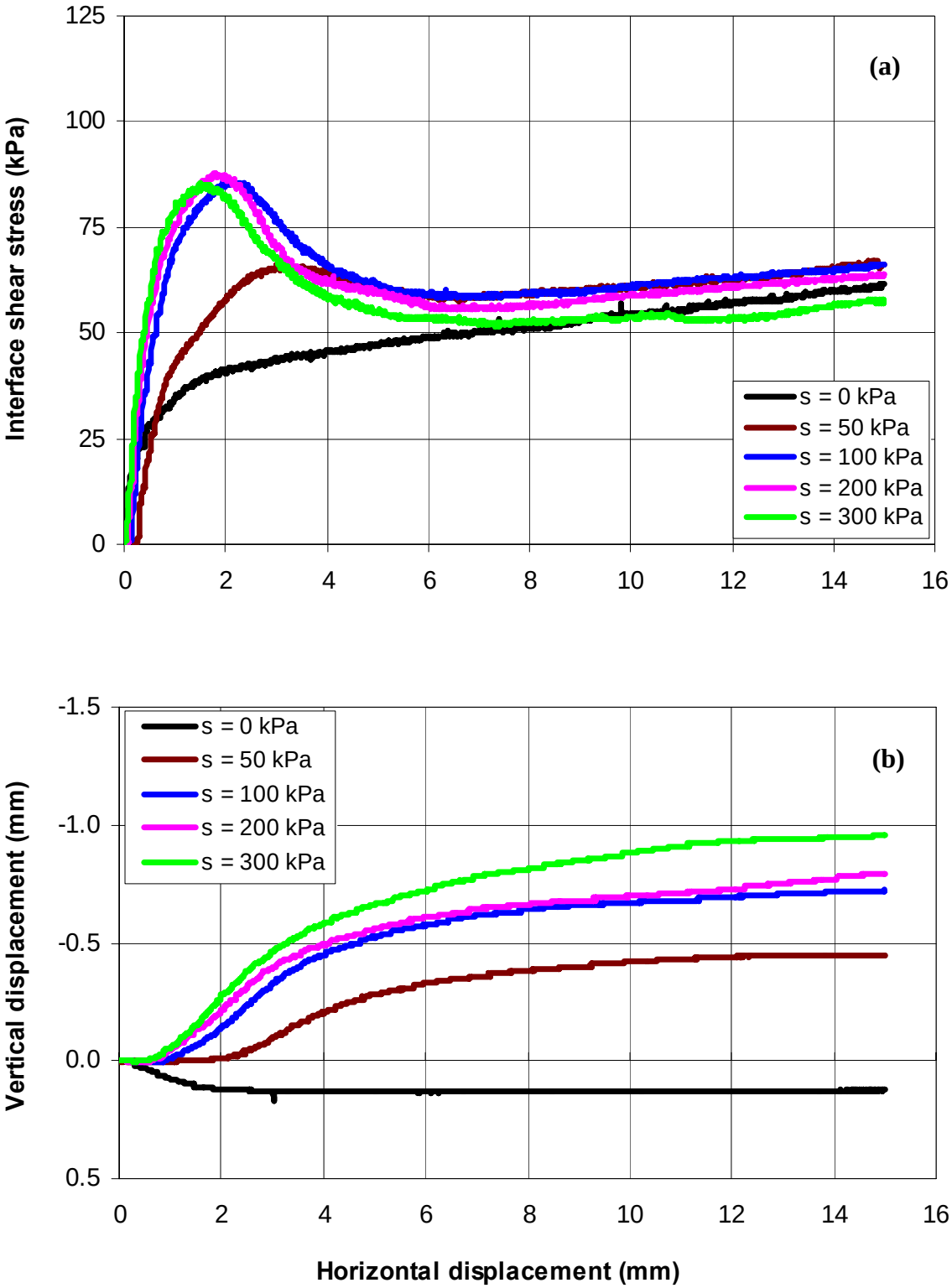

Figure 7.11 Curves of (a) interface shear stress versus horizontal displacement; and (b) vertical displacement versus horizontal displacement for different suctions under 50 kPa net normal stress and 130 kPa grouting pressure

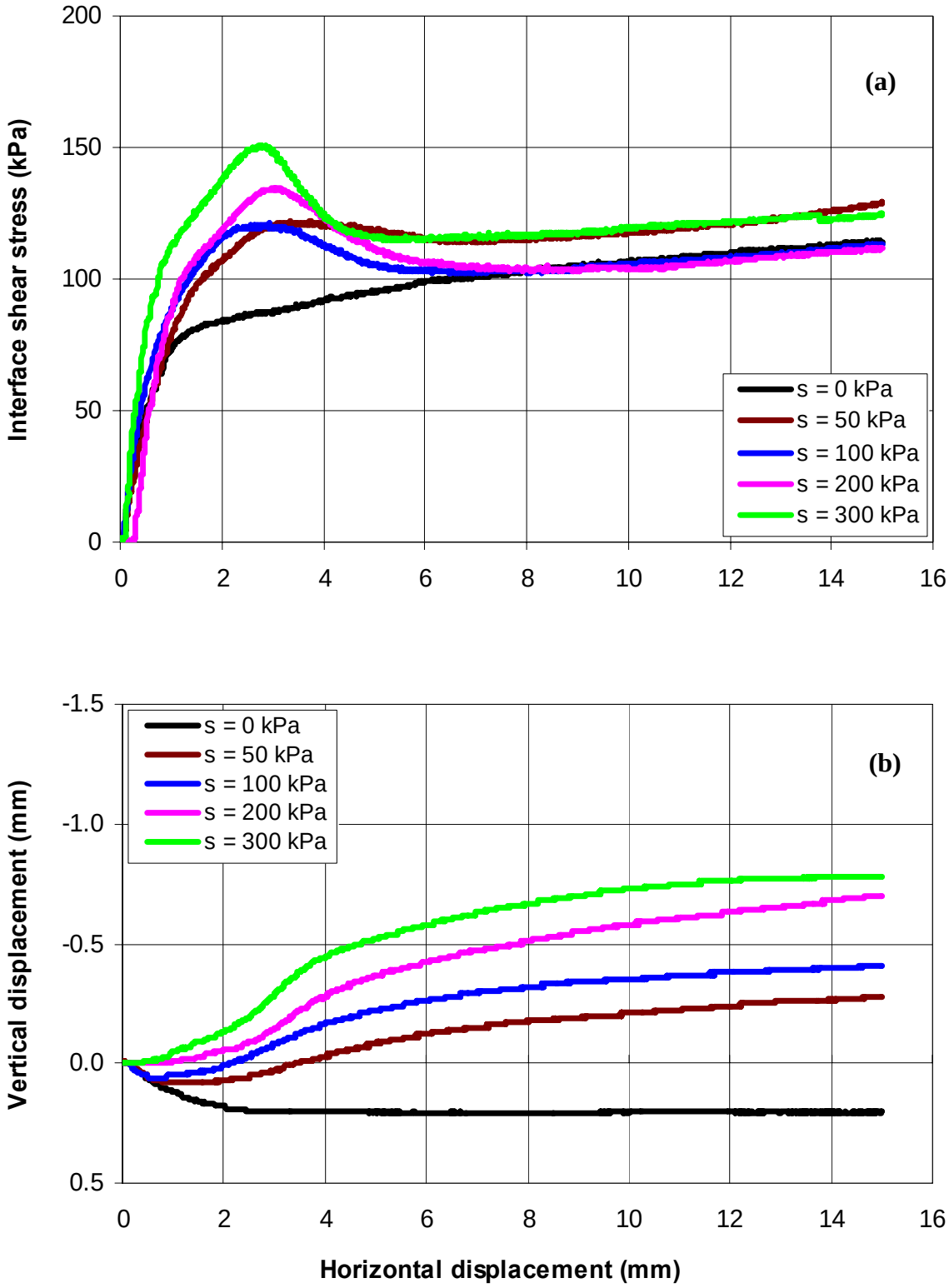

Figure 7.12 Curves of (a) interface shear stress versus horizontal displacement; and (b) vertical displacement versus horizontal displacement for different suctions under 100 kPa net normal stress and 130 kPa grouting pressure

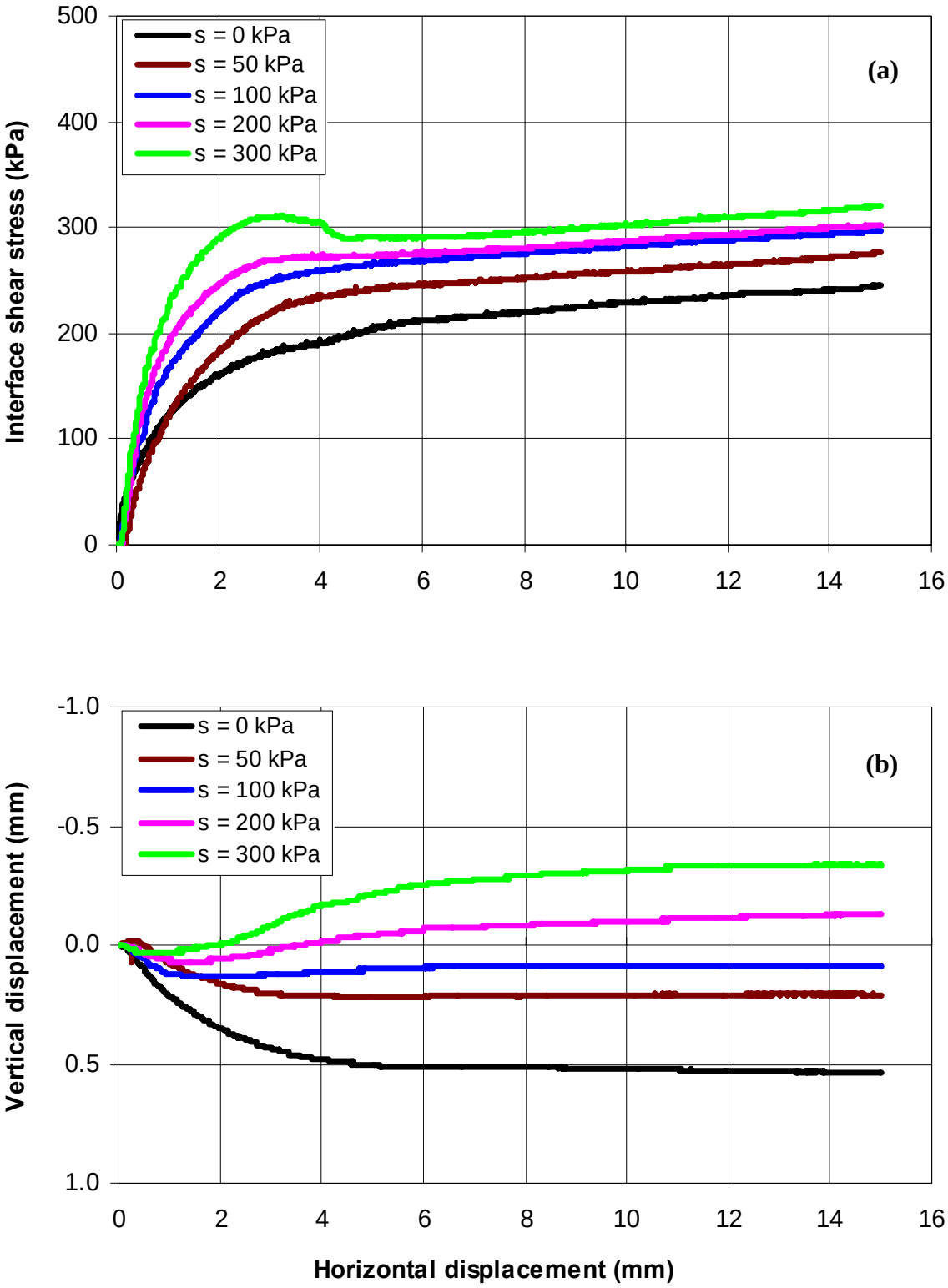

Figure 7.13 Curves of (a) interface shear stress versus horizontal displacement; and (b) vertical displacement versus horizontal displacement for different suctions under 300 kPa net normal stress and 130 kPa grouting pressure

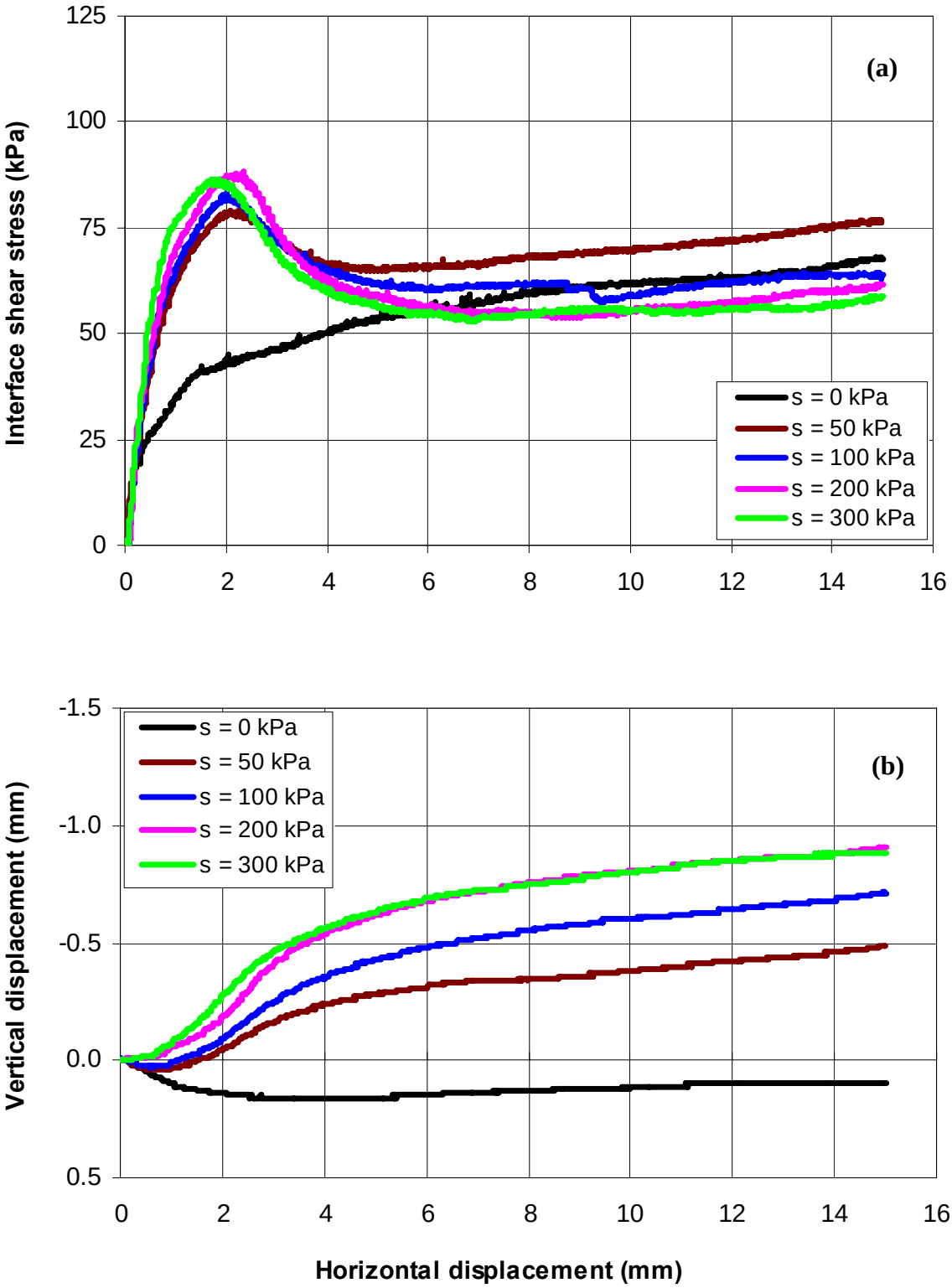

Figure 7.14 Curves of (a) interface shear stress versus horizontal displacement; and (b) vertical displacement versus horizontal displacement for different suctions under 50 kPa net normal stress and 250 kPa grouting pressure

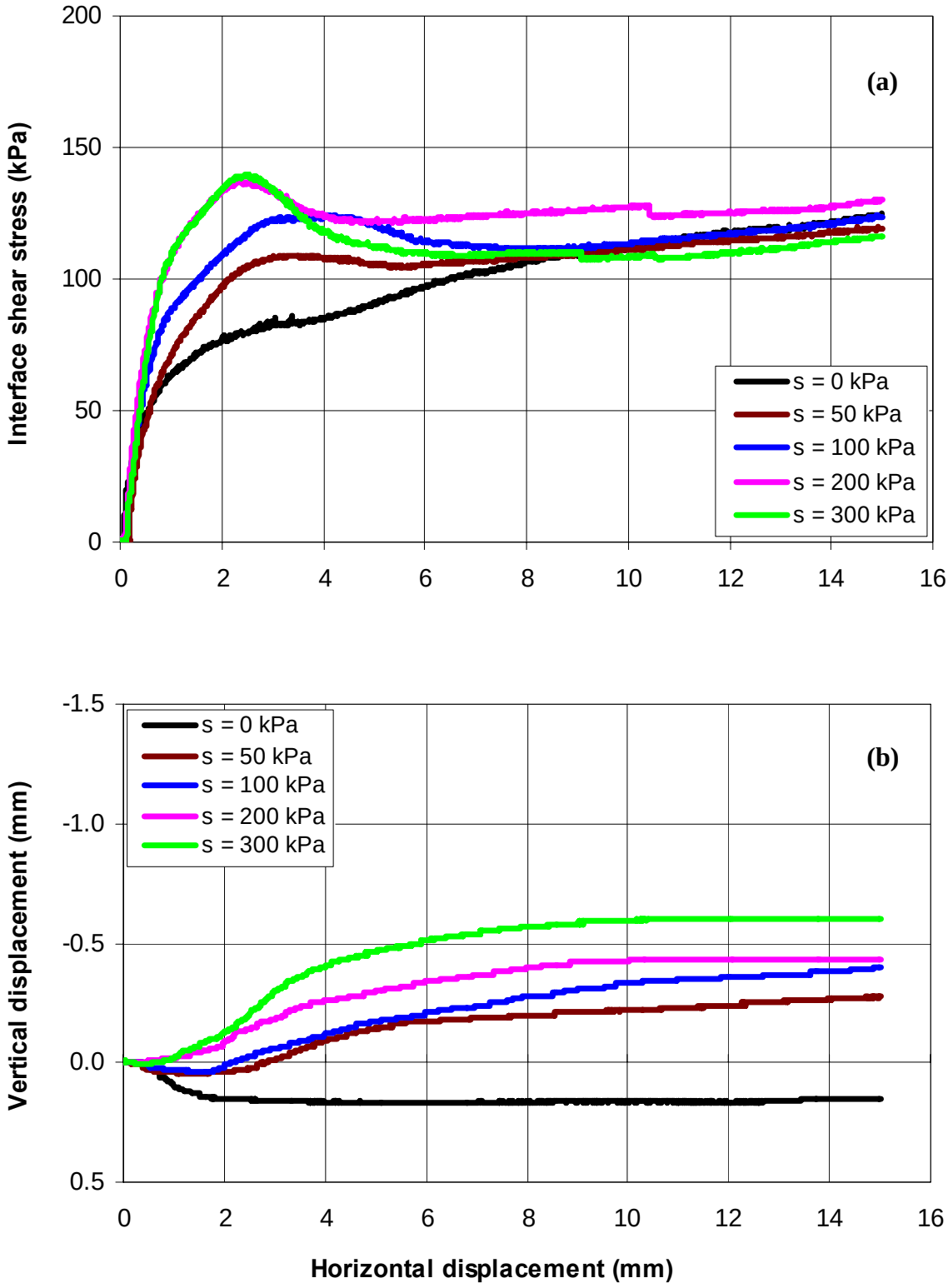

Figure 7.15 Curves of (a) interface shear stress versus horizontal displacement; and (b) vertical displacement versus horizontal displacement for different suctions under 100 kPa net normal stress and 250 kPa grouting pressure

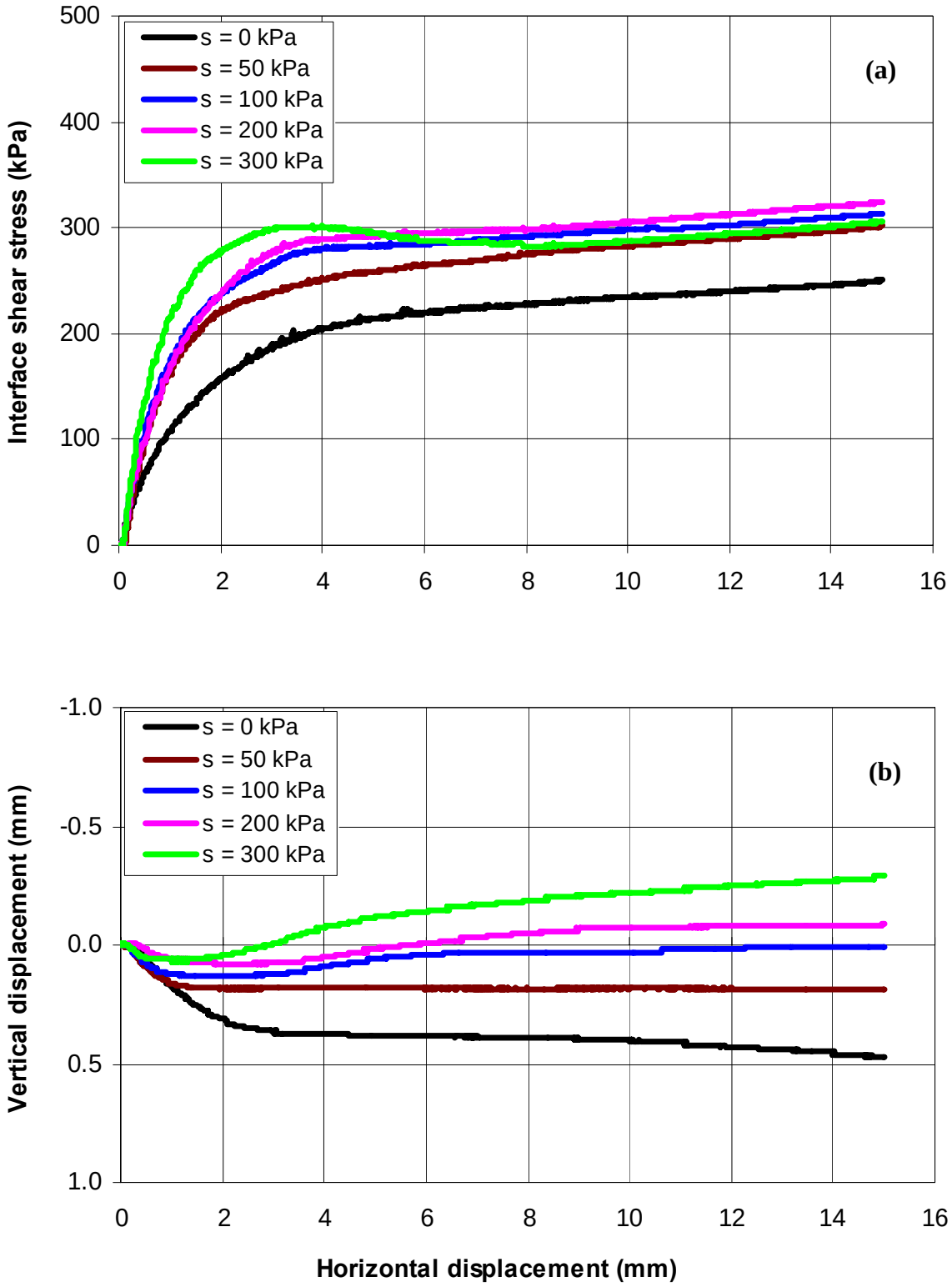

Figure 7.16 Curves of (a) interface shear stress versus horizontal displacement; and (b) vertical displacement versus horizontal displacement for different suctions under 300 kPa net normal stress and 250 kPa grouting pressure

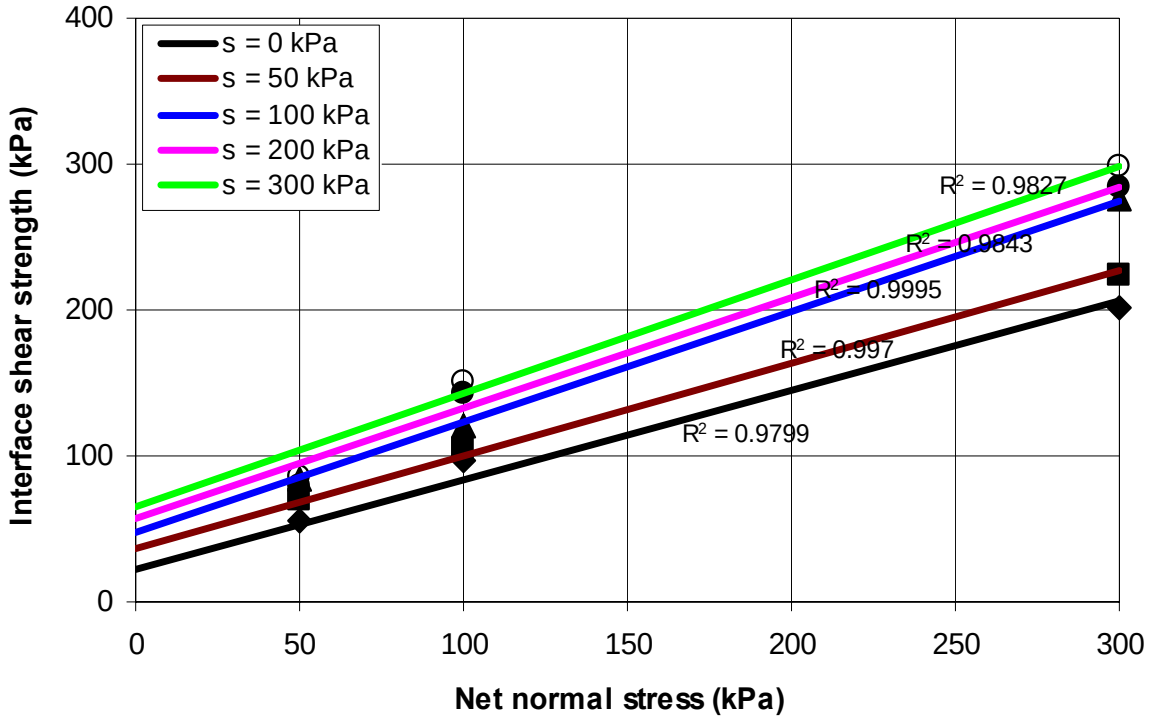

Figure 7.17 Interface failure envelopes corresponding to different suctions for 80 kPa grouting pressure

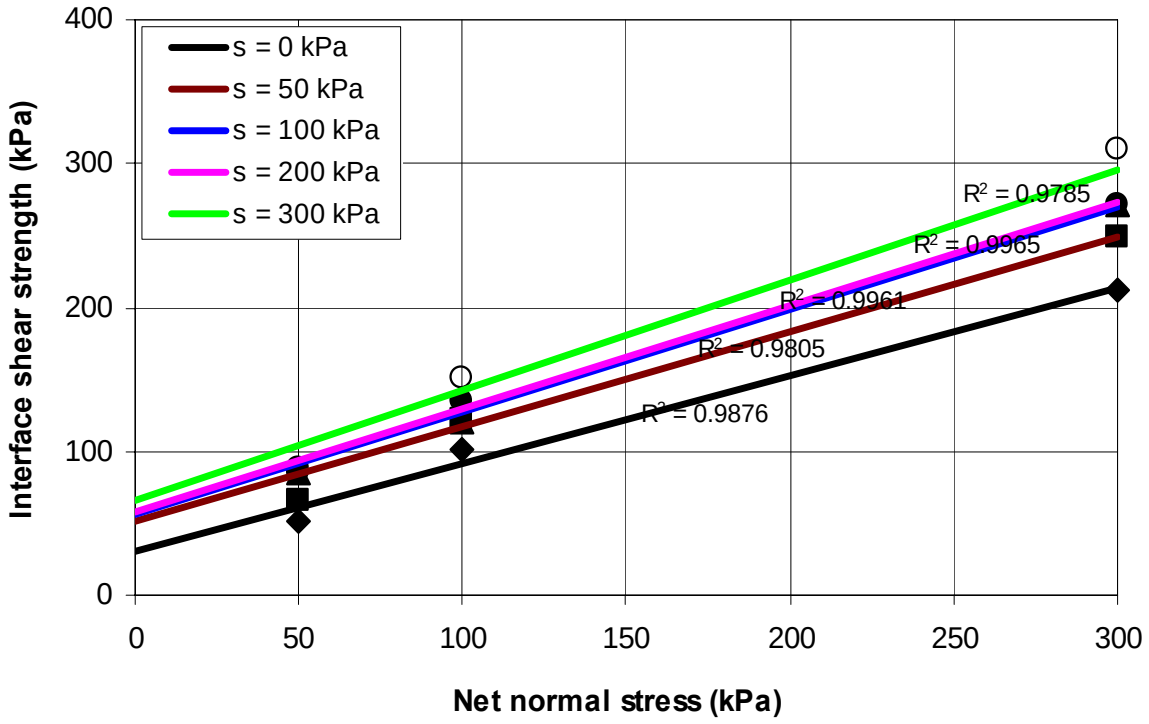

Figure 7.18 Interface failure envelopes corresponding to different suctions for 130 kPa grouting pressure

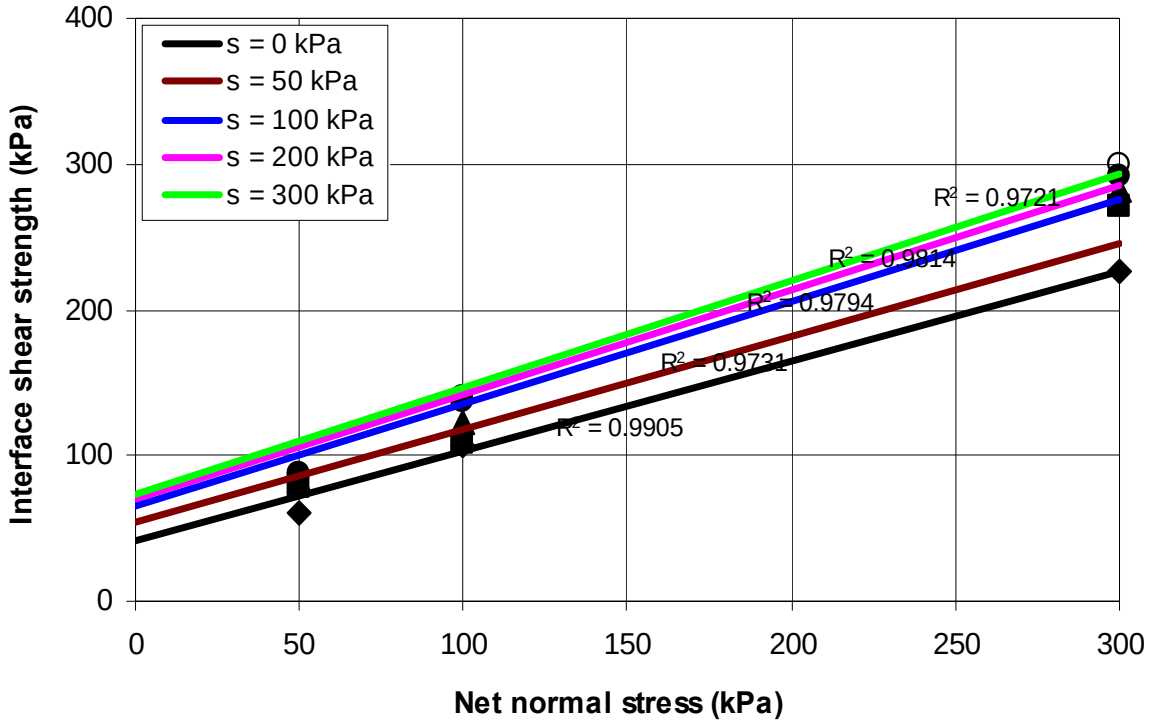

Figure 7.19 Interface failure envelopes corresponding to different suctions for 250 kPa grouting pressure

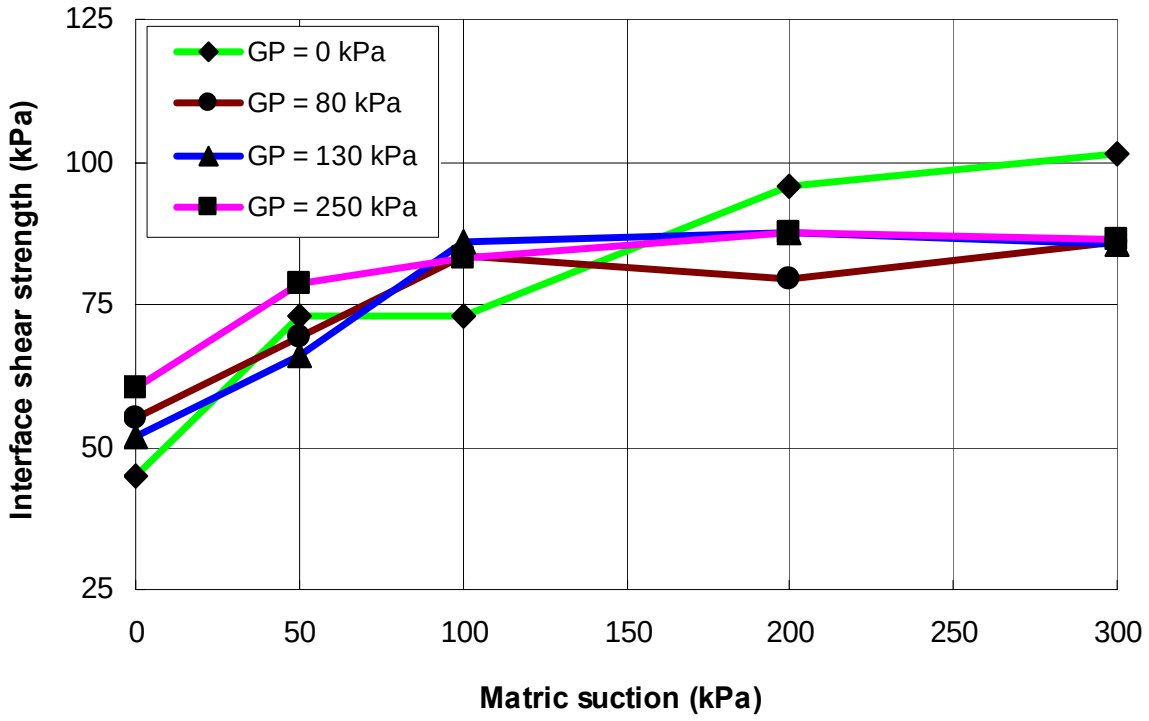

Figure 7.20 Interface suction envelopes for different grouting pressures under 50 kPa net normal stress

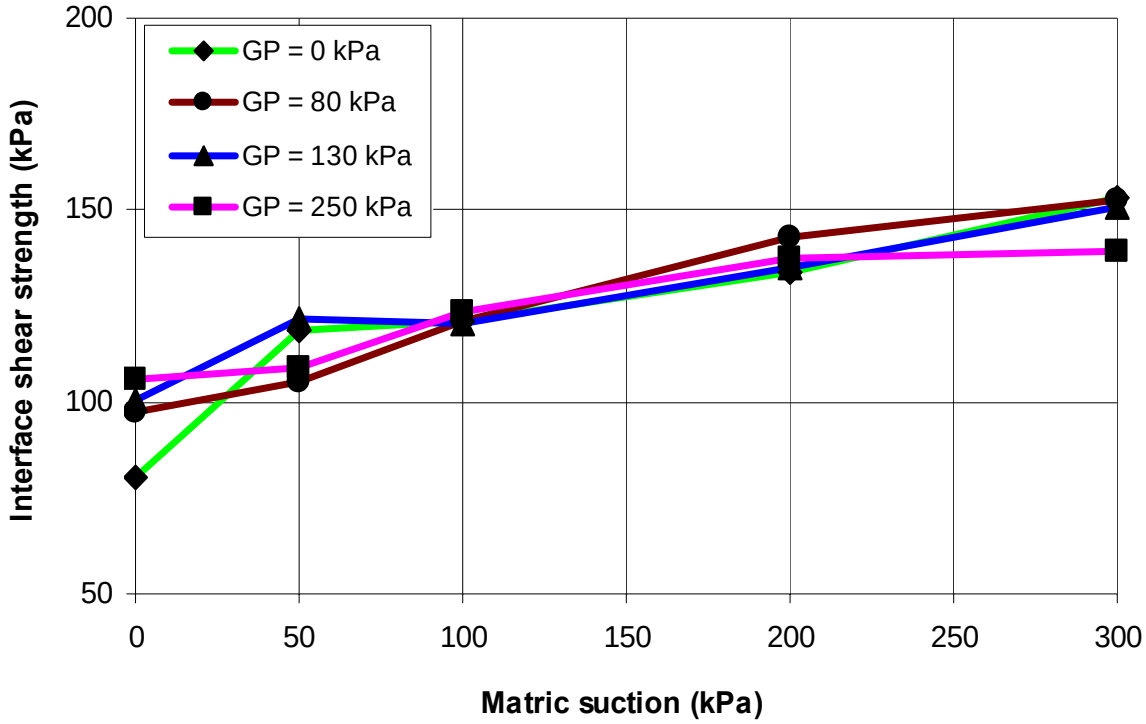

Figure 7.21 Interface suction envelopes for different grouting pressures under 100 kPa net normal stress

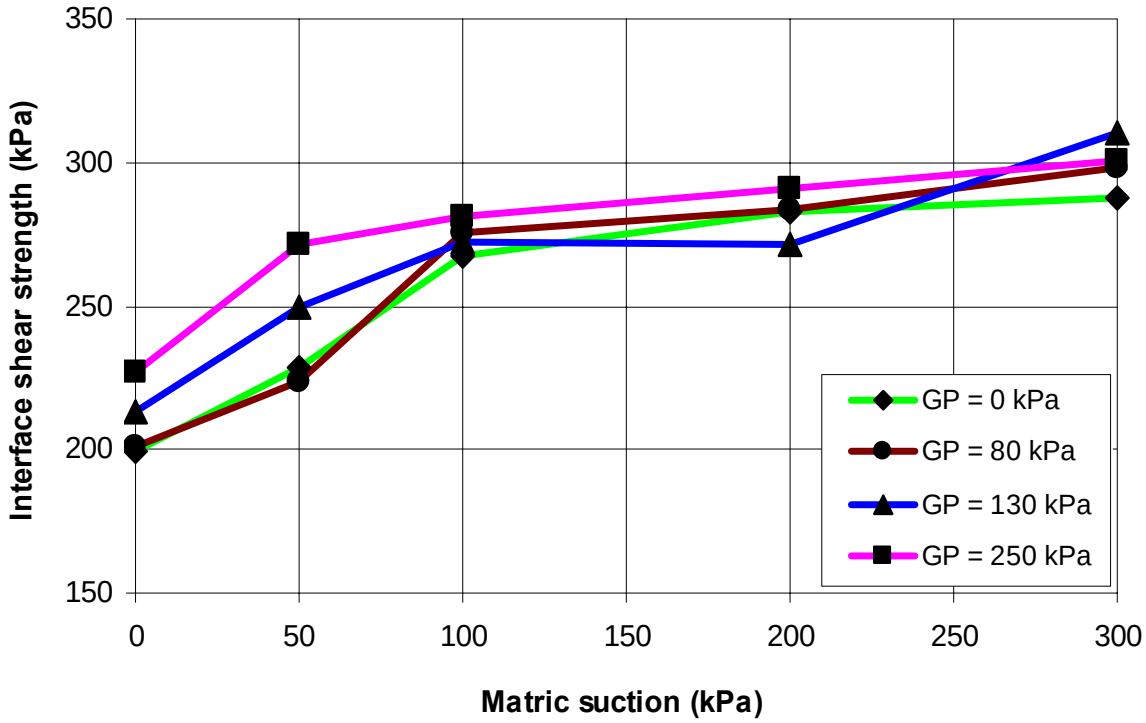

Figure 7.22 Interface suction envelopes for different grouting pressures under 300 kPa net normal stress

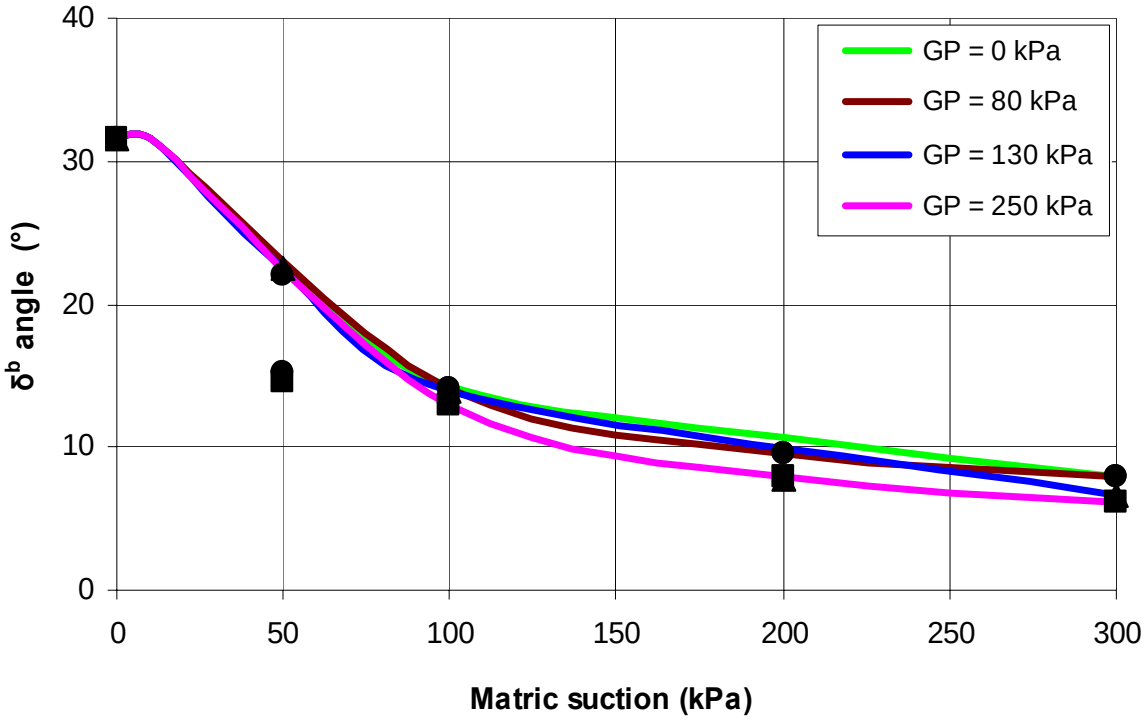

Figure 7.23 Variation of δ^b angle with matric suction for different grouting pressures

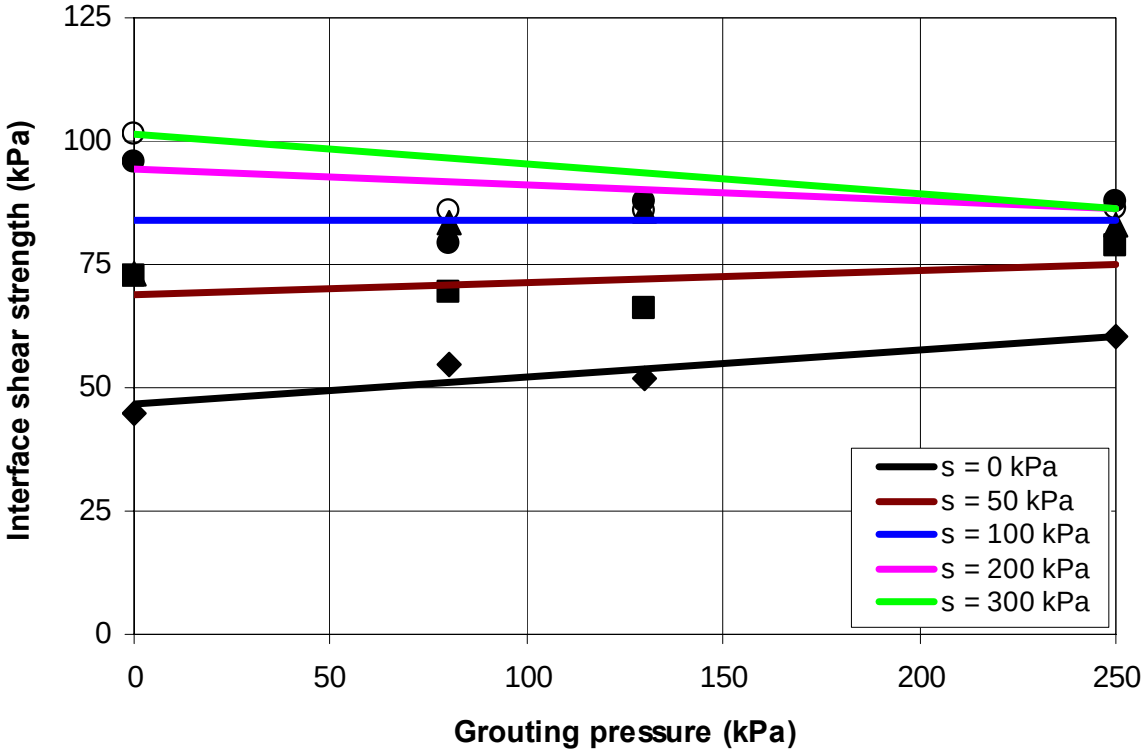

Figure 7.24 Variation of interface shear strength with grouting pressure for different suctions under 50 kPa net normal stress

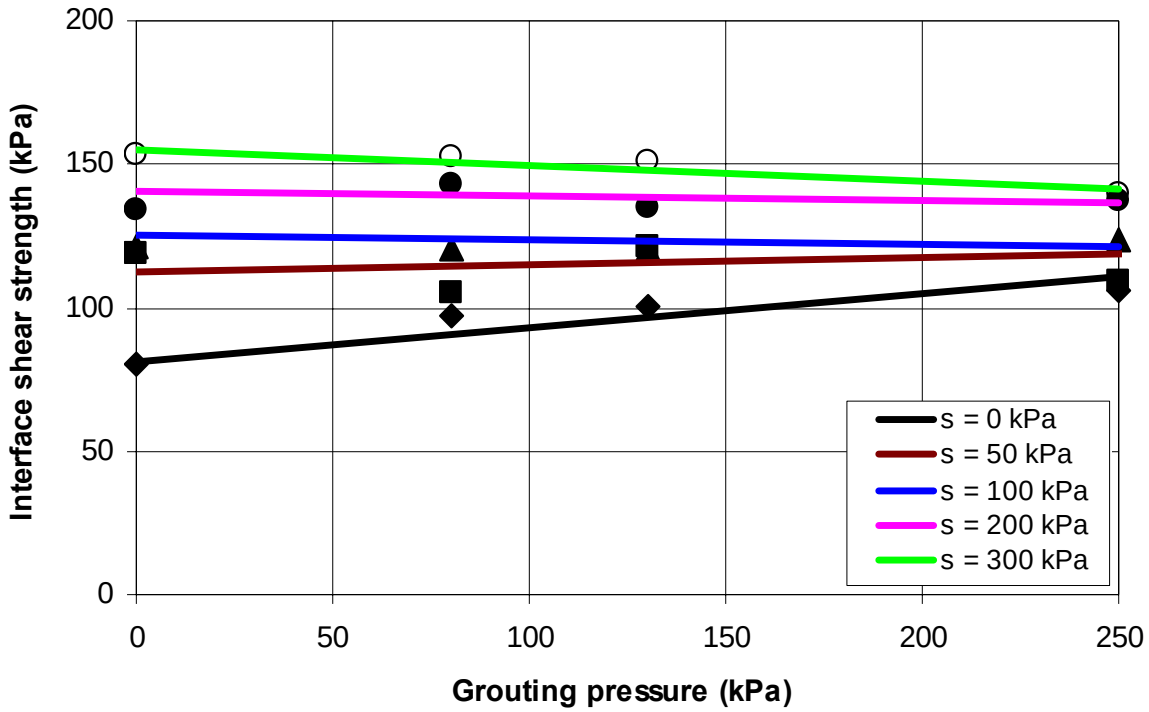

Figure 7.25 Variation of interface shear strength with grouting pressure for different suctions under 100 kPa net normal stress

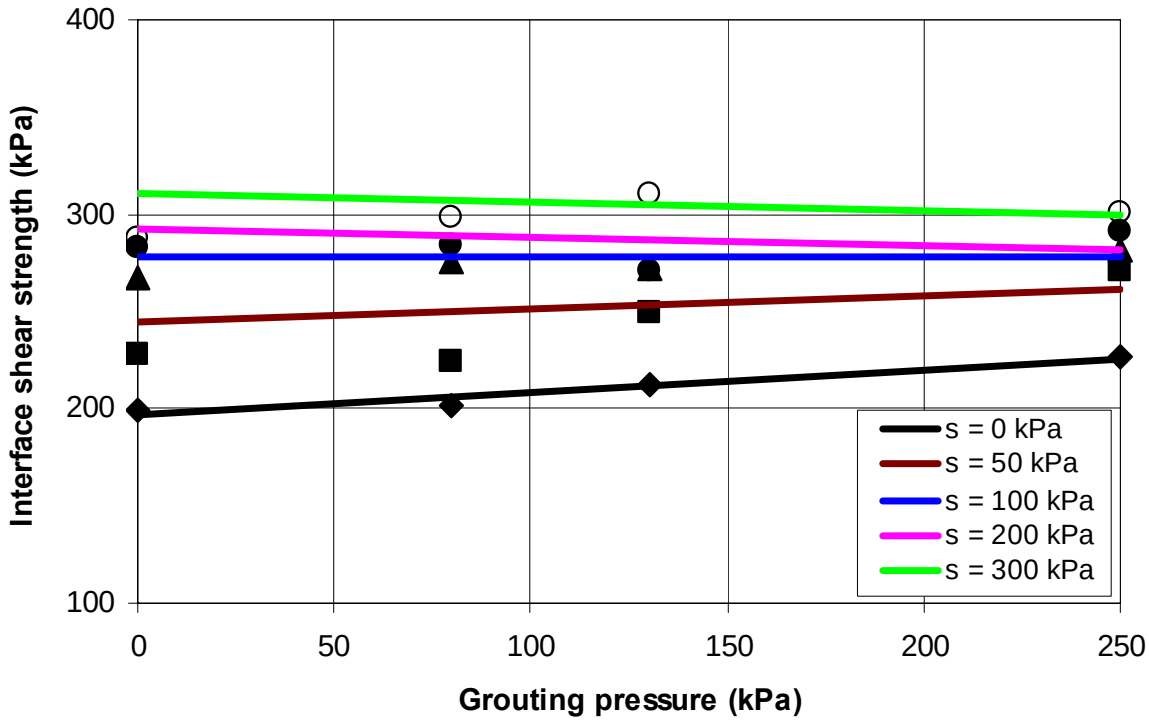

Figure 7.26 Variation of interface shear strength with grouting pressure for different suctions under 300 kPa net normal stress

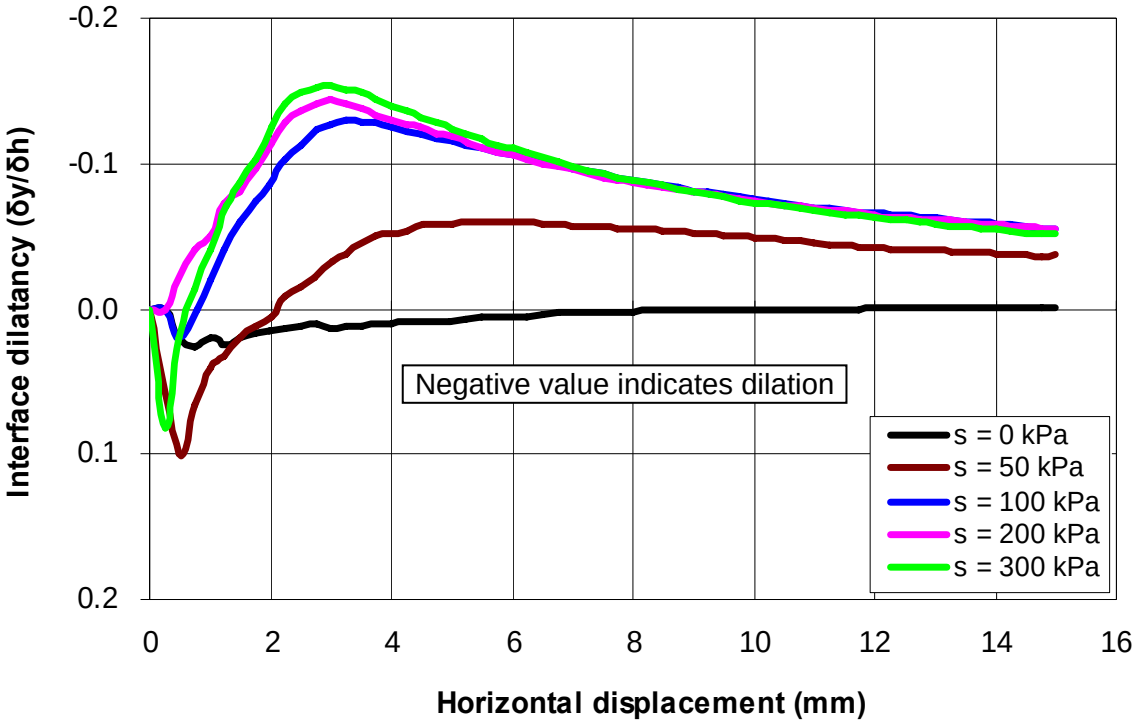

(a) Net normal stress 50 kPa

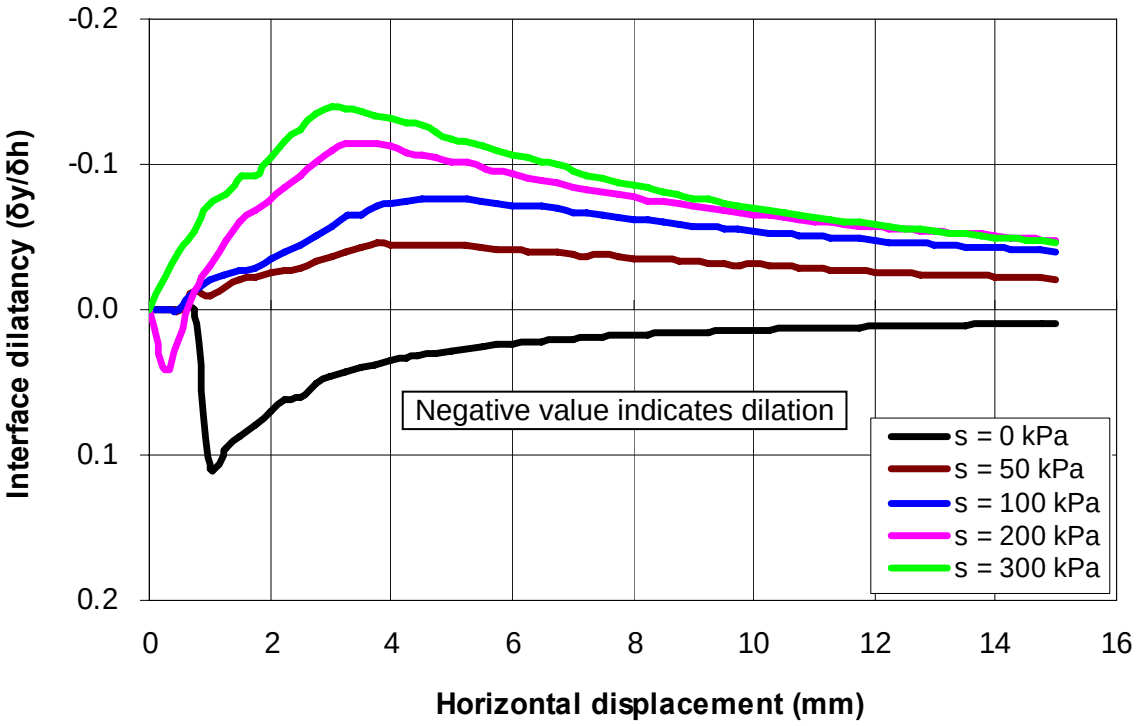

(b) Net normal stress 100 kPa

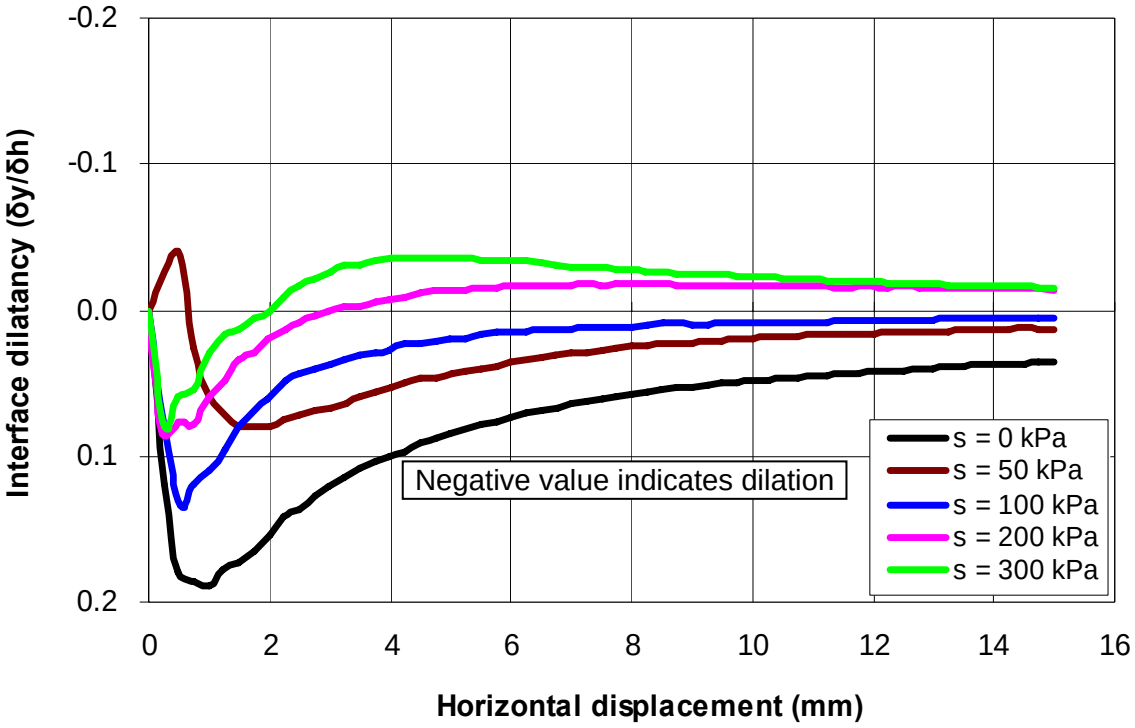

(c) Net normal stress 300 kPa

Figure 7.27 Curves of interface dilatancy versus horizontal displacement for different suctions and net normal stresses (Grouting pressure 80 kPa)

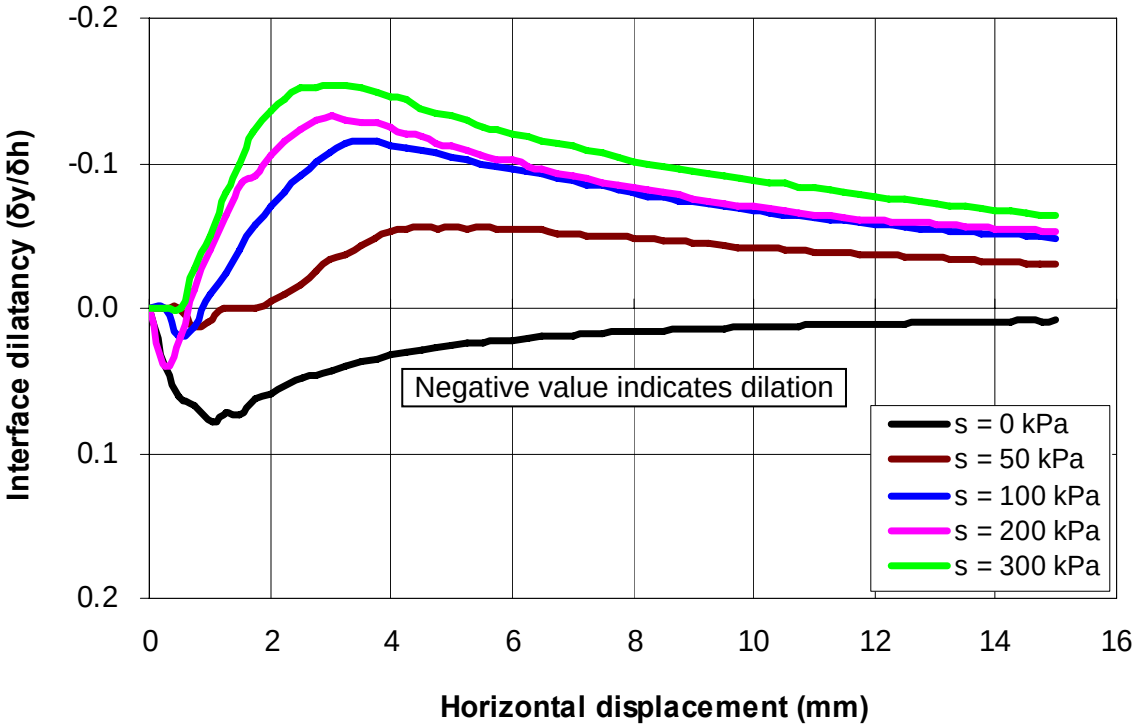

(a) Net normal stress 50 kPa

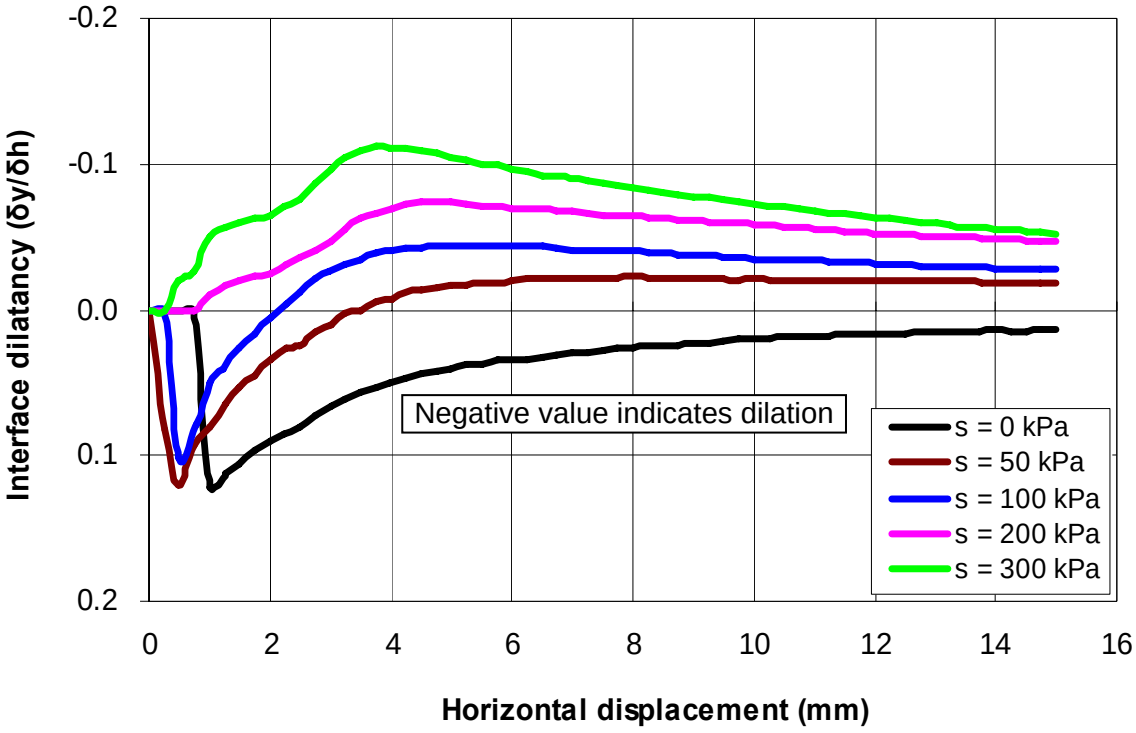

(b) Net normal stress 100 kPa

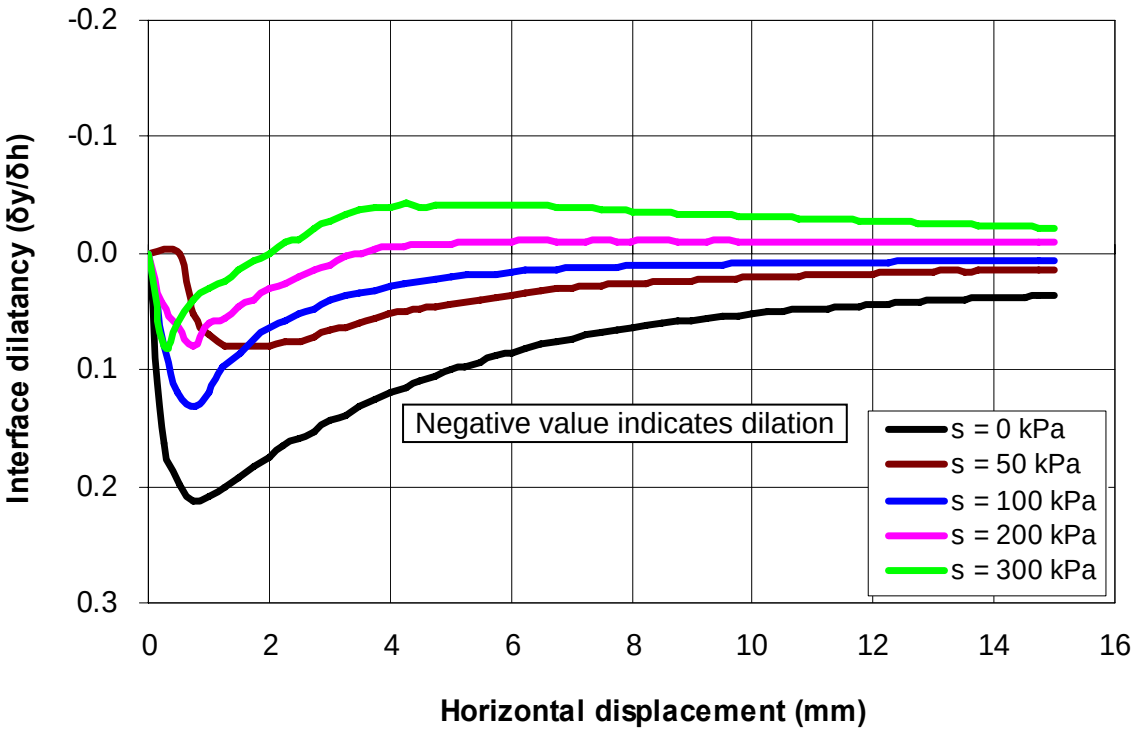

(c) Net normal stress 300 kPa

Figure 7.28 Curves of interface dilatancy versus horizontal displacement for different suctions and net normal stresses (Grouting pressure 130 kPa)

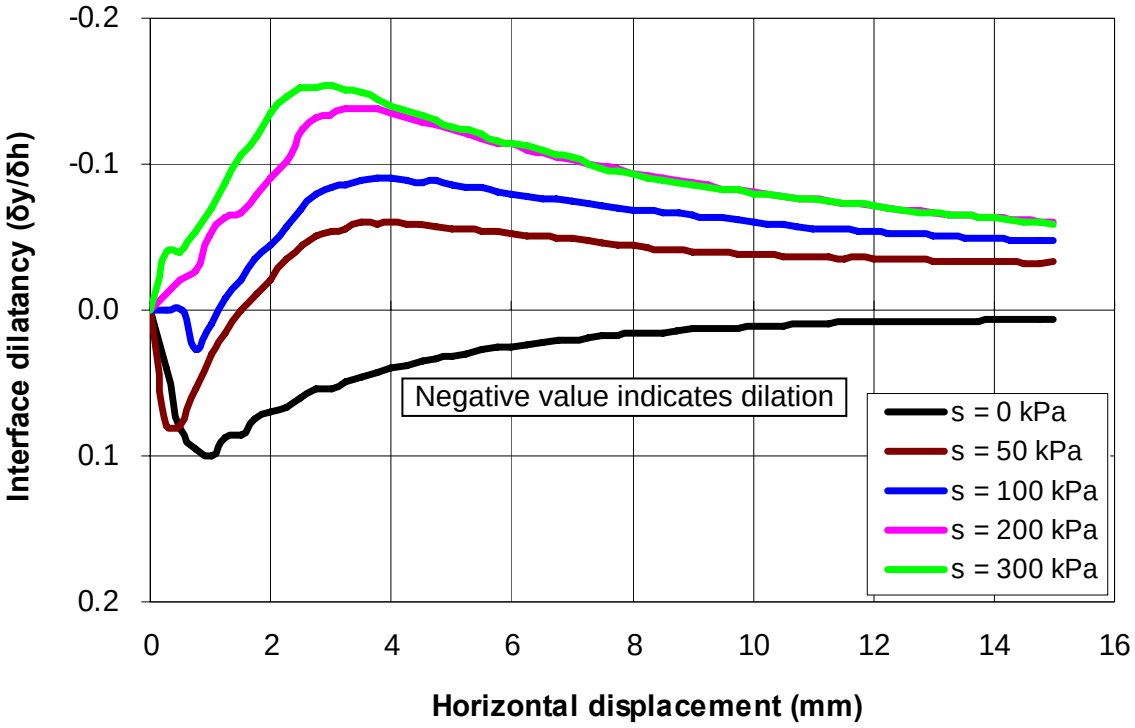

(a) Net normal stress 50 kPa

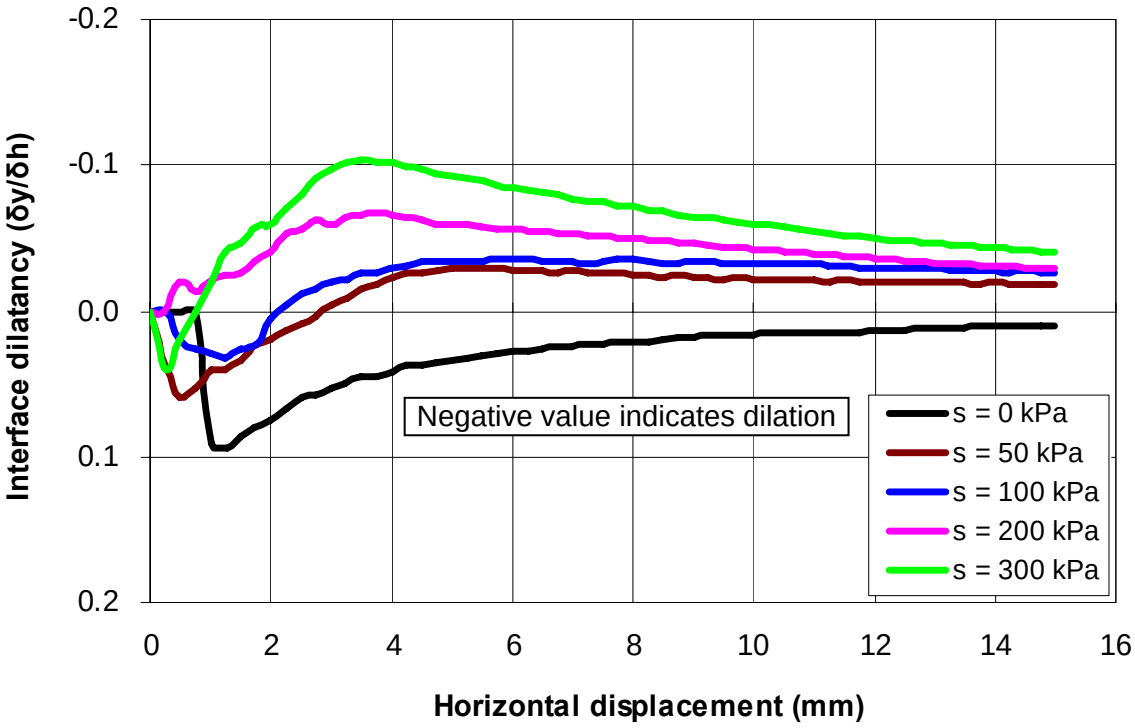

(b) Net normal stress 100 kPa

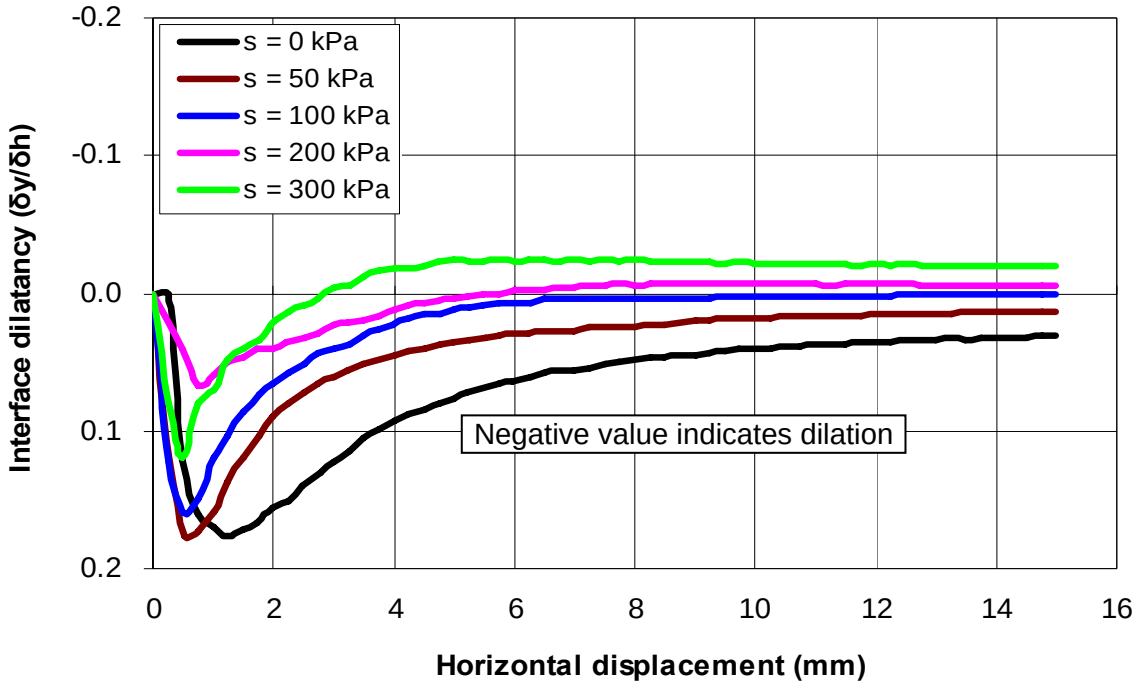

(c) Net normal stress 300 kPa

Figure 7.29 Curves of interface dilatancy versus horizontal displacement for different suctions and net normal stresses (Grouting pressure 250 kPa)

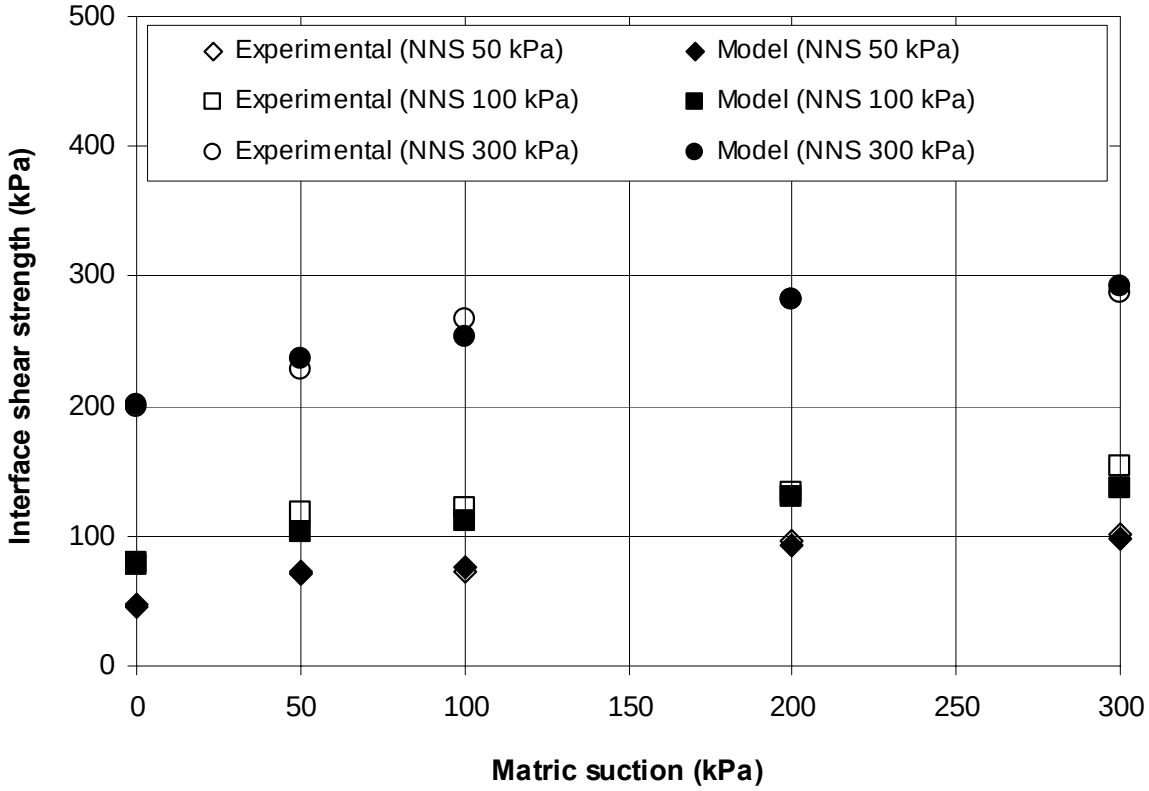

Figure 7.30 Comparison between experimental interface shear strength data and analytical results obtained from the proposed model (Grouting pressure 0 kPa)

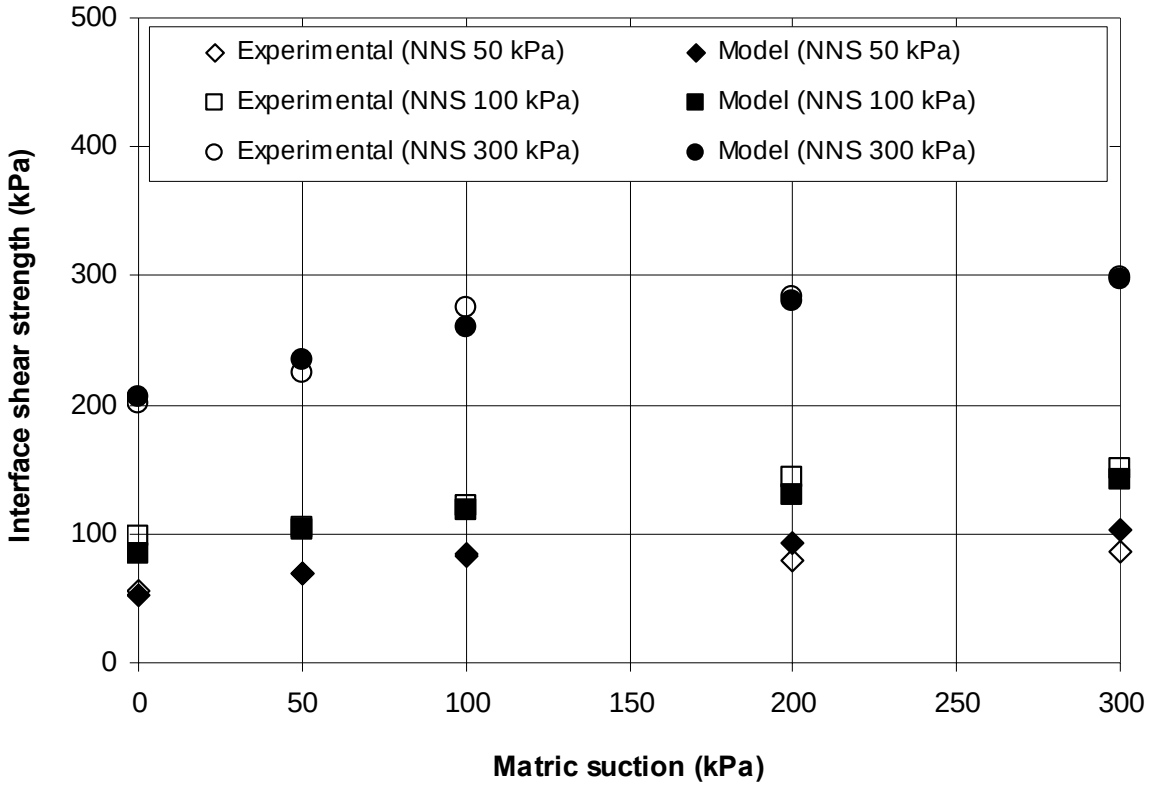

Figure 7.31 Comparison between experimental interface shear strength data and analytical results obtained from the proposed model (Grouting pressure 80 kPa)

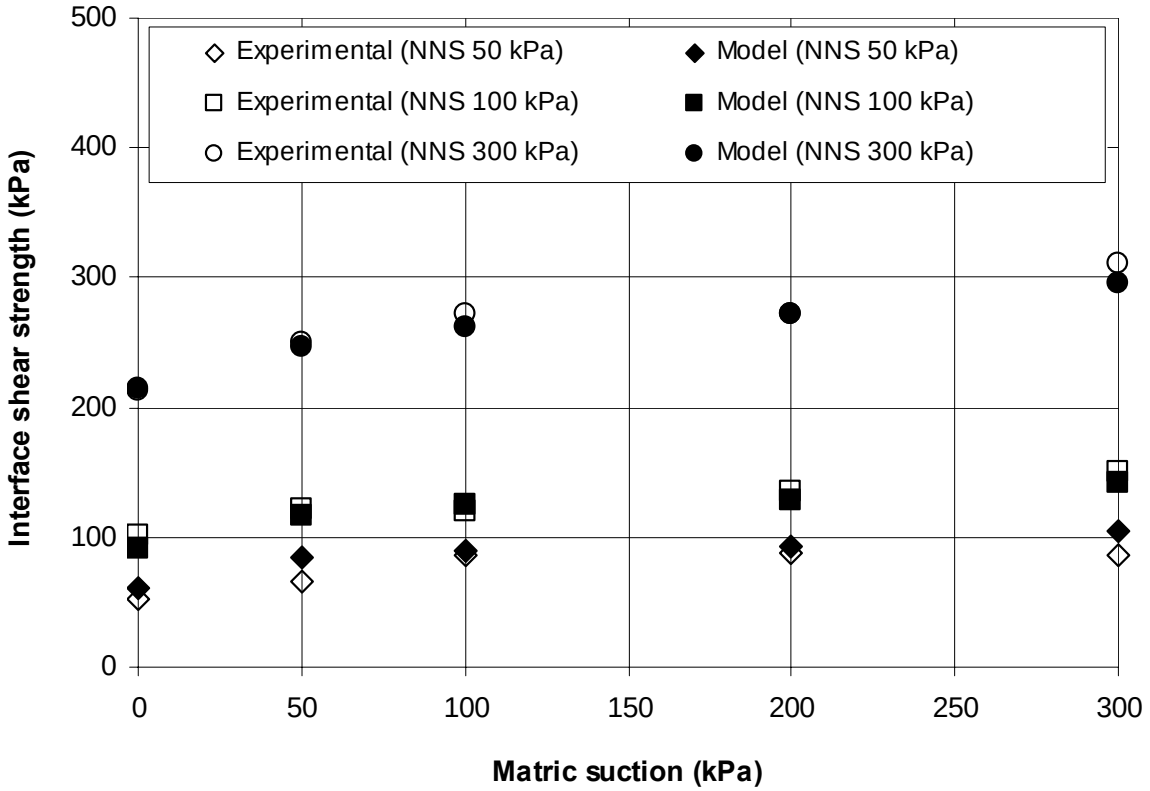

Figure 7.32 Comparison between experimental interface shear strength data and analytical results obtained from the proposed model (Grouting pressure 130 kPa)

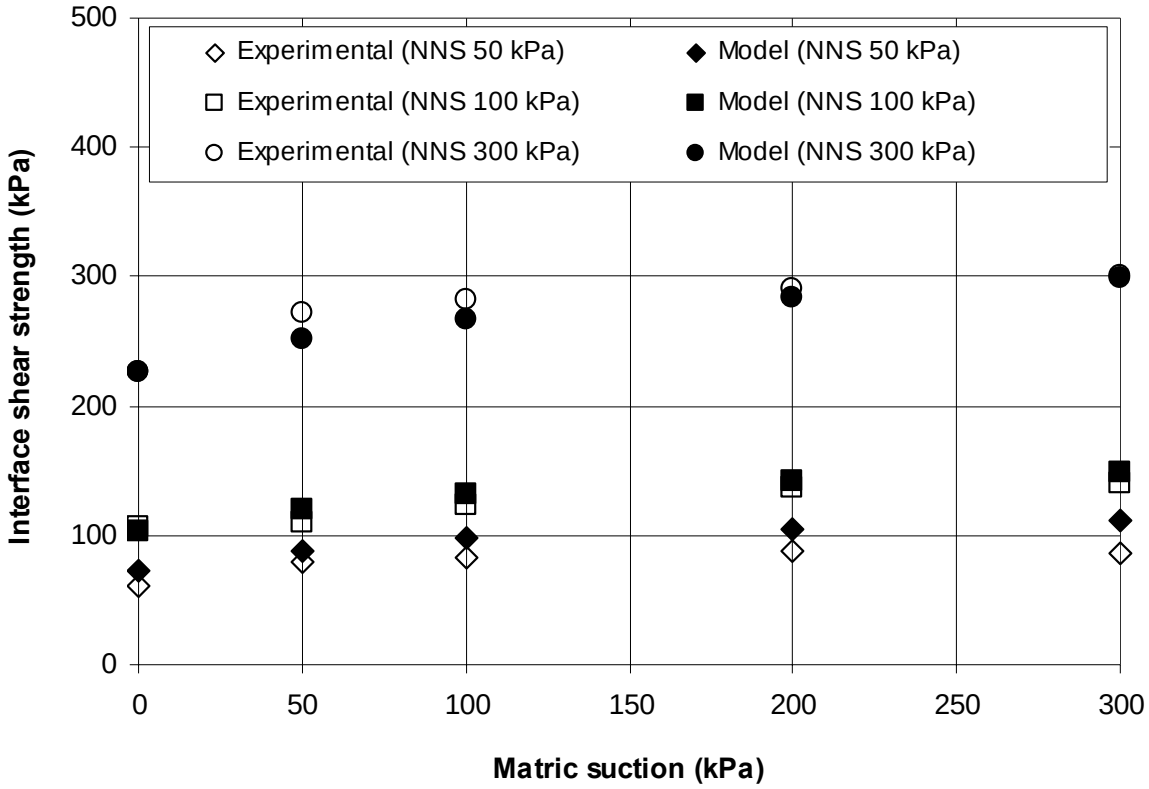

Figure 7.33 Comparison between experimental interface shear strength data and analytical results obtained from the proposed model (Grouting pressure 250 kPa)

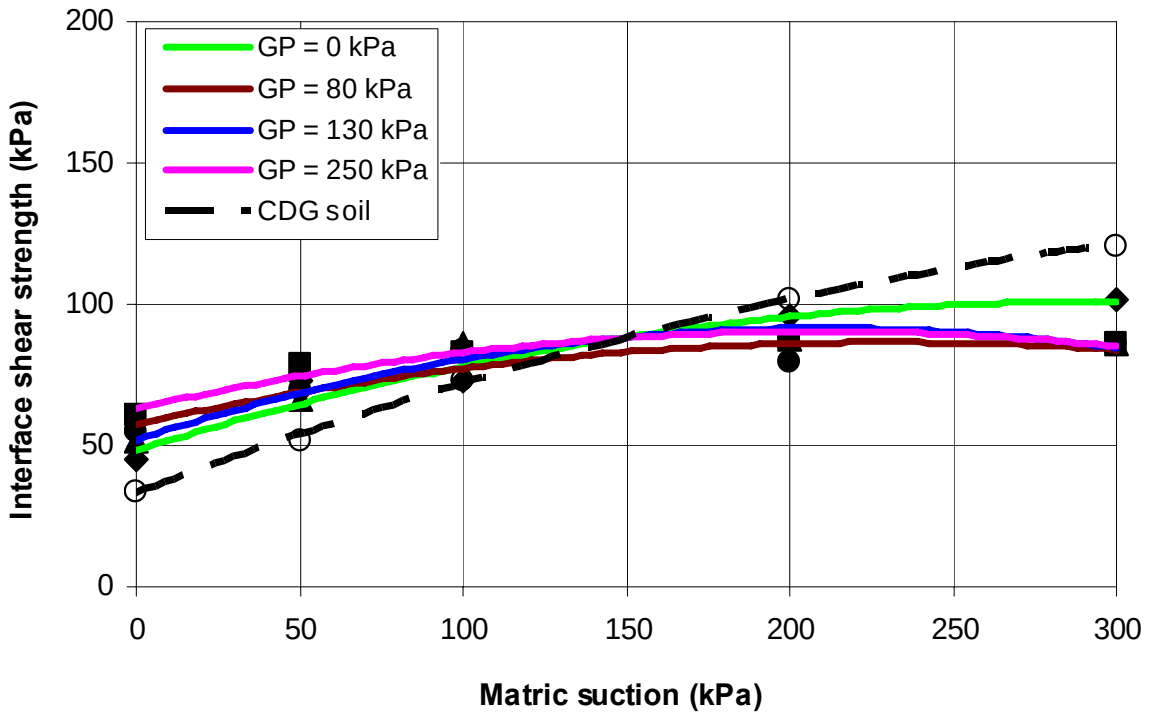

Figure 7.34 Comparison between pressure grouted interface shear strength and shear strength of CDG soil for 50 kPa net normal stress

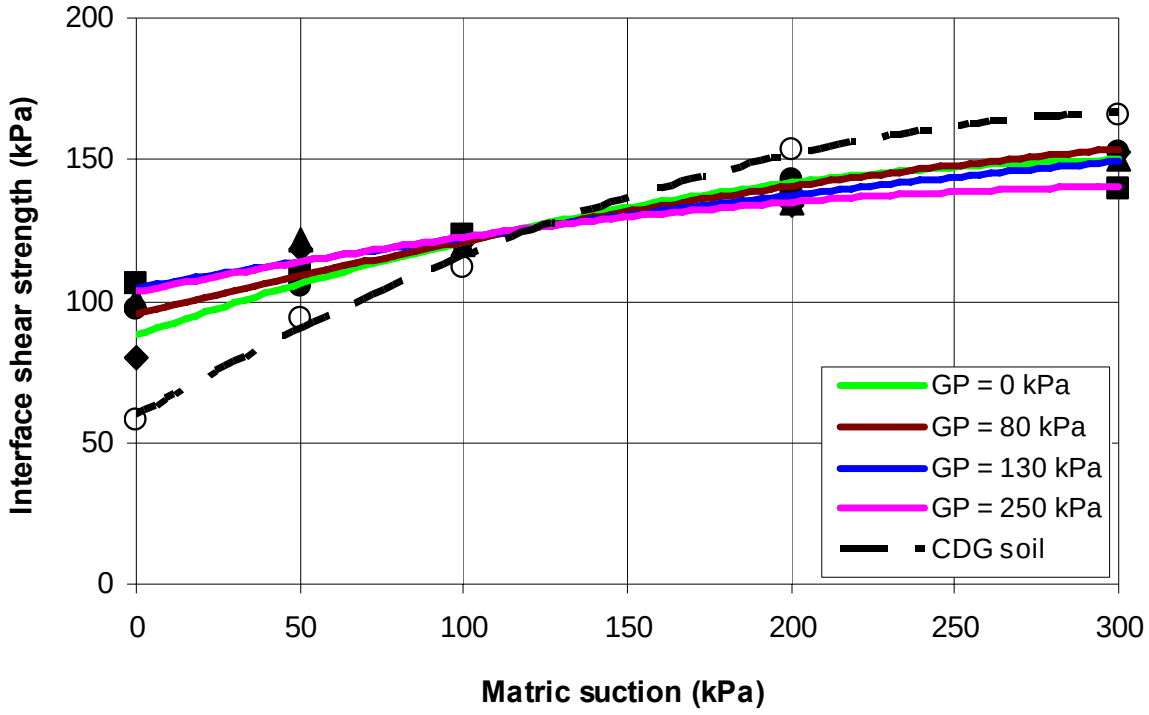

Figure 7.35 Comparison between pressure grouted interface shear strength and shear strength of CDG soil for 100 kPa net normal stress

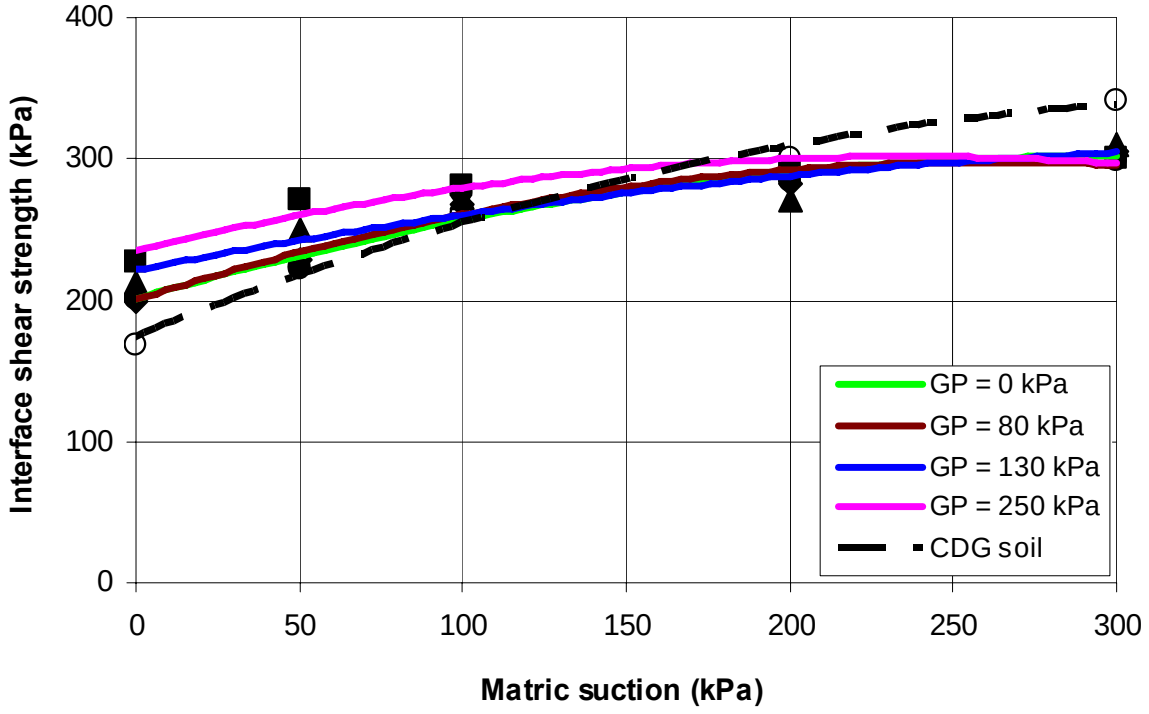

Figure 7.36 Comparison between pressure grouted interface shear strength and shear strength of CDG soil for 300 kPa net normal stress

Chapter 8

CONCLUSIONS AND RECOMMENDATIONS

Single-staged consolidated drained direct shear tests have been conducted on compacted CDG soil and soil-cement interface. A number of influencing factors which may influence the behavior of soil as well as soil-cement interface are investigated in the present study. These influencing factors include: matric suction, net normal stress and grouting pressure. Based on the test results, their interpretations and discussions presented in the previous chapters, the main conclusions of this research study are presented in the following sections, followed by the recommendations for further future research in the topic area.

8.1 CONCLUSIONS FROM UNSATURATED SOIL TESTS

Data from a series of suction controlled direct shear tests on an unsaturated compacted completely decomposed granite (CDG) soil and their interpretation are presented in Chapter 5. An especial attention is paid to the influence of dilation on friction angle and shear strength under different suctions and net normal stresses. A modified shear strength model is proposed to establish the effect of soil dilation on shear strength of unsaturated soils. The following conclusions are drawn based on the discussion presented in the previous chapter:

- For the studied compacted CDG soil, the net normal stress has insignificant influence on SWRC. The SWRC for zero net stress can be used for predicting the shear strength at unsaturated condition. The air entry value of the

compacted CDG soil is obtained as 11 kPa from the soil-water retention curve (SWRC) for zero net stress.

- Matric suction and net normal stress have significant influence on the shear strength characteristics of unsaturated compacted CDG soil. Shear strength increases with matric suction as well as net normal stress. At higher suction with lower net normal stress, the soil shows a strong strain-softening behavior. On the other hand, a strain-hardening behavior is observed at lower suction with higher net normal stress. The shear-compression and shear-dilation behavior of compacted CDG soil are also influenced by matric suction and net stress. A shear-compression is observed under lower suction with higher net stress, and at saturated condition for all net stress. In contrast, a shear-dilation is obvious with the increase of suction for particular net stresses.
- The shear strength increases with net normal stress and suction. The shear strength envelope in the shear strength and the net normal stress space is almost linear. The apparent angle of internal friction $\phi_{\max}$ and cohesion intercept c increase with matric suction. The rate of increment of $\phi_{\max}$ is greater in lower suction range (0 to 100 kPa) than higher suction range (100 to 300 kPa).
- A typical nonlinear suction envelope is observed for unsaturated compacted CDG soil within the suction range 0 to 300 kPa.
- The dilatative behavior of unsaturated compacted CDG soil is greatly influenced by matric suction and net normal stress. The dilatancy essentially increases with an increase of matric suction. The peak dilatancy (negative) is observed at lower net normal stress under higher suctions. Greater dilation angle is found at higher suction with lower net normal stress, and lower or zero dilation angles is obvious under higher net normal stress with lower suction as

well as at saturated condition. The average dilation angle of different net normal stresses increases with matric suction.

- The experimental shear strength data match closely with the predicted shear strength values from the model proposed by Vanapalli *et al.* (1996) using the SWRC at zero net normal stress considering the apparent friction angle.
- Under higher net normal stresses at higher suction range, the experimental shear strength data are little bit greater than the analytical shear strength results obtained from the modified model using SWRC, effective shear strength parameters of compacted CDG soil and analytical values of dilation angles.

8.2 CONCLUSIONS FROM UNSATURATED INTERFACE TESTS

The modified direct shear apparatus used for unsaturated soil tests was upgraded for the interface direct shear tests between CDG soil and cement grout under different suctions and net normal stresses. Cast in-situ interface was formed between soil-cement grout. The interface direct shear test results and their interpretations are presented in Chapter 6. Similar to CDG soil tests, an especial attention is paid to the influence of dilation on interface friction angle and shear strength. The interface strength is compared with the strength of the same soil. The following conclusions are drawn based on the discussion presented in the previous chapter:

- The hardening-softening behavior of interface is significantly influenced by the matric suction and net normal stress. At lower net normal stresses of 50 and 100 kPa the stress-displacement curves show strain-softening behavior for the entire suction range (50 to 300 kPa) except saturated condition. At higher net normal stress of 300 kPa and lower suctions of 0, 50 and 100 kPa, the stress-displacement curves indicate strain-hardening behavior. The interface failure plane becomes densed (similar to overconsolidated soil) than that of

soil-soil direct shear test due to infiltration of cement particles. The shear-compression and shear-dilation behavior of soil-cement interface are also influenced by matric suction and net stress. A shear-compression is observed under lower suction with higher net stress, and at saturated condition for all net stress. In contrast, a shear-dilation is obvious with the increase of suction for particular net stresses.

- Similar to CDG soil, the interface shear strength envelope in the shear strength and the net normal stress space is almost linear. The apparent interface friction angle $\delta_{\max}$ and adhesion intercept c_a increase with matric suction. The apparent interface friction angles for different suctions are greater than or equal to the values of apparent friction angles of soil for the particular suctions. The apparent adhesion values are greater than the apparent cohesion values of soil within the suction range of 0 to 100 kPa, and lower than that within the suction range of 200 to 300 kPa.
- A typical nonlinear suction envelope is observed for CDG soil and cement grout interface within the suction range of 0 to 300 kPa which is similar to the soil-soil direct shear test for the same suction range. The δ^b angle decreases with the increase of suction.
- Similar to CDG soil, the interface dilatancy increases with matric suction. The peak dilatancy (negative) is observed at lower net normal stress (50 kPa) under higher suctions. The dilatancy decreases as the net stress is increased. Greater interface dilation angle is obtained at higher suction with lower net normal stress, and lower or no dilation is observed under higher net normal stress with lower suction, and at saturated condition. However, at higher suction levels, the interface dilation angle is lower compared to soil dilation angle. The average interface dilation angle increases with matric suction.

- A modified model is proposed to predict the shear strength of compacted CDG soil-cement grout interface taking into account the influence of dilation on apparent interface friction angle. The experimental shear strength data are compared with the prediction of the proposed modified model. The interface shear strength predicted from the proposed modified model agrees well with the experimental shear strength data for different net normal stresses and matric suctions.
- Similar to CDG soil, the interface shear strength increases with suction and net normal stress. However, the interface shear strength is higher than the soil shear strength within lower suction range (0 to 100 kPa). Whereas, the shear strength becomes lower than the soil shear strength at higher suction range (200 to 300 kPa). The apparent interface friction angle remains equal to the apparent friction angle of soil for the entire suction range.
- The decrease of apparent adhesion at higher suctions may be due to breaking of bonding between soil and cement particles, and weakening of air-water menisci (contractile skin) at higher suctions.

8.3 CONCLUSIONS FROM PRESSURE GROUTED INTERFACE TESTS

8.3.1 Pressure grouted interface tests at saturated condition

The direct shear test results of soil-cement interface at saturated condition (zero suction) under different grouting pressures and normal stresses, and their interpretations are presented in Chapter 7. The interface behavior is compared with the behavior of the same soil. The following conclusions can be drawn based on the discussion presented in the previous chapter:

- The behavior of shear stress-displacement curves of pressure grouted soil-cement interface tests is similar to that of soil-soil direct shear tests. The interface shear stress increases with net normal stress and grouting pressure. The stress-displacement curves indicate strain-hardening behavior for different grouting pressures under different normal stresses. The interface shear stress under different grouting pressures is greater than the shear stress of CDG soil under particular net stresses.
- A contractive behavior is observed under different net stresses, and the deformation (shear-compression) value increases with net stress. The vertical displacement (downward) values of interface tests are lower for different grouting pressures compared to that of CDG soil under individual net stresses.
- The interface shear strength envelopes for different grouting pressures are approximately linear. The effective apparent interface friction angle δ'' is constant for different grouting pressures, but effective apparent adhesion intercept c_a'' increases with grouting pressure.
- CDG soil-cement grout interface behaves as a rough interface for different grouting pressures since the effective interface friction angle is greater than the effective friction angle of CDG soil. The rough interface is likely formed due to infiltration of cement particles along the failure plane under different grouting pressures.
- The interface shear strength increases with grouting pressure and net stress. The increase of interface shear strength (grouting pressure envelope) is approximately linear, and the declivities are constant for different net stresses.
- A new model is proposed for interface shear strength incorporating the influence of grouting pressure considering grouting pressure as an independent parameter. The experimental data for different grouting pressures and net

stresses are compared with the predictions of new model, and they seem to agree well.

8.3.2 Pressure grouted interface tests at unsaturated condition

The direct shear test results of compacted CDG soil-cement grout interface under different suctions, net stresses and grouting pressures, and their interpretations are presented in Chapter 7. An especial attention is paid on the influence of grouting pressure on the interface dilatancy and strength. The interface strengths for different grouting pressures are compared with the strength of the same soil. A general model is proposed to predict the shear strength of pressure grouted soil-cement interface under different suctions. The following conclusions can be drawn based on the discussion presented in the previous chapter:

- The interface shear stress increases with matric suction for different grouting pressures, and a strain-softening behavior is obvious when the suction value is increased from saturated condition. However, for CDG soil, a strain-softening behavior is observed only at higher suction range.
- Similar to soil-soil direct shear tests, a shear-dilation is obvious for pressure grouted interface as the suction value is increased from saturated condition. However, the shear-dilation values of soil-cement interface for different grouting pressures are lower compared to CDG soil under different suctions.
- The interface shear strength envelopes for different matric suctions corresponding to different grouting pressures are approximately linear. Similar to CDG soil, the apparent interface friction angle $\delta_{\max}$ increases with matric suction for particular grouting pressure. On the contrary, it decreases with grouting pressure for different matric suctions except saturated condition. The

apparent adhesion intercept for different grouting pressures $c_{a(g)}$ increases with matric suction and grouting pressure.

- For gravity grouted interface, the interface shear strength increases with matric suction under different net normal stresses. On the other hand, for pressure grouted interface, the interface strength increases with matric suction at lower suction range (upto 150 to 200 kPa), and after that the strength decreases or remains nearly constant at higher suction range (200 to 300 kPa). Similar to CDG soil, the relationships between interface shear stress τ_f at failure and matric suction $(u_a - u_w)_f$ for different grouting pressures are obviously nonlinear, indicating that the δ^b angle is not constant.
- The interface shear strength increases with grouting pressure at lower suctions of 0 to 50 kPa for particular net stresses. On the contrary, a downward trend is observed for the interface strength under higher suctions of 200 to 300 kPa for different grouting pressures and net stresses. The interface shear strength remains nearly constant with grouting pressure under suction of 100 kPa for different net stresses.
- Similar to CDG soil, the interface dilatancy increases with matric suction, and peak dilatancy (negative) is observed under lower net stress at higher suction. The interface dilatancy decreases with grouting pressure, and the rate of decrement is higher at higher suction range of 200 to 300 kPa than the lower suction range of 50 to 100 kPa. The average interface dilation angle values for different grouting pressures are lower compared to those of compacted CDG soil under the same suctions and net stresses.
- A general model is proposed to predict the shear strength of compacted CDG soil-cement grout interface taking into account the influence of interface

dilation, matric suction, net stress and grouting pressure. The experimental shear strength data are compared with the prediction of the proposed model. The interface shear strength predicted from the proposed model agrees well with the experimental shear strength data for different net normal stresses, matric suctions and grouting pressures, which indicates that matric suction, normal stress and grouting pressure have significant influence on shear behavior of compacted CDG soil and cement grout interface.

- The shear strength of pressure grouted interface is greater than that of CDG soil within the suction range of 0 to 100 kPa for different net normal stresses. In contrasts, the interface shear strength is lower than the shear strength of CDG soil at higher suction range of 200 to 300 kPa. The strength of higher grouting pressure (250 kPa) interface under different net stresses and saturated condition is greater than the strength of CDG soil and gravity grouted interface. This indicates that the stability of slopes can be boosted up at saturated condition by the inclusion of pressure grouted soil nails into the slopes instead of gravity grouted soil nails. At saturated condition and lower suctions, the failure of slope may be happened in the soil as the strength of soil is lower than the strength of interface. On the other hand, at higher suctions, failure of slope may be happened inside the interface zone rather than in the soil as the strength of soil is greater than the interface.
- The behavior of compacted CDG soil-cement grout interface changes from rough interface towards the smooth interface as the grouting pressure is increased.

8.4 RECOMMENDATIONS FOR FUTURE RESEARCH

- In the present study, compacted CDG soil specimens were used for direct shear tests and interface tests. It shall be valuable to investigate the behavior of unsaturated soil and interface by using undisturbed soil samples.
- The preselected interface layer thickness for the present interface study was 2 mm from the cement face. Further study can be conducted to observe the actual extent of infiltration of cement into the soil by varying the interface layer thickness.
- To form the cast in-situ interface, cement grout was used to form the counterface of soil for the present study. Other type of materials like steel and precast concrete can be used as counterface to form an interface.
- A relative compaction of 95% of the maximum dry density of CDG soil was used for the present study. A range of different relative compactions can be used for future studies.
- The curing period of the cement grout was 5 days for the present study. A longer curing period is suggested for future study as the bonding strength at the interface between cement grout and soil is dependent on the curing period.
- The proposed models for compacted CDG soil-cement grout interface were verified with the experimental data within the grouting pressure range of 0 to 250 kPa, net stress range of 50 to 300 kPa, and matric suction range of 0 to 300 kPa. Further study can be performed to verify the proposed model beyond those ranges.
- Numerical study can be conducted to simulate the behavior of compacted CDG soil and cement grout interface, and verify the experimental data as well as proposed models.

REFERENCES

Acar, Y. B., Durgunoglu, H. T., and Tumay, M. T. (1982). Interface properties of sand. Journal of Geotechnical Engineering, **108**(4): 648-654.

Aitchison, G. D. (1959). The strength of quasi-saturated and unsaturated soils in relation to the pressure deficiency in the pore water. *In* Proceedings of the 4th International Conference on Soil Mechanics and Foundation *Engineering*, London, pp 135-139.

Aitchison, G. D. (1960). Relationships of moisture stress and effective stress functions in unsaturated soils. *In* Proceedings of the Conference on Pore Pressure and Suction in Soils. Butterworths, London, UK. pp. 47-52.

Aitchison, G. D., and Donald, I. B. (1956). Effective stresses in unsaturated soils. *In* Proceedings of the 2nd Australia–New Zealand Conference on Soil Mechanics and Foundation Engineering. Christchurch, New Zealand. Technical Publications Ltd., Wellington, New Zealand. pp. 192-199.

Alonso, E. E., Gens, A., and Hight, D. W. (1987). Special problem soils: General report. In Proceedings of the 9th European Conference of Soil Mechanics and Foundation Engineering, Dublin, Vol.3, pp. 1087-1146.

Alonso, E. E., Gens, A., and Josa, A. (1990). A constitutive model for partially saturated soils. Géotechnique **40**(3): 405-430.

Au, S. K. A., Soga, K., and Yeung, A. T. (2006a). A new laboratory apparatus for grout injection studies. Geotechnical Testing Journal, ASTM, **29**(2):.95-101.

Au, S. K. A., Yeung, A. T., and Soga, K. (2006b). Pressure-controlled cavity expansion in clay. Canadian Geotechnical Journal, **43**(7): 714-725.

ASTM. (1992). Standard test method for classification of soils for engineering purposes. D2487-90, West Conshohocken, Philadelphia, pp. 326-336.

Bao, C. G., Gong, B. W., and Zhan, L. T. (1998). Properties of unsaturated soils and slope stability for expansive soils. *In* proceedings of the 2nd International Conference on Unsaturated Soils, Beijing, China, Vol. 2, pp. 71-98.

Brabour, S. L. (1998). The soil-water characteristic curve: a historical perspective. Canadian Geotechnical Journal, **35**: 873-894.

Berglund, C., and Oden, K. (1996). The pullout resistance of different types of nails. MS thesis, Dept. of Geotechnical Engineering, Chalmers University of Technology, Göteborg, Sweden.

Bernier, F., Volckaert, G., Alonso, E., and Villar, M. (1997). Suction-controlled experiments on Boom clay. Engineering Geology, **47**: 325-338.

Bishop, A. W. (1959). The principle of effective stress. Lecture delivered in Oslo, Norway, in 1955. Tecknisk Ukeblad I Samarbeide Med Teknikk, **106**(39): 859-863.

Bishop, A. W., Alpan, I., Blight, G. E., and Donald, I. B. (1960). Factors controlling the shear strength of partly saturated cohesive soil. ASCE Research Conference on Shear Strength of Cohesive Soils, Boulder, Colorado, pp. 505-532.

Bishop, A. W., and Donald, I. B. (1961). The experimental study of partly saturated soil in the triaxial apparatus. *In* Proceedings of the 5th International Conference on Soil Mechanics and Foundation Engineering, Paris, pp. 13-21.

Bishop, A. W., and Henkel, D. J. (1962). The measurement of soil properties in the triaxial test. 2nd edition, London, Edward Arnold (Publisher) Ltd., London, pp. 180-211.

Bishop, A. W., and Blight, G. E. (1963). Some aspects of effective stress in saturated and partly saturated soils. Géotechnique, **13**(3): 177-196.

Bocking, K. A., and Fredlund, D. G. (1980). Limitations of the axis translation technique. *In* Proceeding of the 4th International Conference on Expansive soils, Denver, pp.117-135.

Bosscher, P. J., and Ortiz, G. C. (1987). Frictional properties between sand and various construction materials. Journal of Geotechnical Engineering, ASCE, **113**(9): 1035-1039.

Boulon, M. (1989). Basic features of soil structure interface behaviour. Computer Geotechnics, **7**: 115-131.

Brumund, W. F., and Leonards, G. A. (1973). Experimental study of static and dynamic friction between sand and typical construction materials. Journal of Testing Evaluation, JTEVA, **1**(2): 162-165.

Brooks, R. H., and Corey, A. T. (1964). Hydraulic properties of porous medium. Colorado State University, Fort Collins, Hydrology Paper No. 3.

BS 5930. (1981). Code of Practice for Site Investigations. British Standards Institution (BSI), London, UK.

BS 1881: Part 107. (1983). Method for determination of density of compacted fresh concrete. British Standards Institution (BSI), London, UK.

BS 1881: Part 116. (1983). Method for determination of compressive strength of concrete cubes. British Standards Institution (BSI), London, UK.

BS 1377. (1990). British Standard BS1377: Methods of test for soils for civil engineering purposes. British Standards Institution (BSI), London, UK.

BS 1377-2. (1990). Methods of Test for Soils for Civil Engineering Purpose-Part 2: Classification Tests. British Standards Institution (BSI), London, UK.

Burland, J. B., and Ridley, A. K. (1996). The importance of suction in soil mechanics. *In* Proceedings of the 12th Geotechnical Southeast Asian Conference, Kualalumpur, Malaysia.

Campos, T. M. P., and Carrillo, C. W. (1995). Direct shear testing on an unsaturated soil from Rio de Janeiro. Unsaturated soils, ed. Alonso and Delage., *In* Proceedings of the 1st International Conference on Unsaturated soils, Paris: Balkema, Vol.1, pp. 31-38.

Chen P. Y. M. (1992). Methods of Test for Soils in Hong Kong for Civil Engineering Purposes (Phase 1 Tests). GEO Report No.36, Geotechnical Engineering office, Hong Kong, China.

Chiu, C. F., and Ng, C. W. W. (2003). A state-dependent elasto-plastic model for saturated and unsaturated soils. Géotechnique **53**(9): 809-829.

Chu L. M. (2003). Study on the Interface Shear Strength of Soil Nailing in Completely Decomposed Granite (CDG) Soil. MPhil thesis, The Hong Kong Polytechnic University, Hong Kong, China.

Chu L. M., and Yin J. H. (2005). Comparison of Interface Shear Strength of Soil Nails Measured by Both Direct Shear Box Tests and Pullout Tests. Journal of Geotechnical and Geoenvironmental Engineering, **131**(9): 1097-1107.

Chu, L. M., and Yin, J. H. (2006). Study on soil-cement grout interface shear strength of soil nailing by direct shear box testing method. Geomechanics and Geoengineering: An International Journal, **1**(4): 259-273.

Cui, Y. J., and Delage, P. (1996). Yielding and plastic behaviour of an unsaturated compacted silt. Géotechnique, **46**(2): 291-311.

Delage, P. Howat, M. D., and Cui, Y. J. (1998). The relationship between suction and swelling properties in a heavily compacted unsaturated clay. Engineering Geology, **50**: 31-48.

Desai, C. S., Drumm, E. C., and Zaman, M. M. (1985). Cyclic testing and modeling of interface. Journal of Geotechnical Engineering, ASCE, **111**(6): 793-815.

Dineen, K., and Burland, J. B. (1995). A new approach to osmotically controlled oedometer testing. *In* Proceedings of the 1st International Conference on Unsaturated Soils, Paris, Vol. 2, pp. 459-465.

Donald, I. B. (1956). Shear strength measurements in unsaturated non-cohesive soils with negative pore pressures. *In* Proceedings of the 2nd Australia–New Zealand Conference on Soil Mechanics and Foundation Engineering. Christchurch, New Zealand. Technical Publications Ltd., Wellington, New Zealand, pp. 200-204.

Drumright, E. E. (1989). The contribution of matric suction to the shear strength of unsaturated soils. Ph. D. thesis, University of Colorado, Fort Collins, USA.

Escario, V. (1980). Suction controlled penetration and shear tests. *In* Proceeding of the 4th International Conference on Expansive soils. Denver, ASCE, 2: pp. 781-797.

Escario, V., and Saez, J. (1986). The shear strength of partly saturated soils. Géotechnique, **36** (3): 453-456.

Esteban, V., and Saez, J. (1988). A device to measure the swelling characteristics of rock samples with control of the suction up to very high values. ISRM Symposium on Rock Mechanics and Power Plants. Madrid, Vol. 2, pp. 195-200.

Estabragh, A. R., Javadi, A. A., and Boot, J. C. (2004). Effect of compaction pressure on consolidation behaviour of unsaturated silty soil. Canadian Geotechnical Journal, **41**: 540-550.

Evans, M. D., and Fennick, T. J. (1995). Geosynthetic/soil interface friction angles using a rotation shear device. Geotechnical Testing Journal, **18**(2): 271-275.

Everett, D. H., and Whitton, W. I. (1952). A general approach to hysteresis, International Faraday Society, Vol. 48, pp. 749-752.

Fakharian, K., and Evgin, E. (1996). An automated apparatus for three-dimensional monotonic and cyclic testing of interfaces. Geotechnical Testing Journal, **19**(1): 22-31.

Feuerharmel, C., Pereira, A., Gehling, W. Y. Y., and Bica, A. V. D. (2006). Determination of the shear strength parameters of two unsaturated colluvium soils using the direct shear test. Unsaturated Soils, ASCE, pp. 1181-1190.

Franzen, G. (1998). Soil nailing- A laboratory and field study of pullout capacity. Ph. D. thesis, Chalmers University of Technology, Chalmers, Sweden.

Fredlund, D.G. (1998). Bringing unsaturated soil mechanics into engineering practice. *In* Proceedings of the 2nd International Conference on Unsaturated soils, Beijing, Vol. 2, pp. 1-36.

Fredlund, D. G., and Morgenstern, N. R. (1977). Stress state variables for unsaturated soils. Journal of the Geotechnical Engineering Division, ASCE, **103**(GT5): 447-466.

Fredlund, D. G., Morgenstern, N. R., and Widger, R.A. (1978). The shear strength of unsaturated soils. Canadian Geotechnical journal, **15**(3): 313-321.

Fredlund, D. G., and Rahardjo, H. (1993). Soil Mechanics for unsaturated soils. John Wiley and Sons, Inc., New York.

Fredlund, D. G., Rahardjo, H., and Gan, J. K. (1987). Nonlinearity of the strength envelope for unsaturated soils. Proceedings of the 6th International Conference on Expansive Soils. New Delhi, pp. 49-54.

Fredlund, D. G., and Xing, A. (1994). Equations for the soil-water characteristic curve. Canadian Geotechnical journal, **31**(3): 521-532.

Fredlund, D. G., Xing, A., Fredlund, M. D., and Barbour S. L. (1996). The relationship of the unsaturated soil shear strength to the soil-water characteristic curve. Canadian Geotechnical journal, **33**: 440-448.

Frost, J. D., and Han, J. (1999). Behavior of interfaces between fiber-reinforced polymers and sands. Journal of Geotechnical and Geoenvironmental Engineering, ASCE, **125**(8): 633-640.

Gan, J. K. M. (1986). Direct shear testing of unsaturated soils. MS thesis, University of Saskatchewan, Saskatoon, Sask, Canada.

Gan, J. K. M., and Fredlund, D. G. (1988). Multistage direct shear testing of unsaturated soils. Geotechnical Testing Journal, ASTM, **11**(2): 132-138.

Gan, J. K. M., and Fredlund, D. G. (1992). Direct shear testing of a Hong Kong soil under various applied matric suction. GEO Report No. 11, Geotechnical Engineering Office, Hong Kong, China.

Gan, J. K. M., and Fredlund, D. G. (1994). Direct shear and triaxial testing of a Hong Kong soil under saturated and unsaturated condition. GEO Report No. 46, Geotechnical Engineering Office, Hong Kong, China.

Gan, J. K. M., and Fredlund, D. G. (1996). Shear strength characteristics of two saprolitic soils. Canadian Geotechnical Journal, **33**(4): 595-609.

Gan, J. K., Fredlund, D. G., and Rahardjo, H. (1988). Determination of the shear strength parameters of an unsaturated soil using the direct shear test. Canadian Geotechnical Journal, **25**(8): 500-510.

Gens, A., and Alonso, E. E. (1992). A framework for the behavior of unsaturated expansive clays. Canadian Geotechnical Journal, **29**: 1013-1032.

GEO (Geoguide 3). (1988). Guide to Rock and Soil Descriptions. Geotechnical Engineering Office, Civil Engineering Department, The Government of HKSAR.

Gulhati, S. K., and Satija, B. S. (1981). Shear strength of partly saturated soils. *In* Proceedings of the 10th International Conference on Soil Mechanics and Foundation Engineering, Stockholm, Sweden, Vol. 1, pp. 609-6612.

Hamid, T. B., and Miller, G. A. (2009). Shear strength of unsaturated soil interfaces. Canadian Geotechnical Journal, **46**(5): 595-606.

Han, K. K. (1997). Effect of hysteresis, infiltration and tensile stress on the strength of unsaturated soil. Ph. D. thesis, School of Civil and Structural Engineering, Nanyang Technological University, Singapore.

Head, K. H. (1956). Manual of soil laboratory testing. John Wiley & Sons Inc., New York.

Heymann, G. (1993). Soil nailing systems as lateral support for surface excavations. MS thesis, Faculty of Engineering, Univ. of Pretoria, Pretoria, South Africa.

Heymann, G., Rhode, A.W., Schwartz, K., and Friedlaender, E. (1992). Soil nail pullout resistance in residual soils. In Proceedings of the International Symposium on Earth Reinforcement Practice, Kyushu, Japan, Vol. 1, pp. 487-492.

Hilf, J. W. (1956). An investigation of pore water pressure in compacted cohesive soils. Technical Memo 654, Denver, Bureau of Reclamation.

Hillel, D. (1998). Environmental Soil Physics. San Diego, CA, USA: Academic Press.

Ho, D. Y. F., and Fredlund, D. G. (1982). Increase in strength due to suction for two Hong Kong soils. Engineering and Construction in Tropical Soils, ASCE, Honolulu, Hawaii, pp. 263-293.

Hossain, M. A., and Yin, J. H. (2010). Behavior of a compacted completely decomposed granite soil from suction controlled direct shear tests. Journal of Geotechnical and Geoenvironmental Engineering, ASCE, **136**(1): 189-198.

Jewell, R. A., and Wroth C. P. (1987). Direct shear tests on reinforced sand. Géotechnique, **37**(1): 53-68.

Juca, J. F. T., and Frydman, S. (1996). Experimental techniques. *In* Proceedings of the 1st International Conference on Unsaturated Soils, Paris, Vol. 3, pp.1257-1292.

Junaideen, S. M., Tham, L. G., Law, K. T., Lee, C. F., and Yue, Z. Q. (2004). Laboratory study of soil nail interaction in loose, completely decomposed granite. Canadian Geotechnical Journal, **41**: 274-286.

Juran, I., Shaffiee, S., Schlosser, F., Humbert, P., and Guenot, A. (1982). Study of soil-bar interaction in the technique of soil nailing. *In* Proceedings of the 8th European Conference on Soil Mechanics and Foundation Engineering, pp. 513-516.

Karube, D. (1988). New concept of effective stress in unsaturated soil and its proving test. *In* Advanced triaxial testing of soil and rock. American Society for Testing and Materials, Philadelphia, ASTM STP 977, pp. 539-552.

Kassif, G., and Ben Shalom, A. (1971). Experimental relationship between swelling pressure and suction. Géotechnique, **21**(3): 255-259.

Khalili, N., and Khabbaz, M. H. (1998). A unique relationship for χ for the determination of the shear strength of unsaturated soils. Géotechnique, **48**(5): 681-687.

Kishida, H., and Uesugi, M. (1987). Tests of the interface between sand and steel in the simple shear apparatus. Géotechnique, **37**(1): 45-52.

Komornik, A., Livneh, M., and Smucha, S. (1980). Shear strength and swelling of clays under suction. *In* Proceedings of the 4th International Conference on Expansive soils. Denver, CO, Vol. 1, pp. 206-226.

Kulhawy, F. H., and Peterson, M. S. (1979). Behavior of sand-concrete interfaces. *In* Proceedings of the 6th Pan-American Conference on Soil mechanics and Foundation Engineering, Vol. 7, pp. 225-236.

Lagerwerff, J. V., Ogata, G., and Eagle, H. E. (1961). Control of osmotic pressure of culture solutions with polyethylene glycol. Science, **133**: 1486-1487.

Lamborn, M. J. (1986). A micromechanical approach to modeling partly saturated soils. M. Sc. thesis, Texas A & M University, College Station, Tex.

Lee, C. F., Law, K. T., Tham, L. G., Yue, Z. Q., and Junaideen, S. M. (2001). Design of a large soil box for studying soil-nail interaction in loose fill. Soft soil engineering, pp. 413-418.

Lee, I. M., Sung, S. G., and Cho, G. C. (2005). Effect of stress state on the unsaturated shear strength of a weathered granite. Canadian geotechnical Journal, **42**: 624-631.

Leong, E. C., and Rahardjo, H. (1997). Review of soil-water characteristic curve equation. Journal of Geotechnical and Geoenvironmental Engineering, ASCE, **123**: 1106-1117.

Liang, R. Y., and Feng, Y. (2002). Development and application of anchor-soil interface models. Journal of Soil and Foundations, **42**(2): 59-70.

Likos, W. J., and Lu, N. (2003). Automated humidity system for measuring total suction characteristics of clay. Geotechnical Testing Journal, **26**(2): 1-12.

Lloret A, Villar, M. V., Sanchez, M., Gens, A., Pintado, X., and Alonso, E. E. (2003). Mechanical behaviour of heavily compacted bentonite under high suction changes. Géotechnique, **53**(1): 27-40.

Mancuso, C., Vassallo, R., and d'Onofrio, A. (2002). Small strain behavior of a silty sand in controlled-suction resonant column-torsional shear tests. Canadian Geotechnical Journal, **39**(1): 22-31.

Mazo, O. C., Saez, J., and Esteban, F. (1995). Laboratory tests and equipment with suction control. In Proceedings of the 1st International Conference on Unsaturated soils, Paris, Vol. 3, pp. 1509-1515.

McKee, C. R., and Bumb, A. C. (1984). The importance of unsaturated flow parameters in designing a monitoring system for a hazardous wastes and environment emergencies. Hazardous materials Control Research Institute National Conference, Houston, Tex., March, pp. 50-58.

McKee, C. R., and Bumb, A. C. (1987). Flow-testing coalbed methane production wells in the presence of water gas. SPE Formation Evaluation, December, pp. 50-58.

Melinda, F., Rahardjo, H., Han, K. K., and Leong, E. C. (2004). Shear strength of compacted soil under infiltration condition. Journal of Geotechnical and Geoenvironmental Engineering, ASCE, **130**(8): 807-817.

Miller, G. A., and Hamid, T. B. (2007). Interface direct shear testing of unsaturated soil. Geotechnical Testing Journal, **30**(3): 182-191.

Milligan, G. W. E., and Tei, K. (1998). The pull-out resistance of model soil nails. Journal of Soils and Foundations, **38**(2): 179-190.

Mualem, Y. (1973). Modified approach to capillary hysteresis based on a similarity hypothesis. Water Resources Research, **9**(5): 1321-1331.

Mualem, Y. (1974). A conceptual model for hysteresis. Water Resources Research, **10**(3): 514-520.

Ng, C. W. W., and Chiu, C. F. (2003). Laboratory study of loose saturated and unsaturated decomposed granitic soil. Journal of Geotechnical and Geoenvironmental Engineering, ASCE, **129**(6): 550-559.

Ng, C. W. W., and Pang, Y. W. (2000). Influence of stress state on soil-water characteristics and slope stability. Journal of Geotechnical and Geoenvironmental Engineering, ASCE, **126**(2): 157-166.

Ng, C. W. W., and Yung, S. Y. (2008). Determination of the anisotropic shear stiffness of an unsaturated decomposed soil. Géotechnique, **58**(1): 23-35.

Ng, C. W. W., and Zhou, R. Z. B. (2005). Effects of soil suction on dilatancy of an unsaturated soil. *In* Proceedings of the 16th ICSMGE, Osaka, Japan, Vol. 2, pp. 559-562.

Noorany, I. (1985). Side friction of piles in calcareous sands. *In* Proceedings of the 11th International Conference on Soil mechanics and Foundation Engineering, San Francisco, Vol. 3, pp. 1611-1614.

O'Rourke, T. D., Druschel, S. J., and Netravali, A. N. (1990). Shear strength characteristics of sand-polymer interfaces. Journal of Geotechnical Engineering, ASCE, **116**(3): 451-469.

Paikowsky, S. G., Player, C. M., and Connors, P. J. (1995). A dual interface apparatus for testing unrestricted friction of soil along solid surface. Geotechnical Testing Journal, **18**(2): 168-193.

Palmeira, E. M., and Milligan, G. W. E. (1989). Scale and other factors affecting the results of pull-out tests of grids buried in sand. Géotechnique, **39**(3): 511-524.

Panchanathan, S., and Ramaswamy, S. V. (1964). Skin friction between sand and construction materials. Indian National Society of Soil Mechanics and Foundation Engineering, **3**(4): 325-336.

Peck, A. J., and Rabbidge, R. M. (1969). Design and performance of an osmotic tensiometer for measuring capillary potential. Proceedings of Soil Science Society of America, **33**: 196-202.

Peterson, R.F.W. (1988). Interpretation of triaxial compression test results on partly saturated soils. *In* Advanced triaxial testing of soil and rock. American Society for Testing and Materials, Philadelphia, ASTM STP 977, pp. 512-538.

Potyondy, J. G. (1961). Skin friction between various soils and construction materials. Géotechnique, **11**(4): 339-353.

Pradhan, B. (2003). Study of pullout behaviour of soil nails in completely decomposed granite fill. Master's thesis, The University of Hong Kong, Hong Kong, China.

Pun, W. K., and Shiu, Y. K. (2007). Design practice and technical developments of soil nailing in Hong Kong. *In* Proceedings of HKIE Geotechnical Division, 27th Annual Seminar: Geotechnical Advancements in Hong Kong since 1970s, Hong Kong, pp. 197-212.

Rahardjo, H., and Leong, E. C. (1997). Soil-water characteristic curves and flux boundary problems. Unsaturated Soil Engineering Practice, New York, ASCE, pp. 88-112.

Rao, K. S. S, Allam, M. M., and Robinson, R. G. (1996). A note on the choice of interfacial friction angle. Proceedings of Institute of Civil Engineers, Geotechnical Engineering, **119**(1): 123-128.

Rao, K. S. S, Allam, M. M., and Robinson, R. G. (2000). Drained shear strength of fine-grained soil-solid surface interfaces. Proceedings of Institute of Civil Engineers, Geotechnical Engineering, **143**: 75-81.

Rassam, D. W., and Williams, D. J. (1999). A relationship describing the shear strength of unsaturated soils. Canadian Geotechnical Journal, **36**: 363-368.

Rui, C. (2007). Experimental study and constitutive modelling of stress-dependent coupled hydraulic hysteresis and mechanical behaviour of an unsaturated soil. Ph. D. thesis, The Hong Kong University of Science and Technology, Hong Kong, China.

Satija, B.S. (1978). Shear behaviour of partly saturated soils. Ph. D. thesis, Indian Institute of Technology, Delhi, India.

Schlosser F., and Guilloux A. (1981). Le Frottement dans les sols. Revue Francaise de Geotechnique, No. 16, pp. 65-77.

Schofield, R. (1935). The pF of the water in soil. Trans. 3rd Int. Congress Soil Sci., Vol. 2: 37-48.

Shakir, R. R., and Zhu, J. (2009). Behavior of compacted clay-concrete interface. Journal Frontiers of Architecture and Civil Engineering in China, **3**: 85-92.

Sharma, J. S., Fleming, I. R., and Jogi, M. B. (2007). Measurement of unsaturated soil-geomembrane interface shear-strength parameters. Canadian Geotechnical Journal, **44**: 78-88.

Sharma, R. S. (1998). Mechanical behavior of unsaturated highly expansive clays. Ph. D. thesis, Oxford University.

Sillers, W. S., and Fredlund, D. G. (2001). Statistical assessment of soil-water characteristic curve models for geotechnical engineering. Canadian Geotechnical Journal, **38**: 1297-1313.

Sivakumar, V. (1993). A critical state framework for unsaturated soils. Ph. D. thesis, University of Sheffield.

Slatter, E. E. , Jungnickel, C. A., Smith, D. W., and Allman, M. A. (2000). Investigation of suction generation in apparatus employing osmotic methods. *In* Proceedings of the Conference on Unsaturated Soils for Asia, Singapore, pp. 297-302.

Su L. J. (2006). Laboratory pull-out testing study on soil nails in compacted completely decomposed granite fill. Ph. D. thesis, The Hong Kong Polytechnic University, Hong Kong, China.

Su, L. J., Chan T. C. F., Shiu, Y. K., Cheung, T., and Yin, J. H. (2007). Influence of degree of saturation on soil nail pullout resistance in compacted completely decomposed granite fill. Canadian Geotechnical Journal, **44**(11): 1314-1428.

Su, L. J., Chan T. C. F., Yin, J. H., Shiu, Y. K., and Chiu, S. L. (2008). Influence of overburden pressure on soil-nail pullout resistance in compacted fill. Journal of Geotechnical and Geoenvironmental Engineering, **134**(9): 1339-1347.

Tarantino, A., and Mongiovi, L. (2000). A study of the efficiency of semi-permeable membranes in controlling soil matrix suction using the osmotic technique. *In* Proceedings of the Conference on Unsaturated Soils for Asia, Singapore, pp. 303-308.

Tarantino, A., Mongiovi, L., and Bosco, G. (2000). An experimental investigation on the independent isotropic stress variables for unsaturated soils. Géotechnique, **50**(3): 285-292.

Toll, D. G. (1990). A framework for unsaturated soil behaviour. Géotechnique, **40**(1); 31-44.

Uesugi, M., Kishida, H., and Uchikawa, Y. (1990). Friction between dry sand and concrete under monotonic and repeated loading. Soil and Foundations, Japanese Society of Soil Mechanics and Foundation Engineering, **30**(1): 115-128.

Van Genutchen, M. T. (1980). A closed-form equation for predicting the hydraulic conductivity of unsaturated soils. Soil Science Society of American Journal, **44**(5): 892-898.

Vanapalli, S. K. (1994). Simple test procedure and their interpretation in evaluating the shear strength of an unsaturated soil. Ph. D. thesis, University of Saskatchewan, Saskatoon, Canada.

Vanapalli, S. K., Fredlund, D. G., and Pufahl, D. E. (1999). The influence of soil structure and stress history on the soil-water characteristic of a compacted till. Géotechnique, **49**(2): 143-159.

Vanapalli, S. K., Fredlund, D. G., Pufahl, D. E., and Clifton, A. W. (1996). Model for the prediction of shear strength with respect to soil suction. Canadian Geotechnical Journal, **33**: 379-392.

Vilar, O. M. (2006). A simplified procedure to estimate the shear strength envelope of unsaturated soils. Canadian Geotechnical Journal, **43**: 1088-1095.

Wheeler, S. J. (1988). The undrained shear strength of soils containing large gas bubbles. Géotechnique, **28**(3): 399-413.

Wheeler, S. J., and Karube, D. (1996). Constitutive modelling. *In* Proceedings of the 1st International Conference on Unsaturated. Soils, Paris, Vol.3, pp. 1323-1356.

Wheeler, S. J., Sharma, R. J., and Buisson, M. S. R. (2003). Coupling of hydraulic hysteresis and stress–strain behaviour in unsaturated soils. Géotechnique **53**(1): 41–54.

Wheeler, S. J., and Sivakumar, V. (1995). An elasto-plastic critical state framework for unsaturated soil. Géotechnique, **45**: 35-53.

Williams, J., and Shaykewich, C. F. (1969). An evaluation of polyethylene (PEG) 6000 and PEG 20000 in the osmotic control of soil water matric potential. Canadian Journal of Soil Science, **102**(6):394-398.

Wong, H. Y. (1995). Soil nails design manual for slopes (with worked example), Architectural Services Department.

Yeung, A. T., Cheng Y. M., Lau C. K., Mak L. M., Yu R. S. M., Choi Y. K., and Kim J. H. (2005). An innovative Korean system of pressure-grouted soil nailing as a slope stabilization measure. *In* the Proceedings of The HKIE Geotechnical Division 25th Annual Seminar, 4 May 2005, Hong Kong, published by HKIE-GDC and HKGES, pp. 43-49.

Yin, J. H., Su, L. J., Cheung, R. W. M., Shiu, Y. K., and Tang, C. (2008). The influence of grouting pressure on the pullout resistance of soil nail in compacted completely decomposed granite fill. Géotechnique, **59**(2): 103-113.

Yin, J. H., and Zhou, W. H. (2009). Influence of grouting pressure and overburden stress on the interface resistance of a soil nail. Journal of Geotechnical and Geoenvironmental Engineering, ASCE, **135**(9): 1198-1208.

Yin, Z. Z., Zhu, H., and Xu, G. H. (1995). A study of deformation in the interface between soil and concrete. Computers and Geotechnics, **17**: 75-92.

Ying, J., Liao, H., and Yin, J. H. (2006). An experimental study on the shear strength of undisturbed loess. Unsaturated Soil, Seepage and Environmental Geotechnics, ASCE, (GSP 148): 127-135.

Yoshimi, Y., and Kishida, T. (1981). Friction between sand and metal surface. *In* Proceedings of the 10th International Conference on Soil Mechanics and Foundation Engineering, Vol. 1, pp. 831-834.

Zeghal, M., and Edil, T. B. (2002). Soil structure interaction analysis: modeling the interface. Canadian Geotechnical Journal, **39**: 620-628.

Zhan, L. T. (2003). Field and Laboratory study of an unsaturated expansive soil associated with rain-induced slope instability. Ph. D. thesis, The Hong Kong University of Science and Technology, Hong Kong, China.

Zhan, L. T., and Ng, C. W. W. (2006). Shear strength characteristics of an unsaturated expansive clay. Canadian Geotechnical Journal, **43**: 751-763.

Zhou, W. H. (2008). Experimental and theoretical study on pullout resistance of grouted soil nails. Ph. D. thesis, The Hong Kong Polytechnic University, Hong Kong, China.

Zur, B. (1966). Osmotic control of the matric soil-water potential. Soil Science, **102**: 394-398.